The role of the transcription factor JAGGED in early floral organogenesis

A thesis submitted to the University of East Anglia

for the degree of Doctor of Philosophy

Katharina Schiessl

John Innes Centre

Norwich, UK

May 2014

Abstract

Initiation of organ primordia from pools of undifferentiated cells requires coordinated cytoplasmic growth, oriented cell wall extension, and cell cycle progression. It is debated which of these processes are primary drivers for organ morphogenesis and directly targeted by developmental regulators. The single zinc finger transcription factor *JAGGED (JAG)* is a direct target of several floral organ identity genes and is expressed in early organ primordia (Dinneny et al., 2004; Ohno et al., 2004; Gomez et al., 2005; Kaufmann et al., 2009). Loss of function *jag* mutants have narrow floral organs with reduced distal growth. Quantitative 3D imaging has revealed that *JAG* is required for the transition from meristematic to organ primordium cell behaviour. The transition involves an increase in the rates of cell division and cell growth, a shift from isotropic to anisotropic growth, and modifications in cell size homeostasis in primordia (Schiessl et al., 2012). In this project, ChIP-Seq was combined with transcriptome analysis to identify global direct target genes of JAG.

Consistent with the roles of JAG during organ initiation and organ growth, I found that *JAG* directly repressed genes involved in meristem development, such as the *TALE PROTEIN BELL1* and genes involved in organ boundaries specification such as *PETAL LOSS*. In addition, JAG directly regulated genes involved in growth regulatory pathways, tissue polarity, cell wall modification, and cell cycle progression. For example, JAG directly repressed the cell cycle inhibitors *KIP RELATED PROTEIN 2* and *4 (KRP2/4).* The *krp2* and *krp4* mutations suppressed *jag* loss of function defects in organ growth and cell type patterning. In particular, loss of *KRP4* rescued the defects of cell size homeostasis in the primordia of the *jag* loss of function mutant. In summary, this work revealed that JAG directly coordinates organ patterning with cellular processes required for tissue growth.

Acknowledgments

I would like to thank Robert Sablowski for supervision and excellent support on the project, and for his help with the 3D analysis of cell geometry.
I would like to thank Lars Østergaard, Rico Coen, and Susana Sauret-Gueto for support during my PhD.
I would like to thank all the supervisors and my colleagues from the SYSFLO training network.
I would like to thank Jose Muiño for help with ChIP-Seq and microarray analysis.
I would like to thank Grant Calder for his support and Kim Findlay for SEM imaging.
I would like to thank all people in Biffen and especially my colleagues for their support: Cristina, Maria, Pauline, Swathi, Jessica, Nick, Nico, Tom, Stefano, Antonio, and Diego
I would like to thank Tim Wells for looking after my plants so well.
I would like to thank Cindy and Barbara for looking after me.
I would like to thank Beth, Katie, Wiebke, and Erika for sharing a lovely time.
I would like to thank Professor Marie-Theres Hauser for her encouragement to do a PhD.
I would like to thank Katharina, Maria and Leo, Ingrid and Franz for their support from Austria.
I would like to thank my dear love Paul.

My PhD was funded by the Marie Curie Initial Training Network "Training in Systems Biology" (SYSFLO) (Grant 237909).

Table of Contents

Abbreviations

BiFC	Bimolecular Fluorescence Complementation
ChIP	Chromatin Immunoprecipitation
ChIP-Seq	Chromatin Immunoprecipitation followed by High throughput Deep Sequencing
Col	Columbia
DEX	Dexamethasone
DNA	Deoxyribonucleic acid
dNTP	Deoxynucleotide triphosphate
DTT	Dithioreitiol
EDTA	Ethylenediaminetetraacetic acid
EdU	5-ethynyl-2′-deoxyuridine
EMS	Ethyl methanesulfonate
GA	Gibberellins
GFP	Green fluorescent protein
GO	Gene Ontology
GR	Glucocorticoid receptor
GUS	ß-glucuronidase
L-*er*	Landsberg *erecta*
PCR	Polymerase chain reaction
PI	Propidium iodide
RNA	Ribonucleic acid
ROS	Reactive oxygen species
SEM	Scanning electron microscopy
T-DNA	Transfer DNA
WT	Wild type

Chapter 1 - General Introduction

1.1. What does it take to produce a determinate plant organ?

Plants undergo post-embryonic organogenesis and continuously produce lateral organs such as leaves and flowers during their lifetime. What does it take to produce a floral organ? Organs initiate from a small number of founder cells which are recruited from pools of undifferentiated cells within meristems. Their development is under tight control of gene regulatory networks that regulate the timing and position of organ initiation, organ identity, organ patterning (establishment of organ boundaries, organ margins and growth axes), growth and morphogenesis to final size, shape, and function. To reach final organ size, shape and function, cells in an organ initial increase in number by cell division, increase in volume by cell growth – expansion, and acquire specific cell identities by cell differentiation. These cellular processes are also coordinated in the spatial and temporal context of the developing organ primordium by developmental regulators.

1.2. The shoot apical meristem is an indeterminate source of undifferentiated cells

The shoot apical meristem consists of undifferentiated cells that divide to maintain the pool of cells from which founder cells are continuously recruited into organ primordia at the flanks of the shoot apical meristem. In the central zone of the dome-shaped shoot apical meristem, cells divide relatively slowly and grow at equal rates resulting in a cell population that have uniform sizes, are isotropic in shape and have small vacuoles. With every round of cell division, daughter cells are pushed into the peripheral zone, where they divide twice as fast as cells in the central zone, to be recruited as founder cells into lateral organ primordia (Reddy et al., 2004; Carraro et al., 2006; Besnard et al., 2011; Schiessl et al., 2012).

Development of the shoot apical meristem and its size homeostasis are regulated by meristem maintenance genes such as the *KNOTTED 1-like homeobox (KNOX)* genes *SHOOTMERISTEMLESS (STM)* and *BREVIPEDICELLUS (BP),* and by the *WUSCHEL-CLAVATA*

pathway (Schoff et al., 2000; Long et al., 1996; Byrne et al., 2002). *WUSCHEL* and *KNOX* genes promote cytokinin biosynthesis and cytokinin signalling which plays a major role in promoting cell proliferation and in preventing differentiation (reviewed by Veit, 2009; Holst et al., 2011). By contrast, *KNOX* genes repress biosynthesis and promote degradation of gibberellins resulting in a high cytokinin/gibberellins ratio in the shoot apical meristem (reviewed by Veit, 2009).

In the peripheral zone of the shoot apical meristem, organs sequentially initiate at sites of high auxin accumulation. During vegetative growth, the shoot apical meristem gives rise to leaf primordia and after plants have undergone the transition to flowering, the shoot apical meristem becomes an inflorescence meristem that gives rise to floral primordia. Floral primordia consist of a determinate floral meristem from which the floral organs are initiated (recently reviewed by Ó' Maoiléidigh et al., 2014). In the *Arabidopsis* flower, the floral organs initiate in concentric whorls, with four sepals in the outermost whorl protecting four petals in the second whorl, six stamen in the third whorl and two fused carpels in the centre of the flower. Flower development in *Arabidopsis* was described and staged by Smyth et al. (1990), who defined the initiation of floral primordia from the inflorescence meristem as stage 1, the emergence of the first sepal primordium from the floral meristem as stage 3, subsequent emergence of petal and stamen primordia as stage 5 and the appearance of the gynoceum as stage 6. These stages are followed by stages 7-11, which involve processes of organ expansion and cell type specification, followed by stage 12, when the flower opens for anthesis, on average 13.25 days after initiation of the floral primordium (Smyth et al., 1990).

The gene regulatory network that defines floral primordia identity and the identity of the different floral organs has been well studied over the past thirty years: Floral primordia identity is promoted by the transcription factor *LEAFY (LFY)* and the partly redundant transcription factors *APETALA1 (AP1)*, *CAULIFLOWER (CAL)*, and *FRUITFUL (FUL)*. Once floral organ primordia are established, *LFY* and *AP1* promote the expression of floral organ identity genes. Floral organ identity genes, predominantly MADS-box transcription factors, act in a combinatorial manner to superimpose the organ identity of sepals, petals, and the reproductive organs on groups of founder cells in the floral meristem (Coen and Meyerowitz, 1991; Krizek and Fletcher, 2005; Ó' Maoiléidigh et al., 2014).

Because floral organ identity genes function as master regulators, their direct downstream targets could provide important clues about what it takes to produce an organ including the gene regulatory network of floral organogenesis. Global transcription profiling and genome-wide analysis of DNA binding sites revealed that the floral primordium identity gene *LFY* and floral organ identity genes such as *SEPALATA3* (*SEP3*) and *APETALA3/PISTILATA* (*AP3*/*PI*) target predominantly transcription factors involved in hormone response (specifically auxin response), meristem development, and organ growth such as members of the *TEOSINTE BRANCHED1/CYCLOIDEA/PCF* (*TCPs*), *GROWTH REGULATORY FACTORS* (*GRFs*), *GRF INTERACTING FACTORS* (*GIFs*), *AINTEGUMENTA*/ *AINTEGUMENTA-LIKE* protein families (Kaufmann et al., 2009; Winter et al., 2011; Wuest et al., 2012). Consequently, these transcription factors have been considered as putative master regulators and have been analysed in more detail, but still little is known about how the gene regulatory network of early organogenesis is interconnected with organ patterning, growth, and morphogenesis to produce floral organs with their final size, shape and function.

1.3. Initiation of organ primordia

During organ initiation, a group of around sixty undifferentiated meristem cells are recruited as pre-founder cells in the flanks of the shoot apical meristem. These pre-founder cells are still part of the shoot apical meristem, but undergo transcriptional changes and express the early markers of founder cell identity such as *REVOLUTA (REV)* and the auxin efflux carrier *PIN-FORMED 1 (PIN1)* (Heisler et al., 2005; reviewed by Carraro et al., 2006). Only a limited and reproducible number of true founder cells are recruited from the pool of pre-founder cells to form the organ primordium. For example, four cells are the foundation of a floral primordium at the inflorescence meristem and between four and sixteen cells are the core founder cells of leaf and floral organ primordia (Bossinger and Smyth, 1996; Donnelly et al., 1999; Roeder et al., 2010). Founder cells undergo a transition from meristem growth behaviour to a primordium growth behaviour that involves an increase in cell proliferation rates and cell growth rates by about three-fold compared to meristem cells (Reddy et al., 2004; Schiessl et al., 2012)

and a loss of coordination between these two processes (Schiessl et al., 2012). In order to bulge out and to form an early organ primordium that is distinct from the morphology of the shoot apical meristem, founder cells change division planes and shift from isotropic to anisotropic cell growth behaviour (Grandjean et al., 2004; Reddy et al., 2004; Schiessl et al., 2012; Burian et al., 2013).

While undergoing this transition, founder cells acquire a transcriptional profile that significantly differs from meristem cells: Downregulation of meristem identity genes such as the *KNOX* genes *SHOOTMERISTEMLESS (STM)* and *BREVIPEDICELLUS (BP)* is considered a hallmark in the recruitment of founder cells from the peripheral zone of the shoot apical meristem (Carraro et al., 2006). In *Arabidopsis* leaves, the MYB transcription factor *ASYMMETRIC LEAVES1* (*AS1*) and its co-activator the lateral organ boundary domain transcription factor *ASYMMETRIC LEAVES2* (*AS2*) have been identified as early primordium markers that down-regulate KNOX genes. Conversely, *STM* represses *AS1*, suggesting that there is a mutual antagonism between KNOX genes and early primordium markers (Byrne et al., 2000 and 2002). Additionally, the growth-promoting AP2/ERF transcription factor *AINTEGUMENTA (ANT)* and the related *AINTEGUMENTA-LIKE 6 (AIL6)* have been identified as early markers of primordium identity. In initiating floral primordia*, ANT* and *AIL6* and the floral primordium identity gene *LEAFY* are directly promoted by the *AUXIN-RESPONSE FACTOR 5/MONOPTEROS* (*ARF5*/*MP*) in response to auxin accumulation (Krizek, 2009; Yamaguchi et al., 2013).

1.4. Establishing growth axes in early organ primordia

One of the first patterning processes in incipient lateral organ primordia is to determine growth directions relative to the position of the meristem, which consequently establishes a proximal/distal axis, medial/lateral and an adaxial/abaxial axis for polar organ growth. Primordia initiate at sites of high accumulation of the growth promoting hormone auxin. The auxin efflux carrier *PIN1* has been found as an early marker of pre-founder cell identity and PIN1 proteins point to the distal tip of early organ primordia, suggesting that an auxin gradient may be involved in the establishment of the proximal/distal growth axis (Benkova et al., 2003; Heisler et al., 2005; Sauret et al., 2013).

Auxin accumulation at the site of primordium initiation promotes the early down-regulation of meristem identity genes such as *STM* and *BP* in primordium founder cells, while adjacent undifferentiated cells maintain high expression levels of meristem identity genes. Therefore, it has been suggested that down-regulation of KNOX genes defines the initial process of proximal/distal organ patterning relative to the meristem (Bolduc et al., 2012). KNOX genes are also down-regulated by *AS1* and the associated transcriptional activators *BOP1/BOP2*, which are expressed specifically at the site of incipient floral primordia and at the adaxial base of sepals and petals and have been shown to play a role in adaxial/abaxial patterning (Ha et al., 2003 and 2007; Jun et al., 2010). In addition, BOP1/2 have been shown to be expressed in the proximal region of leaf primordia where they restrict blade tissue growth and therefore have been suggested to be involved in proximal/distal organ patterning (Norberg et al., 2005). Besides this information, little is known about the gene regulatory network and the molecular mechanisms that establish the proximal/distal growth axis downstream of or independently from the effects of auxin gradients during early organogenesis.

Primordia initiate as radially symmetric cylindrical bulges that soon acquire a flattened shape in the case of leaves, sepals and petals and establish an adaxial/abaxial growth axis. Unlike for the proximal/distal processes, the gene regulatory network that defines the adaxial/abaxial patterning is well established, with HD-ZIPIII transcription factors *PHAVOLUTA*, *PHABULOSA* and *REVOLUTA* defining the adaxial domain and members of the *KANADI* and *YABBY* transcription factor families defining the abaxial side (reviewed by Barkoulas et al., 2007).

1.5. Organ boundaries and margins delimit lateral organs

Concomitantly with the determination of the founder cells, adjacent cells are recruited as boundary cells that separate the primordium from the neighbouring meristem cells and from neighbouring organs (reviewed by Aida and Tasaka, 2006). In addition, boundaries play a major role in separating domains during organ patterning where they form juxtapositions between domains that are important sources of signals (reviewed by Barkoulas et al., 2007; Nawy et al., 2010).

Boundary cells are small, thick-walled cells that elongate parallel to the tissue plane into concave, saddle-shaped cells. Owing to their position, boundaries are regions under high mechanical stress with tension in longitudinal direction and compression towards the medial/lateral direction. It has been disputed whether boundary cells divide not at all or at very slow rates parallel to the longitudinal axis of the boundary (Breuil-Broyer et al., 2004; Aida and Tasaka, 2006; Burian et al., 2013). RNA *in situ* hybridisation suggested that cell cycle related genes that are highly expressed in organ primoridia are excluded from the band of adjacent boundary cells (Breuil-Broyer et al., 2004). As a band of non-proliferating or slowly proliferating cells, boundary cells serve as a stable barrier to avoid overgrowth into neighbouring domains. It has also been speculated that boundary cells may also serve as a barrier for the movement of proteins and signalling molecules. As a result, loss of boundary cell identity causes organ fusions and loss or conversion of tissues and whole organs (Aida and Tasaka, 2006).

Organ boundary cell identity is determined by the expression of organ boundary-specifying genes such as members of the *NAC* transcription factor family *CUP-SHAPED COTYLEDONS* (*CUC*), the *GATA* transcription factor *HANABA TARANU* (*HAN*) and the floral organ specific boundary genes trihelix transcription factor *PETAL LOSS (PTL)*, and the C2H2 single zinc finger transcription factors *SUPERMAN* (*SUP*) and *RABBIT EAR (RBE)* (reviewed by Aida and Tasaka, 2006). In *Arabidopsis*, the three members of the *CUC gene* family, *CUC1-3*, promote boundary formation throughout postembryonic development. *CUC* genes are expressed in a narrow strip of cells between the meristem and emerging organs and between neighbouring organs. In floral buds, *CUC2* and *CUC3* expression marks the band of boundary cells prior to primordia emergence, providing evidence that boundary establishment is one of the early steps of organogenesis. In *Arabidopsis*, *cuc*

double loss of function mutants show fusions in all lateral organs, providing evidence that *CUC* genes play a crucial role in organ separation (Breuil-Broyer et al., 2004; Hibara et al., 2006; reviewed by Aida and Tasaka, 2006). On the other hand, ectopic expression of boundary-specifying genes leads to repressed cell proliferation and tissue growth, therefore expression domains of boundary-specifying genes are strictly delimited by growth promoting factors such as *AS1/AS2* (Xu et al., 2008).

According to their function, it could be speculated that boundary-specifying genes negatively regulate cell proliferation and cell growth, but only a few downstream targets have been identified so far. For example, global transcription profiling showed that upon ectopic expression of *HAN,* cell cycle genes and cell wall related genes were differentially expressed (Zhang et al., 2013). However, no direct molecular or genetic interactions have been revealed between boundary specifying genes and regulators of the cell cycle.

Not only organ boundaries to neighbouring cells but also organ margins have to be defined in order to determine final organ size, shape and function. In this context, members of the *CINCINNATA-like TEOSINTE-BRANCHED1/CYCLOIDEA/PCF (CIN-like TCP)* family have been shown to play a crucial role in promoting cell differentiation during leaf development, particularly affecting the leaf margins (Nath et al., 2003; Koyama et al., 2007 and 2010). By contrast, *CUC* genes are expressed in the sinus of developing serrations of organ margins and promote undifferentiated cell fates by promoting KNOX gene expression (Hasson et al., 2011). During leaf differentiation, members of the *CIN-like TCP* genes have been shown to indirectly repress *CUC* gene expression in leaf margins by promoting expression of the *MYB* transcription factor *AS1* and the *microRNA 164*, which targets transcripts of *CUC1* and *CUC2* for degradation. In *tcp* loss of function mutants, ectopic expression of *CUC* genes promoted ectopic expression of *KNOX* genes leading to delayed cell differentiation. Consequently, *tcp* mutants have wavy leaves with severely serrated margins, serrated sepals and wavy petals (Koyama et al., 2007; Koyama et al., 2010; Koyama et al., 2011)

The boundary specifying gene *PTL* is not only expressed in the floral primordia, but also in the distal margins of petal and sepal primordia, suggesting that *PTL* may have a role in restricting organ outgrowth in margins. This hypothesis is further supported by the fact that ectopic expression of PTL leads to severe reduction in organ growth (Brewer et al., 2004; Lampugnani et al., 2012).

1.6. Organ growth and morphogenesis

In early primordia, cells undergo several rounds of mitotic divisions. This phase of primordium formation is also referred to as primary morphogenesis. In a second phase of morphogenesis, cells exit mitotic cell proliferation, undergo endoreduplication, post-mitotic cell expansion and cell differentiation to acquire final cell sizes, shapes, and functions (Donnelly et al., 1999; Gonzalez et al., 2010; Asl et al., 2011; Adriankaja et al., 2012; Powell and Lenhard, 2012). Over the time-course of development, organs are shaped by variations in local division rates, growth rates, growth directions, the timing of exit from division and growth, and onset of differentiation. These processes have to be coordinated within and between tissues of an organ to maintain tissue integrity (Roeder et al. 2010; Kuchen et al., 2012; Sauret et al., 2013). For example, within developing leaves, growth ceases in a coordinated pattern from the tip to the base in an apical-basal cell cycle arrest front, where cells undergo the transition from mitotic cell proliferation to endoreduplication and cell expansion followed by stomatal cell differentiation (Donnelly et al., 1999; Gonzalez et al., 2010; Asl et al., 2011). Similarly, Roeder et al. (2010), who followed the development of sepal primordia, found that the top half of the cells in early sepal primordia generates the tip of the sepal, indicating that the cells on top stop dividing after only few cycles of division. In the central region, cells divide and enter endoreduplication in order to become giant cells. Cells at the base stay in proliferation phase the longest, undergoing comparatively more cell divisions, and thus generating the basal half of the sepal. In the case of petals, mitotic cell division rates are different between the proximal and distal area, but appear to decrease more homogenously within the entire organ over the time-course of development. Moreover, petal cells do not undergo endoreduplication and keep expanding until flowering. Clonal analysis in developing petal primordia has shown that the formation of a petal lobe requires an increase in growth rates perpendicular to the proximal/distal axis in the distal areas (Sauret et al., 2013).

Together, these studies provide evidence that plant organ growth and morphogenesis depend on the regulation of cell division and cell expansion in a spatial and temporal context.

1.7. The plant mitotic cell cycle

The mitotic cell cycle is the core process that gives rise to new daughter cells and determine the final number of cells in an organ. The mitotic cycle in eukaryotes is divided in four phases: Cells that enter a round of mitotic division start in interphase/gap phase 1 (G1), enter S-phase (DNA replication phase), in which the nuclear DNA is replicated, gap phase 2 (G2), where cells check the integrity of the newly synthesised DNA and prepare for division, followed by M-phase, where sister chromatids separate and cells undergo cytokinesis (De Veylder et al., 2003). During this process, the cytoplasmic and nuclear contents are divided by formation of a new plasma membrane that separates the two new daughter cells along the division plane, whose location in plants is pre-determined by a preprophase band consisting of microtubules and actin filaments (reviewed by Jürgens, 2005).

Cells divide symmetrically (proliferative division) or asymmetrically (formative division). For example, in the central zone of the meristem, proliferative cell divisions maintain a pool of undifferentiated cells with uniform cell sizes. By contrast, in the peripheral zone and in organ primordia, cells also undergo asymmetric cell divisions, which are considered an important mechanism to establish divergent cell fates during growth and morphogenesis, for example in stomatal development (reviewed by Blomme et al., 2013). In addition to the mitotic cell cycle that gives rise to two daughter cells, endoreduplication is a cell cycle where DNA replication phase is not followed by cytokinesis, resulting in an increase of nuclear DNA content with ploidy levels higher than 2C (De Veylder et al., 2011).

The transition between cell cycle phases strongly depends on the activity of cyclin-dependent kinases (CDKs). CDKs are activated by CDK-ACTIVATING KINASES (CAKs). Besides positive and negative phosphorylation events, CDK activity is positively regulated by binding of cyclins that are periodically expressed and degraded by ubiquitin-dependent proteolysis. Complexes with specific cyclins determine phase-specific activity and substrate specificity of CDKs during progression through the cell cycle. In total, 13 CDKs and 49 cyclins have been identified in *Arabidopsis* (Inze and De Veylder, 2006; reviewed by Harashima et al., 2013; Blomme et al., 2013) with *CDKA;1* being the most important cyclin-dependent kinase that is required throughout the cell cycle and has been shown to

keep cells in a cell proliferation competent state. At the transition from G1 to S-phase, phosphorylation of RBR1 by CDKA;1 – CYCD complexes relieves the repression of the transcriptional activator complex E2FA/B-DP that promotes expression of genes involved in DNA synthesis, chromatin dynamics and progression through S-phase, such as the origin recognition complex (*ORC*) genes and mini-chromosome maintenance complex (*MCM*) genes. The transition from G2 to M-phase is mediated by specific mitotic CDK-cyclin complexes involving CDKA, B-type CDKs, A-type CYCLINs, and B-type CYCLINs that regulate the activation of MYB3R proteins. MYB3R proteins act as transcriptional activators of M-phase specific genes that share an M-specific activator (MSA) *cis* regulatory element in their promoter region. Interestingly, also mitotic CDKs and cyclins have been found to have MSA elements in their promoters, suggesting a regulatory feed back loop between these regulators of cell cycle progression (reviewed by de Veylder et al., 2003 and 2007; Harashima et al., 2013).

1.7.1. Plant cell cycle regulation

Progression through the phases of the cell cycle is directed by CDK-cyclin complexes, consequently, they are the prime targets for cell cycle regulation. Cell cycle progression is predominantly regulated by post-translational modifications of CDK-CYCLIN complexes such as phosphorylation/dephosphorylation, protein-protein interactions, and most importantly, targeted proteasome-dependent degradation (reviewed by Blomme et al., 2013).

Proliferating cells arrest or commit to enter a new round of DNA replication at the transition from G1/S phase. Therefore, CDKA-CYCLIN D complexes which regulate this transition are prime targets to regulate cell proliferation rate and the duration of cell proliferation phase. In this context, *KIP-related proteins* or *INHIBITOR/INTERACTOR OF CDK* (*KRPs* or *ICKs*) and members of the *SIAMESE* (*SIM*) and the *SIAMESE-related* (*SMR*) proteins are two groups of cell cycle regulators with CDK- and cyclin-binding motifs that have been shown to specifically interact with CDKA and D-type cyclins *in vitro* and *in vivo* (De Veylder et al., 2001; Churchman et al., 2006). In *Arabidopsis*, seven members of the *Kip-related proteins*, four core members and 16 putative members of the *SIAMESE* and *SIAMESE-related proteins* have been identified (De Veylder et al., 2001; Churchman et al., 2006; John Larkin, personal communication). While *SIM/SMR* proteins are plant-specific,

Kip-related proteins show some sequence similarity to mammalian *Kip/Cip* proteins that regulate G1 to S phase transition, have checkpoint functions and regulate exit from cell proliferation (reviewed by Besson et al., 2008). Ectopic expression of several different members of *KRPs* and *SIM/SMR* proteins led to a reduction of final cell number and reduced organ sizes (De Veylder et al., 2001; Churchman et al., 2006; Bemis and Torii, 2007; Roeder et al., 2010). In particular, *SIM/SMR* proteins have been shown to promote endoreduplication (Churchman et al., 2006). For example, *SMR1* is highly expressed in flowers, where it promotes the formation of giant cells in sepals. Giant cells have been described to exit mitotic proliferation prematurely, to undergo several rounds of endoreduplication to subsequently grow to the enormous sizes compared to their neighbouring cells (Roeder et al., 2010). Mild ectopic expression of *KRP2* also promoted endoreduplication (Verkest et al., 2005).

There are numerous additional examples where modulating the expression levels and/or activity of core cell cycle components altered the final number of cells in an organ and affected final cell sizes, cell type patterning, or final organ size and morphology. For example, a decrease in CDKA activity led to disorganisation and onset of cell differentiation in the meristem and to smaller organs with increased cell sizes (Gaamouche et al., 2010). Similarly, loss of CAK function resulted in dwarfed plants with small, curled, and serrated leaves. By contrast, ectopic expression of *Arabidopsis CYCD;2, CYCD;4* and *CYCD;5* caused an increase in cell proliferation rates by accelerated progression through G1/S-phase transition and resulted in leaves with an increased number but smaller cells (Qi and John, 2007). Mild ectopic expression of *CYCD3;1* resulted in increased leaf size owing to an increase in cell numbers. By contrast, ectopic expression of *CYCD3;1* under the *35S* promoter resulted in smaller leaves with hyperplasia and delayed cell differentiation (Dewitte et al., 2003).

The APC/C (anaphase promoting complex/cyclosome) is a multidomain E3-ligase which specifically targets mitotic CDK-cyclin complexes for protein degradation at the G2 to M-phase transition. Therefore, APC/C plays a crucial role in mediating the onset of endoreduplication (De Veylder et al., 2003 and 2007). Misexpression of subunits and interactors of APC/C affected final cell number, the degree of endoreduplication and overall organ size. For example, the dwarfed *hobbit* mutant has a loss of function mutation in one of the subunits of APC/C. By contrast, the loss of function mutant of the

SAMBA protein, an interactor of the APC/C, shows an increase in overall leaf size which manifests itself already at the early stages of organ initiation, when an increased number of cells is recruited into the organ primordia owing to an increase in cell number in the peripheral zone of the shoot apical meristem (reviewed by Blomme et al., 2013).

Based on this variety of phenotypes caused by modulation of cell cycle components, it can be speculated that developmental regulators target the components of the core cell cycle machinery to fine tune local cell proliferation rates and exit from cell proliferation in order to regulate final organ size. However, only few functional and molecular links have been provided for the interaction between developmental regulators and the core cell cycle machinery. For example, the transcription factor TCP20 has been reported to directly bind to the promoter region of *CYCB1;1* (Li et al., 2005) and the transcription factor *AINTEGUMENTA* (*ANT*) has been proposed to promote growth by activating expression of *CYCD3* (Mizukami and Fischer, 2000). However, whether this interaction is direct or indirect still remains unclear.

By contrast, plant hormones, in particular cytokinins, auxins and gibberellins, have been shown to modulate cell cycle progression by targeting components of the core cell cycle machinery. Cytokinins play a crucial role in maintaining cell proliferation in the meristem. Cytokinins have been shown to target *CYCD3*, which is a limiting factor at the G1 to S-phase transition (Dewitte et al., 2007). In this context, meristem maintenance genes have been suggested to indirectly promote expression of D-type cyclins via cytokinin signalling (Dewitte et al., 2007). During lateral root formation, *KRP2* levels were repressed upon auxin accumulation (Himanen et al., 2002; Sanz et al., 2011). Also gibberellin-mediated growth responses target the cell cycle machinery. In this respect, DELLA proteins, which restrain plant growth in the absence of gibberellins, have been shown to restrain cell proliferation rates by promoting the expression of the cell cycle inhibitors *KRP2*, *SIM*, *SMR1* and *SMR2* (Achard et al., 2009), in addition to their well known function in restraining cell expansion.

1.8. Plant cell expansion

1.8.1. Cellular and vacuolar growth

In plants, increase in cell volume is achieved on the one hand by increase in cytoplasmic and nuclear content, and on the other hand by enlargement of the vacuoles through water uptake (reviewed by Schopfer, 2006; Sablowski and Carnier Dornelas, 2013). During cytoplasmic growth, cells increase their macromolecular content and the number of cellular compartments and organelles. This process is particularly important in proliferating cells, where the cytoplasmic content has to be divided in order to produce two viable daughter cells. Cytoplasmic growth, which is strongly linked to biosynthesis of proteins, carbohydrates and lipids, turns a growing cell into a sink for energy and nutrients. An important regulator of cytoplasmic growth is the *Target of Rapamycin* (*TOR*) pathway, which integrates the nutrient status (levels of sucrose and glucose in plants, amino acid levels in yeast and mammals) with the regulation of ribosome biogenesis, which drives mRNA translation and protein biosynthesis, and sugar-related metabolic processes such as starch and lipid metabolism. Modulation of *TOR* expression in plants resulted in smaller and larger plant organs accordingly and has, thus, provided evidence that TOR activity is a limiting factor for overall plant organ growth (reviewed by Henriques et al., 2014).

In comparison, vacuolar growth is predominantly achieved by uptake of water, is less energy and nutrient consuming and leads to comparatively larger cell volumes predominantly during post-mitotic expansion of cells. In meristems and early organ primordia, cells increase in volume predominantly by cytoplasmic growth, while post-mitotic growth of differentiated cells is predominantly achieved by vacuolar growth. In both growth-related processes, cell wall modifications play a major role to facilitate the increase in cell volume (reviewed by Wolf et al., 2012).

1.8.2. Cell expansion is dependent on processes in the cell wall

Plant cells are surrounded by cell walls that hold against the turgor pressure of the protoplast, give shape to the cell, and connect neighbouring cells. Therefore, expansion of a single cell but also local tissue growth and overall organ growth need to be coordinated with reversible and irreversible cell wall remodelling processes.

In young growing cells, the cell walls are 0.1 to 1.0 µm thick dynamic structures that undergo continuous remodelling in composition and in physical and chemical properties. The cell wall is a composite material made of stiff but tensionally resistant cellulose microfibrils, which are embedded in a matrix of hemicelluloses, pectins and cell wall proteins. Hemicelluloses consist of xyloglucan, arabinoxylan and mannan backbones, with branches that are decorated with galactose, fucose, arabinose, and glucuronic acid residues. Xyloglucan as the predominant hemicellulose can bind to the surface of cellulose microfibrils and crosslink them or get trapped within microfibrils. Pectins consist of homogalacturonan and rhamnogalacturonan chains with a wide range of sugars such as xylose, arabinose, fucose, galactan, rhamnose side chains that are modified with additional methyl and acetyl groups. These side chains can interact with cellulose microfibrils. Pectins can form hydrated gels that allow cellulose fibrils to slide and contribute to cell wall loosening. By contrast, pectins can also crosslink with calcium and borate to form a rigid matrix. In addition to cell wall carbohydrates, structural proteins such as glycine-rich glycoproteins can make up to 10% of the cell wall of a growing cell (reviewed by Cosgrove, 2005; Wolf and Greiner et al., 2012, Wolf et al., 2012).

In expanding cells, the turgor pressure generates a tensile stress and upon cell wall loosening, cell walls are irreversibly stretched to accommodate the expanded cell volume (reviewed by Cosgrove, 2005). In order to allow turgor-driven cell expansion and to maintain cell wall integrity at the same time, the processes of cell wall loosening and wall extension have to be in balance with the process of cell wall stiffening and deposition of new wall material. In this respect, cell growth has been described as an oscillating process that is controlled by a mechano-sensing feed back loop. It involves, in order: cell wall relaxation, cell wall extension, sensing of the stretching, cell wall stiffening and deposition of new cell wall material that promotes a new round of cell wall relaxation and extension (Wolf et al., 2012). Cell wall hydration and swelling is mediated by plasma membrane proton ATPases that pump protons into the apoplast, causing hyperpolarisation of the

plasma membrane and acidification of the apoplast, which leads to rapid hydration and swelling of the cell wall. Acidification of the apoplast promotes the activity of expansins, pectin methylesterases and cell wall degrading enzymes, resulting in the loosening and extension of the cell wall. Extension of the cell wall stretches the plasma membrane and opens stretch sensitive calcium channels, which in turn increase the level of free cytosolic calcium. High cytosolic calcium levels inhibit proton ATPases. In addition, proton channels open, which drain the apoplast of protons; the alkalinisation of the apoplast inhibits expansins and cell wall degrading enzymes. In addition, high cytosolic calcium levels also activate NADPH-oxidase that generates and releases superoxide into the cell wall leading to cross-linking of cell wall components and partial dehydration of the cell wall. In the following step, newly synthesised cell wall polymers are deposited and integrated into the extended cell wall (reviewed by Wolf et al., 2012).

Cell wall reinforcement is particularly achieved by cellulose synthase complexes which migrate along the plasma membrane and deposit new cellulose microfibrils. Cortical microtubules have been shown to guide the insertion and trajectories of the cellulose synthase complexes (Paredez et al., 2006). During growth, the hydrostatic turgor pressure in a cell is strictly isotropic, however, the local force and stress it generates on the cell wall surfaces is dependent on the shape of the cell. The degree of reversible (elastic) and irreversible (plastic) deformation (strain) that stress causes in the wall is dependent on the resistance of the wall. The resistance of the cell wall to local stress is modulated by wall reinforcement and loosening processes that can be anisotropically distributed within a cell and therefore translate isotropic force into specific strain directions. Cellulose microfibrils restrict the elastic deformation parallel to the direction of alignment resulting in growth perpendicular to the direction of cellulose microfibril reinforcement. Thus, in elongating cells circumferential microfibrils act as main contributors of longitudinal growth. For example, in mutants with disrupted microtubules or cellulose deficiency, cell growth shifts from anisotropic to isotropic growth, suggesting that both microtubule organisation and cellulose microfibril alignment play a major role locally and anisotropically to reinforce the cell wall during cell growth (reviewed by Baskin et al., 2005; Hamant et al., 2008; Burian et al., 2013).

It is debated how local stress and strain generated by anisotropic growth processes are perceived and how they can subsequently feed back to direct microtubule alignment and

the directional alignment of cellulose microfibrils during organogensis. These questions are currently subject to biophysical approaches and computational modelling efforts (Hamant et al., 2008; Burian et al., 2013). In addition, the function of cell wall matrix components such as expansins and pectin methylesterases in anisotropic growth remains to be elucidated. Furthermore it remains unclear how biomechanical and biochemical signals, in particular auxin and gibberellins are integrated in the context of the regulatory network of organogenesis. Andriankaja et al., (2012), who tracked leaf development using transcriptional profiling, found that at the transition from proliferation phase to post-mitotic expansion a considerable number of cell wall-related genes was transcriptionally up-regulated, for example members of the expansin family and the cellulose synthase-like family, suggesting that up-regulation of cell-wall related genes plays a key role in facilitating post-mitotic growth and cell differentiation. In addition, modulating the activity of cell wall-related expansins and pectin methyl esterases and their inhibitors have been shown to have dramatic effects on organ initiation and final organ size (Peaucelle et al., 2011; Zenoni et al., 2011). However, only few direct functional and molecular links between transcriptional growth regulators and cell wall-related genes have been established yet. Revealing the mechanisms of anisotropic growth, and how they are linked to growth regulatory genes, will be key to understanding organ growth.

1.9. Coordination of cell proliferation and cell growth

Although cell cycle progression and cell expansion function together to promote tissue and organ growth, little is known about the regulation between these processes. Particularly in tissues with high mitotic cell division rates, cell cycle progression and cell growth have to be coordinated in order to maintain cell size homeostasis over several rounds of divisions. Work in the unicellular, eukaryotic fission yeast and budding yeast has revealed that cells have to reach a minimum cell size before they can progress into S-phase, generating a dependency of cell cycle progression on cell size (Jorgensen and Tyers, 2004). In plants, minimum size thresholds for cell cycle progression have been proposed by Francis (1998) and by Donnelly et al., (1999), however no size threshold mechanisms have been identified in plants so far. Experiments inhibiting either cell growth or cell cycle have supported the idea that also in plants cell cycle progression

depends on cell growth, while cell growth does not depend on cell division (Grandjean et al., 2004). In multicellular organisms, it has been suggested that these cell autonomous dependencies are modulated by developmental regulators during organ growth and morphogenesis (Jorgensen and Tyers et al., 2004).

In this context, plant hormones, in particular auxin and gibberellins in crosstalk with brassinosteroids have been shown to promote cell expansion but are also able to transcriptionally target cell cycle regulators. For example, expansins have been shown to have auxin and gibberellin transcriptional response elements in their promoters and in particular CDK inhibitors such as *KRP2* and *SMR1* are targeted by DELLA proteins and auxin (reviewed by Lee and Kende, 2002; reviewed by Perrot-Rechenmann, 2010; Sablowski and Carnier Dornelas, 2013; Himanen et al., 2002; Achard et al., 2009; Sanz et al., 2011). Therefore, one hypothesis could be that growth regulators may specifically target hormone signalling to mediate the coordination of cell growth and cell cycle progression.

A striking example of developmentally controlled cell size changes is the formation of giant and non-giant cells in the abaxial sepal epidermis. Studying this process, Roeder et al. (2010) showed that modulation of the cell cycle duration in tissues with uniform growth rates plays a role in determining final cell sizes and in cell type specification. However, little is known about how this coordination is achieved in the first place and how it could be modulated during organ morphogenesis. It has been suggested that such a coordinating factor would either have to be able to generate a dependency of one process on the other, or be able to control both processes in parallel. In the special case of mitotic cell division, these processes have to be reset in the two newly separated daughter cells after cytokinesis (Jorgensen and Tyers 2004). In relation to the coordination between cell growth and cell cycle, we are faced with one of the unsolved key questions in biology (recently reviewed by Marshall et al., 2012): How do cells measure their size or monitor processes that lead to changes in their size? And, is this the mechanism by which cells maintain size homeostasis?

1.10. Links between cellular processes required for growth and genes that regulate organ growth

In the search for regulatory factors that affect final organ size, several mutants and transgenic lines with increased or decreased cell numbers and cell sizes have been identified (reviewed by Krizek, 2009a; Breuninger and Lenhard, 2010).

Many of them have been reported to promote the duration of cell proliferation phase (primary morphogenesis) and only comparatively few have been shown to increase the rate of proliferation or the process of cell expansion. This has resulted in the idea that the transition from cell cycle exit to endoreduplication and expansion phase is a key contributor to determine final number of cells and final organ size. For example, the transcription factor *ANT* has been shown to promote cell proliferation by acting as a transcriptional activator of the D-type cyclin *CYCD3,* which as described above is a limiting factor for the G1/S-phase transition and plays a major role in preventing exit from the mitotic cycle (Mizukami and Fischer, 2000). Reinforcing the connection between D-type cyclins and organ growth, *CYCD3;2* was the only core cell cycle gene identified to be transcriptionally down-regulated during the transition from cell proliferation to post-mitotic phase by Andriankaja et al. (2012). Over-expression of *ANT* caused an increase of final organ size with increased number of cells owing to prolonged cell proliferation phase while loss of ANT function caused smaller organs with a reduced number of cells (Krizek, 1999). Furthermore, *GRFs* and their co-activators *GIFs* act redundantly to promote and prolong cell proliferation (Horiguchi et al., 2005). By contrast, members of the *CIN-like* transcription factor family have been shown to promote exit from cell proliferation and onset of cell differentiation (Koyama et al., 2010). Finally, JAGGED (JAG) has been proposed to control cell proliferation to promote growth of shoot organs (Dinneny et al., 2004; Ohno et al., 2004), as described in more detail below.

While the examples above relate to the control of cell cycle progression, a few developmental regulators appear to target both cytoplasmic growth and cell cycle progression. For example, TCP20 has been reported to be able to bind to the promoters of *CYCB1;1* and of several ribosomal subunits, linking cell cycle activity with cytoplasmic growth (Li et al., 2005). Furthermore, it was speculated that apart from promoting the expression of *CYCD3*, *ANT* may target cell growth-related processes, because ectopic

CYCD3 expression did not cause an increase in organ size as observed when *ANT* was ectopically expressed. However, mild ectopic expression of *CYCD3* under its endogenous promoter was reported to increase final organ sizes (Krizek, 1999; Mizukami and Fischer 2000; Dewitte et al., 2003 and 2007). Overall, although connections have been found between regulatory genes and growth-related cellular processes, the molecular details and functional relevance of these links remain unknown.

In addition to transcriptional regulators, genes involved in targeted protein degradation, for example the ubiquitin receptor *DA1* and the E3 ubiquitin ligases *DA2* and *BIG BROTHER*, are associated with the ubiquitin-dependent proteasomal protein degradation pathway. Because their loss of function mutants show an increase in overall flower size, while ectopic expression reduces flower sizes, it has been suggested that *DA1*, *DA2* and *BB* target growth promoting factors (Disch et al., 2006; Li et al., 2008; Xia et al., 2013). In a non-cell autonomously manner, the phytochrome P450 protein *KLUH CYP78A5* has been shown to promote the duration of cell proliferation. While being expressed in the organ margins it promotes proliferation in the central regions of the organ by an unidentified mobile factor and, additionally, has been reported to coordinate organ sizes within an inflorescence (Anastasiou et al., 2007; Eriksson et al., 2010).

Modulating the activity of factors like *ANT*, *GRFs/GIFs*, *DA1, BB,* or *KLUH*, predominantly causes changes in overall organ size. By contrast, *STEROL METHLYTRANSFERASE 2* (*SMT2*) has been found to suppress endoreduplication in petals and loss of *SMT2* in the *frill1* mutant causes serrations in petals and sepals and thus has an effect on final size and shape (Hase et al., 2005). A more severe alteration in morphology has been observed in the *bop1/2* loss of function mutants, where leaf blade tissue proliferates ectopically along the petiole. Furthermore, the *bop1/2* mutant shows ectopic formation of floral bracts, a leaf-like structure subtending floral buds, which does not form in wild-type *Arabidopsis* flowers (Norberg et al., 2005). It was therefore suggested that *BOP1/2* not only restricts tissue growth, but also may interact with organ patterning genes (axis-specifying genes and boundary-specifying genes) to coordinate growth behaviour in relation to boundaries and axes. However, little is known about the link between growth regulators and genes involved in early organ patterning.

1.11. Research Questions and Objectives

During my PhD project I focussed on the question of how regulatory genes link early events of organ patterning to the cellular processes required for organ outgrowth and morphogenesis. This relates to the broader question of how the processes of cell proliferation and cell growth are coordinated to sculpt an organ of specific size, shape and function.

1.11.1. The role of the transcription factor JAG during early organogenesis

In order to address these questions, I studied the function of the transcription factor JAGGED (JAG), which has been characterised for its macroscopic phenotype of serrated, narrow leaves, narrow sepals and petals with defective distal growth and defects in cell type patterning. *JAG* (*At1g68480)* encodes a protein comprising a putative nuclear localisation signal close to the N-terminus, a single C_2H_2 zinc finger domain of 31 amino-acids, followed by a proline rich sequence, and a leucine rich EAR motif at the C terminus (Ohno et al. 2004). JAG forms a monophyletic group with *NUBBIN* (*NUB*) and shows 35% overall amino-acid sequence similarity to the boundary specifying gene *SUPERMAN* (*SUP*) (Dinneny et al. 2004).

Using *HISTONE 4* expression as a cell cycle marker Dinneny et al. (2004) revealed that in the *jag* mutant cells exit cell proliferation earlier during flower development than in the wild type, suggesting that *JAG* has a function in promoting cell proliferation. Similarly to loss of *BOP1/2* function, ectopic *JAG* expression caused extended leaf blade growth and was sufficient and necessary to induce ectopic bract outgrowth in *Arabidopsis.* In flowers, ectopic expression of *JAG* under the flower-specific *AP1* promoter caused organ fusions and ectopic growth of sepal tissue along the pedicels. This is in contrast to the regulatory function of *ANT*, which is not sufficient to cause ectopic bract formation and extended ectopic tissue growth (Ohno et al., 2004).

JAG has been identified to be a direct downstream target of the floral organ identity genes *SEPALATA3*, *APETALA3/PISTILATA*, and *AGAMOUS*, suggesting that *JAG* acts immediately downstream of floral organ identity genes. This early function of JAG was further supported by its expression pattern: During floral organogenesis, JAG was strongly expressed in initiating organ primordia but excluded from the inflorescence meristem or floral primordia. Over the time-course of organogenesis, JAG expression was restricted to

the distal regions of the organ primordia and faded away when cell proliferation ceased and organs started to expand and to differentiate (Dinneny et al., 2004; Ohno et al., 2004).

In the context of these findings, the transcription factor *JAG* was considered an ideal candidate to investigate how the gene regulatory network directing floral organogenesis is wired to the control of cell proliferation, cell growth and cell type patterning. Apart from being a direct downstream target of several floral organ identity genes, little is known how JAG is connected to the gene regulatory network of organogenesis: *JAG* has been shown to be repressed by the transcriptional co-activators *BOP1/BOP2* and by the boundary specifying gene *HANABA TARANU* (*HAN*) (Norberg et al., 2005; Zhang et al., 2013).

1.11.2. Objectives

Here, I aimed to identify direct downstream transcriptional targets of *JAG* that might reveal molecular links to cell proliferation and cell growth during early organogenesis. I used global transcriptome profiling combined with genome-wide analysis of DNA binding sites to identify direct downstream targets of *JAG*. Furthermore, I used reverse genetics, reporter lines, and quantitative 3D imaging to confirm and to further investigate the functional relevance of the interaction between *JAG* and downstream candidate genes at cellular and molecular levels.

Chapter 2 - Global expression analysis

2.1. Introduction

Plants grow and develop new organs over their entire lifetime, first producing leaves and after floral transition producing floral organs as diverse as sepals, petals and reproductive organs. To produce floral organs of species-specific size, shape and function, fundamental but coordinated changes in gene transcription are required. The gene regulatory network that predetermines floral organ identity in floral primordia has been studied in great detail over the past 20 years. MADS-domain transcription factors have been identified as key players of this gene regulatory network and their function has been conceptualised in the extended ABCE model (Coen and Meyerowitz, 1991; reviewed by Krizek and Fletcher, 2005; reviewed by Ó' Maoiléidigh et al., 2014). Recent advances in global transcriptome profiling and genome-wide mapping of DNA binding sites have generated very detailed information on the regulatory functions of MADS-domain transcription factors with high spatial and temporal resolution (Wellmer et al., 2006; Kaufmann et al., 2010; Wuest et al., 2012). By contrast, little is known about the gene regulatory network that directs organ outgrowth once organ identity has been defined. Because development of a floral organ of final size, shape and function from a few founder cells requires an increase in cell number and cell size, and cell type specification, the gene regulatory networks downstream of floral organ identity genes need to co-ordinate the processes of cell growth, cell proliferation and cell differentiation in the spatial and temporal context of a developing organ.

In this respect, the C_2H_2 single zinc finger transcription factor JAGGED (JAG) is a good candidate to study: *JAG* is expressed in incipient and early organ primordia and it has been shown to act as a direct downstream target of the floral organ identity genes *SEPALATA3* (*SEP3*)*, APETALA3/PISTILATA* (*AP3/PI*), and *AGAMOUS* (*AG*) (Dinneny et al., 2004; Ohno et al., 2004; Gomez et al., 2005; Kaufmann et al., 2010, Wuest et al., 2012). Loss of function *jag* mutants show growth defects in early organ primordia (Schiessl et al., 2012) and have narrow mature floral organs with reduced distal growth (Dinneny et al., 2004; Ohno et al., 2004;). Furthermore, it has been shown by quantitative 3D imaging

that JAG promotes cell growth, growth anisotropy and cell proliferation, and modulates cell size homeostasis in early organ primordia (Schiessl et al., 2012).

In summary, this has led to the hypothesis that *JAG* is a key upstream regulator of early organogenesis acting immediately downstream of floral organ identity genes. In order to further investigate how JAG promotes cell growth and cell proliferation and how it modulates the coordination of these two processes, I aimed to find the direct downstream targets of JAG.

2.2. Identifying genes under transcriptional control of JAG

In order to monitor the global transcriptional response to changes in JAG function in early floral organogenesis, I performed an expression array experiment using unopened flower buds from inflorescence apices that were dissected and left to recover for 24 hours. In a first expression array experiment, I compared *jag-1* with wild-type inflorescence apices to assess the steady state effects of loss of endogenous JAG function. In order to detect genes with an immediate and early transcriptional response to JAG, I generated a dexamethasone (DEX)-inducible *35S:JAG-GR* construct where the *JAG* cDNA was translationally fused to the dexamethasone-inducible glucocorticoid receptor (GR) under control of the constitutive *35S* promoter, using a cloning strategy similar as described in Gallois et al. (2002). To show that *35S:JAG-GR* was fully functional, I confirmed that the construct was able to induce the previously observed phenotype of ectopic *JAG* activity (twisted and elongated petals and sepals) in both the wildtype and *jag-2* L-*er* mutant background by dexamethasone treatment (Figure 2.1.A-D). In addition, ectopic activation of JAG-GR in seedlings by supplementing the germination medium with 10 µM DEX resulted in cup-shaped and fused cotyledons seven days after germination (Figure 2.1.C-D). Subsequently, leaves developed which had no clear petiole and were broader at the base. While wild-type plants grown on DEX medium developed normal leaves and flowered after 4 weeks, the plants harbouring the *35S:JAG-GR* construct failed to flower, instead producing an increased number of leaves (Figure 2.1.E-F), providing evidence that constitutive ectopic expression of JAG causes severe developmental and morphological changes.

For the expression array experiment, the inflorescence apices of *35S:JAG-GR* L-*er* wild-type plants were dipped with solutions of 0.1% ethanol as control treatment (mock) and 10 µM dexamethasone with 0.1% ethanol for ectopic JAG-GR activation. In order to filter for candidate genes that are putative immediate targets of JAG, I included a cycloheximide treatment for inhibition of *de novo* protein synthesis, comparing plants treated with 10 µM dexamethasone, 0.1% ethanol and 10 µM cycloheximide, or 10 µM cycloheximide, 0.1% ethanol. Furthermore, a *jag-1* versus wild type comparison was included, using the *35S:JAG-GR* line in L-*er* wild-type background and the *jag-1* loss of function mutant, both mock-treated with 0.1% ethanol. All dipped inflorescences were incubated for 5 h under daylight conditions. For each treatment, three biological replicates were harvested with 12 inflorescence apices (flowers < stage 10) per sample. RNA samples were prepared and hybridised with Affymetrix ATH1 oligonucleotide arrays. The raw data and experiment metadata were made available at http://affymetrix.arabidopsis.info/, experiment ID: NASCARRAYS-605. Array data (CEL files) were normalised using the GCRMA method (Gharaibeh et al., 2008), differential expression was tested using t-test statistics and False Discovery Rate (FDR) control method described by Benjamini and Hochberg (1995) (data analysis performed with bioinformatics support from Jose Muiño). A gene was considered significantly differentially expressed with an absolute value of the $\log_2$ ratio > 0.5 and FDR <0.01.

2.3. Results of the global expression array analysis

In total, 495 genes were identified to be significantly differentially expressed in response to ectopic JAG-GR activation ($\log_2$ ratio >0.5, FDR<0.01), with 232 up-regulated and 263 down-regulated genes (Figure 2.2.; full analysis shown in Apendices Tables A and B). In order to assess the steady state effects of endogenous JAG function on gene expression I compared inflorescence apices of mock-treated *jag-1* to that of mock-treated *35S:JAG-GR* (with gene expression comparable to wild type). This comparison resulted in 1289 genes that were up-regulated in mock-treated *jag-1* compared to the mock-treated *35S:JAG-GR* and 1158 down-regulated genes (Figure 2.2.).

In the next step, I overlapped the sets of differentially expressed genes obtained from both comparisons. In detail, 39 genes were repressed by *JAG-GR* activation and up-

regulated in the *jag-1* mutant. This overlap was significantly higher than expected by chance (p= 1.20 x 10^{-4}, Fisher's exact test) within the 16164 genes that were considered as the total gene set expressed in inflorescence apices because they had expression levels above the minimum expression level detected in our expression array experiment. By contrast, 23 genes overlapped between genes activated by ectopic JAG-GR activation and genes with significantly lower expression levels in the *jag-1* mutant, which was not significantly higher than expected by chance (p = 0.071, Fisher's exact test). This is consistent with the proposed repressor function of JAG (Dinneny et al., 2004; Ohno et al., 2004). Surprisingly, 88 genes responded in the same way to JAG-GR activation and to loss of endogenous JAG function leading to an enrichment with significant values of p= 3.08 x 10^{-14} for genes activated by JAG-GR and in *jag-1* and p= 2.28 x 10^{-3} for genes repressed by JAG-GR and with lower expression in *jag-1* (Fisher's exact test). Comparison of tissues with severe phenotypic differences (*jag-1* versus wild-type floral buds) and inhibited growth processes of the relevant tissues in *jag* loss of function mutant may be the main cause that genes repressed by *JAG-GR* are also found to be down-regulated in the mutant. By contrast, negative feedback or the absence of tissue-specific co-factors might alter the function of ectopically activated JAG-GR, in the case of genes activated by JAG-GR and with higher expression in the mutant (Figure 2.2.).

In preparation for the ChIP-Seq experiments, I aimed to filter for putative direct transcriptional targets of JAG. In the presence of cycloheximide, 581 genes were significantly down-regulated and 312 genes were significantly up-regulated upon ectopic JAG-GR activation, suggesting that the numbers of genes responding to ectopic *JAG-GR* activation are higher in the presence of the cycloheximide treatment than in the absence of the drug. The overlap of the two sets of differentially expressed genes obtained from ectopic *JAG-GR* activation in the absence and in the presence of cycloheximide resulted in 75 up-regulated genes (Figure 2.3.A) and 96 down-regulated genes (Figure 2.3.B) and provided a first preliminary global overview of putative direct transcriptional targets of JAG.

2.4. Functional categorisation of genes controlled by JAG

Gene Ontology (GO) analysis of the 495 JAG-GR responsive genes using BAR SuperViewer (http://bar.utoronto.ca/ntools/cgi-bin/ntools_classification_superviewer.cgi) revealed that JAG targets genes with a significant enrichment for the molecular function of transcription factor activity (p-value= 1.302×10^{-8}) and kinase activity (p-value= 7.308×10^{-4}). This is in line with JAG being a regulator of floral organogenesis upstream in the gene regulatory network of floral organogenesis. Furthermore, JAG targets showed a significant enrichment for the molecular function of hydrolases ($p=2.45 \times 10^{-4}$) , transferases (1.691×10^{-3}) and transporters ($p=1.302 \times 10^{-8}$). The annotation of JAG targets was enriched for subcellular localisation at the plasma membrane ($p=3.28 \times 10^{-10}$) and cell wall ($p= 2.67 \times 10^{-9}$), in line with the observation from the quantitative 3D imaging experiments that JAG promotes growth (Schiessl et al., 2012), considering that cell expansion and increase in cell volume as well as anisotropic growth processes are strongly dependent on the physical properties of the plasmamembrane and the cell wall.

Using the GO software tool BINGO (Maere et al., 2005) to identify significantly enriched GO terms (corrected p-value < 0.01) for biological processes (Figure 2.4.A-B) (data analysis performed with bioinformatics support from Jose Muiño), JAG targeted genes involved in meristem development and meristem maintenance, for example the TALE proteins *BELL-domain 1* (*BEL1*), *BREVIPEDICELLUS* (*BP*), and *SHOOTMERISTEMLESS* (*STM*) are repressed upon JAG activation. Repression of meristem identity genes is in line with the observations from the quantitative 3D imaging approach that the transition from meristem cell behaviour to primordium cell behaviour is JAG-dependent. Furthermore, the GO terms response to auxin stimulus and gibberellin stimulus and other GO terms related to these two hormones were enriched, suggesting that JAG is involved in the coordination of auxin- and gibberellin-mediated processes. Furthermore, the GO term "response to abscisic acid stimulus" was enriched. In addition, more than 10 out of 68 significantly enriched GO terms were related to processes in the cell wall, suggesting that JAG promotes growth by promoting cell wall related processes. The GO analysis for biological processes of the mutant versus wild-type comparison was less informative, with a general enrichment for developmental processes, stress responses, and a strong

enrichment for genes involved in pollen development, suggesting that the loss of JAG function has broad secondary downstream effects on overall transcription as would be expected from the severe phenotypic changes observed in the *jag* loss of function mutants.

2.5. Discussion

Here, I aimed to obtain an overview of the putative transcriptional targets of the single C_2H_2 zinc finger transcription factor *JAG* in early floral organogenesis by using a global expression array approach. Comparison of transcript levels between *jag-1* and wild-type inflorescences apices resulted in more than 2200 significantly up- and down-regulated genes, which include direct and indirect targets but also the broader transcriptional downstream consequences of the morphological changes caused by the loss of JAG function. Conversely, constitutive ectopic JAG expression also causes severe phenotypic changes and appears to repress flowering (Figure 2.1.E-F). Therefore, I decided to use a DEX-inducible system in wild-type background, which allowed for activation of ectopic JAG-GR once floral organs with wild-type morphology had developed.

Activation of ectopic JAG-GR by dexamethasone treatment of wild-type inflorescences harbouring the *35S:JAG-GR* construct followed by five hours of incubation resulted in 495 differentially expressed genes between DEX-treated and mock-treated *35S:JAG-GR* plants of comparable wild-type tissue morphology. Changes in expression of these 495 genes were considered short-term transcriptional responses to ectopic JAG activation in inflorescence apices. In addition, by expressing *JAG-GR* under the control of the *35S* promoter, I aimed to detect local interactions in very early developmental stages of primordia development that would otherwise be diluted by the comparatively larger amounts of older bud tissue in a wild-type background with endogenous JAG expression domain and function.

Interestingly, there was only limited overlap between the lists of significantly differentially expressed genes obtained from the 35S:JAG-GR (DEX versus mock treatment) experiment and the wild type versus jag-1 mutant comparison, with 39 genes being repressed upon ectopic JAG-GR activation and being ectopically expressed in the *jag-1* loss of function mutant and 23 genes being activated upon ectopic JAG activation

and having lower expression levels in the *jag-1* mutant compared to wild type. In particular, this set of genes responded to changes in JAG function in two independent experiments, strongly suggesting that these genes are regulated by JAG. Among them, the meristem maintenance genes *SHOOTMERISTEMLESS* (*STM*) and *BREVIPEDICELLUS* (*BP*), and the boundary specifying gene *PETAL LOSS* (*PTL*) were found, which I subsequently used as test candidates to establish and optimise the chromatin immunoprecipitation (ChIP) protocol.

In this context, the cycloheximide treatment provided a first overview of potential direct downstream targets of JAG. For example, the TALE proteins *BELL-domain 1* (*BEL1*) and *BP* were found to be repressed upon ectopic JAG-GR activation in the presence and absence of cycloheximide, suggesting that they are direct transcriptional targets of JAG. *BEL1* was later found to be a direct target of JAG by ChiP-Seq, while *BP* was found to have no DNA binding sites in close vicinity of its gene locus at all. *PTL*, for which I found two significantly enriched DNA binding sites in the ChIP-Seq experiment, was not identified as a direct target in the cycloheximide experiment. This suggests that the cycloheximide treatment is prone to false positives and false negatives, which was further supported by the fact that the number of differentially expressed genes was significantly increased in the presence of cycloheximide compared to when cycloheximide was absent. In this regard, it is known that cycloheximide can affect mRNA stability (e.g. Sablowski and Meyerowitz, 1998). Furthermore, indirect repression of a gene *via* activation of a miRNA does not require *de novo* protein syntyhesis and would not be expected to be inhibited by cycloheximide. Therefore, cycloheximide treatment should only be considered as a rough guide in the search for direct downstream candidates of transcription factors.

A considerable number of genes, 88 in total, showed an inconsistent transcriptional response in the comparison between ectopic JAG activation and loss of JAG function, suggesting that comparing tissues of different morphologies (*jag-1* versus wild-type inflorescence apices see Figure 2.1.A,C) detected a broad range of indirect downstream consequences caused by the developmental changes of the loss of *JAG* function. For example, the petal specific MYB-related transcription factor *MYB16* promotes conical cell differentiation in the distal lobe of the petal (Baumann et al., 2007) and is repressed upon *JAG-GR* activation. However, *MYB16* is also down-regulated in the absence of JAG function, most likely because the distal petal lobe is poorly developed in the *jag* loss of

function mutant. However, the *jag*-1 versus wild type comparison provided us with a global overview and served as a general confirmation of the processes targeted by JAG.

Gene ontology analysis revealed that JAG predominantly regulates transcription factors and kinases, providing evidence for the hypothesis that JAG functions as an early upstream regulator in the gene regulatory network of floral organogenesis. Furthermore, the enriched GO terms provided support for the functions of JAG obtained from the quantitative 3D imaging approach (Schiessl et al., 2012). Firstly, JAG represses genes involved in meristem development and meristem maintenance, suggesting that the transition from meristematic growth behaviour to primordium growth behaviour requires the repression of meristem maintenance genes. Secondly, JAG regulates genes with hydrolase, transferase, and transporter activities which function at the interface between plasma membrane and cell wall, suggesting that JAG promotes growth by regulating genes involved in growth-related cell wall processes. In the context of cell growth related processes, JAG also regulated genes involved in response to gibberellin stimulus and auxin biosynthesis processes. Auxin and gibberellin have been reported to promote cell growth and cell expansion during organ development (Reinhardt et al., 2003; reviewed by Perrot-Rechenmann et al., 2013; Leyser 2010; Ljung 2013; peAchard and Genschik, 2009).

In summary, the expression array analysis revealed a list of putative downstream candidates of JAG and provided support for the JAG functions we have observed from the quantitative 3D imaging approach. It provided a starting point to further confirm and investigate candidates that were related to the processes of transition from meristematic to primoridium cell behaviour and cell growth. Furthermore, it provided putative direct downstream targets that served as test candidates for establishing and optimising the ChiP protocol which allowed me to identify DNA binding sites of JAG to further confirm direct transcriptional targets of JAG in the gene regulatory network of floral organogenesis.

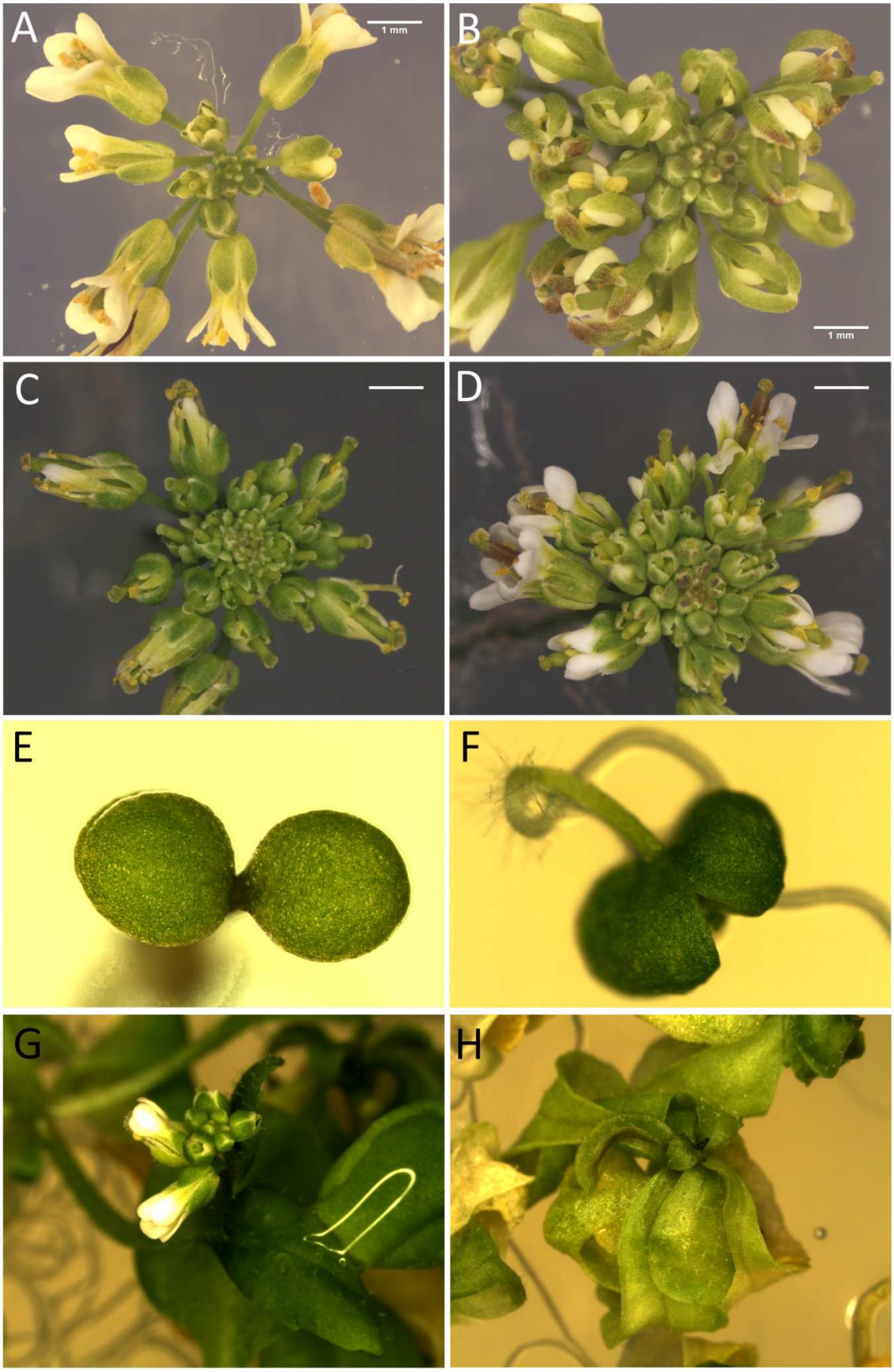
A
1 mm
B
1 mm
C
D
E
F
G
H

Figure 2.1. *35S:JAG-GR* construct in wild type L-*er* background (A-B, E-H) and in *jag-2* L-*er* mutant background (C-D). Scale bars: 1 mm (A-D), not available (E-H).

(A) *35S:JAG-GR* in wild-type L-*er* inflorescence 10 days after mock-treatment showing a wild-type phenotype; (B) *35S:JAG-GR* in wild-type L-*er* inflorescence 10 days after DEX-treatment with ectopic JAG phenotype of elongated, twisted sepals and petals; (C) *35S:JAG-GR* in *jag-2* L-*er* inflorescence 10 days after mock-treatment with *jag-2* phenotype with reduced outgrowth of sepals and petals; (D) *35S:JAG-GR* in *jag-2* L-*er* inflorescence 10 days after DEX-treatment with rescued sepal and petal outgrowth; (E) *35S:JAG-GR* in wild-type L-*er* 7 days after germination on germination medium supplemented with 0.1% EtOH (mock) developing wild type cotyledons; (F) *35S:JAG-GR* in wild-type L-*er* 7 days after germination on germination medium supplemented with 10 µM DEX developing fused cup-shaped cotyledons. (G) *35S:JAG-GR* in wild-type L-*er* grown on germination medium supplemented with 0.1% EtOH (mock) with wild-type inflorescence; (H) *35S:JAG-GR* in wild-type L-*er* grown on germination medium supplemented with 10 µM DEX with increased numbers of leaves but not flowering, leaves were elongated and appeared to predominantly consist of blade tissue with no clear separation between blade and petiole.

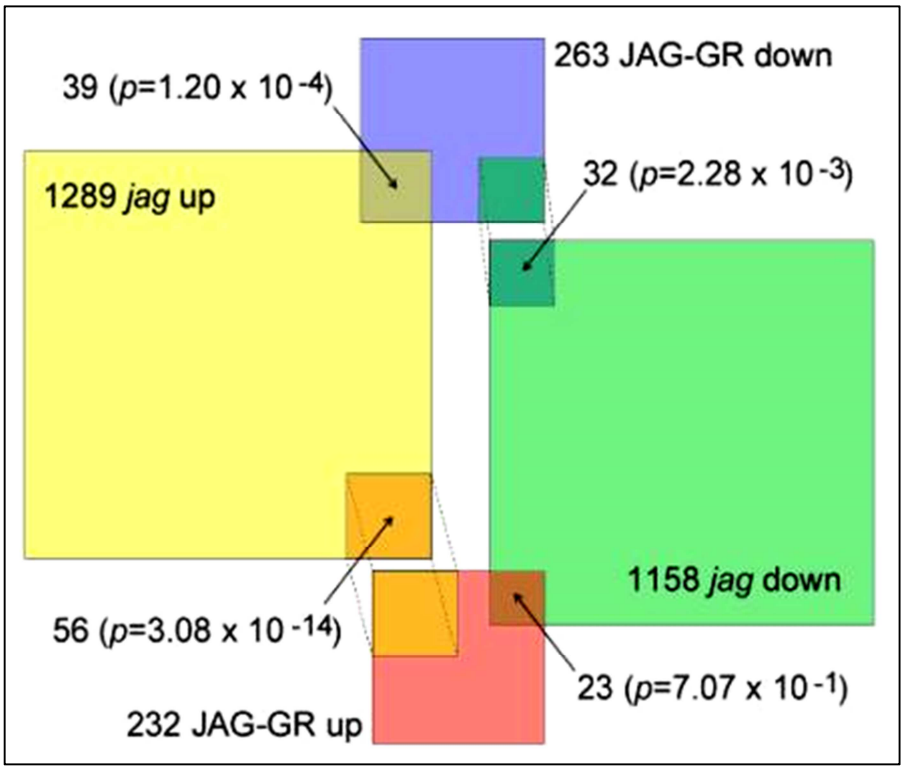

Figure 2.2. Overview of the expression profiling experiment.

Overlap between gene sets that were differentially expressed in response to ectopic JAG-GR activation (blue: repressed, red: activated) or in the comparison between *jag-1* and wild-type buds (yellow: up-regulated in the mutant, green: down-regulated in the mutant); when calculating p-values for the overlaps (Fisher's exact test), only genes present on the Affymetrix ATH1 oligonucleotide array that were also expressed above detection threshold level in at least one replicate of our experiment using inflorescence apices were considered as the total number of genes (16164 genes) to avoid detecting correlations that are merely based on tissue-specific differences; (graph produced with bioinformatics support from Jose Muiño).

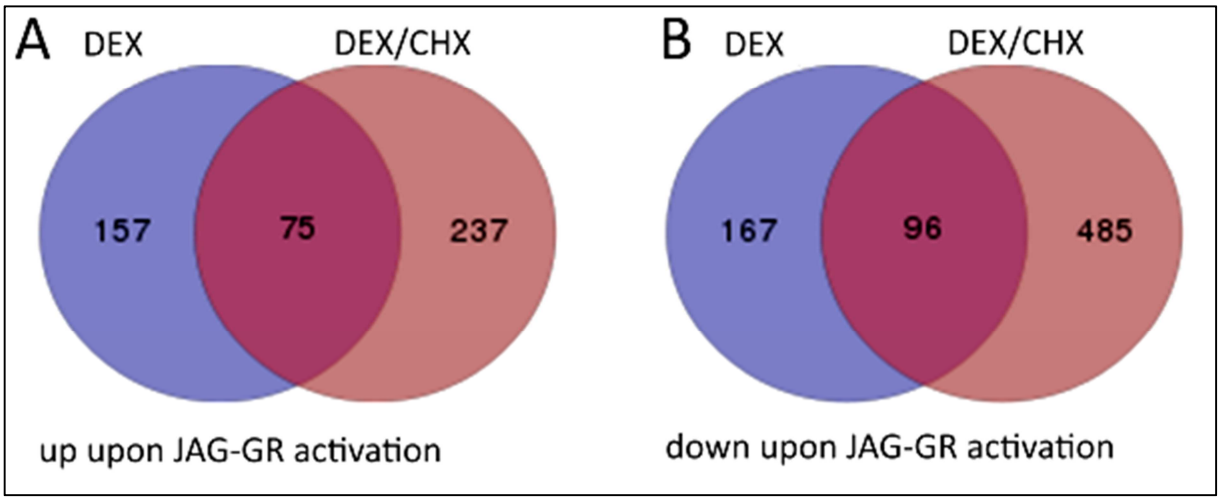

Figure 2.3. Differentially expressed genes upon ectopic JAG activation in the absence and presence of the protein inhibitor cycloheximide.

(A) Overlap between gene sets that were up-regulated in response to ectopic JAG-GR activation (blue: DEX-treatment, no cycloheximide (CHX), red: DEX-treatment combined with cycloheximide (CHX); (B) Overlap between gene sets that were down-regulated in response to ectopic JAG-GR activation (blue: DEX-treatment, no cycloheximide (CHX); (graph produced with bioinformatics support from Jose Muiño).

A

Enrichment of GO terms (biological processes) in the set of 495 genes responsive to JAG-GR activation

GO-ID	p-value	x	n	X	N	Description
9908	3.30E-02	13	198	403	15988	flower development
48509	4.65E-02	6	56	403	15988	regulation of meristem development
9739	3.22E-04	13	104	403	15988	response to gibberellin stimulus
10476	2.47E-02	5	30	403	15988	gibberellin mediated signaling pathway
9684	2.47E-02	3	7	403	15988	indoleacetic acid biosynthetic process
6569	2.47E-02	2	2	403	15988	tryptophan catabolic process
9737	4,70E-02	14	239	403	15988	response to abscisic acid stimulus
42545	2.47E-02	10	119	403	15988	cell wall modification
71554	2.77E-02	15	238	403	15988	cell wall organization or biogenesis
9831	3.67E-02	4	22	403	15988	plant-type cell wall modification involved in multidimensional cell growth

B

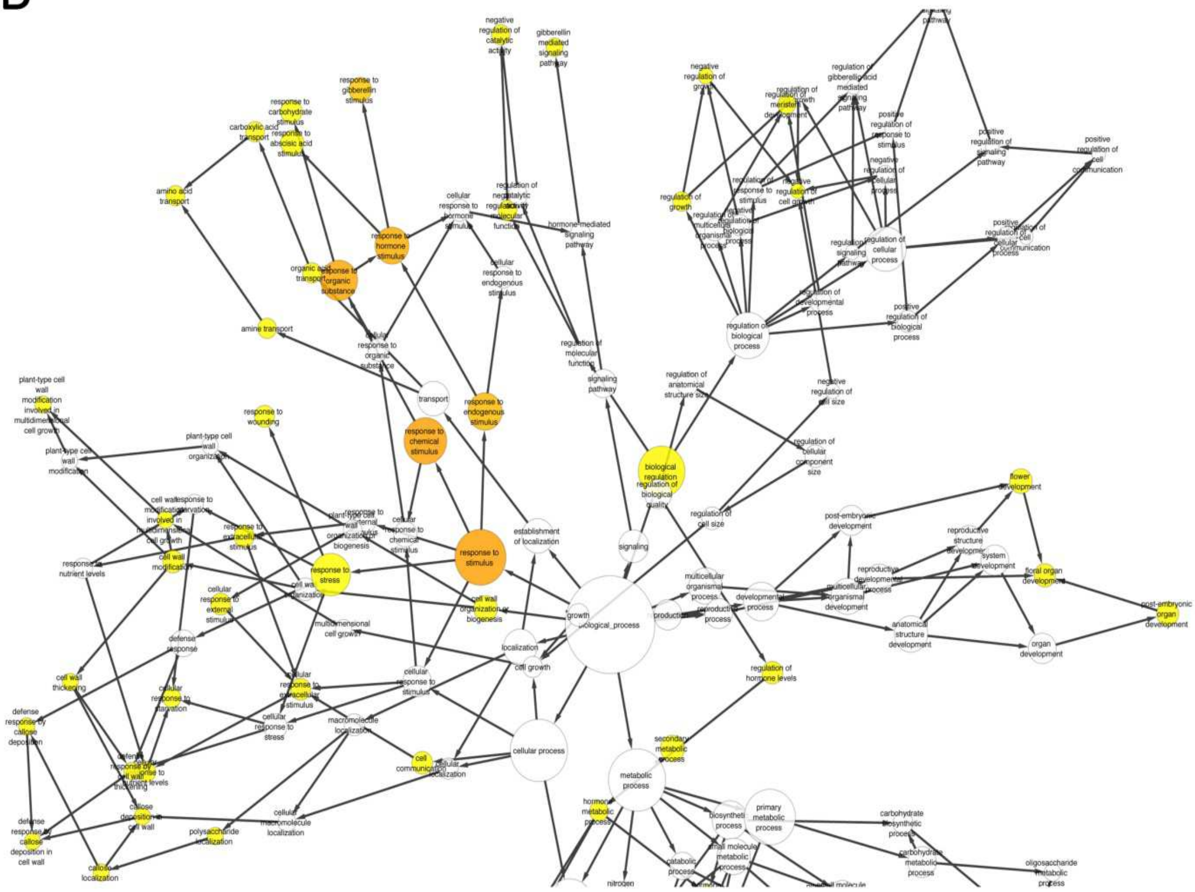

Figure 2.4. Enrichment for Gene Ontology (GO) terms within the sets of genes that were differentially expressed upon ectopic JAG-GR activation.

(A) GO terms (biological process) enriched within the set of genes that were differentially expressed upon ectopic JAG-GR activation; p-values are the corrected p-values calculated by BINGO (Maere et al., 2005) using a Hypergeometric Test and p-value correction

according to Benjamini and Hochberg (1995), with x being the number of genes belonging to the specific GO-ID found in the total number our gene set (X), while n is the number of genes identified for the specific GO-ID and N is the total number of annotated genes considered in the BINGO analysis. (B) Graphical representation of the enriched GO terms (biological process) within the set of genes described in (A); enrichment map representing the hierarchy of the network of biological processes; produced within the Cytoscape environment (Saito et al., 2012); GO terms that were found significantly enriched including all parental categories are represented in the map as nodes; the size of the node is proportional to the number of differentially expressed genes represented in the GO term, node colour corresponds with the significance based on the BINGO analysis described in (A) with white (insignificant), from yellow p=0.01 to dark orange p= 0.01 10^{-5}; nodes were automatically arranged so that highly similar gene sets are placed together, as a result highly redundant gene sets cluster; edges between nodes represent weighted links between the nodes according to the number of overlapping genes; (graphs produced with bioinformatics support from Jose Muiño)

Chapter 3 - Combined analysis of ChiP-Seq and global expression array

3.1. Introduction

Recent advances in genome-wide mapping of DNA binding sites and next generation sequencing techniques, for example Chromatin Immunoprecipitation followed by Illumina Deep Sequencing (ChiP-Seq), have generated data on DNA binding affinities, *cis*-binding motifs and regulatory functions of transcription factors with high spatial and temporal resolution. In particular, the function of the floral meristem identity gene *LEAFY* (*LFY*) and the combinatorial functions of the MADS-domain transcription factors in the gene regulatory network of floral organ identity have been elucidated by these methods in great detail (Winter et al., 2011; Kaufmann et al., 2010; Wuest et al., 2012). To further investigate how *JAG* is interconnected with the gene regulatory network of early floral organogenesis, we aimed to identify direct transcriptional targets bound *in vivo* by JAG by ChIP-Seq. Furthermore, we combined the data obtained from ChIP-Seq and global transcription profiling by expression array (Chapter 2). Using this combined approach I aimed to identify direct downstream targets bound by JAG that are also under transcriptional regulation by JAG. Moreover, I aimed to separate the targets and processes that are under direct immediate regulatory control of JAG from the processes further downstream.

3.2. Chromatin Immunoprecipitation (ChIP)

To further confirm direct transcriptional downstream targets of JAG I aimed to find the DNA binding sites bound by JAG *in planta* in the context of early floral organogenesis. In particular, I aimed to identify DNA binding sites of JAG in floral organ tissue bound by JAG in its endogenous wild-type expression domain and function. I pursued two approaches in parallel: I cloned the coding sequence of *JAG* under its endogenous promoter to generate GFP-tagged fusion lines. In addition, I aimed to produce anti-JAG antibodies to be able to pull down native JAG protein.

3.2.1. ChIP using the *35S:JAG-GR* construct in combination with anti-GR antibodies

In order to test the ChIP protocol and to identify DNA binding sites that can serve as positive controls for the global ChIP-Seq approach, I performed preliminary ChIP experiments with the DEX-inducible *35S:JAG-GR* construct in wild-type background (Chapter 2, Figure 2.1.A-B). For the first ChIP experiments, the DEX inducible *35S::JAG:GR* line combined with anti-GR antibodies was used to compare inflorescence apices treated with 10 µM dexamethasone and 0.1 % ethanol or 0.1% ethanol (mock) that had been incubated for four hours. In order to identify enriched DNA binding regions in the precipitated DNA of DEX-induced compared with mock-induced inflorescence apices, qPCR was performed with oligo pairs mapping the promoter regions upstream of the transcriptional start of *BP* and *BEL1* in 300 to 600 bp intervals, in accordance with the average fragment size of 500 bp after sonication. For *BEL1* I identified an enriched DNA binding site 1.77 kb upstream of the start codon (Figure 3.1.). For BP, I identified an enriched DNA binding site 2.6 kb upstream of the start codon (Figure 3.2.). These two enriched binding sites for *BEL1* and *BP* were used as internal positive controls to test for reproducibility and sensitivity in the subsequent ChIP-Seq experiments.

3.2.2. Producing anti-JAG antibodies

To complement the ChIP strategy using commercially available anti-GR antibodies to immunoprecipitate ectopic JAG-GR, I aimed to raise antibodies against recombinant JAG protein, which would allow me to pull down native JAG protein from any *Arabidopsis* line without the need for protein tags. Two strategies were pursued to produce recombinant JAG protein in amounts sufficient to raise polyclonal anti-JAG antibodies: Firstly, it was aimed to express recombinant JAG protein in the prokaryotic host *E. coli*. Secondly, the transient expression system *pEAQ specialK* (Sainsbury et al., 2009) in the eukaryotic host *Nicotiana bentamiana* was used as an alternative strategy to produce recombinant JAG protein. The binary vector *pEAQspecialK* that combines a modified Cowpea mosaic virus (*CPMV-HT*) sequence with the viral suppressor of silencing *35S-P19* cassette was specifically tailored for high level transient protein expression in plants (Sainsbury et al., 2009). In order to express recombinant JAG protein, I inserted *JAG* cDNA into the binary vector *pEAQspecialK* generating an N-terminal histidine (His) tagged JAG fusion protein. Subsequently, I transformed the binary vector into the *Agrobacterium strain L* (Sainsbury et al., 2009) and infiltrated young leaves of *Nicotiana bentamiana* with the aim to harvest mg-amounts of recombinant JAG protein. However, agro-infiltration of six *Nicotiana bentamiana* plants resulted in hypersensitive response in all infiltrated leaves after five days (Figure 3.3.A). By contrast, plants either infiltrated with the *pEAQspecial-GFP-HT* (positive control) (Figure 3.3.B) or with empty *pEAQspecial-HT* (negative control) did not show signs of hypersensistive response. The positive control plants expressed GFP (personal communication Pooja Saxena) seven days after infiltration. From this experiment, we concluded that transient over-expression of *JAG* was lethal for the *Nicotiana bentamiana* cells, and thus, no leaf material and recombinant JAG protein could be harvested.

In a second strategy to produce recombinant JAG protein, I aimed to over-express *JAG* in *E.coli strain BL21*. For this, *JAG cDNA* was cloned into the expression vector system *pRSETA* which harbours a polylinker for restriction digestion cloning downstream the viral, IPGT inducible *T7* promoter and the sequence encoding a *poly-His* tag. Directional cloning resulted in an N-terminal *poly-His* tag fusion of the expressed protein for later purification of the protein by immobilized metal affinity chromatography. Expression of the protein at the estimated size range of 30 kDa was confirmed by SDS-PAGE gel

electrophoresis (Figure 3.4.). For large-scale production, *BL21* harbouring the construct was grown in 500 ml liquid cultures to an OD of 0.5-0.7 and induced with IPGT (100 µM) and grown for four hours. Protein purification was performed under native conditions as the protein was found to be soluble after sonication. For purification of the JAG poly-His tag protein TALON metal affinity resin beads (TAKARA Clontech) in combination with imidazole elution were used (Figure 3.5.A) followed by several concentration steps to a final concentration of 70 µg/ml (Figure 3.5.B). In total, about 40 litre of bacterial culture were purified and concentrated to produce 600 µg of recombinant JAG protein at a final concentration of 70 µg/ml. The protein was used to immunise two rats in a 28-day immunisation program conducted by EUROGENTEC (Seraing, Belgium).

In order to test the specificity and sensitivity of the anti-JAG rat antibodies, I performed Western blots with 1:500 diluted rat serum. In the first step, I confirmed that the antibodies raised against recombinant JAG protein could detect recombinant JAG protein. Western Blots loaded with 7 ng to 350 ng of the recombinant protein showed a detection limit at 70 ng of total recombinant protein split in three bands (Figure 3.6.A) as previously observed in the SDS-PAGE gels.

In a second step I confirmed that the anti-JAG antibodies could detect plant JAG protein from crude plant protein extracts. Western blots were performed with five µl of crude plant extracts boiled in 2X Laemmli Buffer, prepared from inflorescences of wild type L-*er*, DEX-induced *35S:JAG-GR* in L-*er* background, and *jag-1*. In the DEX-induced WT-*35S:JAG-GR* samples, anti-JAG antibodies detected 1-2 bands at a size of 58 kDa, which is in accordance with the *in silico* size prediction for the JAG-GR fusion protein (57 kDa). However, no endogenous JAG protein was detected in any of the WT samples using this method. However, most importantly, the Western Blots loaded with crude plant protein extracts did not show any unspecific bands implying that the anti-JAG antibodies are specific to the JAG protein (Figure 3.6.B).

3.2.3. ChIP using *pJAG:JAG-GFP* combined with anti-GFP antibodies

In parallel to producing anti-JAG antibodies, I generated a 10.4 kb *pJAG:JAG-GFP* construct harbouring a 6.5 kb upstream promoter fragment, 1.6 kb coding sequence translationally fused to GFP cDNA (0.7 kb), and a 1.6 kb 3' fragment downstream of the stop codon. The *pJAG:JAG-GFP* construct complemented the flower phenotype in the *jag-2* L-*er* loss of function mutant background (Figure 3.7.) and showed JAG-GFP expression in early sepal primordia (Figure 3.8.). For chromatin immunoprecipitation, inflorescence apices with flowers of stage <10 were used. Commercial monoclonal anti-GFP antibodies bound to microbeads (Milteyi Biotec) were used for precipitation and purification of the formaldehyde fixed JAG-GFP protein-DNA complexes in the *pJAG:JAG-GFP* complemented *jag-2* line and in WT L-*er* plants serving as a negative control. To test for enrichment of JAG DNA binding sites in the precipitated DNA derived from *pJAG:JAG-GFP jag-2* samples compared with the WT L-*er* control samples, qPCR was performed with primers covering the previously identified JAG binding site in the *BEL1* promoter region and primers covering regions of the *Mu-like* transposon as a negative control (Figure 3.9.A). ChiP using *pJAG:JAG-GFP* in combination with the anti GFP-antibody coated microbeads provided consistent enrichments over several test experiments and was therefore the method of choice to perform the final ChIP-Seq experiment.

3.3. Illumina deep sequencing and ChIP-Seq data analysis

Immunoprecipitated DNA samples of three biological replicates for JAG-GFP and wild type with good enrichment were used to generate Tru-Seq libraries of a fragment size between 200 bp and 500 bp. Subsequently, Illumina deep sequencing was performed using 50 bp rapid runs. Deep sequencing resulted in average 20,000,000 reads per library. Subsequently, the sequence reads obtained for each library (in FASTQ format) were mapped to the unmasked Arabidopsis genome (TAIR10; ftp://ftp.arabidopsis.org/) using the SOAPaligner (v2) (Li et al., 2008). On average 3,000,000 reads per library could be mapped to regions in the Arabidopsis genome and a high percentage of reads was identified as unique positional reads, suggesting that only few duplication artefacts were generated during library preparation, thus, supporting good quality of the data.

To test for enrichment of DNA binding sites, the reads of each of the three JAG-GFP biological replicates were individually compared to the pooled reads of all three biological replicates of WT L-*er* (WT L-*er* all) using CSAR (Muiño et al., 2011a). All three biological replicates had comparable significance threshold values for the maximum peak scores between 1.85 and 1.88 at a false discovery rate (FDR) 0.01. *BELL-domain 1 (BEL1)* that had been previously identified as a direct JAG target (Schiessl et al., 2012) was used as one of the internal controls and showed reproducible significant JAG binding in all ChIP-Seq replicates (Figure 3.9.B), reconfirming the choice of FDR <0.01 and the corresponding ChIP score threshold values (Figure 3.9.B). Comparisons of the three JAG-GFP samples and the pooled WT L-*er* sample resulted in 12606 significantly enriched DNA binding sites for all three biological replicates in total that mapped within 3 kb upstream and 1.5 kb downstream of coding sequences in the *Arabidopsis* genome (Figure 3.10.A) (analysis performed with bioinformatics support from Jose Muiño).

In a first step, I aimed to see how the 12606 significant DNA binding sites were distributed on the genome in relation to the start and end of coding sequences (Figure 3.10.A). Therefore, the maximum peak scores that mapped within 3 kb upstream and 1.5 kb downstream of a coding sequence were categorised according to their distance to the start codon and stop codon of the nearest genes. This categorisation showed that JAG DNA binding sites showed a binding pattern typical for transcription factors (Kaufmann et al., 2010; Wuest et al., 2012) with 59% of all DNA binding sites mapping upstream of start codons. Furthermore, 13 % of the DNA binding sites were found within gene regions and 28% of the JAG DNA binding sites mapped within a distance of up to 1.5 kb downstream of the stop codon (Figure 3.10.B). In a next step, target genes were assigned to the binding sites that mapped within the distance of 3 kb upstream and 1.5 kb downstream of the coding sequence on the same strand or on the opposite strand. Accordingly, a total number of 11336 unique genes summed up from three biological replicates were assigned to 12606 significant peaks in all three replicates, whereby a single DNA binding site could be assigned to several genes, and on the other hand, a gene could be assigned to more than one DNA binding site.

In summary, replicates JAG-GFP 1, JAG-GFP 2 and JAG-GFP 3 had 4235, 3449 and 3652 genes assigned, respectively. In an overlap of the target genes identified in each of three biological replicates, 1634 genes were represented with significantly enriched peaks in all

three experiments and were therefore considered as a consistent core set of genes targeted by JAG (Figure 3.10.A; full analysis shown in Appendices Tables C-F).

3.4. Identification of DNA binding sequence motifs for JAG

DREME (Bailey, 2011) was used to search for sequence motifs associated with the top 1000 binding sites identified from the ChIP-Seq analysis of all 3 replicates. Four motifs were detected by DREME within a window of 100 bp centered on the binding peaks (Figure 3.11.A). In particular, the proportion of binding sites with the A(ATC)AGAGA motif, showed a strong enrichment with increasing ChIP-Seq score values, suggesting that this motif is recognised by JAG and potential JAG co-factors. The A(ATC)AGAGA motif is similar to the sequence bound by the Drosophila GAGA factor, which like JAG contains a single C2H2 zinc finger. By contrast, the (AC)CAAAA motif did not show an enrichment for the whole range of ChIP-Seq score values (Figure 3.11.B) (analysis performed with bioinformatics support from Jose Muiño).

3.5. Functional characterisation of direct targets of JAG

To gain an overview of the biological processes the 1634 direct JAG targets are involved in, we used the gene ontology (GO) analysis tool BINGO (Maere et al., 2005). In the BINGO analysis for 1634 direct ChIP targets, 153 GO terms were significantly enriched (corrected p-value < 0.01), thereof 18 GO terms were specifically involved in flower development, in particular, “reproductive developmental process”, reflecting that the ChIP experiment was performed with inflorescence apices. The GO term “regulation of transcription” showed strong enrichment, suggesting that JAG interacts with a large number of other regulatory genes and that JAG as a direct target of floral organ identity genes acts upstream in the gene regulatory network of organogenesis (Figure 3.12.). Furthermore, when correlating the proportion of JAG target genes with their ChIP-Seq score values, genes grouped in the GO terms “regulation in gene expression” and “reproductive developmental process” showed an increase with increasing ChIP-Seq score values (Figure 3.13.).

In addition, the GO terms “meristem maintenance” and “meristem development”, and several GO terms related to the plant hormones auxin and gibberellins were significantly enriched, suggesting that one of the key functions of JAG as a growth promoting factor is to orchestrate hormone-mediated cell communication in tissue and organ growth. In addition, the GO terms “response to abscisic acid” and “response to water stress” were enriched, suggesting that JAG targets genes involved in osmotic processes. Furthermore, several GO terms related to growth axis specification, such as “specification of axis polarity”, “abaxial/adaxial axis specification” and “abaxial/adaxial pattern formation” were enriched in the 1634 direct ChIP targets (Figure 3.12.; full analysis shown in Appendices Tables C-F) (analysis performed with bioinformatics support from Jose Muiño).

3.6. Identifying targets that are *in vivo* bound by JAG and under transcriptional control of JAG

Using the region between 3 kb upstream of the start codon and 1.5 kb downstream of the stop codon to associate DNA binding sites to gene models, we assigned several DNA binding sites to more than one gene. To resolve which of these genes are targeted by JAG, it can be assumed that the target genes are more likely to change expression in response to changes in JAG function. Therefore, we overlapped the total number of 2447 differentially expressed genes including genes responsive to JAG-GR activation and to steady state changes in the *jag-1* mutant with the 1634 high-confidence ChIP-Seq targets (Figure 3.14.). In addition, this allowed us to select direct JAG targets that are functionally relevant in the context of floral organ development.

The set of JAG-GR responsive genes was strongly enriched in the ChIP-Seq targets with 94 genes out of 495 genes being also directly bound by JAG. This enrichment was more pronounced for genes repressed by JAG-GR ($p = 1.16 \times 10^{-25}$, Fisher’s exact test) than for activated genes ($p = 1.22 \times 10^{-2}$). Specifically, the proportion of genes repressed by JAG-GR rose with increasing ChIP-Seq peak scores while the up-regulated genes did not (Figure 3.15.). In comparison, 164 genes out of 2447 genes differentially expressed between *jag-1* and the wild type were found among the direct ChIP-Seq targets. Thereof, 11 genes showed a consistent response to JAG-GR activation and in the *jag-1* wild-type

comparison, among them for example, the organ boundary specifying gene *PETAL LOSS* (*PTL*) and the meristem regulatory gene *CLAVATA1* (*CLV1*) (Brewer et al., 2004; Clark et al. 1997). ChIP-Seq targets that are differentially expressed in the mutant versus wild-type comparison but did not respond to ectopic JAG-GR activation may correspond to genes that are regulated by JAG in combination with cell type-specific co-factors or their transcriptional response may have been diluted by the cellular response to ectopic JAG-GR activation, therefore, the overlap with these differentially expressed genes was included in the list of functional relevant *in vivo* bound JAG target genes. In total, 235 genes overlapped between the ChIP-Seq analysis (FDR < 0.01) and the expression array experiment (log_2 ratio > 0.5, FDR < 0.01) (full analysis shown in Appendices Tables C and D) and are hence *in vivo* bound and transcriptionally regulated by JAG. On the other hand, 1007 direct ChIP target genes that were represented on the Affymetrix ATH1 oligonucleotide array did not show significant differences in gene expression (log_2 ratio > 0.5, FDR <0.01) (full analysis shown in Appendices Table E). Since we only used very young unopened flower buds from dissected inflorescences, and JAG has been shown to be expressed until flower stage 8-10 (Dinneny et. al., 2004; Ohno et al., 2004; Dinneny et al., 2006; Sauret et al., 2013, Smyth et al., 1990) the non-responsive genes could be relevant in later stages of floral organ development or in another developmental context, for example, leaf development. Furthermore, 392 genes that are direct *in vivo* bound targets of JAG were not represented on the Affymetrix ATH1 oligonucleotide array and therefore no information about expression is available for these direct targets (full analysis shown in Appendices Table F). However, the annotated genes of this group match the GO terms previously identified for JAG-GR responsive and ChIP-Seq targets, such as response to hormones and cell wall related processes. Furthermore, several of these targets belong to protein families that are directly regulated by JAG, for example members of the *GROWTH REGULATING FACTOR* (*GRF*) family, or protein families that are closely functionally associated to direct targets of JAG, for example, members of the *OVATE* family which are functionally associated with *TALE* proteins. In addition, JAG binds to several members of *microRNA* families involved in plant development, for example *microRNA 396* that regulates members of the *GRF* family (Rodriguez et al., 2010).

In addition to identifying functionally relevant direct JAG targets, the overlap also filtered for indirect JAG targets, with 399 genes responding to ectopic JAG-GR activation

but not being directly bound by JAG. The vast majority of differentially expressed genes between the *jag-1* mutant and the wild type were not bound by JAG and are therefore considered as indirect further down-stream targets.

3.6.1. Functional categorisation of directly regulated JAG targets

Compared to the GO analyses for the 1634 ChIP targets and the 495 differentially expressed genes upon ectopic JAG activation, the GO analysis for the 235 directly regulated genes showed fewer GO terms and less specific biological processes, because the reduced number of genes included into the analysis weakened statistical power. However, several GO terms related to floral organ development, regulation of transcription, abscisic acid and auxin related processes were significantly enriched. In line with the functions of JAG in promoting cell proliferation and cell growth, the directly regulated JAG targets showed enrichment for the GO terms “negative regulation of cell size” and “negative regulation of cell growth”, which includes the two trihelix transcription factors *PTL* and *GTL1* (Brewer et al., 2004, and Breuer et al., 2009) and *ATHB16* involved in cell expansion (Wang et al., 2003), all repressed by JAG. In addition, the GO term “negative regulation of cyclin-dependent protein kinase activity” was significantly enriched, with two members of the *Kip-related proteins*, *KRP2* and *KRP4* (De Veylder et al., 2001) being directly repressed by JAG (Figure 3.16.).

3.7. Discussion

3.7.1. Summary and limitations of the combined ChIP-Seq and expression analysis

Combining data of genome-wide DNA binding sites with global transcriptome analysis has been shown to be a useful tool to investigate the function of transcription factors in developmental gene regulatory networks (Kaufmann et al., 2010; Wuest et al., 2012). Here we identified the genome-wide DNA binding sites of JAG expressed under its endogenous promoter, which were associated with 1634 direct target genes. The overlap of the ChIP-Seq targets with the genes differentially expressed upon changes in JAG function identified 235 genes that are directly bound and transcriptionally regulated by JAG. Combining the ChIP-Seq with the global expression analysis generated a framework for the hierarchy of the gene regulatory network directing the process of early

organogenesis. Furthermore, the overlap provided a way to filter for genes that are specifically relevant in floral organogenesis, particularly in the cases when DNA binding sites were assigned to more than one gene in close vicinity. The overlap of 235 directly bound and transcriptionally regulated genes is comparable in size with previously published overlaps of ChIP-Seq and transcriptome data: For example, Kaufmann et al. (2010) who performed a ChIP-Seq on the MADS domain transcription factor *SEP3* and overlapped it with corresponding transcriptome data, identified a core set of 249 direct target genes, while Wuest et al. (2012) performed a ChIP-Seq on the Class B MADS domain transcription factor *AP3/PI* and identified 1500 direct ChIP targets, with 469 genes of them being differentially expressed upon changes in AP3/PI function.

The fact that the majority of genes bound by JAG did not seem to change in expression in response to JAG could suggest that a large number of JAG binding sites are functionally irrelevant. However, it must be kept in mind that the extent of the overlap between ChIP-Seq and expression data depends on the context in which the expression data are collected. The experiments reported here used dissected inflorescence apices containing young floral buds, so genes that have been excluded from the set of direct, transcriptionally responsive JAG targets may still be functionally relevant in other contexts where JAG is relevant, such as leaf development.

The degree of overlap between the ChIP-Seq and expression data also depends on the statistical thresholds used. My set of 235 gene candidates was generated by using stringent significant threshold values of FDR <0.01 for the ChIP-Seq and the microarray analysis. In the case of the ChIP-Seq I additionally only considered target genes that showed enriched DNA binding sites in all three biological replicates independently. At this level of stringency, all 1634 direct target genes can be considered as interesting candidates even if they did not show a differential response in the expression array. For example, increasing the significance threshold value in the expression array analysis from FDR < 0.01 to FDR< 0.05 identified 66 additional genes to be directly differentially expressed upon changes in JAG function. A further caveat in my approach was that almost 25% (392 out of 1634) of all genes identified as direct targets in the ChIP-Seq were not represented on the Affymetrix ATH1 oligonucleotide array. In particular, we were not able to assess the expression profiles of microRNA targets. In the future, RNA-Seq could be used to improve detection of differentially expressed transcripts.

Collecting expression data for a wider range of developmental stages and tissues could reveal additional direct and transcriptionally responsive JAG targets, but the overlap between multiple developmental programs in different tissues and cell types can make it difficult to interpret the functional significance of the regulatory interations. To minimise this problem, Kaufmann et al. (2010) and Wuest et al. (2012) used the *ap1 cal* mutant, which produces inflorescence meristem tissue but is defective in floral primordia initiation, as the genetic background for the DEX-inducible *35S:AP1-GR*. This resulted in synchronised induction of floral primordia and floral organs, producing large quantities of floral tissue of the same developmental stage and allowing the analysis of stage-specific expression profiles and DNA binding dynamics over the time-course of flower development (Gomez et al., 2005; Wellmer et al., 2006; Kaufmann et al., 2010; Wuest et al., 2012). I attempted to use this system to focus on genes controlled by JAG at early stages of organ development, but my preliminary experiments using the DEX-inducible *ap1 cal 35S:AP1-GR* system in combination with the anti-JAG antibodies did not provide consistent results. The experiments were hampered by premature induction of floral primordia in the absence of dexamethasone, accompanied by an increased number of floral bracts. Ectopic floral bract formation in *Arabidopsis* has been associated with loss of *LEAFY* (*LFY*) and *LATE MERISTEM IDENTITY1* (*LMI1*) function, and also with ectopic *JAG* expression. The ChIP-Seq data provided evidence that JAG regulates several of the floral meristem identity genes, among them *LEAFY* (*LFY*), and *LATE MERISTEM IDENTITY1* (*LMI1*), which are early floral meristem identity genes but also suppress ectopic bract formation. Together, these results suggest that *JAG* may be ectopically expressed in the *ap1 cal AP1-GR* system, precluding its use to analyse specifically the early roles of JAG.

To increase the resolution of my analysis of the downstream functions of JAG, the list of candidate genes can be further investigated in a stage-specific manner by RNA *in situ* hybridisation, marker lines and reverse genetics. Alternatively, laser capture microdissection and fluorescence activated cell sorting of JAG-GFP cells would provide a domain- and developmental stage-specific transcriptome profile.

3.7.2. The transcription factor *JAG* predominantly acts as a transcriptional repressor

The original gene annotation revealed that JAG harbours a repressive N-terminal EAR (ethylene-responsive amphiphilic repressor) motif, suggesting that it functions as a transcriptional repressor (Ohno et al., 2004). Combining ChIP-Seq data with transcriptome analysis data allowed me to further investigate the repressor function of JAG. While there is a significant correlation between genes down-regulated upon ectopic JAG activation and genes up-regulated in *jag-1* compared to wild type (mock-treated *35S:JAG-GR*), there is no significant overlap between genes up-regulated upon ectopic JAG activation and genes down-regulated in the *jag-1* mutant (Chapter 2). Furthermore, in the group of the 235 genes that are directly regulated by JAG, significantly more genes were repressed upon JAG activation than up-regulated. Moreover, among the 1,634 ChIP-Seq core target genes, the proportion of genes repressed by JAG-GR rose with increasing ChIP-Seq peak scores, while this was not the case for genes activated by JAG-GR. In this respect, our combined approach provided further evidence that JAG preferentially functions as a transcriptional repressor.

Further analysis of the role of JAG in transcriptional control would be facilitated by identifying the DNA sequences bound by JAG. In this respect, three significantly enriched DNA binding motifs were found in the vicinity of ChIP-Seq peaks, in particular the A(ATC)AGAGA motif showed similarity to a sequence bound by the Drosophila GAGA factor which also contains a single zinc finger domain (van Steensel et al., 2003). However, no obvious similarities to other DNA binding motifs of plant transcription factors have been found yet. For example, the three significantly enriched DNA binding motifs found for JAG did not include the core AGT binding motif identified for the single C_2H_2 zinc finger transcription factor *SUPERMAN* (*SUP*) (Dathan et al., 2002). This is in line with findings by Ohno et al. (2004), who have shown that *SUP*, *JAG* and *NUB* share high sequence similarity in the C_2H_2 zinc finger sequence, but that the sequence conferring DNA binding specificity differed significantly among them, suggesting that *SUP* and *JAG* have different downstream targets (Ohno et al., 2004).

The enriched DNA binding motifs identified in the ChIP-Seq analysis could be further confirmed by electrophoretic mobility shift assays (EMSA) or Surface Plasmon Resonance (SPR) as described by Stevenson et al. (2013). In this regard, the already produced recombinant JAG protein as well as the established protocol for recombinant JAG protein

expression and purification will prove useful. In addition, the rat anti-JAG antibodies generated for this project will provide an alternative to commercially available antibodies and can be used to pull down native JAG protein *in vitro* and in different genetic backgrounds, independently from tagged JAG fusion proteins.

3.7.3. Functional characterisation of JAG targets

The combined approach described in this chapter provided an overview of direct and indirect functions in biological processes and molecular mechanisms targeted by the growth regulatory gene *JAG*. The GO analyses of biological processes for the 1634 ChIP target genes and for the 495 genes differentially expressed showed a significant enrichment for the GO term regulation of transcription factor activity, suggesting that JAG, as a direct target of floral organ identity genes, acts upstream in the gene regulatory network of floral organogenesis once organ identity has been defined.

Furthermore, there was an overlap in the GO terms related to floral organ development, meristem maintenance and meristem development, suggesting that JAG directly targets these processes in order to promote the transition from meristem to primordium growth behaviour, but also promotes organ outgrowth and organ patterning. This is further supported by the enrichment of GO terms involved in axis specification found for the 1634 ChIP targets, suggesting that JAG directly targets genes involved in specifying the growth axis of organs, a key process in organ outgrowth and tissue patterning. Tissue patterning requires cell to cell communication, and in this context the GO terms response to auxin stimulus and response to gibberellin stimulus, and several auxin-and gibberellin-related GO terms were significantly enriched in both GO analyses. Both hormones have been reported to have key functions in promoting cell growth and tissue growth, suggesting that JAG promotes growth and possibly growth anisotropy by directly modulating hormone-mediated cell communication processes related to auxin and gibberellins (reviewed by Achard and Genschik, 2009; reviewed by Leyser, 2010 and Ljung, 2013). In addition, also response to abscisic acid was found among the enriched GO terms in both analyses. Abscisic acid has been reported to negatively regulate leaf growth in response to osmotic stress by the regulation of osmotic processes at the plasmamembrane, which are also crucial for turgor pressure driven cell expansion (Bacon et al., 1998, Parent et al., 2009), suggesting that JAG mediates its growth-promoting

effects using a similar pathway associated with osmotic processes in the plasmamembrane. Together, these enriched GO terms suggest that the growth regulator JAG links tissue patterning with tissue growth.

In addition, negative regulation of cell size and cell growth and negative regulation of cyclin-dependent protein kinase activity were among the enriched GO terms for the overlap between transcriptome and ChIP-Seq candidates, supporting the observations from the quatitative 3D live-imaging approach (Schiessl et al., 2012) that JAG promotes not only cell growth but also cell proliferation. In respect of the latter, the combined approach revealed that JAG directly represses the CDK inhibitors *KRP2* and *KRP4* which are members of the *Kip-related proteins* (De Veylder et al., 2001). This appeared particularly exciting, because quantitative 3D imaging using the S-phase marker EdU (also see Chapter 7) revealed that JAG modulates cell size homeostasis at the G1-/S-phase transition (Schiessl et al., 2012), therefore *KRP2* and *KRP4* were considered as promising candidates to further investigate how JAG uncouples entry into S-phase from cell size in sepal primordia. Moreover, the interaction of JAG with *KRP2* and *KRP4* provided the first evidence that JAG can directly interact with the core regulatory network of the cell cycle. Interestingly, no significant enrichment for cell wall related processes was found among the GO terms for the 1634 direct ChIP targets, suggesting that cell wall processes are predominantly indirectly regulated by JAG to promote cell growth and cell expansion. Furthermore, GO terms related to nutrients were not significantly enriched in the direct targets of JAG compared with the genes responsive to ectopic JAG activation, suggesting that modulation of nutrient levels are downstream of the immediate growth promoting effects of JAG.

In summary, combining the ChIP-Seq data with the global transcriptome provided a global view of the hierarchy of gene expression downstream of JAG. I identified a core set of target genes that are directly *in vivo* bound and transcriptionally regulated by JAG in the context of floral organogenesis. Furthermore, I could separate this core set of direct targets from indirectly regulated genes and processes. For example, the processes of meristem maintenance and response to auxin were directly targeted by JAG, whereas processes related to the cell wall appeared to be mostly indirectly regulated by JAG. Together, the direct and indirect candidate genes provided a platform to elucidate the molecular mechanisms of organogenesis and laid the foundation for further

understanding the role of growth regulators in the gene regulatory network of floral organogenesis. In the following chapters (Chapter 4-7), the interaction of JAG with target genes involved in floral patterning, meristem maintenance and cell cycle regulation is analysed in detail, while Chapter 8 discusses in more depth genes and functions that provide novel and unexpected leads to understand JAG function.

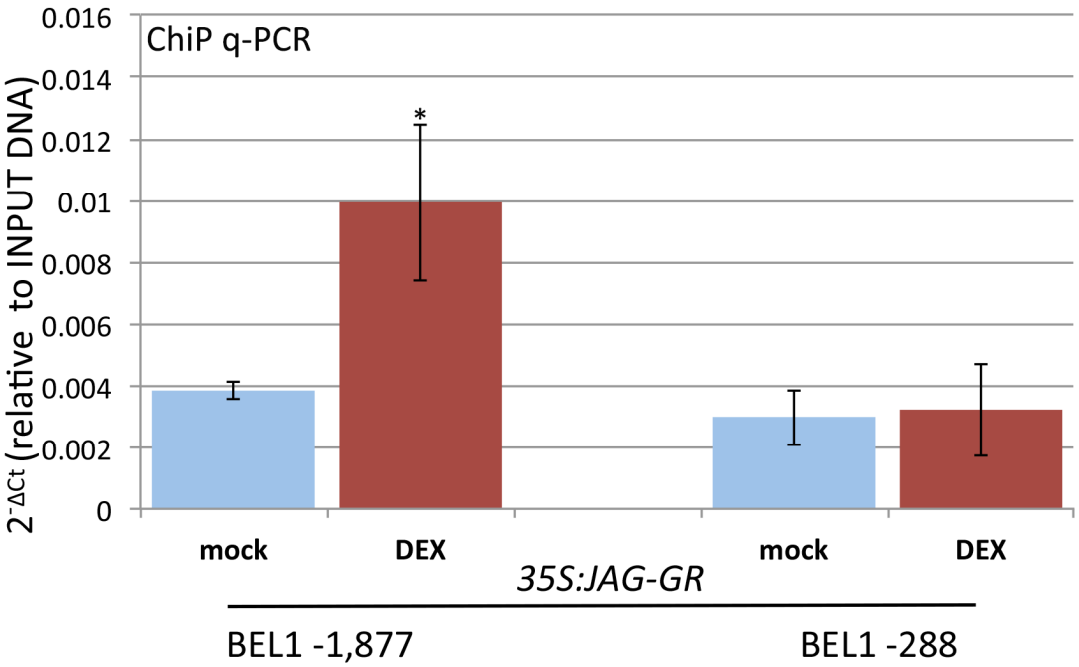

Figure 3.1. Ectopic JAG-GR binds to the promoter region of *BEL1*.

Chromatin immunoprecipitation (ChIP) using anti-GR antibodies and inflorescence apices of *35S::JAG-GR* plants 4 h after mock treatment (light blue) or treatment with dexamethasone 10 µM (red); target sequences 1.9 or 0.3 Kb upstream of the *BEL1* transcriptional start; bars show the average and standard deviation of three biological replicates; numbers below the bars indicate the left border of the q-PCR amplicon relative to the coding sequence; asterisks indicate significant difference to the mock control ($p < 0.05$, Student's *t*-test).

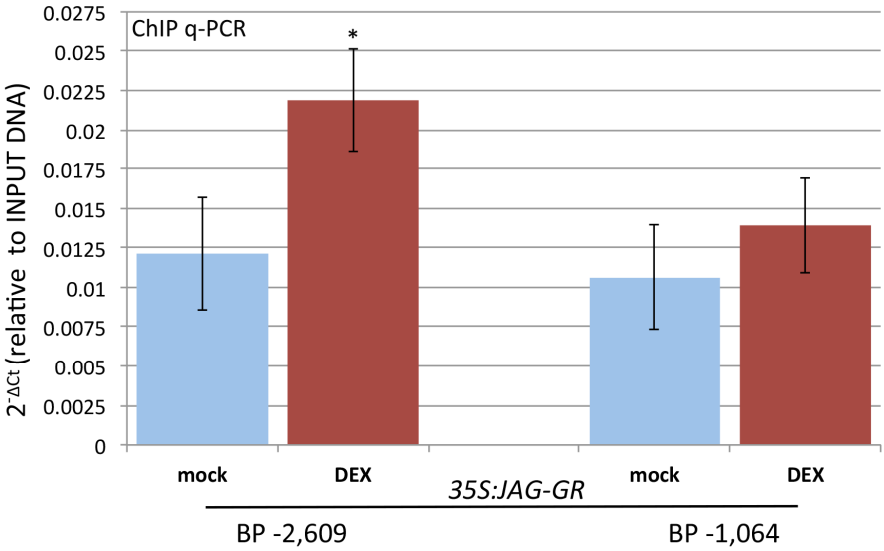

Figure 3.2. Ectopic JAG-GR binds in the promoter region of BP.

Chromatin immunoprecipitation (ChIP) using anti-GR antibodies and inflorescence apices of *35S::JAG-GR* plants 4 h after mock treatment (light blue) or treatment with dexamethasone 10 µM (red); target sequences 2.6 and 1.1 Kb of upstream of the *BP* transcriptional start; bars show the average and standard deviation of three biological replicates; numbers below the bars indicate the left border of the q-PCR amplicon relative to the coding sequence; asterisks indicate significant difference to the mock control ($p < 0.05$, Student's *t*-test).

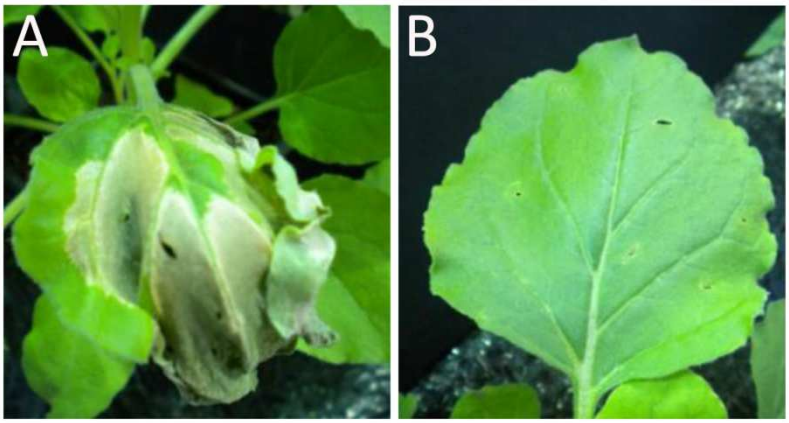

Figure 3.3. Transient expression of recombinant JAG poly-His tag protein in *Nicotiana bentamiana* leaves. (A) Leaf infiltrated with *pEAQspecial* harbouring the *JAG cDNA* (hypersensitive response) 5 days after infiltration; (B) Leave infiltrated with *pEAQspecial-GFP-HT* (positive control) 5 days after infiltration.

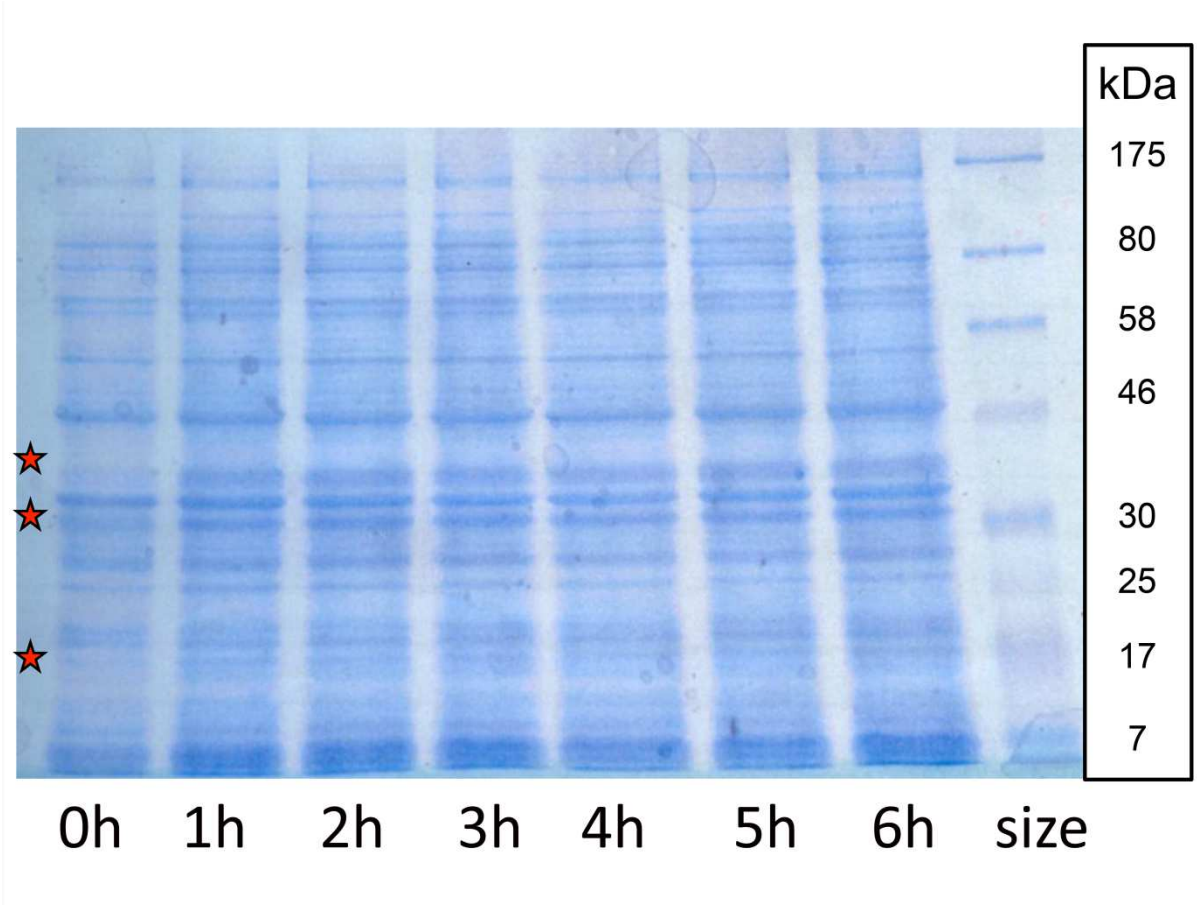

Figure 3.4. Expression of recombinant JAG poly-His tag protein in *E.coli* strain *BL21.*
SDS-PAGE gel loaded with recombinant JAG poly-His tag protein sampled at different time-points after induction with 100 µM IPGT (time-point 0h), from time-point 1h onwards three bands at 30 kDa (predicted size of JAG poly-His tag), slightly above 30 kDa, and around 20 kDa were induced (indicated by red asterisks).

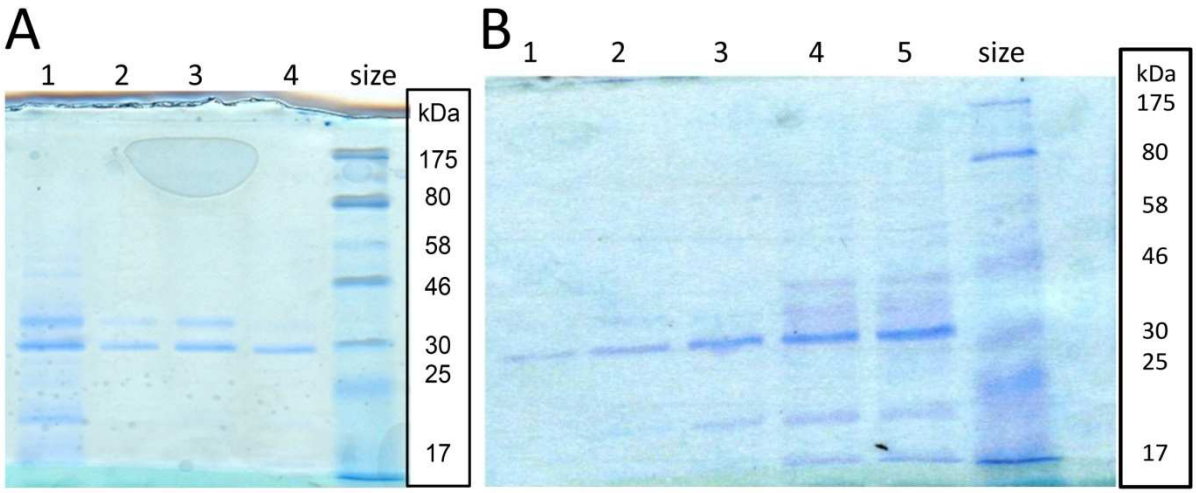

Figure 3.5. Purified and concentrated recombinant JAG poly-His tag protein on SDS-PAGE gels. (A) SDS-PAGE gel of column-purified and imidazole eluted samples: 1-4 are sequential samples of 1.5 ml eluted fractions, with the last fraction (4) showing an increase for the 30 kDa band. (B) Samples of several elution fractions were combined and concentrated to a final concentration of 70 ng/ml; samples 1-5 show gradual enrichment of the 30 kDa band over 5 concentration steps.

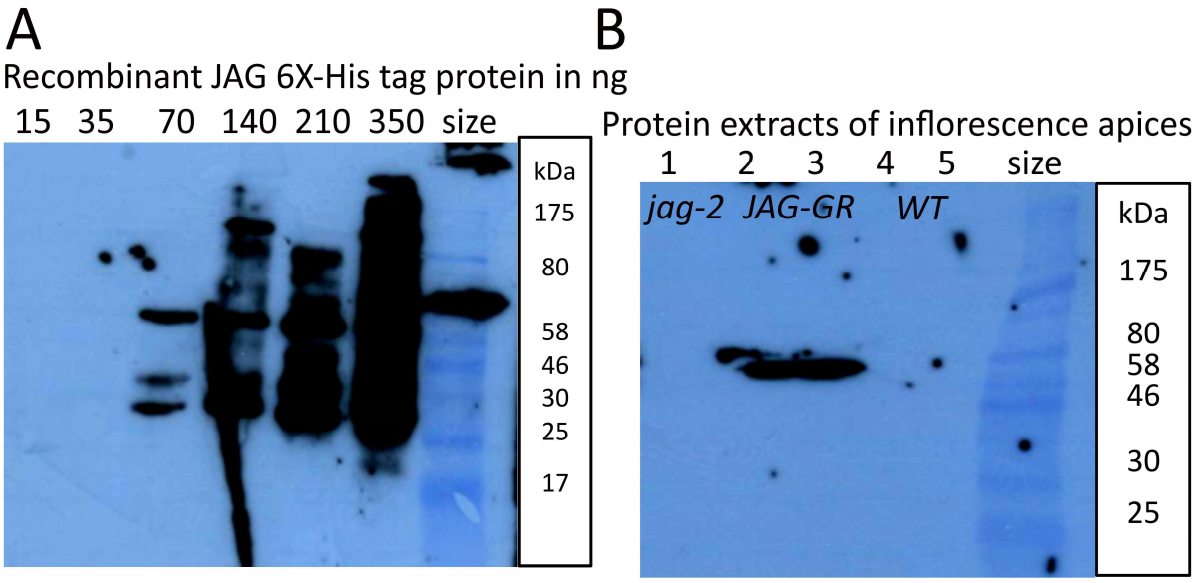

Figure 3.6. Testing of the rat anti-JAG antibodies against JAG protein in Western Blots. (A) Detection test for anti-JAG antibodies using different concentrations of recombinant JAG poly His-tag protein showed a detection limit at 70 ng with a 1:500 anti-JAG antibody dilution. (B) Detection test for anti-JAG antibodies using crude plant protein extracts of inflorescences of different genotypes:(1) *jag-2* L-*er*, (2-3) *35S:JAG-GR* in wild-type L-*er*,(4-5) wild-type L-*er*.

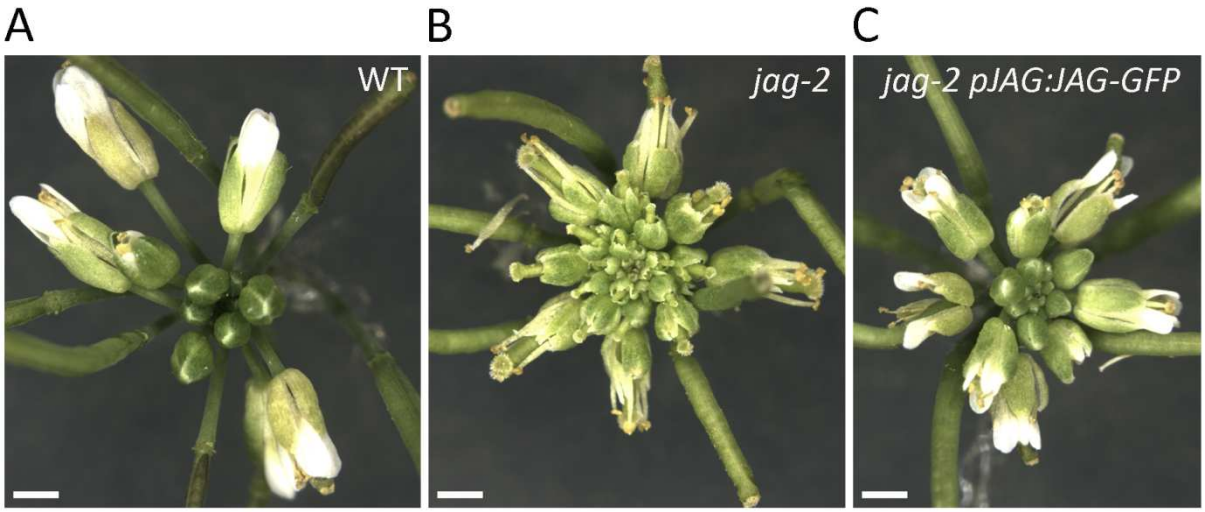

Figure 3.7. Complementation of the *jag-2* mutant with *pJAG:JAG-GFP.*

Scale bars: 1mm; (A) wild-type L-*er* inflorescence; (B) *jag-2* L-*er* inflorescence: sepals and petals with reduced distal growth, carpels protruding from the unopened younger flower buds, and petals with translucent appearance; (C) *pJAG:JAG-GFP* in *jag-2 L-er* with fully complemented distal outgrowth of sepals and petals, petals regaining white appearance, and sepals completely enclosing the organs of the inner whorls in unopened younger flower buds.

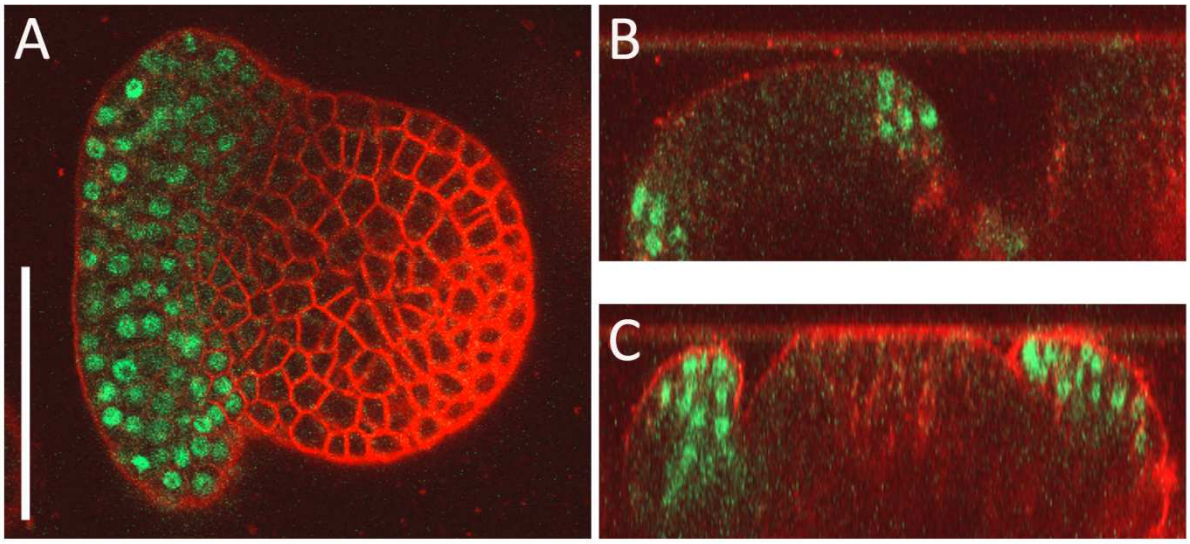

Figure 3.8. JAG-GFP expression in the *pJAG:JAG-GFP jag-2* L-*er*.

Scalebar (A-C): 50 µm; (A-C) Confocal image of a stage 3 floral bud with the first pair of sepal primordia emerging; JAG-GFP showed a nuclear-localised expression pattern throughout the emerging primordia, but was not expressed in the floral meristem; (A) cross section from a confocal stack; (B-C) 3D projections of the confocal stack generated in Fiji (Schmid et al., 2010).

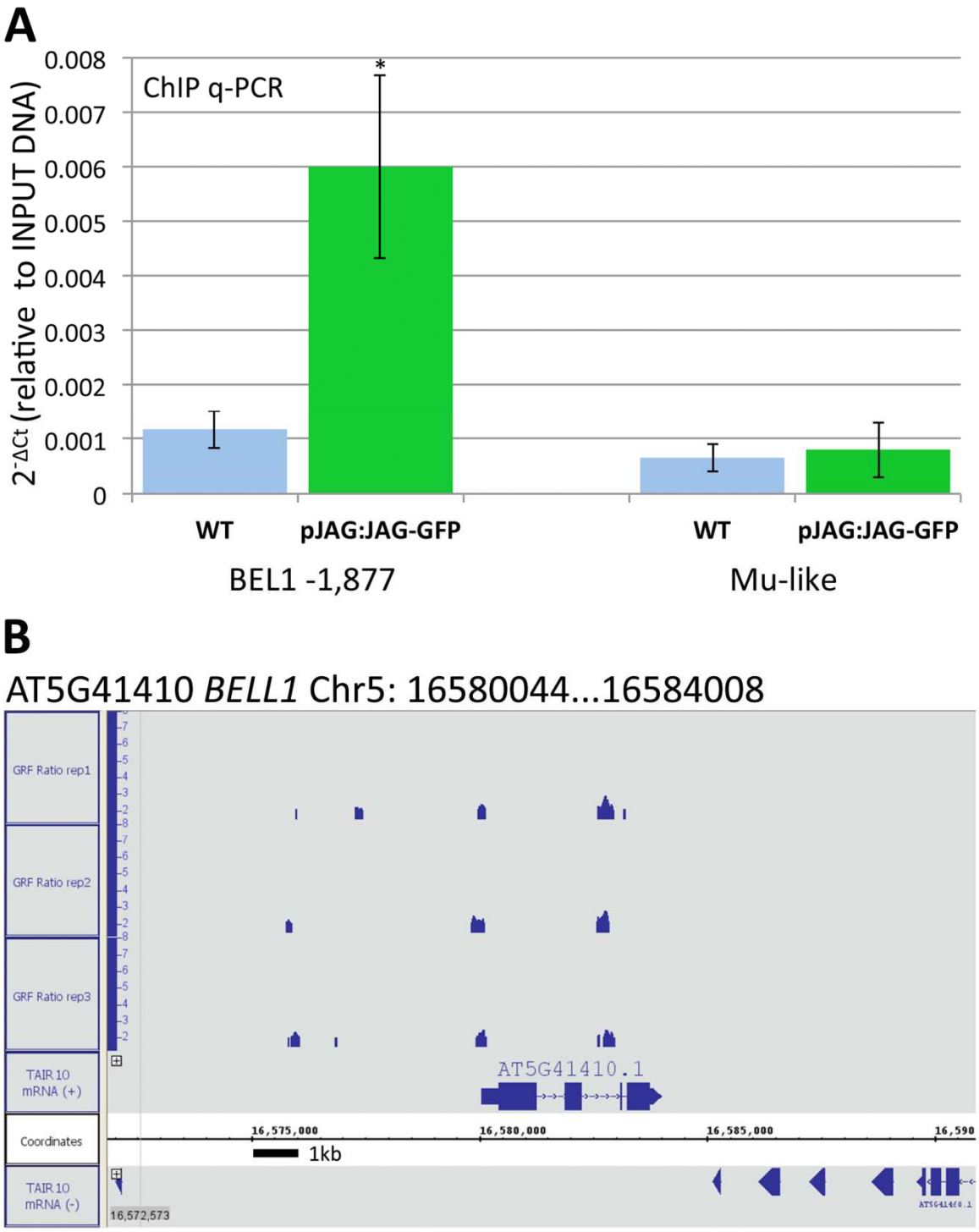

Figure 3.9. Testing the sensitivity and reproducibility of the ChIP with endogenous JAG-GFP in combination with anti-GFP antibodies. (A) Binding of JAG-GFP to the upstream region of *BEL1* confirmed by ChIP-qPCR; target sequence 1.9 upstream of the *BEL1* transcriptional start was significantly enriched (as previously identified as a positive control, see Figure 3.2.) in comparison to the *Mu-like* gene that served as a negative control and did not show a significant enrichment in the JAG-GFP precipitated DNA; bars

show the average and standard deviation of three biological replicates; numbers below the bars indicate the left border of the q-PCR amplicon relative to the coding sequence; asterisks indicate significant difference to the negative WT control ($p < 0.01$, Student's *t*-test). (B) Visualisation of read enriched regions mapping to the TAIR10 Arabidopsis reference genome (x-axis) using the Integrated Genome Browser (Nicol et al., 2009), ChIP-Seq peak score values (y-axis) based on the ratios of normalised reads between JAG-GFP and control samples were calculated for every single nucleotide position using CSAR software (Muiño et al., 2011a), the maximum score value within the candidate peaks was used to test for significance of the enrichment; enrichments detected in each of the three replicates within 3 kb upstream and 1.5 kb downstream of the coding sequences for the *BEL1* locus on chromosome 5 confirm that *BEL1* is one of the 1634 highly reproducible target genes.

A

DNA binding sites and ChIP target genes at FDR < 0.01

	number of enriched DNA binding sites					number of target genes
	-3kb to -1.5 kb	-1.5 kb to 0 kb	within cds	0 kb to +1.5 kb		
Replicate GFP-1	1107	1635	632	1384		4235
Replicate GFP-2	863	1395	500	1054		3449
Replicate GFP-3	976	1442	521	1097		3652
total	**2946**	**4472**	**1653**	**3535**	**12606**	**11336**
percentage	**0.23**	**0.35**	**0.13**	**0.28**		
			number of reproducible genes			**1634**

B

Spatial distribution of DNA binding sites relative to cds

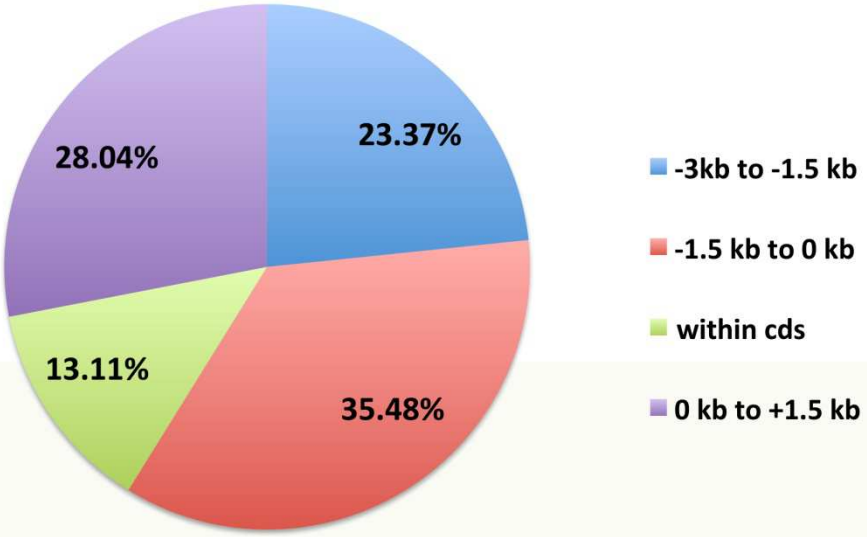

Figure 3.10. Analysis of the ChIP-Seq data. (A) Number of the significantly enriched DNA binding sites and associated target genes with binding sites in -3kb and +1.5 kb vicinity of their coding sequence for each of the three biological replicates and in total. (B) Pie chart of the spatial distribution of DNA binding sites relative to the coding sequences in close vicinity, numbers are the percentage for each distance category (-3kb to -1.5 kb, -1.5 kb to transcriptional start, within CDS, 0 kb to 1.5 kb downstream of the stop codon) relative to the total number of 12606 significantly enriched DNA binding sites identified within -3kb and +1.5 kb vicinity of coding sequences in the three biological replicates (graphs produced with bioinformatics support from Jose Muiño).

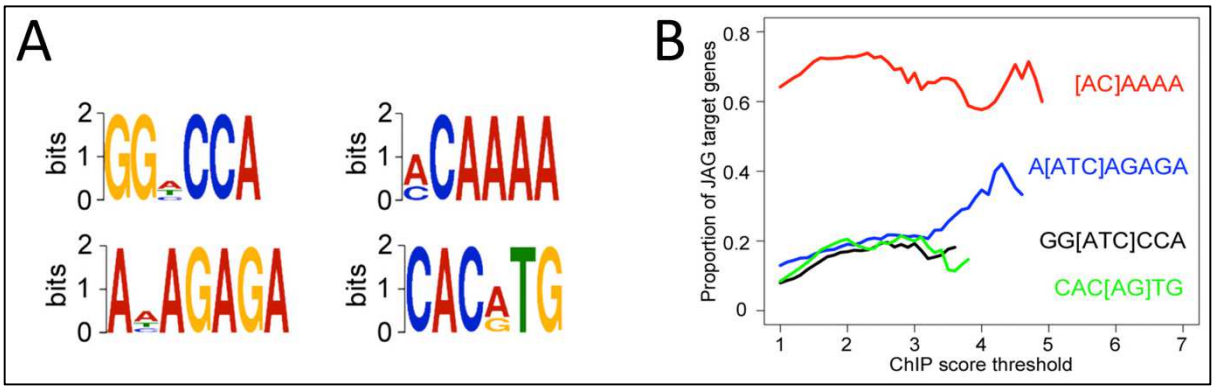

Figure 3.11. Enriched DNA binding motifs of JAG. (A) Affinity logos for motifs enriched within 100 bp of JAG DNA binding peaks; (B) Enrichment for the motifs shown in (A) as a function of ChIP-Seq scores, the horizontal axis shows the ChIP-Seq score values above the threshold; the single ChIP-Seq score attributed to each gene was from the replicate with the lowest value; proportion of genes were only displayed, when the total number of genes above a given ChIP-Seq score was 3 or higher (graphs produced with bioinformatics support from Jose Muiño).

A

Enrichment of GO terms (biological processes) in the set of 1634 ChIP-Seq target genes

GO-ID	p-value	x	n	X	N	Description
10468	1.23E-20	193	1641	1274	22278	regulation of gene expression
48507	5.06E-03	15	95	1274	22278	meristem development
10073	1.48E-02	10	56	1274	22278	meristem maintenance
9908	4.05E-07	37	228	1274	22278	flower development
3006	1.01E-03	75	828	1274	22278	reproductive developmental process
9733	6.40E-09	46	282	1274	22278	response to auxin stimulus
9850	4.49E-02	7	37	1274	22278	auxin metabolic process
9737	6.67E-05	36	272	1274	22278	response to abscisic acid stimulus
9788	2.39E-02	5	17	1274	22278	negative regulation of abscisic acid mediated signaling pathway
9414	1.48E-02	22	188	1274	22278	response to water deprivation
10476	4.61E-03	8	31	1274	22278	gibberellin mediated signaling pathway
9739	6.87E-04	18	107	1274	22278	response to gibberellin stimulus
9798	3.52E-05	10	27	1274	22278	axis specification
9955	6.70E-05	9	23	1274	22278	adaxial/abaxial pattern formation
9944	3.19E-04	7	16	1274	22278	polarity specification of adaxial/abaxial axis

B

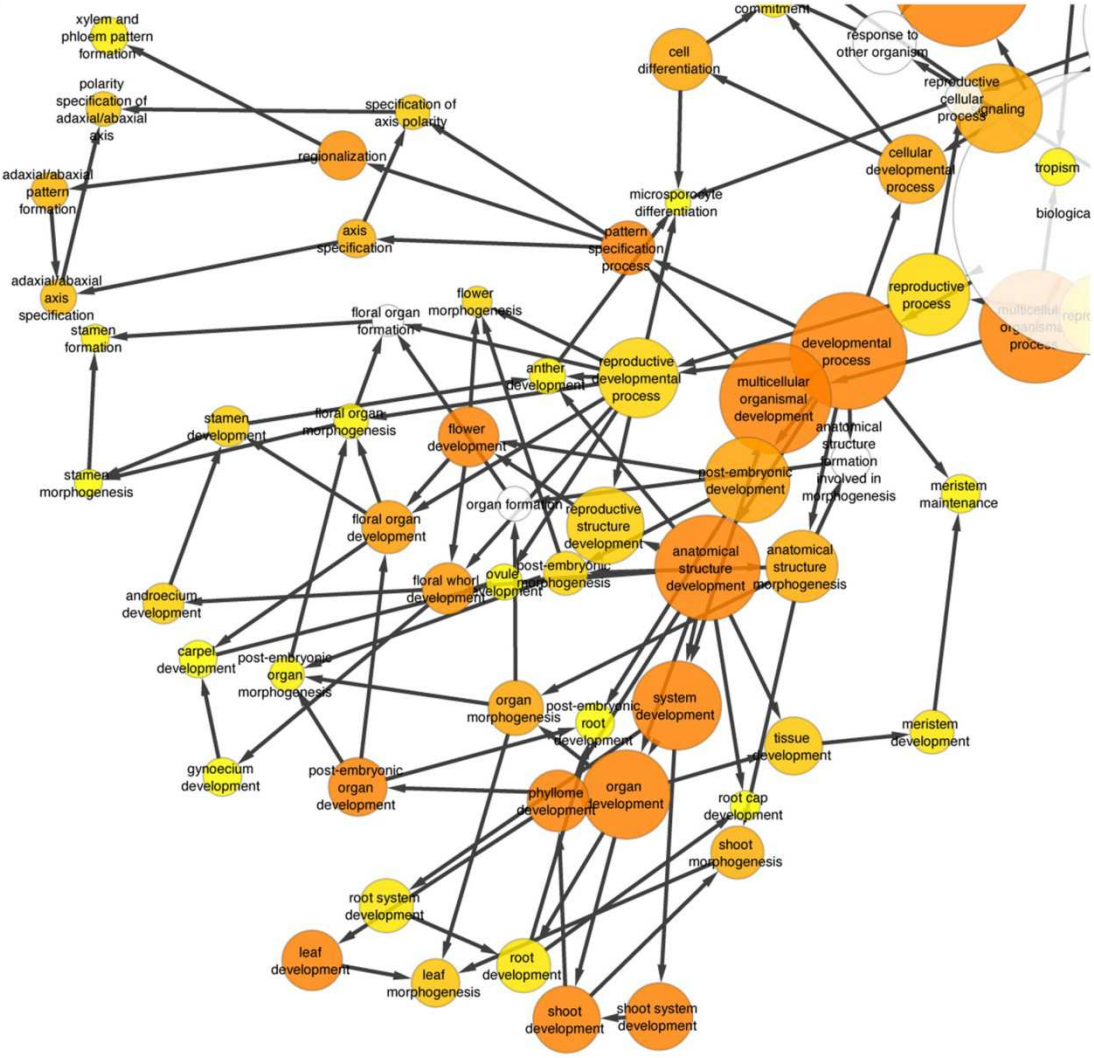

C

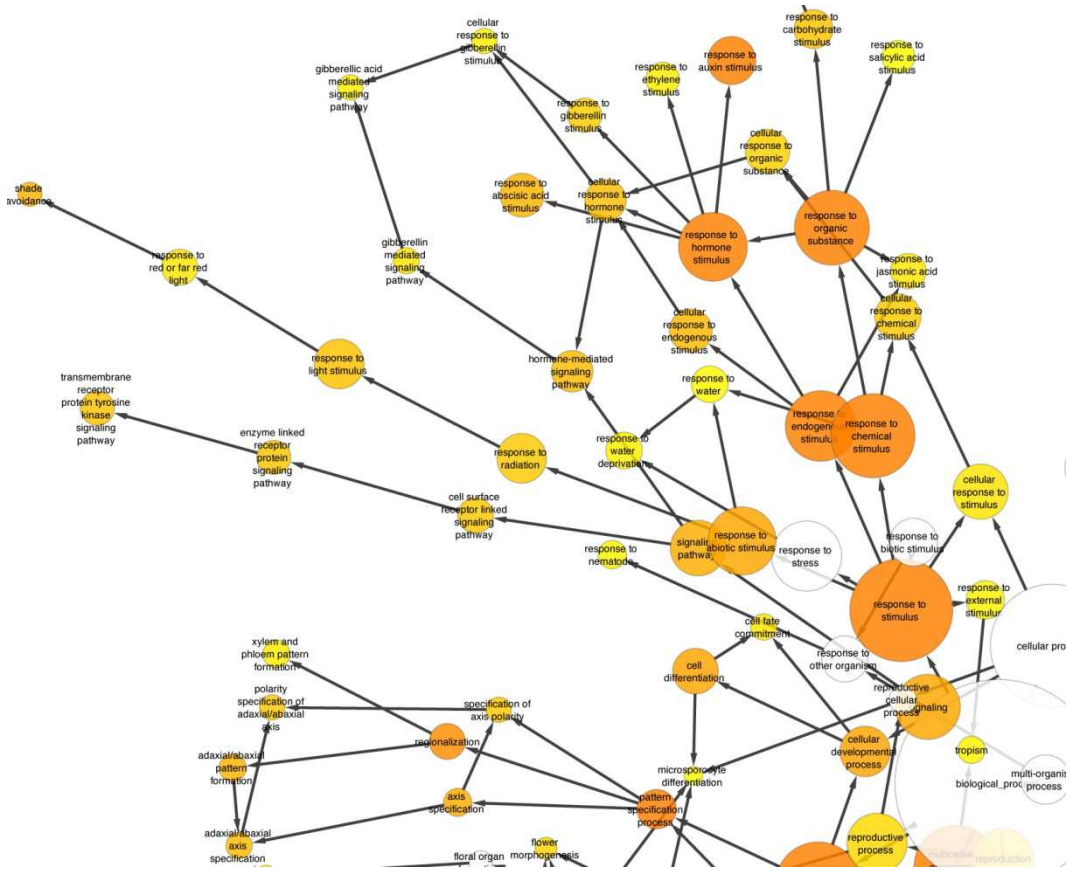

Figure 3.12. Enrichment for Gene Ontology associated with the direct 1634 reproducible target genes *in vivo* bound by JAG. (A) GO terms (biological process) enriched within the set of ChIP target genes. The p-values are the corrected p-values calculated by BINGO, with x being the number of genes belonging to the specific GO-ID found in the total number our gene set (X), while n is the number of genes identified for the specific GO-ID and N is the total number of annotated genes considered in the BINGO analysis. (B and C) Graphical representation of the enriched GO terms (biological process) within the set of genes described in (A); enrichment map representing the hierarchy of the network of biological processes; produced within the Cytoscape environment (Saito et al., 2012); GO terms that were found significantly enriched including all parental categories are represented in the map as nodes; the size of the node is proportional to the number of ChIP targets represented in the GO term, node colour corresponds with the significance based on the BINGO analysis described in (A) with white (insignificant), from yellow p=0.01 to dark orange p= 0.01 10^{-5}; nodes were automatically arranged so that highly similar gene sets are placed together, as a result highly redundant gene sets cluster;

edges between nodes represent weighted links between the nodes according to the number of overlapping genes; (B) enrichment map with a focus on developmental processes and morphogenesis and (C) with a focus on hormone stimulus; (graphs produced with bioinformatics support from Jose Muiño) .

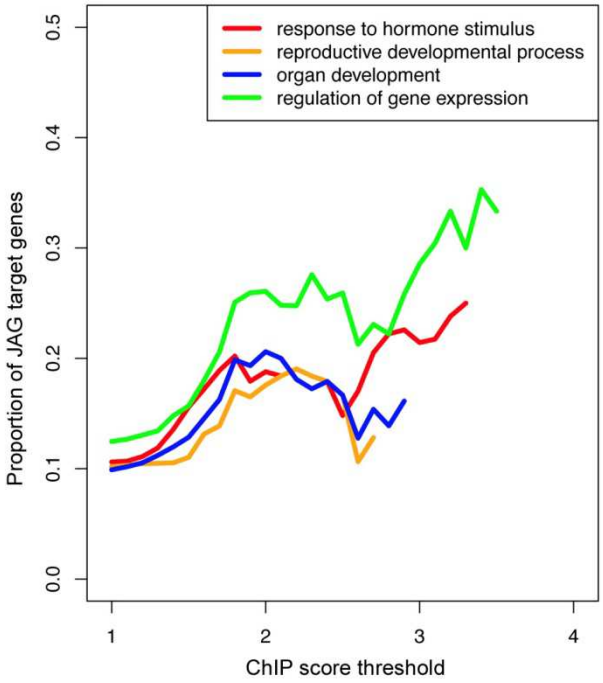

Figure 3.13. Enrichment for Gene Ontology terms associated with differentially expressed, direct JAG target genes with ChIP-Seq scores above the threshold shown in the horizontal axis. The single ChIP-Seq score attributed to each gene was from the replicate with the lowest value; proportion of genes were only displayed, when the total number of genes above a given ChIP-Seq score was 3 or higher; (graph produced with bioinformatics support from Jose Muiño).

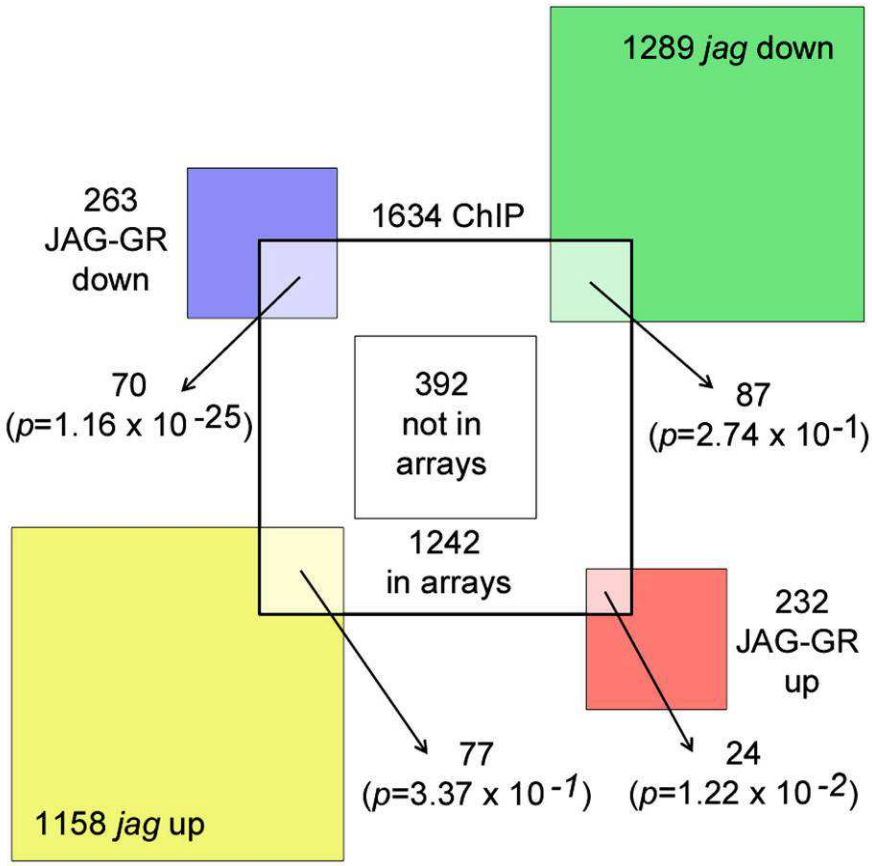

Figure 3.14. Overlap of ChIP-Seq targets with genes differentially expressed upon changes in JAG function. Overlap between the sets of differentially expressed genes shown in Chapter 2, Figure 2.2. and the combined set of 1634 reproducible ChIP-Seq targets shown in Figure 3.9.A; when calculating p-values for the overlaps (Fisher's exact test), only genes that were present in both the ChIP-Seq and expression array lists were considered; (graph produced with bioinformatics support from Jose Muiño).

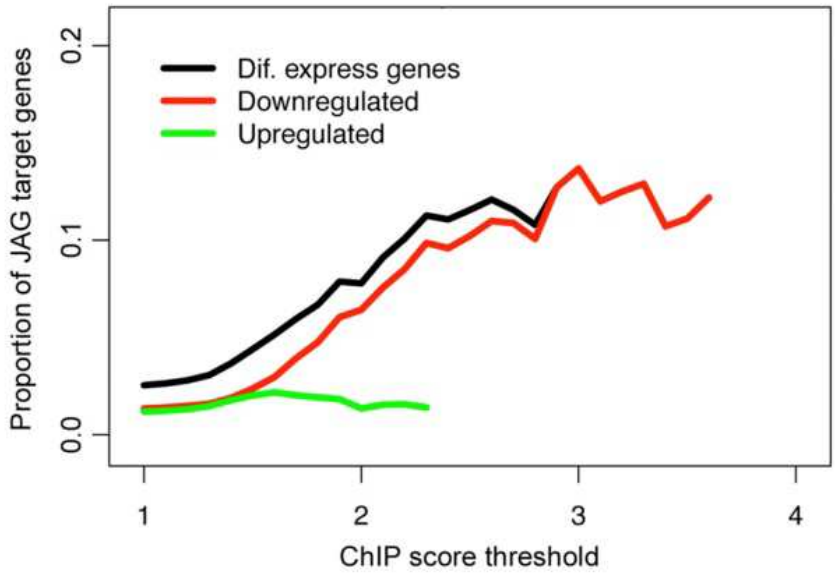

Figure 3.15. Enrichment of ChIP-Seq scores for differentially expressed (repressed and activated) genes. Enrichment for repressed and activated genes with ChIP-Seq scores above the threshold shown in the horizontal axis, within the set of 495 genes that were differentially expressed upon ectopic JAG-GR activation; the single ChIP-Seq score attributed to each differentially expressed gene was from the replicate with the lowest value; proportion of genes were only displayed, when the total number of genes above a given ChIP-Seq score was 3 or higher; (graph produced with bioinformatics support from Jose Muiño).

Enrichment of GO terms (biological processes) in the set of 235 differentially expressed ChiP-Seq targets

GO-ID	p-value	x	n	X	N	Description
9908	8.31E-05	13	198	201	15988	flower development
45449	1.15E-04	34	1160	201	15988	regulation of transcription
9733	3.89E-02	9	234	201	15988	response to auxin stimulus
9737	4.24E-02	9	239	201	15988	response to abscisic acid stimulus
45736	4.14E-02	2	7	201	15988	negative regulation of cyclin-dependent protein kinase activity
45926	2.19E-03	3	8	201	15988	negative regulation of growth
45792	2.20E-02	2	5	201	15988	negative regulation of cell size

Figure 3.16. Enrichment for Gene Ontology terms associated with the 235 differentially expressed, direct JAG target genes. The p-values are the corrected p-values calculated by BINGO, with x being the number of genes belonging to the specific GO-ID found in the total number our gene set (X), while n is the number of genes identified for the specific GO-ID and N is the total number of annotated genes considered in the BINGO analysis; (graph produced with bioinformatics support from Jose Muiño).

Chapter 4 - JAG directly represses genes involved in meristem maintenance and organisation

4.1. Introduction

Results obtained from quantitative 3D imaging identified JAG as a regulator in the transition from meristematic to primordia cell behaviour in early stages of organ growth. The transition involves decreased coordination of cell size and DNA synthesis, an increase in the rates of cell growth and division, and a shift from isotropic to anisotropic growth. Consequently, cells in the sepal primordium of *jag* loss of function mutants fail to make this transition and behave like meristem cells (Schiessl et al., 2012; note that the imaging data presented in the paper were not obtained by me, therefore I cited the paper whenever imaging results were concerned; also note that the imaging protocol presented in the paper differed from the imaging protocol used in Chapter 7). It has been shown that organ identity genes such as *ASYMMETRIC LEAVES1/2 (AS1/2)* and their interactors, for example, *BLADE ON PETIOLE1/2* (*BOP1/2),* but also auxin maxima generated at the site of incipient organ primordia, repress meristem maintenance genes (Ori et al., 2000; Jun et al., 2010; Hay et al., 2006), showing that establishing primordia identity requires down-regulation of meristem maintenance genes. In this context, I hypothesised that JAG would also antagonise meristem development genes.

A particularly important group of meristem regulatory genes are the TALE proteins, which are highly conserved developmental regulators also present in animals and fungi. In plants, they form a tightly interconnected regulatory network to co-ordinate meristem establishment and maintenance throughout post-embryogenic development (reviewed by Hay and Tsiantis 2010). TALE proteins share a homeodomain (HD) that allows them to bind to DNA and to act as transcription factors. Additionally, (BLH) proteins such as *BEL1* and *SAW2* have a BELL domain that facilitates protein-protein interactions, and class I KNOX-type homeodomain proteins such as *BP* and *STM* have a MEINOX domain that allows interaction with other TALE proteins to control transcription. Members of the class I KNOX and BLH protein families heterodimerise in multiple combinations and form a closely linked transcriptional and post-translational regulatory network that controls maintenance and organisation of meristems and organ development during all stages of

post-embryonic plant development. One of their main functions is to keep stem cell populations in a pluripotent state and to prevent them from differentiation.

Heterodimerisation is crucial for the function of TALE proteins to determine subcellular localisation, target specificity and affinity, as shown for the interaction of STM with BLH proteins. STM has no nuclear localisation signal and relies on the interaction with BLH proteins harbouring a nuclear localisation signal to be localised in the nucleus (Cole et al., 2006). In addition, BLH proteins harbour nuclear export signal sequences within their BELL domain, which are recognised by nuclear export receptors. Co-localisation experiments suggested that the interaction of STM-BLH masks the nuclear export signal and localises the heterodimers to the nucleus where they can function as transcription factors (Cole et al., 2006). For example, in the inflorescence meristem, the interaction of STM with three BLH proteins, namely ATH1, REPLUMLESS (RPL), and POUNDFOULISH (PNF) has been studied in detail (Rutjens et al., 2009). The triple *ath1 rpl pnf* loss of function mutant, but none of the single or double loss of function mutants showed the *stm* loss of function phenotype of a depleted, prematurely determinate meristem, suggesting that STM function relies on the interaction with these BLH proteins that act redundantly. In addition, it has been shown that BP and RPL heterodimers function in internode patterning (Kanrar et al., 2006).

Far less is known about the protein-protein interactions of BEL1 and SAW2. Yeast two-hybrid assays have shown that BEL1 and SAW2 can form heterodimers with BP and STM (Reiser et al., 1995; Kumar et al., 2007) *in vivo*. Interaction of BEL1 with BP and STM was confirmed *in planta* by BIFC. Overlap between the expression patterns of *BEL1* and *STM* in the central zone of the inflorescence meristem and between *BEL1* and *BP* at the base of early floral meristems suggested that these TALE proteins can function together (Bellaoui et al., 2001). In particular, this has been supported by the *bel* mutant phenotype that showed a determinate inflorescence meristem, suggesting that the STM-BEL1 heterodimer contributes to the indeterminacy of wild-type inflorescence meristems (Bellaoui et al., 2001). However, this phenotype is variable and appears to depend on the *bel* allele (personal communication, Stefano Bencivenga).

STM has a broad function in establishing and maintaining stem cell populations. It is required for the establishment of the shoot meristem during embryogenesis and subsequent maintenance of all apical meristems (Long et al., 1996). Accordingly, *stm* loss

of function mutants fail to establish a pool of pluripotent stem cells in the early shoot apical meristem and consequently cannot develop beyond the seedling stage. *BP* is a close *STM* homolog and is expressed in the basal region of the vegetative shoot meristem and in the boundaries of the inflorescence meristems were it regulates initiation of floral meristems and the development of the stems and flower pedicels (Venglat et al., 2002). *BP* can also assume the role of *STM* in meristem and boundary maintenance (Byrne et al., 2002; Belles-Boix et al., 2006).

Functional analysis has shown that both STM and BP modulate hormone homeostasis in the meristem in order to maintain pluripotent stem cell populations. STM and BP promote high cytokinin levels and low gibberellic acid (GA) levels, which promote cell division and prevent cell elongation and differentiation, respectively. The cytokinin biosynthesis gene *IPT7* has been identified as a major target of STM and BP, and expression of the *IPT7* gene under the *STM* promoter partially rescued the *stm* loss of function phenotype (Yanai et al., 2005; Jasinski et al., 2005). Furthermore, ectopic expression of *STM* and *BP* resulted in ectopic expression of the cytokinin response factor *ARR5:GUS* reporter in lateral organ primordia, suggesting that ectopic KNOX gene expression leads to increased levels of cytokinin in organ primordia (Yanai et al., 2005). Conversely, it has been shown in several species that *KNOX* genes can repress the GA biosynthesis gene *GA 20-oxidase* (*GA20ox1*) (Sakamoto et al., 2001; Hay et al., 2002; Cheng et al., 2004). Activation of *35S:STM-GR* resulted in increased *GA2ox2* and *GA2ox4* expression levels, two genes involved in deactivation of GA, and in maize it has been shown that the KN1 (KNOTTED1) protein can directly bind to a *cis*-regulatory element of the *GA2ox1* promoter to promote deactivation of GA (Bolduc et al., 2009). In Arabidopsis wild-type plants, *GA2ox* genes were found to be expressed at the base of meristems at the boundary to organ primordia, suggesting that the expression of GA-deactivating *GA2ox2* and *GA2ox4* protects the meristem from GA influx from developing organ primordia (Yasinski et al., 2005). Expression of both *BP* and *STM* is excluded from founder cells and their absence in founder cells has been considered as the earliest marker for organ primordia formation in contrast to meristem cell identity (Smith et al., 1992; Long et al., 1996). As expected, overexpression of *BP* using the *35S* promoter had severe effects on lateral organ development: simple leaves were overall smaller in size and formed lobes in the basal serrations due to a lack of growth in the sinus. Flowers were

smaller with thinner sepals and narrow greenish translucent elongated petals (Chuck et al., 1996). More interestingly, fully functional inflorescence meristems formed from veins leading to the first basal lobe of cauline leaves that gave rise to wild-type flowers. In these ectopic meristems, *STM* was expressed once the meristem dome had been established, suggesting that ectopic *BP* expression is sufficient to initiate meristems in lateral organs (Chuck et al., 1996).

In summary, TALE proteins form a complex network promoting pluripotent, indeterminate meristematic cell behaviour. However, for organ development cells need to change their growth pattern and fate. Therefore, TALE proteins need to be tightly controlled during floral organogenesis. Accordingly, my initial expression array analysis revealed that *BEL1*, *BP* and, *STM* were repressed by JAG. Therefore, I characterised in detail the interaction between *JAG* and *BEL1, BP*, and *STM*, using qRT-PCR, RNA *in situ* hybridisation, reporter lines and reverse genetics. I also aimed to identify DNA binding sites of JAG in close vicinity to the *BEL1, BP* and *STM* loci. Subsequently, combined analysis of expression array and ChIP-Seq data confirmed that JAG directly repressed not only BEL1, but also further *BELL1-like homeodomain* (*BLH*) genes, including *SAWTHOOTH2* (*SAW2/BLH4*) (Kumar et al., 2007), *ATH1* and *REPLUMLESS* (*RPL*) (Gomez et al., 2005; Rutjens et al., 2009), in addition to the *class II KNOX* gene *KNAT4*. Furthermore, the combined ChIP-Seq and arrays data revealed that the regulation of *BREVIPEDICELLUS (BP)* and *SHOOTMERISTEMLESS (STM)* was indirect, and extended the interactions with JAG to a wider range of meristem regulatory genes apart from the TALE family.

4.2. Results

4.2.1. JAG represses *BEL1* and *BP*

Global expression profiling showed that *BP* and its interactor *BEL1* are both significantly (FDR<0.01) repressed by ectopic JAG activation. Because the ChIP-Seq data was not available at that point, I relied on the ectopic activation experiment using DEX treatment in the presence and absence of the protein synthesis inhibitor cycloheximide to filter for putative direct targets. Both *BP* and *BEL1* were also significantly repressed upon ectopic JAG activation in the presence of cycloheximide, suggesting that they were immediate transcriptional targets of JAG. Consistently, *BP* and *BEL1* were down-regulated

in the control treated *35S:JAG-GR* wild type L-*er* background compared with the control treated *jag-1* loss of function background, showing that both candidates are ectopically expressed in *jag-1*.

To confirm the global expression profiling data, I performed qRT-PCR on inflorescence apices tissue of wild-type plants harbouring the *35S:JAG-GR* construct. For ectopic JAG activation, the plants were subjected to a DEX treatment and ethanol-control treatment in the presence and absence of the protein synthesis inhibitor cycloheximide and incubated for 4 hours. Transcript levels of *BEL1*, *BP* and *STM* were significantly reduced upon ectopic JAG activation in the absence and presence of cycloheximide compared with the ethanol-treated controls. In addition, qRT-PCR results confirmed that mRNA levels for *BEL1, BP,* and *STM* were significantly increased in the *jag-2* mutant flower apices compared with the wild-type flower apices, suggesting ectopic expression of these genes in the *jag* mutant (Figure 4.1.).

4.2.2. *JAG* restricts the expression domains of *BEL1* and *BP* in early flower buds

To further verify that *BEL1, BP, and STM* were repressed and restricted to their wild-type expression domains by endogenous *JAG*, I performed RNA *in situ* hybridization comparing expression in wild-type and *jag-2* sections of early floral buds. Expression of *BEL1* was observed in the sepal primordia of *jag-2* buds, but not in the wild-type controls (Figure 4.2.A-B). In additon, I observed strong expression in developing ovules in wild-type and in *jag-2* buds, which served as a control for the known expression pattern of *BEL1* (Reiser et al., 1995) (Figure 4.2.C-D). For *BP*, the known expression pattern in flower pedicels and stems (Lincoln et al., 1994; Kumar et al., 2007) was comparable in wild-type and *jag-2* plants (Figure 4.2.E, F). In addition, *jag-2* buds showed ectopic expression at the base of organ primordia, which was particularly obvious in the emerging carpel primordia of stage 6 buds (Figure 4.2.E, F). For *STM,* I observed expression in the inflorescence and floral meristems of wild type and *jag-2* plants as previously reported (Long et al., 1996; Kumar et al., 2007). However, I did not observe consistent differences in expression domains between *jag-2* and wild type in early sepal primordia (data not shown).

Further evidence for ectopic expression of *BP* in the *jag-1* single mutant background was provided by a *pBP:GUS* reporter construct that was crossed into the *jag-1 Col*

background. A significantly stronger GUS signal was observed in young floral buds with the *pBP:GUS* reporter construct in the *jag-1* single mutant compared with the wild-type background (Figure 4.3.).

4.2.3. Effects of ectopic *BP* in the *jag-1* loss of function mutant flower

In the next step, I asked whether the ectopic *BP* expression observed in the early flower buds of the *jag* loss of function mutants had an effect on the flower phenotype. To investigate this, I generated a *bp jag-1* double loss of function mutant in *Col* background. In the *bp* mutant, internodes are compact and pedicels are shorter because of fewer cell divisions and the downwards-pointing flowers are generated by an asymmetric effect in the abaxial side compared to the adaxial side (Venglat et al., 2002). The *bp jag-1* double loss of function mutant showed an additive phenotype, with downwards-pointing pedicels (as typically observed in *bp* single mutants) and narrow and reduced sepals and petals (as observed in *jag* single mutants). No macroscopic rescue of the *jag-1* floral phenotype was observed at any developmental stage, suggesting that ectopic expression of *BP* is not the predominant cause for the defective organ outgrowth phenotype in the *jag-1* mutant (Figure 4.4.).

4.2.4. Endogenous JAG binds to promoter regions of *BEL1* but not *BP*

Results from expression arrays, qRT-PCR and RNA *in situ* hybridisation provided independent evidence that *BP* and *BEL1* were repressed by JAG. In the next step, I aimed to identify *in vivo* binding sites of JAG in the promoter regions of *BP* and *BEL1* by ChIP.

Previously, I identified a DNA binding site 1.877 kb upstream of the *BEL1* start codon using *35S:JAG-GR* line combined with anti GR-antibodies (Figure 4.5.).This binding site coincided with one of the peaks produced in the ChIP-Seq analysis (Figure 4.6.A) and was confirmed by an independent ChIP q-PCR experiment using *pJAG:JAG-GFP* apices (Figure 4.6.B). In addition, JAG bound to the second intron of the *BEL1* gene (Figure 4.6.A). By contrast, I did not observe any enriched DNA-binding sites within the 3 kb upstream and 1.5 kb downstream region of *BP* for JAG-GFP under its endogenous promoter, suggesting that although *BP* may be a direct target of ectopically expressed JAG (Figure 4.7.), it rather appears to be an indirect target of the endogenous JAG in its normal expression domain. For example, JAG may indirectly regulate *BP* by the TALE protein *SAWTOOTH2 (SAW2)* that has been reported to repress the meristem identity gene *BP* in organ

primordia (Kumar et al., 2007) and was identified as a directly activated ChIP target by JAG (Chapter 3). For *STM*, a similar indirect transcriptional effect of JAG, possibly via TALE proteins, can be hypothesised.

4.2.5. ChIP-Seq revealed that JAG directly targeted additional genes involved in meristem organisation

The combined expression array and ChIP-Seq analysis described in Chapters 2 and 3 revealed that JAG repressed several additional genes involved in meristem development. For example, JAG directly represses the floral meristem regulator *LEAFY (LFY)* (Weigel et al., 1992; William et al., 2004) and its direct targets *LATE MERISTEM IDENTITY 1* (*LMI1*) (Saddic et al., 2006) and *LATE MERISTEM IDENTITY 2 (LMI2)* (Pastore et al., 2011) (Figure 4.8.A-D). Both *LMI1* and *LMI2* have been shown to interact with *LFY* to promote expression of downstream floral meristem identity regulators. While *LMI1* has been shown to be able to directly bind and activate *CAULIFLOWER* (*CAL*) but not *APETALA1* (*AP1*) in a ChIP experiment, *LMI2* specifically promotes *AP1* expression (Saddic et al., 2006; Pastore et al., 2011).

Interestingly, loss of *LMI1* function in a weak *lfy* allele background also increases the numbers of floral bracts, suggesting a role for *LMI1* in suppression of bract formation (Saddic et al., 2006). Ectopic bract formation has also been observed in the *JAG* gain-of-function allele *jag-5D* (Dinneny et al., 2004), suggesting that ectopic repression of *LMI1* by ectopically expressed *JAG* could at least in part be the cause for ectopic bract formation. Apart from floral meristems and early floral primordia, *LMI1* is also expressed in the margins of sepals, petals and leaves. Leaves of the *lmi1* mutant have deep lobes, a phenotype that is reminiscent of the ectopic expression of the *Class I KNOX* gene *BP*. Consistently, *lmi1* leaves were reported to ectopically express *BP* (Saddic et al., 2006), suggesting that *LMI1* is involved in the regulation of the meristem identity gene *BP* in leaves. In my experiments, repression of *LMI1* by ectopic *JAG-GR* activation in inflorescences was further confirmed by qRT-PCR. Additionally *LMI1* showed ectopic expression in *jag-1* mutant compared to wild-type inflorescences (Figure 4.8.D).

JAG also directly repressed another floral meristem identity regulator downstream of *LFY*, the MADS BOX transcription factor *SHORT VEGETATIVE PERIOD (SVP)* (Gregis et al., 2008 and 2009). *SVP* functions together with *AGAMOUS-LIKE 24* (*AGL24)* to act

redundantly with *AP1* and *CAL* in floral meristem formation, for example the *ap1 svp agl24* triple mutant mimics the *ap1 cal* mutant in the inability to form floral primordia, consisting only of inflorescence meristems (Gregis et al., 2009). In this context, it was also shown that the MADS box transcription factor *SUPRESSOR of CO1* (SOC1), which is also bound *in vivo* by JAG, can resume the function of *SVP* and *AGL24* in floral meristems in their absence (Gregis et al., 2009).

Furthermore, JAG directly repressed genes involved in the regulation of meristem organisation and size. For example *CLAVATA1 (CLV1)* (Figure 4.8.E) (Clark et al., 1997; Schoof et al., 2000), which acts in the *CLAVATA*-*WUSCHEL* pathway to control meristem size, was directly repressed upon *JAG-GR* activation and ectopically expressed in the *jag-1* mutant in the expression array and in the independent qRT-PCR experiment. Closely related to *CLV1*, two members of *BARELY ANY MERISTEM* (*BAM*) receptor kinase-like family *BAM1* and *BAM2* are direct targets of JAG, and *BAM3* is indirectly down-regulated. BAM1 and BAM2 are expressed in the flanks of shoot and floral meristems and in primordia of leaves, sepals, and petals (DeYoung et al., 2006). Loss of *BAM1* and *BAM2* function caused a decrease in shoot and floral meristem sizes, suggesting that both genes have opposite functions to *CLV1* in meristem size regulation (DeYoung et al., 2006). In addition, *bam1 bam2* double loss of function mutants developed smaller asymmetric leaves with defects in vein formation and curled margins, and floral organs showed growth defects similar to the *jag* loss of function mutant with the gynoecia protruding from unopened flower buds and reduced size of mature petals (DeYoung et al., 2006), suggesting that BAM1/BAM2 play a role in promoting organ development.

In respect to the transition from meristem to founder cell identity, JAG directly targeted the *GRAS* transcription factor *LOST MERISTEMS 1* (*LOM1*) (Figure 4.8.F), which is expressed at the meristem flanks specifically at the boundary to organ primordia. There, it promotes the transition of cells from the peripheral meristem zone into organ primordia. In the *lom1* mutant the vegetative shoot and inflorescence meristems increased in width, became flatter, produced significantly fewer primordia and terminated earlier than in the wild type. In the *lom1* mutant, the shoot apical meristem develops several additional sub-epidermal layers due to changes in cell division patterns. Using *ANTEGUMENTA (ANT)* expression as a marker for founder cell identity it was shown that stem cells over-proliferate in the peripheral zones, acquire founder cell identity but

fail to be recruited into initiating organ primordia, suggesting that *LOM* promotes cell differentiation at the transition from founder cells to organ primordia identity (Schulze et al., 2010).

4.3. Discussion

4.3.1. Wider implications of the interactions between JAG and members of the TALE protein family

One of the key functions of JAG is to facilitate the transition from a meristem to a primordium cell behaviour (Schiessl et al., 2012). As described above, TALE proteins form a regulatory network that promotes meristem development and sustains a pluripotent stem cell population. In this context, I showed that JAG indirectly represses the *KNOX* genes *BP* and *STM*, while the *BLH* gene *BEL1* is directly repressed by JAG. All three genes were ectopically expressed in the inflorescences of the *jag* loss of function mutants. For *BP* and *BEL1* we could show ectopic expression specifically in floral primordia of the *jag* mutant compared to wild type by *in situ* hybridisation and by using a *BP:GUS* reporter construct. Because plants with ectopic BP expression (*35S:BP)* showed a green inflorescence phenotype and lobed serrated leaves (Chuck et al., 1996) I speculated that ectopic *BP* expression would at least in part be the cause for the *jag* floral phenotype. However, I did not observe rescue of the *jag* loss of function phenotype in the *jag bp* double mutant. This suggested that *BP* is not the primary cause for the *jag* loss of function phenotype and that there is possibly functional redundancy with other *KNOX* genes, for example, its closest homolog *STM*.

A regulatory interaction similar to *JAG* and *BP* was observed between BP and the *BLH* genes *SAW1* and *SAW2,* which are the closest homologs to *BEL1* and whose protein products interact with the BP and STM proteins (Kumar et al., 2007). In contrast to *BEL1,* which is expressed in meristems and is directly repressed by JAG, *SAW2* is absent from meristems but expressed in organ primordia and is directly activated by JAG. *BP* was ectopically expressed in leaves and inflorescences of the *saw1 saw2* double mutant, which shows an increased number of leaf serrations. But as seen for *bp jag-1*, in the *saw1 saw2 bp* triple loss of function mutant no rescue of the phenotype was observed, suggesting that even if *JAG* repressed *BP* indirectly via direct activation of *SAW2* there

would still be redundancy due to *mis*-expression of other KNOX genes such as *STM*. In this respect, ectopic expression of *SAW1* caused the same floral phenotype as the mild *stm* loss of function mutant of fused sepals and petals, suggesting that *SAW1* and *SAW2* are able to repress *STM* in lateral organs (Kumar et al., 2007). I have not tested the transcript levels of *STM* and the other Class I KNOX genes such as *KNAT2* and *KNAT6* or Class II KNOX genes in the *bp jag* double mutant. The Class II *KNOX* gene *KNAT4* is directly down-regulated by JAG (see Chapter 3), although *KNAT*2 and *KNAT6* do not appear to be directly or indirectly targeted by JAG.

In addition, *BP* is under transcriptional regulation by several organ-specifying genes, for example the Myb domain transcription factor *AS1* and lateral organ boundaries domain (LOB) protein *AS2*, which both are repressed by STM in the meristem (Byrne et al., 2000; 2002). Consequently, repression of *STM* in the founder cells promotes *AS1* and *AS2* expression in incipient leaf and floral primordia, where both genes act together to repress *BP* (Ori et al., 2000; Byrne et al., 2002; Guo et al., 2008 and Ikezaki et al., 2009). Ori et al (2000) showed that *as1* and *as2* mutants show ectopic expression of *BP* but not *STM* in primordia. In *as1* and *as2* flowers, buds opened prematurely, sepals and petals were shorter and curved outwards (Ori et al., 2000). Interestingly, *as1 as2 bp1* triple mutants have additive phenotypes with reduced narrow sepals and petals, suggesting that also in the *as1 as2* mutant context ectopic *BP* expression is not the single cause for the reduced defective flower phenotype. Furthermore, Xu et al. (2008) reported additive and more severe phenotypes for *as1 jag* and *as2 jag* double mutants compared to either single mutant with severely reduced filamentous sepals and petals, suggesting that *JAG* and *AS1/AS2* act in parallel regulatory pathways to promote floral organ development. It has also been shown that *AS1/AS2* and *SAW1/ SAW2* act in parallel pathways to repress *BP*, because the double mutant appeared to have deeper lobes at the serrations, suggesting an additive effect (Kumar et al., 2007).

In the case of the *as1*, there is evidence that *BP*, and the other Class I *KNOX* genes *KNAT2* and *KNAT6* act redundantly in repressing GA biosynthesis. In *as1* mutants, *GA 20-oxidase1* (*GA20ox1*) transcript levels were decreased to 50% of the wild-type expression, while introducing loss of *BP1*, *KNAT2* and *KNAT6* together restored *GA20ox1* expression to wild-type levels, suggesting that these three Class I *KNOX* genes act redundantly to repress GA biosynthesis (Ikezaki et al., 2009). Furthermore, it has been shown that *KNAT2*

and *KNAT6* were ectopically expressed in the *bp* loss of function mutant (Ragni et al., 2008), suggesting that there is regulatory interaction between *BP*, *KNAT2* and *KNAT6*.

The regulatory function of STM in repressing *AS1* and *AS2* in the meristem and its repression in founder cells raises the question of what represses *KNOX* genes in the founder cells at first place. In shoot apical meristems, organ primordia are positioned by auxin maxima generated via local polar auxin transport in the peripheral zones of the floral meristems, involving the activity of the polar efflux carrier PIN1 and its interacting protein kinase PINOID (PID) (Benkova et al., 2003). Once the position of the incipient organ is established, meristem cells need to terminate meristem cell identity and acquire the identity of organ primordium cells. Evidence for an interaction between *KNOX* genes and auxin patterning came from the phenotype of the *pin1 bp* double mutant, where loss of *BP* function in the *pin1* mutant background partially rescued organ initiation at the boundaries of the shoot apical meristem (SAM). Conversely, a decrease in *PIN1* expression caused ectopic expression of *KNOX* genes (Hay et al., 2006), suggesting that repression of *KNOX* genes in the founder cells could be directly caused by auxin maxima.

In line with this hypothesis, it has been shown that mutations in the *AUXIN RESPONSE FACTORS (ARF) ARF6* and *ARF8* caused ectopic expression of *KNOX* genes and defects in floral organogenesis (Tabata et al., 2010). In the *arf6 arf8* double mutant, perianth organs do not elongate, some floral buds arrest closed with immature reproductive organs and with the stigma protruding. More interestingly, petals of the *arf6 arf8* double mutant show defects in vein formation and in the differentiation of the conical cells in the distal petal region, petal phenotypes reminiscent of the *jag* loss of function mutant (Dinneny et al., 2004; Ohno et al., 2004; Chapter 6) and of the *35S:BP* line (Chuck et al., 1996). Loss of *BP* or *STM* function in the *arf6 arf8* double mutant in part suppressed the double mutant flower phenotype and, in particular, rescued the conical cells in the distal petal region (Tabata et al., 2010). In this context, it would be very interesting to investigate to what degree the regulatory effect of JAG in targeting genes involved in auxin biosynthesis genes and auxin response (Chapters 3 and 8) serves the purpose of indirectly down-regulating *KNOX* genes in early stages of organogenesis. Interestingly, JAG directly binds to promoter region of *miR167*, which directly targets *ARF6* and *ARF8* (Chapter3).

In relation to hormone homeostasis, *BEL1* has recently been linked to hormonal effects in ovule development. In the ovule primordia, *BEL1* is activated by WUSCHEL (WUS) and

restricted to the central zone by endogenous cytokinin, where it has been shown to restrict the expression of the auxin efflux carrier PIN1 (Bencivenga et al., 2012). *BEL1* could have a similar function in the inflorescence and floral meristem and the early depletion of the inflorescence meristems in the *bel* mutant (Bellaoui et al., 2001) could be caused by ectopic PIN expression and down-regulation of *KNOX* genes. On the other hand, ectopic expression of BEL1 in emerging floral organ primordia could influence PIN1 expression and polar auxin localisation. In particular, defects in vein formation, as observed in the *jag* mutant, the *arf6 arf8* double mutant and in the *35S:BP* line, have been linked to defects in auxin dynamics (Tabata et al., 2010; Chuck et al., 1996). Antagonistic interactions between cytokinin, auxin and GA in meristem development have been reported: exogenous cytokinin application could partially rescue the *stm* mutant phenotype, but this effect was diminished by co-application of GA and auxin (Yanai et al., 2005).

As mentioned above, *KNOX* genes promote a low cytokinin to gibberellic acid ratio allowing for cell elongation and cell differentiation. It is interesting to note that JAG directly targets genes involved in cytokinin activation, for example several members of the *LONELY GUY* family (Kuroha et al., 2009) and that JAG directly up-regulated the GA deactivating enzyme *GA2ox1*. Another interesting group of genes closely related to the functional network of TALE proteins and related to GA levels is the plant specific family of OVATE proteins. JAG directly targets several members of the *OVATE* family, whose protein products negatively regulate *KNOX* gene activity by relocating the complexes from the nucleus to the cytoplasm (Hackbusch et al., 2005). In a large-scale yeast two-hybrid and BIFC screen, BEL1 interacted with OPF1, OPF4 and OPF5, and in particular, BEL1, SAW2 (BLH4) and OPF5 were part of a highly interconnected group of TALE and OVATE proteins (Hackbusch et al., 2005). OVATE proteins share an OVATE domain for protein-protein interaction and a nuclear localisation signal. Co-localisation experiments with BLH-RFP fusion proteins and OFP1-GFP in tobacco leaves showed that the otherwise nuclear-localised BLH-RFP fusion proteins localised to the cytoskeleton in the cell periphery in the presence of OFP1-GFP activity (Hackbusch et al., 2005). Providing further support to the hypothesis of post-translational modification, the expression levels of TALE proteins were not changed but the expression levels of *Ga20ox1* was severely decreased in the plants over-expressing OPF1 (Hackbusch et al., 2005). Accordingly, OVATE proteins,

in particular OFP1, have been identified as a transcriptional repressor and ChIP experiments identified *Ga20ox1* as a direct target of OFP1 (Wang et al., 2007and 2011). Ectopic expression of *OPF1* (Hackbusch et al., 2005) and a dominant gain of function mutant of *OFP1* (Wang et al., 2007) showed similar phenotypes, with reduced length of all aerial organs including floral organs with styles protruding from the closed young buds and overall stunted plants with thick stems, due to reduced cell elongation. In the dominant negative mutant, application of exogenous GA in part rescued the phenotypic effects, suggesting that alterations in GA levels are, at least in part, the cause for the ectopic *OPF1* phenotype (Wang et al., 2007). Because no DNA binding domain was identified in the OFP1 protein, it was further suggested that BP and OFP1 act as a complex to directly bind to the promoter region and the second intron of *Ga20ox1* (Wang et al., 2011).

4.3.2. JAG directly targeted genes at the interface between meristem and organ identity

Floral organogenesis does not only require repression of meristem identity, cells also need to acquire founder cell identity and subsequently primordia cell identity. In this context, JAG directly targeted *BAM1/BAM2* that are involved in regulation of the peripheral meristem zones and *LOM*, which is required for the transition from founder cell to primordium cell identity. All three genes have been identified as direct ChIP-Seq targets of JAG, however, in contrast to the TALE proteins, no significant changes in gene expression were detected. Expression of these genes is restricted to only a few cells in the very early stages of organ development and may therefore be diluted in a global expression array using inflorescence apices. However, in order to study the early effects of JAG at the interface of founder cell recruitment into incipient organ primordia, it would be interesting to follow the expression patterns of *LOM* by RNA *in situ* hybridisation or *in vivo* via a *LOM:GFP* reporter line.

Specific for floral organ development, JAG directly repressed the floral meristem identity genes *LFY, BOP1/2, LMI1, LMI2*, and *SVP* (Weigel et al., 1992; Ha et al., 2003; Saddic et al., 2006; Pastore et al., 2011; Gregis et al., 2008 and 2009) (Figure 4.8. A-D, F). This is further supported by the fact that ectopic expression of *JAG* in the inflorescence meristem can promote primordium cell behaviour over meristem cell behaviour which leads to outgrowth of ectopic bracts at the expense of floral primordia. The fact that

ectopic *JAG* can induce floral bracts at the expense of floral organ primordia could be interpreted as further support for the hypothesis that *JAG* is required to promote primordium cell behaviour over meristem cell behaviour, but that in the case of bracts, *JAG* is not only required but even sufficient for organ outgrowth. It has been previously shown that *BOP1/2* repress *JAG* (Norberg et al., 2005), while *JAG* was not found among the direct ChIP targets of LEAFY by Winter et al. (2011), suggesting that *BOP1/2* are the predominant repressors of *JAG* in the inflorescence meristem to promote floral meristem identity in the floral buds.

With these new candidates in mind, it would be interesting to investigate the effects of organ primordia formation on the cellular behaviour of floral meristems in particular in the peripheral zones. Therefore, the 3D imaging and analysis of cell geometry (as described in Schiessl et al., 2012 and in the Chapters 6 and 7) could be extended to early floral primordia (stage 1 and 2). Furthermore, it would be interesting to study the cellular processes in the incipient floral organs as early as stage 2. However, future investigations may be complicated by the fact that *JAG* and *NUB* have been shown to act redundantly in the regulation of bract formation and repression of *BOP1/2*. In this context, Norberg et al. (2005) showed that the *bop1 bop2 jag* triple mutant still produced floral bracts, suggesting that *JAG* and *NUB* act redundantly in promoting floral bract formation. Similarily, no significant differences in expression levels of *BOP1* and BOP2 were found in response to changes in JAG function, further suggesting that *JAG* and *NUB* function redundantly to repress *BOP1/2* (Norberg et al., 2005). While the question of redundancy between *JAG* and *NUB* could easily be addressed in future work, this could not be resolved by Norberg et al. in 2005, because no *nub* loss of function mutants had been identified back then.

In summary, I confirmed that JAG represses several key regulators of meristem organisation and meristem maintenance. Thus, JAG is one of the key regulators of this complex regulatory framework that defines pluripotent stem cell identity and meristem development. With this work I provided molecular evidence for the hypothesis, originally derived from quantitative 3D imaging, that JAG is required for the transition from a meristematic to primordium cell behaviour (Schiessl et al., 2012). It would be interesting to clarify the exact timing and the exact number and position of cells expressing JAG in

early primordia development by live 3D cell-tracking combined with reporter lines, to obtain high resolution data that can place JAG function in the order of events of early floral organogenesis. Furthermore, I also provided molecular support for previously reported genetic interactions, for example, that *JAG* acts in a similar pathway as other organ specifying genes such as *AS1* and *AS2* (Xu et al., 2008). In particular, considering that TALE proteins have been shown to predominantly function via regulation of hormone homeostasis, it will be interesting in the future to link direct and indirect targets of JAG involved in the biosynthesis, degradation and perception of auxin, cytokinin and gibberellins to the regulation of TALE proteins and the early transition from a meristematic to a primordium cell behaviour.

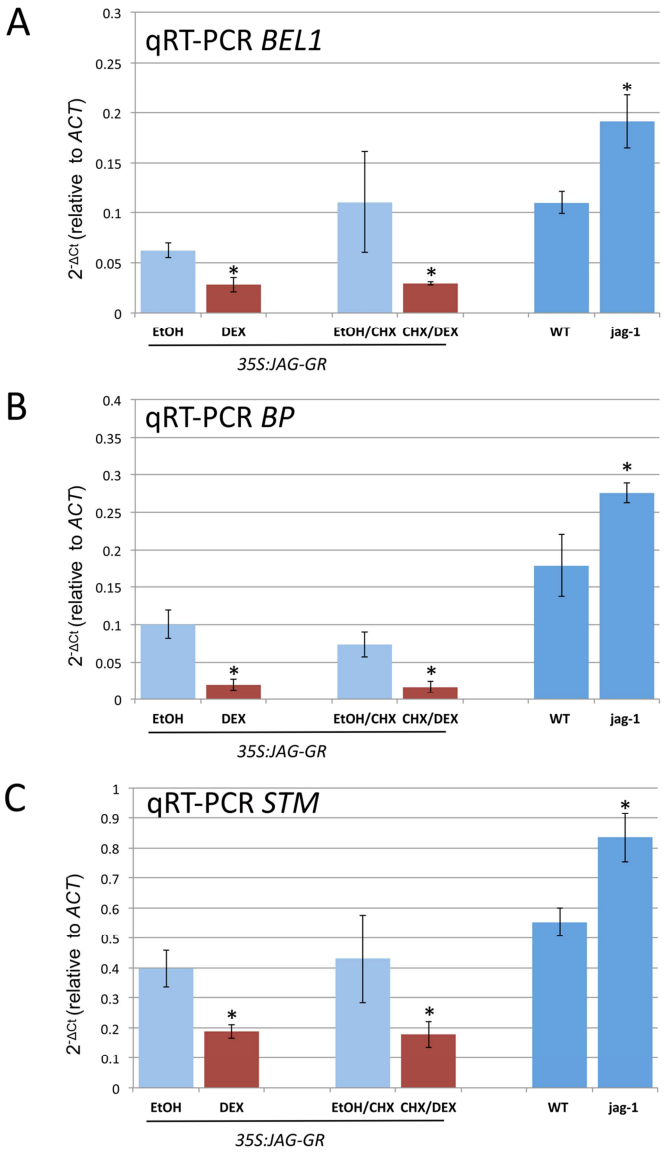

Figure 4.1. JAG represses *BEL1*, BP and STM. Expression levels (relative to the *ACT2* constitutive control) of *BEL1* (A), *BP* (B) and *STM* (C) mRNA measured by qRT-PCR in inflorescence apices of *35S::JAG-GR* plants 4h after mock treatment (light blue) or treatment with dexamethasone 10 µM (red); CHX indicates samples from plants that were also treated with cycloheximide 10 µM or untreated wild-type (WT) and *jag-1* plants (dark blue); bars show the average and standard deviation of three biological replicates; asterisks indicate statistically significant differences (unpaired two-sample Student's *t*-test, $p < 0.05$) between dexamethasone-treated samples and corresponding controls or between the untreated wild type and *jag-1* (dark blue bars).

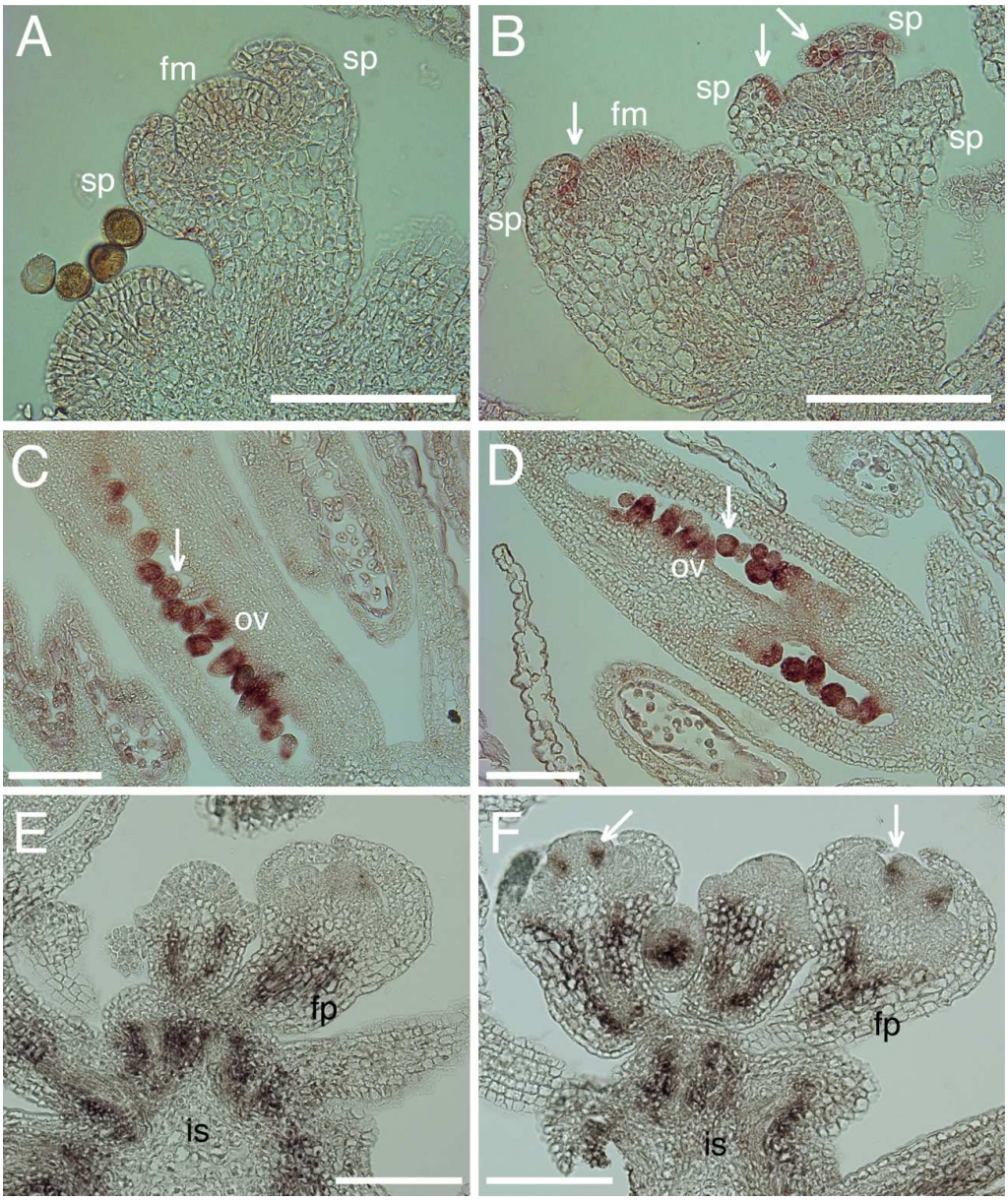

Figure 4.2. RNA *in situ* hybridization showing that *BP* and *BEL1* are ectopically expressed in *jag-2*. Floral meristem: fm; sepal primordium: sp; inflorescence meristem: im; inflorescence stem: is; flower pedicel: fp; ovules: ov; Scale bars: 100 µm.
(A-D) Sections through wild-type (A,C) and *jag-2* (B,D) inflorescence apices hybridized with *BEL1* antisense probe; arrows indicate ectopic *BEL1* expression in *jag-2* sepal primordia (B); arrows in sections through carpels indicate *BEL1* expression in developing ovules (as reported first by Reiser et al., 1995) (C-D).
(E,F) Sections through wild-type (E) and *jag-2* (F) floral buds hybridized with *BP* antisense probe; arrows indicate ectopic *BP* expression in sepal primordia and in carpel primordia (F).

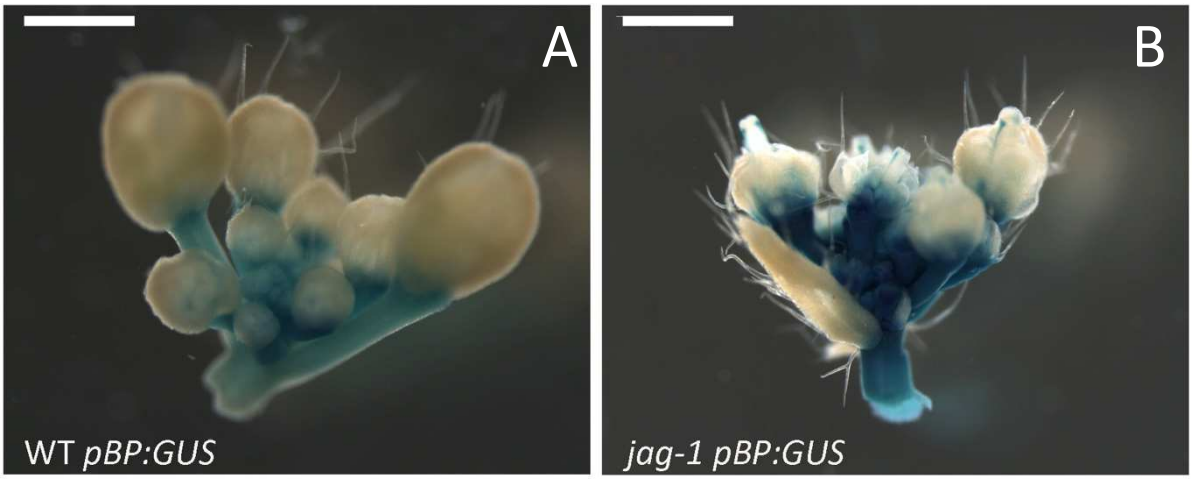

Figure 4.3. Ectopic expression of BP in *jag-1* loss of function mutant and wild-type. Scale bars: 500 µm; *pBP::GUS* in Col-0 wild-type background (A) and *jag-1* Col-0 loss of function background (B) In comparison wild-type where BP expression was restricted to the pedicel and the base of young floral buds. (A), a stronger signal was observed at the base of young *jag-1* floral buds extending into the developing floral organs of (B).

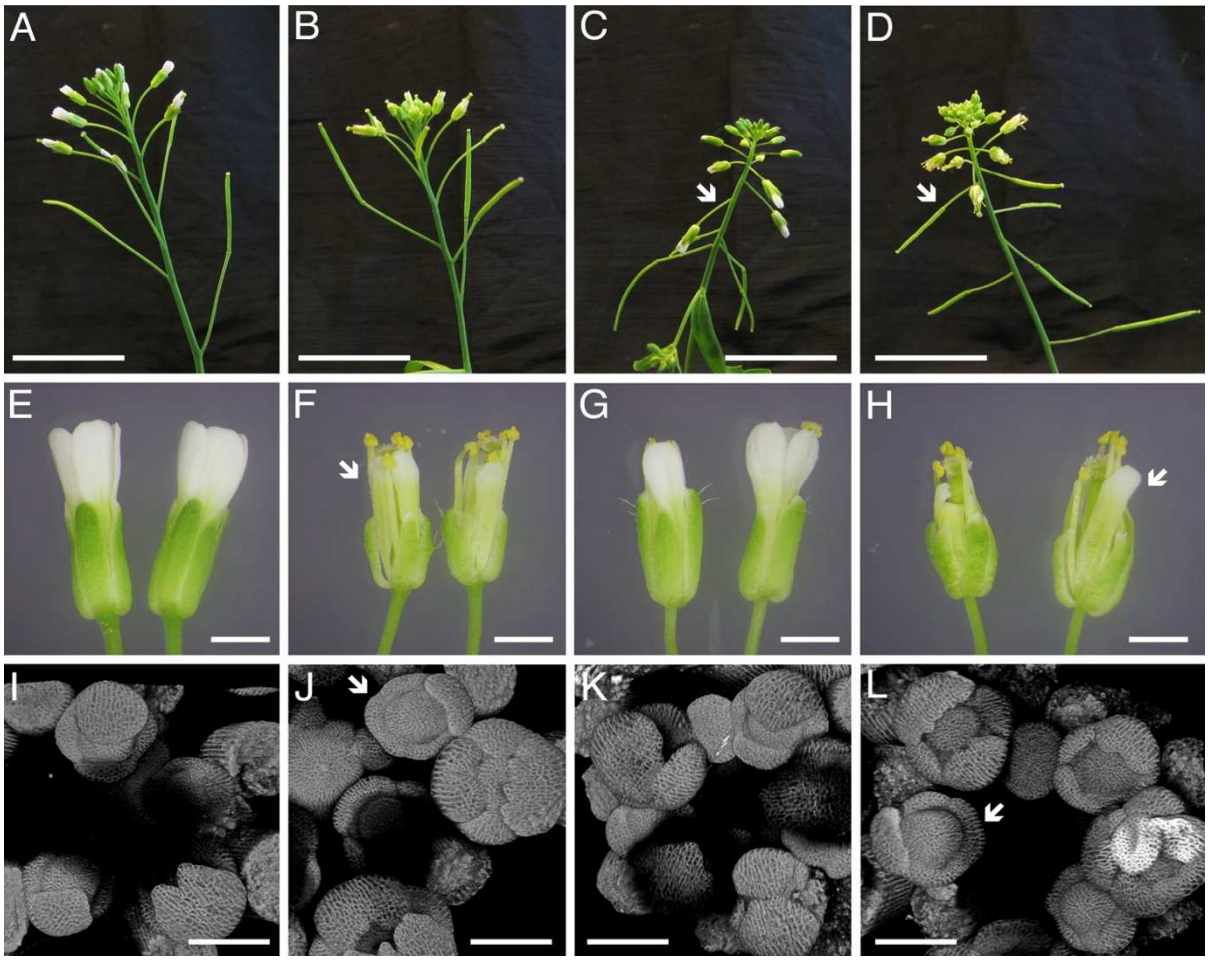

Figure 4.4. Additive phenotypes of the *jag bp double* mutant.

Scale bars: 1 cm (A-H); 1 mm (E-H), 100 µm (I-L).

(A,E,I) Wild-type (Col); (B,F,J) *jag-1*; (C,G,K) bp; (D,H,L) *jag-1 bp*.

(A-D) Inflorescence apices; arrows indicate the downward-pointing pedicels typical of *bp*.

(E-H) Close-up of mature flowers; arrows indicate the defective perianth growth characteristic of *jag* mutants, with narrow sepals and petals which show reduced distal outgrowth.

(I-L) 3-D reconstruction of confocal images of young floral buds; arrows point at buds with the defective sepal primordia characteristic of *jag* mutants.

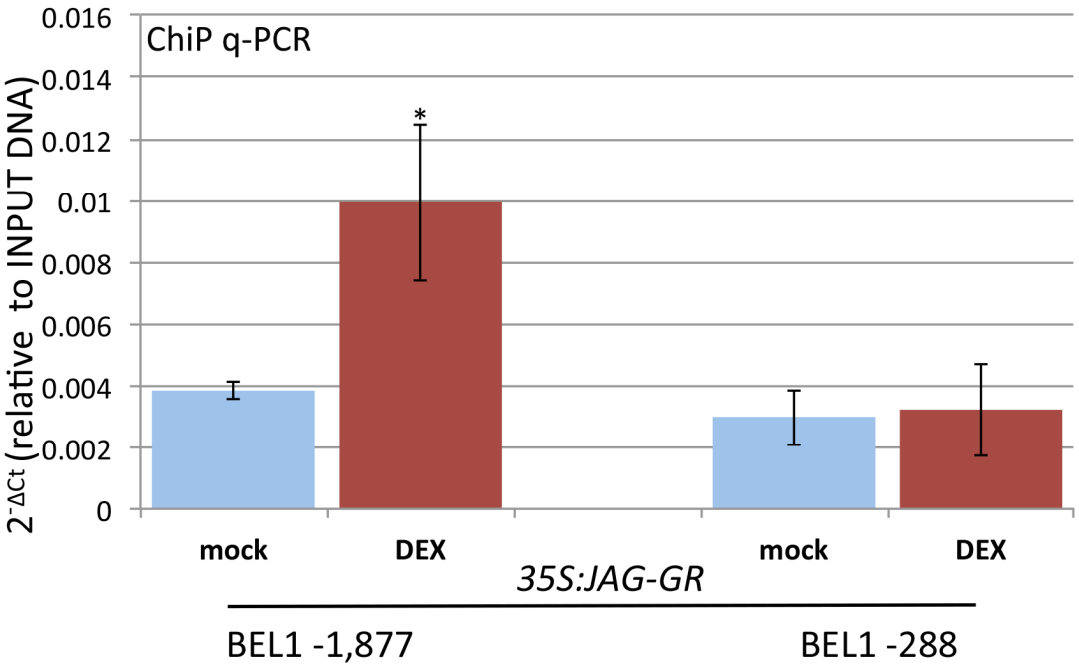

Figure 4.5. Ectopic JAG-GR binds to the promoter region of *BEL1*.

Chromatin immunoprecipitation (ChIP) using anti-GR antibodies and inflorescence apices of *35S::JAG-GR* plants 4 h after mock treatment (light blue) or treatment with dexamethasone 10 µM (red); target sequences 1.9 or 0.3 Kb upstream of the *BEL1* transcriptional start; bars show the average and standard deviation of three biological replicates; numbers below the bars indicate the left border of the q-PCR amplicon relative to the coding sequence; asterisks indicate significant difference to the mock control ($p < 0.05$, Student's *t*-test).

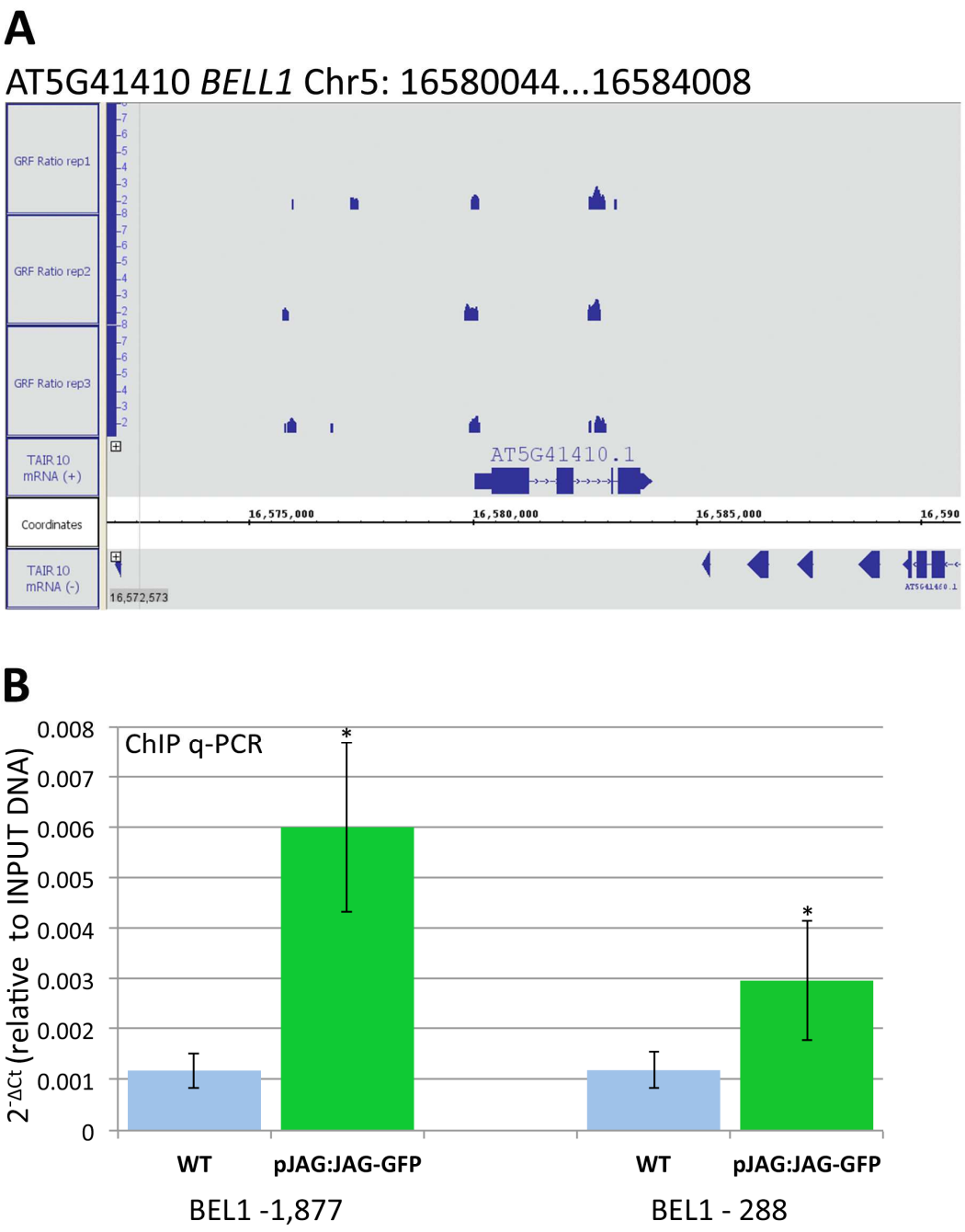

Figure 4.6. Endogenous JAG-GFP directly binds within and upstream of the *BEL1* gene locus. (A) Visualisation of read enriched regions mapping to the TAIR10 Arabidopsis reference genome (x-axis) using the Integrated Genome Browser (Nicol et al., 2009), ChIP-Seq peak score values (y-axis) based on the ratios of normalised reads between JAG-GFP and control samples were calculated for every single nucleotide position using CSAR software (Muiño et al., 2011a), the maximum score value within the candidate peaks was used to test for significance of the enrichment; ChIP-Seq peaks detected in each replicate within 3 kb upstream and 1.5 kb downstream of the coding sequences for the *BEL1* locus

on chromosome 5. (B) Binding of JAG-GFP to the upstream region of *BEL1* confirmed by ChIP-qPCR; target sequences 1.9 or 0.3 Kb upstream of the *BEL1* transcriptional start; bars show the average and standard deviation of three biological replicates; numbers below the bars indicate the left border of the q-PCR amplicon relative to the coding sequence; asterisks indicate significant difference to the negative WT control ($p < 0.01$, Student's *t*-test).

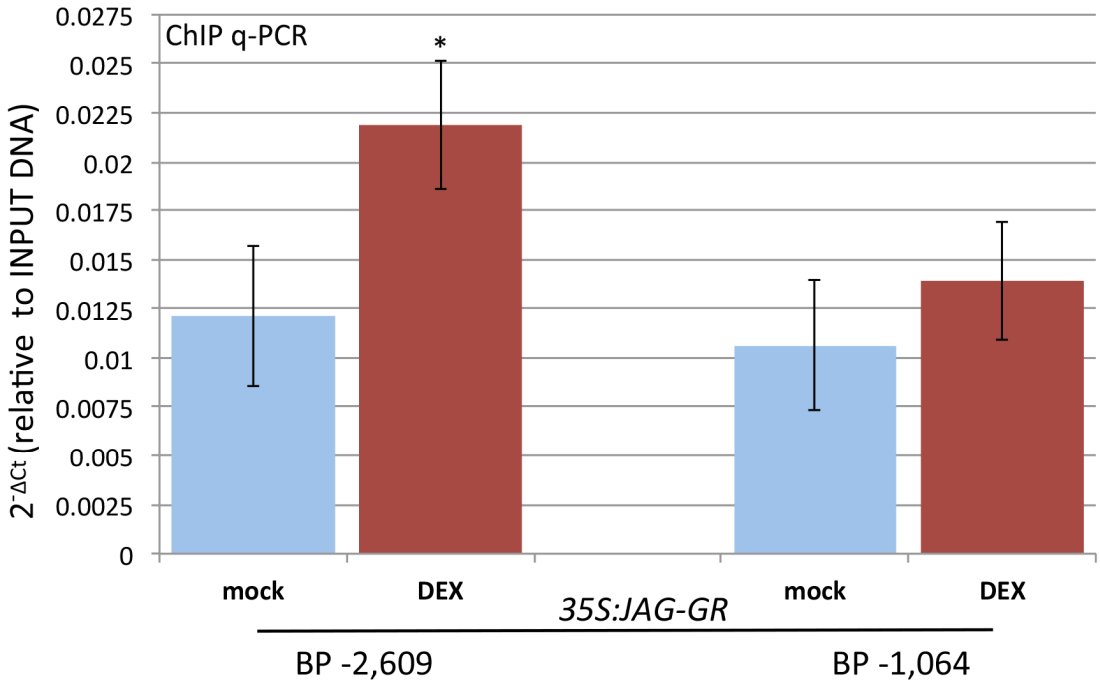

Figure 4.7. Ectopic JAG-GR binds in the promoter region of BP.

Chromatin immunoprecipitation (ChIP) using anti-GR antibodies and inflorescence apices of *35S::JAG-GR* plants 4 h after mock treatment (light blue) or treatment with dexamethasone 10 µM (red); target sequences 2.6 and 1.1 Kb of upstream of the *BP* transcriptional start; bars show the average and standard deviation of three biological replicates; numbers below the bars indicate the left border of the q-PCR amplicon relative to the coding sequence; asterisks indicate significant difference to the mock control ($p < 0.05$, Student's *t*-test).

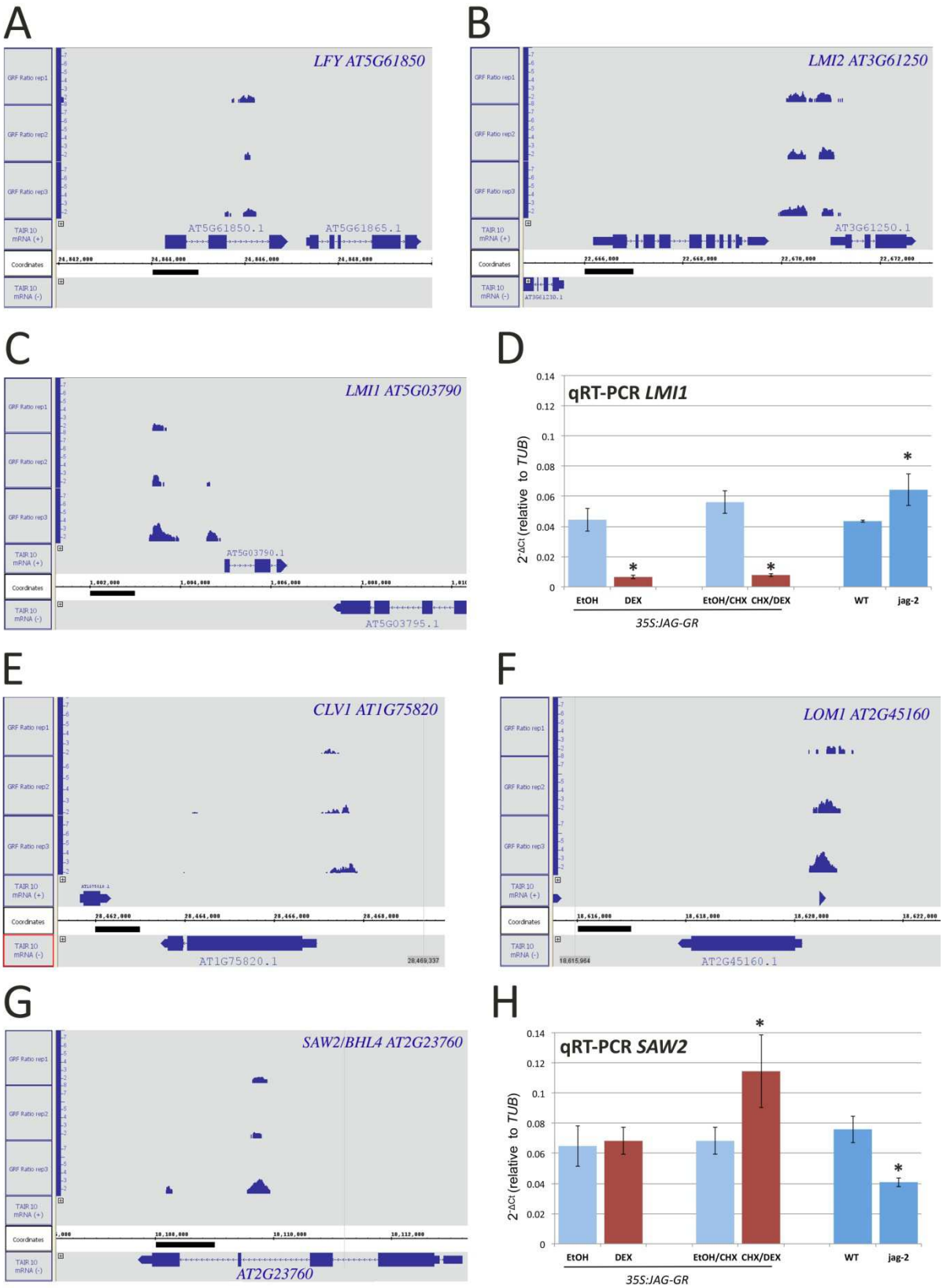

Figure 4.8. JAG directly represses genes involved in meristem organisation.

(A-C, E-G) Visualisation of read enriched regions mapping to the TAIR10 Arabidopsis reference genome (x-axis) using the Integrated Genome Browser (Nicol et al., 2009), ChIP-Seq peak score values (y-axis) based on the ratios of normalised reads between JAG-GFP and control samples were calculated for every single nucleotide position using CSAR software (Muiño et al., 2011a), the maximum score value within the candidate peaks was used to test for significance of the enrichment; ChIP-Seq peaks detected in each replicate within 3 kb upstream and 1.5 kb downstream of the coding sequences for the loci of LFY (A), *LMI2* (B)*, LMI1* (C), *CLV1* (E) *LOM1* (F) and *SAW2* (G); (D, H) Expression levels (relative to the *TUB4* constitutive control) of *LMI1* (D) and *SAW2* (H); mRNA measured by qRT-PCR in inflorescence apices of *35S::JAG-GR* plants 4h after mock treatment (light blue) or treatment with dexamethasone 10 µM (red); CHX indicates samples from plants that were also treated with cycloheximide 10 µM or untreated wild-type (WT) and *jag-2* plants (dark blue); bars show the average and standard deviation of three biological replicates; asterisks indicate statistically significant differences (unpaired two-sample Student's *t*-test, $p < 0.05$) between dexamethasone-treated samples and corresponding controls or between the untreated wild type and *jag-2* (dark blue bars).

Chapter 5 - JAG directly targets boundary specifying genes and organ growth regulatory genes

5.1. Introduction

JAG has been identified as a direct downstream target of the floral organ identity genes *SEPALATA3* (*SEP3*)*, APETALA3/PISTILATA* (*AP3/PI*), and *AGAMOUS* (*AG*) (Dinneny et al., 2004; Ohno et al., 2004; Gomez et al., 2005; Kaufmann et al., 2010, Wuest et al., 2012) and is strongly expressed in early organ primordia (Dinneny et al., 2004; Chapter 3, Figure 3.8.), suggesting that JAG acts as a growth promoting transcription factor during early organogenesis, once organ identity has been established in the founder cells. In Chapter 4, I showed that JAG represses meristem organisation genes in order to promote the transition from meristematic cell behaviour to primordium growth behaviour in early organogenesis. Subsequently, organ boundaries, organ growth axes, local growth rates, and cell identities have to be established in order to allow organs to develop to a final specific size, shape and function. Because *JAG* is expressed throughout organ development and acts as an upstream growth regulator, I expected that JAG would target genes related to these functions. In this context, my initial global expression array analysis (Chapter 2) identified the boundary specifying gene *PETAL LOSS (PTL)* as a high-confidence directly repressed target of JAG.

The trihelix transcription factor *PTL* has been characterised to function as a boundary specifying gene in early sepal and petal development, specifically repressing growth in the boundaries between sepals (Griffith et al., 1999; Brewer et al., 2004). In detail, it has been shown that in stage 4 buds of the *ptl* loss of function mutants, the width of inter-sepal zones is enlarged by almost 40% compared to the wild-type, while other parameters such as overall bud diameter and meristem diameter were not significantly different. In addition, it has been shown that the increase in radial intersepal zone width was due to ectopic cell proliferation resulting in increased cell number rather than due to increase in cell size (Lampugnani et al., 2012). Correspondingly, mature sepals were often wider and fused. Unlike petals sepals initiated in the correct number of four. By contrast, *ptl* loss of

function mutants showed a decrease in petal number from wild-type 4 to 3 and 2 per flower, and in later developing flowers, petals were often completely lost. The petals that arose in *ptl* loss of function mutants are smaller, trumpet-shaped and oriented sideways (Griffith et al., 1999; Brewer et al., 2004). During flower development, *PTL* expression was first observed on the lateral sides of early stage 1 sepal primordia and between the developing sepal primordia from stage 3 onwards. Interestingly, even though *PTL* functions in the initiation and orientation of petals, no *PTL* expression was observed in early petal primordia (Brewer et al., 2004; Lampugnani et al., 2012). Furthermore, *PTL* was expressed around the sepal margins from stage 5 onwards, when the sepals enclose the floral meristem. At later stages, *PTL* expression was also detected in the basal flanks of petal primordia (Brewer et al., 2004; Lampugnani et al., 2012). Promoter deletion experiments have identified a *cis*-regulatory element in the first intron that is accountable for the expression pattern between early sepal primordia and at the basal margin of the petals. By contrast, expression around the sepal margin was not dependent on the *cis*-regulatory element in the first intron, but depended on the presence of the 1.3 kb region upstream of the transcriptional start of *PTL* (Brewer et al., 2004).

Overexpression of *PTL* under the *35S* promoter resulted in growth arrest immediately after germination, demonstrating the severe growth inhibitory function of *PTL*. Similarly, the semi-dominant gain of function mutant *ptl-D* derived from a screen of *35S* enhancer activation-tagging lines was severely dwarfed (Li et al., 2008). Ectopic expression of *PTL* under the flower specific *AP3* promoter (*AP3>>PTL*) using the two-component system (Moore et al., 1998) resulted in severe inhibition of growth in flower primordia and caused the development of filamentous floral structures (Brewer et al., 2004). A similar phenotype of filamentous floral structures replacing sepals and petals was observed in the *as1-101 jag-2* double loss of function mutant. In this double mutant, ectopic *PTL* expression was observed in sepal and petal primordia by RNA *in situ* hybridisation (Xu et al., 2008). Furthermore, ectopic expression of *PTL* in its endogenous domain under regulation of a driver line containing the *PTL* promoter including the first intron (*PTLi>>PTL*) resulted in narrow sepals and petals that were fused at the base (Brewer et al., 2004).

Narrow sepals and petals and organ fusions are also macroscopic features of the *jag* loss of function mutants (Dinneny et al., 2004; Ohno et al., 2004). Previously, genetic

interaction between *PTL* and *JAG* has been reported by Xu et al. (2008), who generated a *ptl jag* double loss of function mutant. The *ptl jag* double mutant showed partial rescue of the wild-type petal phenotype compared with the single *jag* loss of function mutant, suggesting that reduced distal outgrowth of sepals and petals in the *jag* loss of function mutant is at least in part caused by ectopic expression of *PTL*.

In summary, the resemblance between the phenotypes caused by ectopic *PTL* expression and the *jag* loss of function mutants, as well as ectopic expression of *PTL* in *as1 jag* mutant background, provided strong evidence that *PTL* as a boundary specifying gene is repressed by the organ growth-promoting gene *JAG*. This idea was also supported by my initial array experiments (see Chapter 2). Here, I aimed to confirm that JAG directly represses *PTL* in early floral organogenesis. I tested whether JAG transcriptionally represses *PTL* in domains that are relevant for wild-type (normal) outgrowth of sepals and petals. Using ChIP followed by q-PCR and Illumina deep-sequencing, I aimed to reveal DNA binding sites of JAG in close vicinity to the *PTL* locus. The combined analysis of expression array data and ChIP-Seq data (Chapter 3) not only confirmed that *PTL* is a direct target of JAG, but also revealed additional, directly regulated targets of JAG related to organ polarity, growth regulatory pathways and organ boundary specification, which are also discussed in this chapter.

5.2. Results

5.2.1. JAG repressed *PTL*

Global expression profiling data showed that *PTL* is repressed by ectopic JAG activation in the presence and absence of the protein synthesis inhibitor cycloheximide (Chapter 2). Consistently, it was also shown that *PTL* is down-regulated in the mock treated *35S:JAG-GR* wild-type L-*er* background compared with the mock-treated *jag-1* loss of function background, showing that *PTL* is ectopically expressed in *jag-1*. To confirm the global expression profiling data, I performed qRT-PCR on inflorescence apices tissue of wild-type plants harbouring the *35S:JAG-GR* construct. For ectopic JAG activation, the plants were treated with DEX and ethanol-mock in the presence and absence of the protein synthesis inhibitor cycloheximide and incubated for 4 hours (as described in Chapter 2). Transcript

levels of *PTL* were significantly reduced upon ectopic JAG activation in the absence and presence of cycloheximide compared with the ethanol-treated controls (Figure 5.1.).

In addition, I tested *PTL* transcript levels in inflorescence apices of the two-component line (Moore et al., 1998) *AP1:LhG4 OP:JAG (AP1>>JAG)* where *JAG* cDNA is ectopically expressed under the flower-specific *AP1* driver line promoter. From this line, plants with mild and strong ectopic *JAG* phenotypes have been identified (Sauret et al., 2013). While plants with mild ectopic *JAG* phenotypes had broader but unfused sepals and petals that were wider at their base, strong ectopic JAG lines showed fused sepals and deformed and reduced petals. Accordingly, qRT-PCR experiments showed that the *JAG* transcript levels were significantly increased in inflorescence apices of the mild and strong *AP1>>JAG* lines compared with the wild type (Figure 5.2.A), whereas *PTL* expression was significantly reduced in the strong *AP1>>JAG* line compared to the corresponding wild type (Figure 5.2.B). In accordance with a role for JAG in repressing *PTL*, an increase in *PTL* expression levels was observed in inflorescence apices of the *jag-1* loss of function mutant compared with wild type (Figures 5.1. and 5.2.B). To further investigate the expression domains of *PTL* in the *jag-2* loss of function mutant compared to wild type, I crossed the *PTL:GUS* reporter construct in wild-type *Col* background (first described in Brewer et al., 2004) into the *jag-2* L-*er* mutant background and selected for *Col* looking plants. GUS staining experiments showed an overall significantly stronger *PTL:GUS* signal in the inflorescence apices of *jag-2* mutant plants compared to the wild type. A strong signal persisted in older *jag-2* flowers while the signal faded in wild-type flowers (Figure 5.3.A-B). In the early buds (stage 3-5), the GUS signal in the inter-sepal zone was stronger and extended into the margins of early sepal primordia in *jag-2,* while in the wild type the GUS signal was restricted to four clearly defined spots marking the intersepal zones (Figure 5.3.C-D). A particularly strong GUS signal was observed all around the petal margins of *jag-2* flowers and at the proximal region of the developing stamen compared with the wild type, where the signal in the petals was only observed in the margins close to the base and at the base of the stamen (Figure 5.3.E-F). At later stages 8-10, the GUS signal was less pronounced in the margins but extended through the medial petal area in the *jag-2* mutant while in the wild-type petals the signal was not detectable at this stage.

5.2.2. JAG directly binds in close vicinity to the *PTL* locus

Using anti-GR antibodies to immuno-precipitate ectopic JAG-GR protein–DNA complexes in wild-type plants harbouring the dexamethasone inducible *35S:JAG-GR* construct that had been subjected to a 4 hour incubation after dexamethasone- or mock-treatment, a significant enrichment for a region 0.5 kb upstream of the translational start of PTL was confirmed (Figure 5.4.). Subsequently, ChIP-Seq data confirmed that JAG directly targets PTL and the gene has been identified as one of the 235 putative core targets of JAG in the overlap of the ChIP-Seq data and the global expression profiling data (Chapter 3), showing that *PTL* is an *in vivo* binding target of JAG and transcriptionally regulated by it. Two DNA binding sites with significant maximum ChIP-Seq peak scores were detected in close vicinity to the *PTL* locus *(AT5G03680.1)*, one 0.5 kb upstream of the transcriptional start and the other 1.3 kb downstream of the stop codon (Figure 5.5.A). Both DNA binding sites were confirmed in an independent ChIP experiment using the same conditions as for the ChIP-Seq experiment (Chapter 3), followed by q-PCR. For both peaks, the amplicons spanning a region close to the DNA binding site identified by ChIP-Seq were significantly enriched compared to the amplicon spanning a region 1.5 kb upstream of the transcriptional start of the *PTL* gene (negative control) (Figure 5.5.B).

5.2.3. JAG directly targets genes involved in growth regulatory pathways

More recently, combined analysis of ChiP-Seq and expression array data (Chapter 3) revealed that JAG interacted with several growth regulators and genes that direct organ outgrowth, establish organ growth axes, determine local growth rates and cell type patterning. For example, *BLADE ON PETIOLE 1 and 2* (*BOP1, BOP2*) were found to be direct targets of JAG (Figure 5.6.A-B), with *BOP2* being directly repressed by JAG. In particular, *BOP2* is expressed at the site of incipient floral primordia in the inflorescence meristem and later at the adaxial base of sepals and petals, and at the base of the pedicel (Ha et al., 2003; Norberg et al., 2005; Khan et al., 2012). *BOP1*/2 are members of the *BTB POZ ankyrin repeat protein* family, which facilitate protein-protein interactions. Together they can form heterodimers that function as transcriptional co-activators, for example the BOP1/2 heterodimer has been shown to associate to the promoter region of the lateral organ identity gene *ASYMMETRIC LEAVES2* (*AS2*) (Jun et al., 2010). *BOP1/ 2* are expressed at the base of developing lateral organs. Thus, *BOP1/2* act in cells adjacent to

lateral organ boundaries where they negatively regulate meristem maintenance genes, for example *BP* and *STM,* and promote genes that determine the adaxial/abaxial polarity axis in leaves and the radial symmetric arrangement of floral organs in the *Arabidopsis* flower (Norberg et al., 2005). It had been previously shown that *BOP1*/2 repressed *JAG* and that in the *bop1/2* double mutant expression levels of *JAG* and its close homolog *NUB* were increased. Specifically, it has been shown by RNA *in situ* hybridisation that the *JAG* antisense probe hybridised in the wild-type expression domain of *BOP1/2* in the proximal regions of lateral organs in the double loss of function mutant (Norberg et al., 2005). Interestingly, *bop1 bop2* double mutants produce leaves with enhanced proximal growth leading to enlarged lobe areas at the expense of petiole area, and flowers which are subtended by floral bracts. Both phenotypic features are reminiscent of the *jag-5D* gain-of-function allele described by Dinneny et al. (2004). In addition, we also observed leaves with enlarged lobes lacking a distinct petiole in wild-type plants harbouring the *35S:JAG-GR* construct when germinated and grown on media supplemented with 10 µM DEX. These plants failed to flower, in contrast to wild-type plants grown under the same conditions (Chapter 2, Figure 2.1.G-H). Taken together, this suggests that *BOP1/2* and *JAG* act antagonistically, with *BOP1/2* being expressed in the proximal region and *JAG* being expressed in the distal region of lateral organs, possibly establishing the proximal/distal axis of lateral organs.

5.2.4. JAG directly targets genes in the *TCP/GRF* growth regulatory pathway

Relevant to organ growth, JAG directly targeted several genes in the *TCP (TEOSINTE-BRANCHED 1, CYCLOIDEA and PROLIFERATING CELL FACTORS 1 and 2)/GRF (Growth Regulating Factors)* organ growth pathway. For example, *JAG* was found to directly down-regulate *ANGUSTIFOLIA (AN3)* (Figure 5.6.C-D). The *an3* loss of function mutant was characterised by its narrow leaf and petal phenotype that was attributed to a decrease in cell number, but also to changes in polar expansion of epidermal and subepidermal cells. In the *an3* mutant, cells elongated parallel to the proximal/distal axis and did not expand into the medial/lateral axis, giving cells a narrow appearance in leaf cross sections. In line with this observation, microtubule arrangement in parallel to the medial/lateral axis was increased in comparison to the wild type, a phenotype that was restored in a transgenic *an3 AN3* complemented line (Kim et al., 2002). Furthermore, epidermal cells in the *an3*

mutant showed simple cell shapes instead of the of lobed pavement cells (Bai et al., 2010). The *an3* mutant also shows narrow petals due to a decrease in cell number along the medial-lateral axis. In particular, the base of the petals is thin and elongated while the distal lobe was less affected and only showed a slight decrease in max width (Kim et al., 2003; Bai et al., 2010). *AN3* belongs to the *GRF*-interacting factors and functions as a transcriptional co-activator in the interaction with several members of the *GRF* family that have been identified to act as transcriptional activators of cell proliferation (Kim and Kende, 2004). For example, *AN3*, *GRF5* and *GRF9* have overlapping expression patterns in young floral buds and leaf primordia (Horiguchi et al., 2005). The *an3 grf5* double mutant has narrower leaves than either of the single mutants due to a further decrease in cell numbers along the medial/lateral axis.

Overexpression of *AN3* and *GRF5* resulted in similar phenotypes of enlarged leaves that expanded along all axis and did not appear particularly wider, suggesting that *AN3* and *GRF5* can promote cell proliferation in all directions (Horiguchi et al., 2005).
JAG was also found to bind to *GRF4, GRF5, GRF8, GRF9* in the ChIP-Seq analysis but these genes were not differentially regulated in the expression array experiment, except *GRF8* which was found to be down-regulated by *JAG*, a result that could not be confirmed by qRT-PCR. However, qRT-PCR confirmed that *GRF5* is significantly down-regulated upon JAG-GR activation (Figures 5.6.E-F). In addition, JAG directly binds to the promoter region of the *micro RNA miR396,* which targets seven of the nine *GRF* family members for degradation, but interestingly does not affect *GRF5* (Rodriguez et al., 2010). Although *GRF5* is not a target of *miR396*, it acts highly redundantly with the *GRFs* that are targeted by *miR396*, because ectopic expression of *miR396* had an enhanced phenotype in the *grf5* mutant background than in wild type (Rodriguez et al., 2010). In young leaf primordia, cell proliferation is tightly associated with high transcript levels of *GRFs* and *AN3* and low expression levels for *miR396*. Over time-course of development *miR396* expression increases in the distal area marking the front of cell cycle arrest and restricting *GRF* expression to the still proliferating proximal regions of the leaf (Rodriguez et al., 2010).

Also relevant to the interaction with *GRF* genes, JAG directly activated *TCP4* (Figure 5.7.A, C) a member of the *CIN-like TCP* family that activates *miR396* but also represses *AN3* and *GRF5* independently from *miR396* (Rodriguez et al., 2010). Besides the function of *TCP4*, *CIN-like TCP* transcription factors have been shown to play a major role in leaf

differentiation by promoting cell cycle arrest (Nath et al., 2003), and repression of TCP function causes ectopic cell proliferation at the leaf margins and a lack of pavement cell differentiation, both potentially resulting in the wavy and curly leaf phenotype observed in *tcp* mutants. *CIN-like TCP* transcription factors promote cell differentiation by indirectly repressing *CUC* genes, which promote *KNOX* genes and undifferentiated cell fate (Koyama et al., 2010). For this reason, I tested several members of the *ClN-like TCP* transcription factors by qRT-PCR, even though they appear not to be directly targeted by JAG, with the exception of *TCP4*. For example, *TCP3* and *TCP10* were significantly up-regulated upon *JAG-GR* activation and showed significantly lower expression levels in the *jag-1* mutant (Figure 5.7.B, D), while *TCP13* was significantly repressed by JAG and showed significant ectopic expression in *jag-1* in the expression array, suggesting that *TCPs* are important but indirect targets of JAG.

In addition, JAG also directly down-regulated two members of the *POLTERGEIST (POL)* family *POLTERGEIST-like 4 (PLL4)* and *POLTERGEIST-like 5 (PLL5)*, which encode protein phosphatase 2C. While *POL* and *PLL1* act as components in the *CLV1* signalling pathway (Yu et al., 2003), *PLL4* and *PLL5* have been shown to play a role in leaf growth and leaf shape (Song and Clark, 2005). For example, *pll5* leaves were shorter, narrow and curled and the pll4 leaves were longer and wider while the double mutant showed an intermediate phenotype suggesting that these two genes act antagonistically in leaf development. Conversely, it was shown that in the *35S:PLL5* line leaves were rounder and less curled, suggesting that also these genes have an effect on organ development (Song and Clark, 2005).

5.2.5. JAG directly repressed organ boundary specifying genes

In addition to the boundary specifying gene *PTL*, the *GATA3* transcription factor *HANABA TARANU (HAN)* was directly repressed by JAG. *HAN* is expressed at the boundaries between the floral meristem and organ primordia and plays a crucial role in organ separation (Zhao et al., 2004). In addition, HAN also functions in restricting the *WUS* expression domain. Also related to organ boundary formation, JAG directly targeted *miR164,* which has been shown to target *CUC1* and *CUC2*, but not *CUC3* (Laufs et al., 2004; Hasson et al., 2011). Overexpression of the *miR164* caused fused sepals as observed in the *cuc1 cuc2* double mutant, while the a *miR164*-resistant *CUC2* construct

caused thin sepals with increased spacing between the sepals owing to the extended expression of *CUC2* between emerging sepals, suggesting that *miR164* is important in early floral organogenesis (Laufs et al., 2004; Hasson et al., 2011). Interestingly, *CUC3* is indirectly up-regulated upon JAG-GR activation. *CUC3* is expressed at the boundaries between the floral meristem and initiating sepals and functions together with *CUC1* and *CUC2* in floral organ separation (Vroemen et al., 2003; Hibara et al., 2006).

5.3. Discussion

5.3.1. JAG interacts with pathways involved in organ primordium growth

Gobal expression array analysis and, more recently, ChIP-Seq have confirmed that the regulatory function of JAG goes beyond the transition from meristem to primordium cell behaviour and that JAG directly targets key regulators in overall organ development and morphogenesis, which includes pathways to define organ boundaries, to establish growth axes and overall organ morphogenesis. Here, I confirmed in detail that JAG directly represses *PTL*. Furthermore, I confirmed several interesting candidates related to the growth-regulatory network in an independent expression profiling experiment using qRT-PCR.

5.3.2. JAG directly represses the boundary-specifying gene PTL

Firstly, I confirmed in detail that the growth regulatory gene *JAG* directly represses the boundary specifiying gene *PTL*. ChIP-SEQ and ChiP-qPCR analysis have independently confirmed that JAG binds *in vivo* to sites within 3 kb upstream and 1.5 kb downstream of the *PTL* gene. Furthermore, qRT-PCR confirmed that this *in vivo* binding leads to negative regulation of *PTL* expression. Consistently, I showed that *PTL* expression levels are higher in the *jag* loss of function mutant compared to wild type. Moreover, the *PTL:GUS* reporter was ectopically expressed in *jag* loss of function mutant background, particularly in the distal margins of petals. *PTL* expression was extended from the margins to the centre of sepals and petals, confirming an ectopic PTL expression pattern previously shown in the *as1-101 jag-2* double loss of function mutant by RNA *in situ* hybridisation (Xu et al., 2008). Xu et al. (2008) also reported a partial rescue of petal outgrowth in the *as1-101 jag2 ptl* triple mutant, suggesting that reduced distal outgrowth of sepals and petals in the *jag*

loss of function mutant is at least in part caused by ectopic expression of *PTL*. Here I provided further confirmation that *JAG* promotes growth and cell proliferation in organ primordia by directly restricting *PTL* to the margins and boundaries of the developing organs. In addition, I observed a strong ectopic GUS signal in the proximal region of the developing anthers in the *jag-2* mutant compared to wild type. In the *jag-2* mutant, anthers are spade shaped and partially sterile. In this respect, future work could investigate whether ectopic expression of *PTL* in the anthers accounts for their aberrant shape. Sauret et al. (2013) presented a mathematical model that described the outgrowth of petals to final size and paddle-shape based on growth rates parallel and perpendicular to a polarity field. Furthermore, they identified JAG as a potential key regulator and PTL as a potential down-stream target in this process. In this context, it would be interesting to expand the modelling approach to account for shape changes in anthers.

5.3.3. Could PTL repress cell proliferation in the inter-sepal zones by promoting *KRP* function?

PTL has been described as an organ boundary gene, specifying the inter-sepal zones by restricting cell proliferation in this region (Lampugnani et al., 2012). In order to inhibit cell proliferation, *PTL* needs to be able to interact with the regulatory network of the core cell cycle machinery. One way to inhibit cell division would be to activate cell cycle inhibitors. The Kip-related protein family (KRP) has been described to inhibit cell proliferation in plants. The KIP-related proteins interact with CDKA-CYCD complexes to inhibit the transition from G1 to S-phase, the decisive step where cells commit to undergo another round of DNA replication and mitotic division (De Veylder et al., 2001). Overexpression of *KRPs* has been shown to severely inhibit cell proliferation resulting in organs with reduced cell numbers and reduced organ size. For example, over-expression of *KRP2* under the *35S* promoter reduced leave size to 20% of the wild-type leave, caused leave serrations and abnormal flower phenotypes (De Veylder et al., 2001; Zhou et al., 2002 ; Verkest et al., 2005). A link between *PTL* and *KRPs* had been previously suggested by Brewer et al. (2004), who described the ectopic *PTL* phenotype in *AP3>>PTL* lines as similar to the ectopic *KRP1* phenotype of *AP3>>KRP1*, reported in *Brassica napus* by Zhou et al. (2002). Interestingly, confocal imaging and 3D reconstruction of early floral buds (stage 3-5) revealed that the *krp2 krp4 jag* triple mutant shows enlarged inter-sepal zones (Chapter

7, Figure 7.8.D), a phenotype similar to the *ptl* loss of function mutant (Lampugnani et al., 2012). It could therefore be speculated, that *KRP2*, *KRP4* and *PTL* act in the same pathway to restrict cell proliferation in the inter-sepal zones.

Moreover, I observed a significant rescue in sepal and petal outgrowth of mature organs in the *krp2-3 jag-1*, *krp4-1 jag-1* double mutants and in the *krp2-3 krp4-1 jag-1* triple mutant compared with the *jag-1* single mutant (Chapter 6, Figures 6.13., 6.14., and 6.17.). The observation that the *ptl* mutation also partially rescued organ growth in *jag* background raises the question whether loss of *PTL* could reduce expression of *KRP2* and/or *KRP4* in the *jag* mutant. In other words, presuming that all four mutants have similar levels of ectopic *PTL* expression, ectopic *PTL* function could be dependent on *KRP2* and *KRP4* function. The hypothesis that *PTL* function is dependent on *KRP* function could be tested, for example, by reassessing the phenotypes of the lines with ectopic *PTL* expression (Brewer et al., 2004; Li et al., 2008) in the *krp2* and *krp4* loss of function mutant backgrounds.

In addition, I observed that the *KRP2-GFP* expression pattern (Chapter 6, Figure 6.10.) overlaps at least in part with the expression pattern observed with the *pPTL(FI313):YFP* reporter by Lampugnani et al. (2012). The expression domains, in particular, overlap at the boundary as early floral primordia initiate from the inflorescence meristem. At stage 3 to stage 4, expression overlaps between incipient lateral sepal primordia and in the internal floral dome. Furthermore, I have observed *KRP2* expression in sepal margins (KRP2-GFP, Chapter 6, Figure 6.10.) and in developing petal margins (KRP2:GUS, Chapter 6, Figure 6.11.) in later stages of development. In order to test whether *PTL* activates *KRP2* expression, the *pKRP2:KRP2-GFP* reporter could be crossed to the *ptl* mutant background and to the lines with ectopic *PTL* expression (Brewer et al., 2004; Li et al., 2008). ChIP and qRT-PCR experiments could further clarify whether the interaction between the transcription factor *PTL* and the *KRP* genes is direct or involves other downstream mediators. Future work on *KRPs* as potential targets of *PTL* would elucidate the regulatory network downstream of *JAG* and its immediate target, *PTL*. In this respect, it is noteworthy that *KRP2* and *KRP4* are directly down-regulated by JAG (see Chapters 2-3, 6-7), suggesting that modulating *KRP* activity might be a common pathway to restrict and to promote cell proliferation during organ development.

5.3.4. Both *JAG* and *PTL* may indirectly promote petal initiation and outgrowth by modulating auxin function

Another interesting connection between *JAG* and *PTL* arises from the fact that *PTL* has been shown to influence auxin dynamics (Brewer et al., 2004; Li et al., 2008; Lampugnani et al., 2012 and 2013). Initial evidence that auxin changes could be the cause of reduced numbers of petals in the *ptl* loss of function mutant was provided by the disrupted expression of the auxin response marker *DR5* in the petal founder cells. Petal initiation could be rescued by biosynthesis of auxin in the intersepal zones using the bacterial auxin biosynthesis gene *iaaH* under the *PTL* promoter (Lampugnani et al., 2013). Furthermore, loss of function of the auxin influx carrier *AUX1* was found to enhance the *ptl* loss of function phenotype, with petal initiation being completely abolished in the *ptl aux1* double mutant. Ectopic expression of *AUX1* under control of the *PTL* promoter in the *aux1 ptl* double mutant resulted in a significant increase in the number of petals, showing that both auxin biosynthesis and auxin influx in the inter-sepal zones could partly rescue petal initiation in the *ptl* mutant background (Lampugnani et al., 2013).

On the other hand, loss of function mutants of the efflux carrier *PIN1* and its activating kinase *PINOID* (*PID*) showed an increased number of petals. In the *pin ptl* and *pid ptl* double mutants and in either triple mutant with *aux1*, the number of petals is reduced, suggesting that the increase in petal number in the efflux carrier loss of function mutants is dependent on PTL function (Lampugnani et al., 2013). In summary, these genetic interactions provide evidence that PTL is required to modulate appropriate auxin levels in the spatial and temporal context of petal initiation.

Furthermore, it was suggested by Brewer et al. (2004) that *PTL* expression in the margins of the perianth organs functions to define final size and shape. In this context, Sauret et al. (2013) presented a mathematical model that accounted for the broad distal outgrowth of petals leading to their final paddle shape compared with the pointy shape of a leaf. This model was based on an auxin-dependent distal-proximal polarity field that directed local tissue growth perpendicular to it. While in a leaf the polarity field converged in the distal tip, the polarity field diverged towards the distal margins in petals, allowing petals to grow wide at the tip. *JAG* was suggested to be a key regulator in this organ patterning process, because of its striking loss of function mutant phenotype with narrow petals showing reduced distal outgrowth and serrated margins. Moreover, auxin response and

auxin transport patterns were changed in the *jag* loss of function mutant. The auxin response reporter *DR5* as well as the influx carriers *PIN1* and *PIN3* had a weaker, disrupted and narrower distribution in the distal petal margin of *jag-1* compared to the wild type. It was further suggested that changed auxin dynamics in the loss of function mutant might be caused by ectopic expression of *PTL* in the distal margins. In this respect, my results provided further confirmation that the growth promoting effects of *JAG* involve auxin-dependent processes. The interaction with auxin responses is mediated at least in part by directly repressing PTL in the petal margin. However, my ChIP-Seq and expression profiling data revealed that JAG also directly targets genes involved in auxin biosynthesis, transport and response, for example *PID* (Chapters 2-3, 8).

5.3.5. Mutual antagonism between JAG and BOP1/2 may establish the proximal/distal axis

In addition, this work revealed the mutual antagonism between *JAG* and *BOP1/2* and it is tempting to speculate that this antagonism may establish the proximal/distal axis of lateral organ outgrowth. While previous work has focussed on *BOP1/2* repressing *JAG (*Norberg et al., 2005), our data provides evidence that JAG directly represses *BOP2* and binds *in vivo* to *BOP1*. *BOP1/2* and *JAG* expression domains exclude each other along the proximal-distal axis, suggesting that antagonism between proximal *BOP1/2* expression and distal *JAG* expression could determine the proximal-distal polarity axis in leaves and floral organs. In early sepal primordia, for example, *BOP2* is specifically expressed in cells at the adaxial base, while *JAG* is expressed throughout the emerging primordia. In later stages, *BOP1/2* is restricted to the basal region and JAG to the distal region. Both, JAG and BOP1/2 have been shown to be involved in the repression of meristem maintenance genes such as *BP* and *STM*, suggesting that *BOP1/2* and *JAG* promote primordia cell behaviour. Repression of meristem maintenance genes has been considered as the first step to establish the proximal region of developing primordia; subsequent exclusion of the growth promoting factor JAG from proximal regions might be sufficient to establish the proximal/distal axis. In addition, it could be speculated that the *JAG* and *BOP1*/2 recruit different sets of growth promoting pathways (see below).

5.3.6. JAG promotes organ growth independently of the *GRF/TCP* pathway

JAG controls several members in the *AN3/GRF* pathway, for example directly repressing *AN3* and *GRF5* and directly activating *TCP4*. *TCP4* represses *AN3* and *GRF5* and promotes expression of *miR396* that targets GRFs, but is also directly targeted by *JAG*. This suggests that *JAG* generates a tightly interconnected network to repress this growth regulatory pathway.

AN3 and *GRF5* interact to maintain cell proliferation during leaf primordia development and determine the size and shape of leaves and petals. Interestingly, petal width of *an3* and *grf5* mutants has been shown to be more affected in the proximal regions than in the distal regions. This suggests that *AN3* and *GRF5* play a less important role to promote organ growth in the distal region and it can be speculated that this is because they are repressed by JAG in the context of a wild-type petal. Interestingly, in the leaf, AN3 and GRF5 are expressed in the basal regions independently from the region of proliferating cells further distally located. Therefore, in floral organ primordia a similar pattern could restrict *AN3* and *GRF5* to certain regions of the growing organ. Reporter genes as described in Horiguchi et al. (2005) would shed light on the interaction of *AN3, GRF5* and *JAG*.

In relation to the interaction with the GRF growth pathway, it could be further speculated that *JAG* and *BOP* deploy different sets of downstream growth promoting pathways and thereby establish different growth behaviours and organ patterns, a narrow organ growth pattern at the base and an organ pattern of increased width in the distal area. In this context, Sauret et al. (2013) used clonal analysis to follow the rates of growth and cell division parallel and perpendicular to the proximal/distal axis over time-course of petal development in the wild type. This analysis revealed that already in early primordium development clones in the proximal region have a higher length to width ratio than in the distal region and that at petal maturity clones in the distal region are seven-fold longer than wide while in the proximal region they are eleven-fold longer than wide, showing that growth rates perpendicular to the distal-proximal polarity field are increasing towards the distal end of the petal. Furthermore, Sauret et al. (2013) showed that anisotropy of the clones early in primordia development is caused by an increased number of cell divisions along the distal/proximal axis compared with the medial/lateral axis. By contrast, the increase in clone anisotropy at the later stages of development is

caused by increased elongation of the cells, which was particularly pronounced for clones in the proximal regions resulting in a length/width ratio of 11. In addition, the clonal analysis revealed that proximal clones have their main proximal/distal axis aligned with the midline, while the main axis of the distal clones diverged towards the distal petal margin. All in all, this clonal analysis confirmed that there are considerable differences in growth behaviour between the proximal and distal regions of the petal.

In the future, it would be interesting to investigate whether these differences in growth behaviour coincide with the expression domains of *JAG* and *BOP*. For example, ectopic expression of *JAG* in the *AP1>JAG* line resulted in petals that were wider at the base, whereas mature petals of the *jag* loss of function mutant showed a decreased overall width/length ratio of 0.7 in mature petals in comparison to 0.8 in wild type petals (Sauret et al., 2013; Robert Sablowski unpublished), providing evidence that changes in *JAG* expression may cause changes in local growth behaviours. Extending the clonal analysis from the *jag* single mutant to the *bop1/2* double loss of function mutant and the *jag bop1 bop2* triple mutant would elucidate whether the antagonistic interaction between *JAG* and *BOP* is required for different local growth rates parallel and perpendicular to the proximal/distal axis. In addition, this data could be used to further test the mathematical model generated by Sauret et al. (2013) and the model could be extended by taking into account the antagonistic interaction of *BOP* and *JAG* as "proximal and distal organisers". Furthermore, it would be interesting to use reporter lines for *AN3*, *GRF5* and *miR396* in *jag* and *bop1/2* loss of function and gain of function mutant backgrounds, in order to assess whether this growth regulatory pathway is targeted differently by *BOP1/2* and *JAG*. It would also be interesting to investigate the effect on floral organ patterning by modulating *JAG* and *BOP1/2* function in combination with *AN3*, *GRF5* gain and loss of function mutations. This would reveal whether recruiting or suppressing the *AN3/GRF* pathway is one mechanism to maintain and establish different tissue growth behaviours along the basal and distal axis that eventually leads to tissue patterning. A detailed study of the downstream targets of *GRF/AN3* would be required in order to test the hypothesis whether *JAG* and *GRF/AN3* may have different downstream targets and or regulate them differently. Ultimately, reverse genetics would also shed light on the rather crude hypothesis that the antagonistic function between *BOP1/2* and *JAG* could at least in part explain why we find elongated flat cells that are usually found at

the base of wild-type petals in the distal lobe area of *jag* mutant petals instead of conical cells with regular cuticular ridges (as reported by Dinneny et al., 2004; Ohno et al., 2004; Chapter 6, Figure 6.19.).

Apart from *JAG* and *AS2* (Ha et al., 2007; Jun et al., 2010), the global genome-wide targets of the transcriptional co-activators *BOP1/2* have not been identified yet, however, comparison of the direct *JAG* targets with the direct *BOP1/2* targets would provide molecular evidence whether JAG and BOP deploy different sets of downstream target genes that result in different local growth patterns and ultimately shape the organ. In addition, *JAG* directly targeted several genes that have been reported to also have functions in organ shape, for example *PLL4*, *PLL5*, *BAM1* and *BAM2* (Yu et al., 2003; Clark and Song, 2005; DeYoung et al., 2006) and could therefore also be involved in regulating local growth patterns in floral organs. *BOP1/2* have been shown to act as transcriptional co-activators of *AS2* and therefore play a role in establishing the adaxial-abaxial polarity in leaf primordia. In respect to adaxial/abaxial patterning, JAG activated the AGC protein kinase *UNICORN,* which represses members of the *KANADI* protein family that are involved in adaxial/abaxial patterning, to allow for planar symmetric tissue growth. Loss of *UNC* function causes ectopic protrusions in petals (Enugutti et al., 2013). It would be interesting to further investigate the expression pattern of *UNC* in relation to changes in *JAG* and *BOP1/2* function in order to address the question whether adaxial/abaxial patterning and distal/proximal patterning are coordinated and converge at the boundary of BOP1/2 and JAG expression.

5.3.7. Mutual antagonism between JAG and the boundary specifying gene *HAN*

Interestingly, both JAG and BOP1/2 are repressed upon ectopic activation of the GATA3 transcription factor *HAN*. Ectopic activation of DEX-inducible *35:HAN-GR* repressed JAG and BOP1/2, while activating the boundary specifiying genes *RABBIT EARS* (RBE) and *CUC3* (Krizek et al., 2006; Vroemen et al., 2003), suggesting that HAN as a boundary specifiying gene needs to counteracts the growth promoting effects of JAG and BOP1/2. Furthermore, HAN like JAG represses the TALE proteins *BP* and *ATH1*, suggesting that specifying an organ boundary involves down-regulation of meristem maintenance genes. In addition, *HAN* repressed genes involved in response to auxin, cytokinin and gibberellins, cell wall related genes such as expansins, and the cell cycle gene *CYCLIN*

D1;1. In summary, Zhang et al. (2013) showed that the growth inhibiting boundary specifying gene *HAN* targets genes with similar functions as identified for the direct transcriptional targets of JAG in this project. However, *HAN* appears to regulate them the opposite way in order to inhibit cell proliferation and cell growth in the boundaries. Because HAN has been identified as one of the directly repressed core targets of JAG in our combined approach, this work revealed mutual antagonism between the growth promoting gene *JAG* and the boundary specifying gene *HAN.*

In summary, my data suggest that JAG directs local tissue growth, establishment of growth directions and growth axes and the generation of organ boundaries by interacting with members of the major growth regulatory pathways and organ boundary specifying genes. Therefore, JAG acts at the interface between organ identity, organ patterning, and organ growth to produce organs of genetically specified final size and shape.

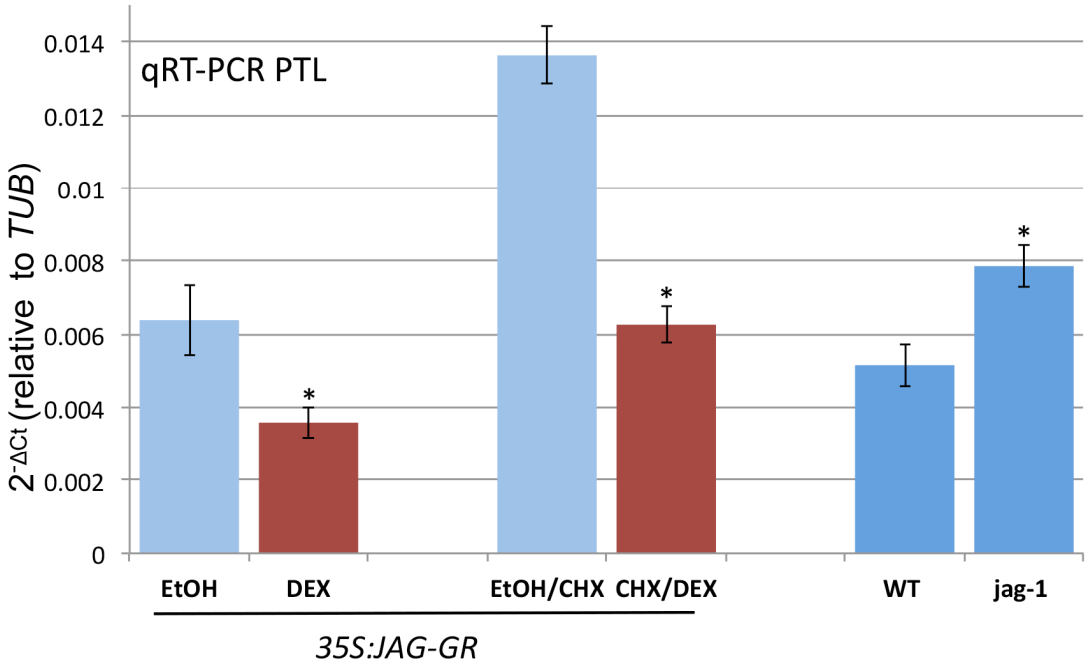

Figure 5.1. JAG represses *PTL*. Expression levels (relative to the *TUB4* constitutive control) of *PTL*; mRNA measured by qRT-PCR in inflorescence apices of *35S::JAG-GR* plants 4h after mock treatment (light blue) or treatment with dexamethasone 10 µM (red); CHX indicates samples from plants that were also treated with cycloheximide 10 µM or untreated wild-type (WT) and *jag-1* plants (dark blue); bars show the average and standard deviation of three biological replicates; asterisks indicate statistically significant differences (unpaired two-sample Student's *t*-test, $p < 0.05$) between dexamethasone-treated and mock-treated samples and between the untreated wild type and *jag-1* (dark blue bars) (compared in a separate independent experiment).

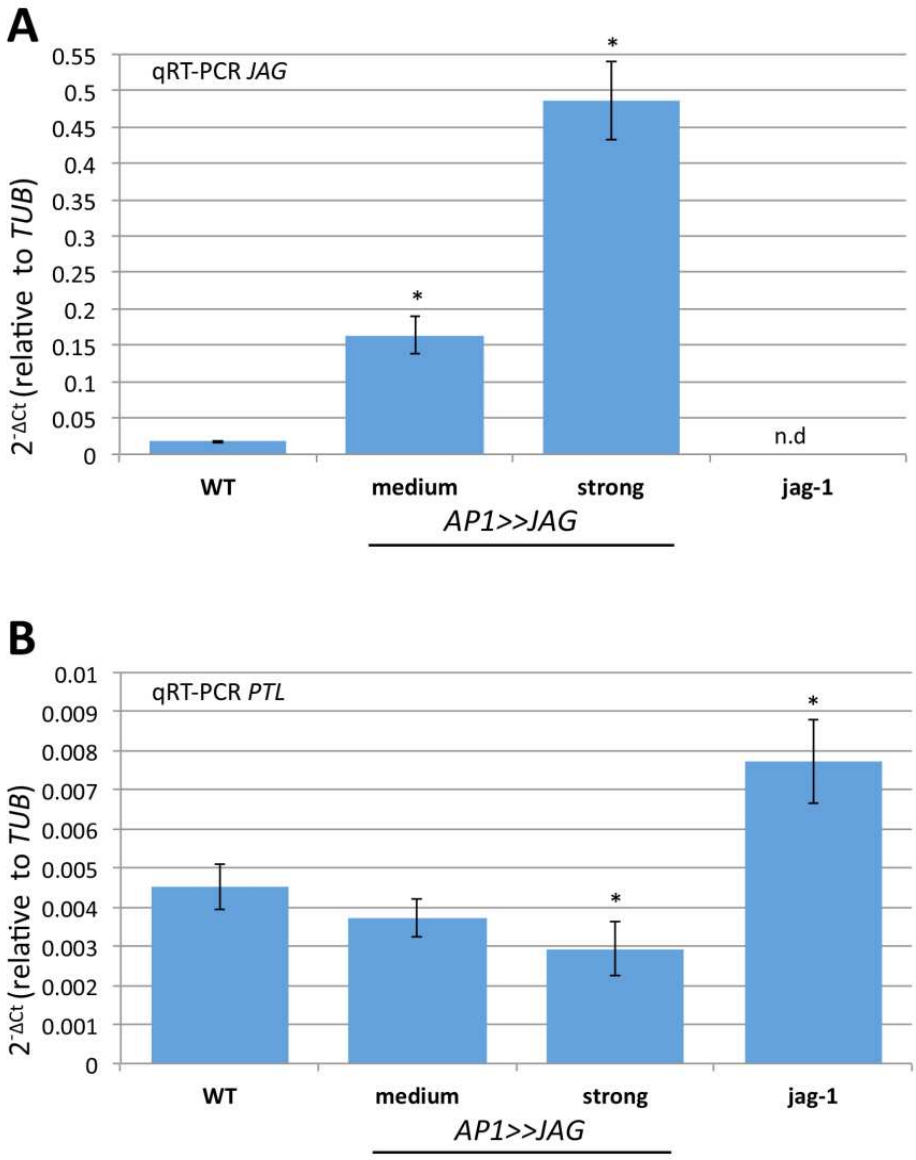

Figure 5.2. *PTL* transcript levels are correlated with *JAG* transcript levels.

(A) *JAG* transcript levels (relative to the *TUB4* constitutive control) were increased in the *AP1>>JAG* line with medium and strong ectopic JAG phenotype and not detectable (n.d.) in the *jag-1* mutant.

(B) Transcript levels (relative to the *TUB4* constitutive control) of *PTL* were decreased in the strong and medium *AP1>>JAG* lines and increased in the *jag-1* mutant compared to wild type; mRNA levels were measured by qRT-PCR in inflorescence apices; bars show the average and standard deviation of three biological replicates; asterisks indicate statistically significant differences to the wild type (unpaired two-sample Student's *t*-test, $p < 0.05$).

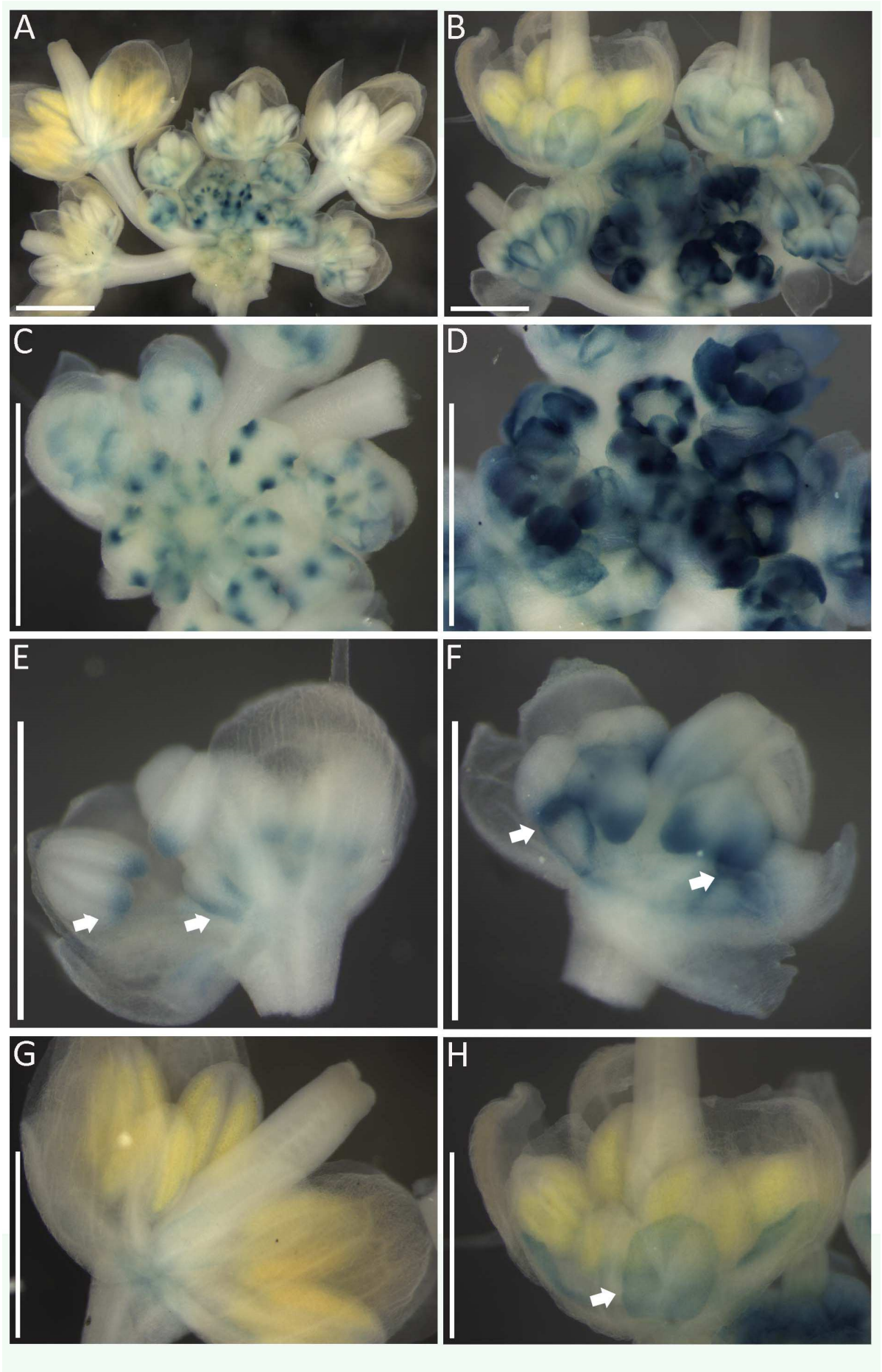
A
B
C
D
E
F
G
H

Figure 5.3. Ectopic *PTL* expression in *jag-2* mutant background.

(A, C, E, G) *pPTL:GUS* expression in inflorescences of wild type, (B, D, F, H) *pPTL:GUS* expression in inflorescences of *jag-2. (A-D)* inflorescence overviews; (E-F) single flowers of comparable stages; Scale bars (A-H): 500 µm; A stronger and extended GUS signal was observed in early floral buds (stage 5-8) of *jag-2* compared with wild type. The strong signal persisted in older flower *jag-2* flowers while the signal faded in wild-type flowers (A-B). The GUS signal in the intersepal zone was stronger and extended into the margins of early sepals in *jag-2* compared with wild type where the GUS signal was restricted to for spots marking the intersepal zones (C-D). From stage 5-8, a particularly strong GUS signal was observed all around the petal margins of *jag-2* flowers and at the proximal region of the developing stamen compared with wild type where the signal in the petals was only observed in the margins close to the base and at the base of the stamen, indicated by arrows (E-F). At later stages 8-12, the GUS signal was less pronounced in the margins but extended through the medial petal area (indicated by arrows), while in the wild-type petals the signal was not detectable at these stages.

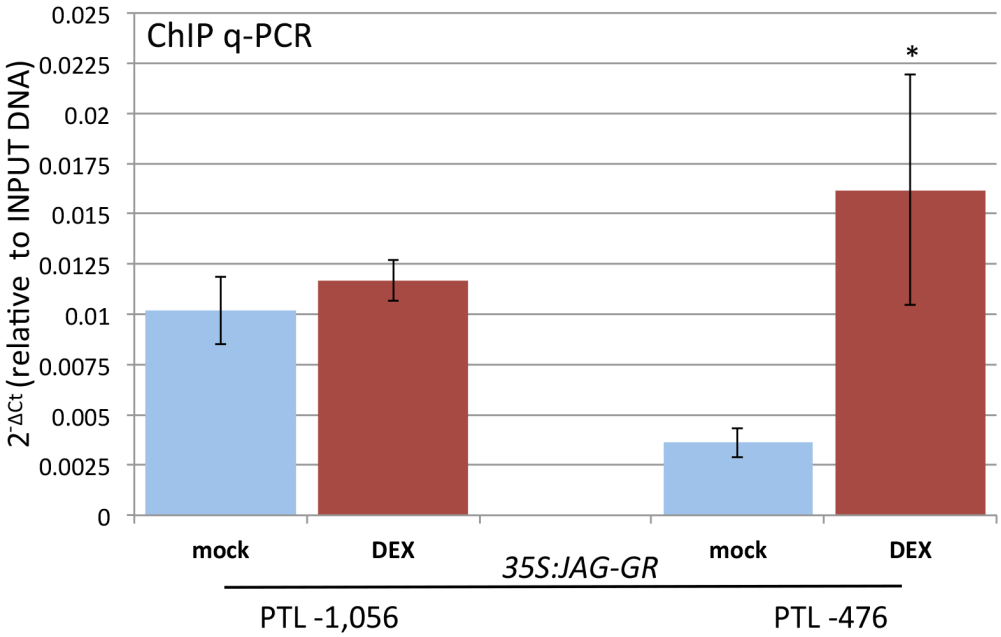

Figure 5.4. Ectopic JAG-GR binds in the promoter region of *PTL*. Chromatin immunoprecipitation (ChIP) using anti-GR antibodies and inflorescence apices of *35S::JAG-GR* plants 4 h after mock treatment (light blue) or treatment with dexamethasone 10 µM (red); target sequences 1.05 Kb and 0.5 Kb of upstream of the *PTL* transcriptional start; bars show the average and standard deviation of three biological replicates; numbers below the bars indicate the left border of the q-PCR amplicon relative to the coding sequence; asterisks indicate significant difference to the mock control ($p < 0.05$, Student's *t*-test).

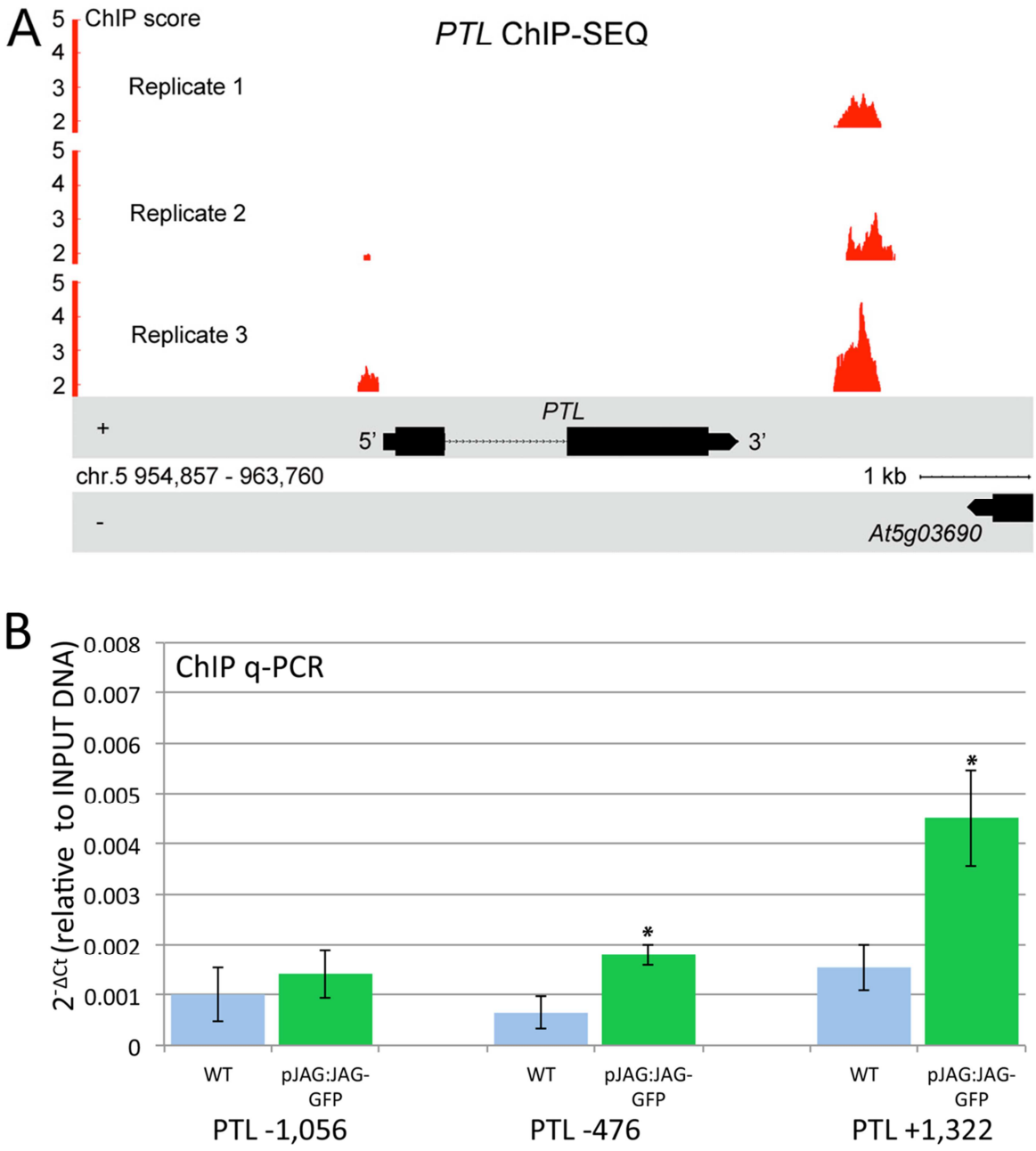

Figure 5.5. Endogenous JAG-GFP directly binds upstream and downstream of the *PTL* locus. (A) Visualisation of read enriched regions mapping to the TAIR10 Arabidopsis reference genome (x-axis) using the Integrated Genome Browser (Nicol et al., 2009), ChIP-Seq peak score values (y-axis) based on the ratios of normalised reads between JAG-GFP and control samples were calculated for every single nucleotide position using CSAR software (Muiño et al., 2011a), the maximum score value within the candidate peaks was used to test for significance of the enrichment; ChIP-Seq peaks detected in each replicate

within 3 Kb upstream and 1.5 Kb downstream of the coding sequences for the *PTL* locus on chromosome 5.

(B) Binding of JAG-GFP to the upstream region of *PTL* confirmed by ChIP-qPCR; numbers below the bars indicate the left border of the q-PCR amplicon relative to the coding sequence; asterisks indicate significant difference to the negative wild-type control ($p < 0.05$, Student's *t*-test).

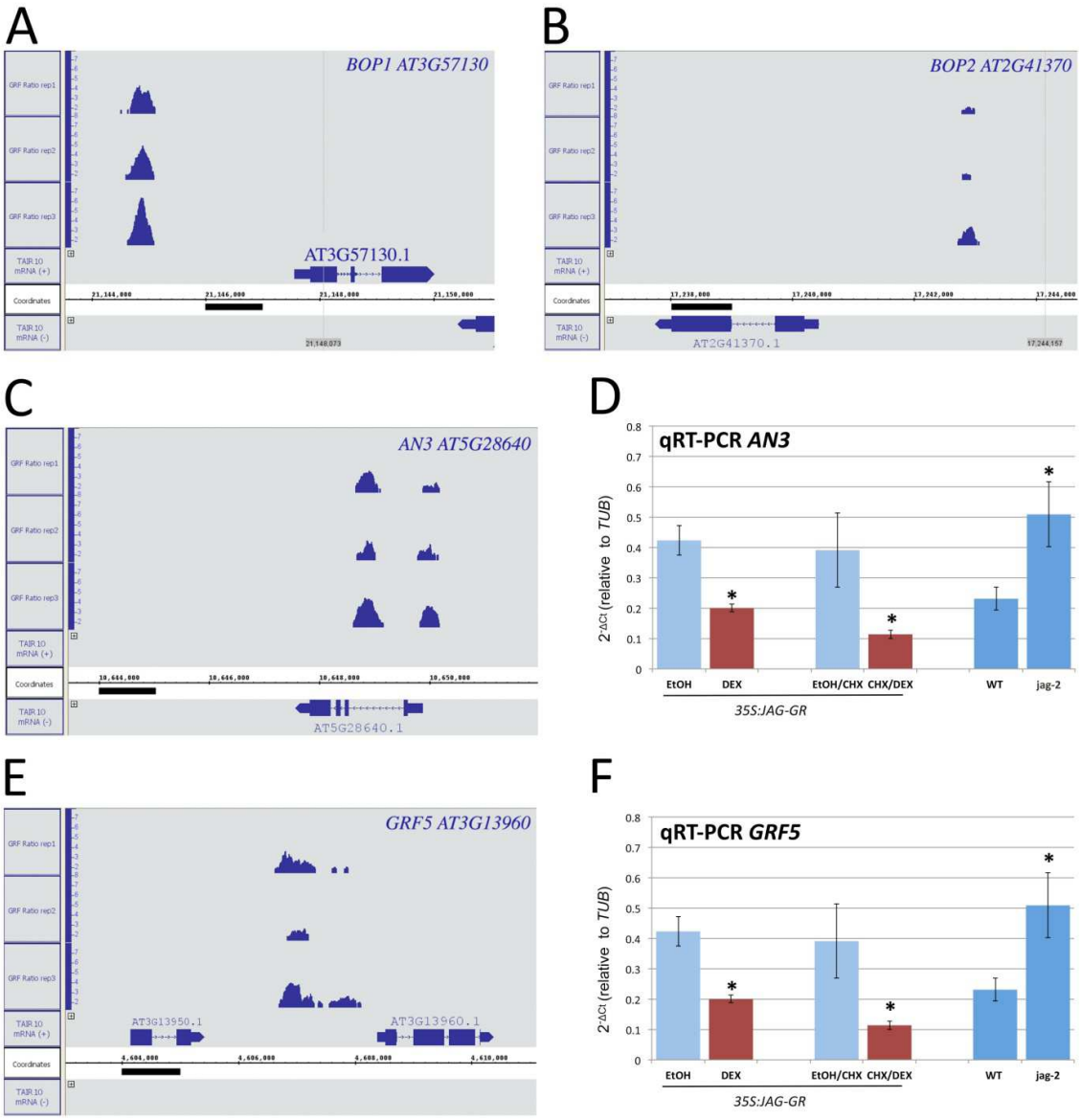

Figure 5.6. JAG directly regulates genes involved in growth regulatory pathways.

(A-C, E) Visualisation of read enriched regions mapping to the TAIR10 Arabidopsis reference genome (x-axis) using the Integrated Genome Browser (Nicol et al., 2009), ChIP-Seq peak score values (y-axis) based on the ratios of normalised reads between JAG-GFP and control samples were calculated for every single nucleotide position using CSAR

software (Muiño et al., 2011a), the maximum score value within the candidate peaks was used to test for significance of the enrichment; ChIP-Seq peaks detected in each replicate within 3kb upstream and 1.5 Kb downstream of the coding sequences for the *BOP1, BOP2, AN3, and GRF5* loci. (D, F) Expression levels (relative to the *TUB4* constitutive control) of *AN3* (D) and *GRF5* (F); mRNA measured by qRT-PCR in inflorescence apices of *35S::JAG-GR* plants 4h after mock treatment (light blue) or treatment with dexamethasone 10 µM (red); CHX indicates samples from plants that were also treated with cycloheximide 10 µM or untreated wild-type (WT) and *jag-1* plants (dark blue); bars show the average and standard deviation of three biological replicates; asterisks indicate statistically significant differences (unpaired two-sample Student's *t*-test, $p < 0.05$) between dexamethasone-treated and mock-treated samples and between the untreated wild type and *jag-2* (dark blue bars).

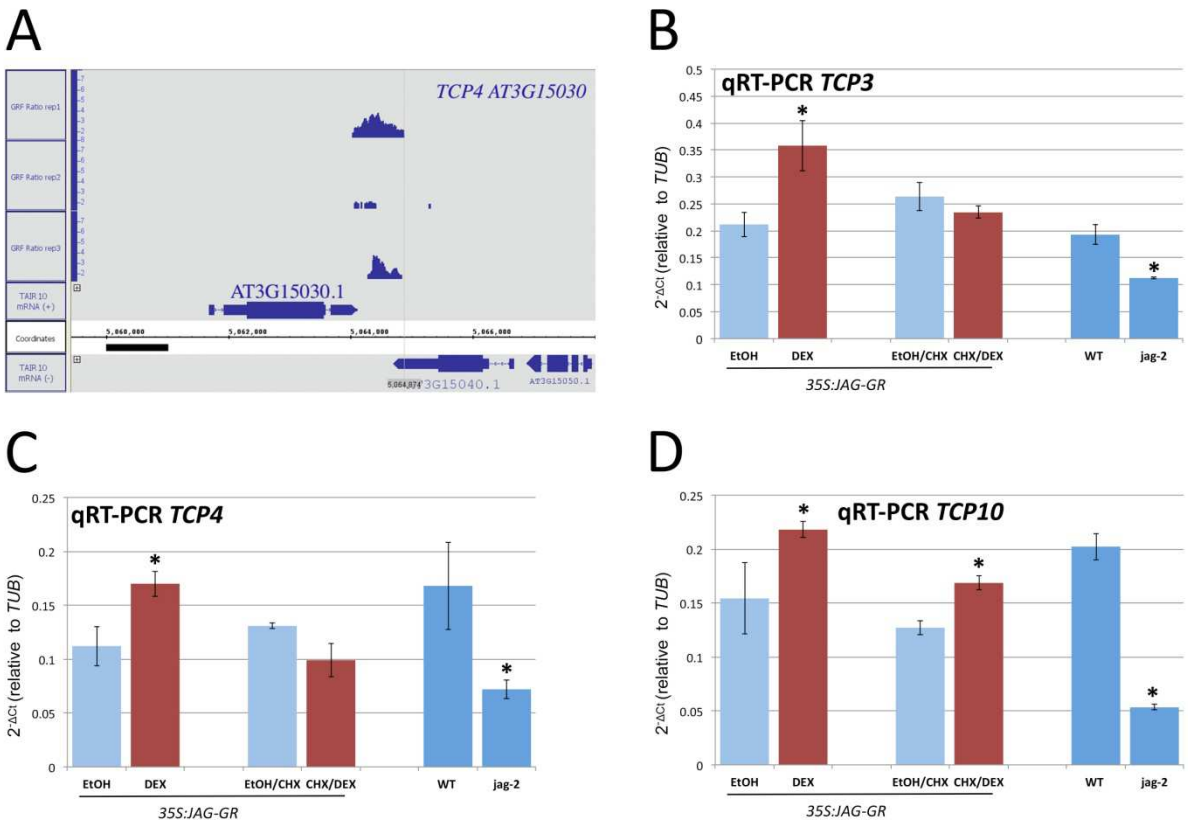

Figure 5.7. JAG directly and indirectly regulates members of the *TCP* family.

(A) Visualisation of read enriched regions mapping to the TAIR10 Arabidopsis reference genome (x-axis) using the Integrated Genome Browser (Nicol et al., 2009), ChIP-Seq peak

score values (y-axis) based on the ratios of normalised reads between JAG-GFP and control samples were calculated for every single nucleotide position using CSAR software (Muiño et al., 2011a), the maximum score value within the candidate peaks was used to test for significance of the enrichment; ChIP-Seq peaks detected in each replicate within 3 Kb upstream and 1.5 Kb downstream of the coding sequences for the *TCP4* locus on chromosome 3. (B-D) Expression levels (relative to the *TUB4* constitutive control) of *TCP3* (B), *TCP4* (C), *TCP10* (D); mRNA measured by qRT-PCR in inflorescence apices of *35S::JAG-GR* plants 4h after mock treatment (light blue) or treatment with dexamethasone 10 µM (red); CHX indicates samples from plants that were also treated with cycloheximide 10 µM or untreated wild-type (WT) and *jag-1* plants (dark blue); bars show the average and standard deviation of three biological replicates; asterisks indicate statistically significant differences (unpaired two-sample Student's *t*-test, $p < 0.05$) between dexamethasone-treated and mock-treated samples and between the untreated wild type and *jag-2* (dark blue bars).

Chapter 6 - JAG interacts with regulators of the core cell cycle machinery

6.1. Introduction

Live-imaging of wild-type and *jag-1* floral buds over a time-course of 48 hours revealed that the increase in cell proliferation rate and cell growth rates observed in cells of wild-type sepal primordia in comparison to cells in the floral meristem is dependent on JAG. In this respect, cells in *jag-1* sepal primordia behave similarly to cells in the wild-type meristem, suggesting that JAG is required for accelerated growth at the onset of primordia differentiation. In addition, combining an S-phase marker with quantitative 3D analysis of cell geometry revealed that JAG modulates the way cell cycle and cell size are coordinated at the transition from G1 to S-phase (Schiessl et al., 2012; note that imaging data presented in the paper were not obtained by me, therefore I cited the paper whenever imaging results were concerned; also note that the imaging protocol presented in the paper differed from the imaging protocol used in Chapter 7).

As a first step to investigate how JAG modulates the coordination of cell volume and cell proliferation, I aimed to investigate how JAG is linked to the core cell cycle machinery. ChIP-Seq and global expression analysis revealed that JAG directly targeted several key regulators of the core cell cycle machinery, which are all interactors of the cyclin-dependent kinase A (CDKA). Specifically, JAG directly repressed two members of the of the *CYCLIN D* family, two members of the *CYCLIN P* family and two members of the *Kip-related protein (KRP)* family of cell cycle inhibitors.

6.2. JAG directly targets several members of the CYCLIN D and CYCLIN P protein family

JAG directly targeted two members of the *CYCLIN D3* subfamily, *CYCD3;1* and *CYCD3;3*. In particular, qRT-PCR showed that *CYCD3;3* was activated upon ectopic JAG activation but also in the *jag-2* mutant (Figure 6.1.A-B). As regulatory subunits, D-type cyclins form complexes with CDKA to promote the G1/S transition by phosphorylating RBR, which

leads to a de-repression of *E2Fa* and its *dimerisation partner* (*Dp*), and consequently to downstream activation of genes required for DNA replication in S-phase. Accordingly, all three members of the cyclin subgroup CYCLIN D3 in *Arabidopsis*, *CYCD3;1-3* are expressed during early to late G1 phase (De Veylder et al., 2003 and 2007).

In floral organ primordia, all three members of the *CYCD3* subfamily are expressed at all stages of development until full anthesis (Dewitte et al., 2007). In petals of the triple loss of function mutant, the total number of cells was reduced to 60% while average cell size was almost doubled, resulting in final organ sizes comparable to wild type for the *cycd3;1-3* triple loss of function mutant. While mature wild type petals do not consist of endoreduplicated cells, it has been shown by flow cytometry that in the *cycd3;1-3* triple mutant a significant number of cells had undergone one or two cycles of endoreduplication leading to a peak at 4C and 8C (Dewitte et al., 2007). In addition, an earlier onset of endoreduplication during leaf development was observed in the triple loss of function mutant, which also lead to increased final ploidy levels in mature leaves. Consistently, ectopic expression of *CYCD3;1* led to increased cell proliferation, a decrease in ploidy levels resulting in mature organs with an increased number but smaller cells (Dewitte et al., 2007). Together, this suggested that *CYCD3;3-1* are not essential for cell cycle progression, but that *CYCD3;1-3* modulate the contribution of cell division, endoreduplication and cell expansion to organ growth and ultimately to final organ size.

It has been shown that cytokinin induces *CYCD3* expression and that ectopic *CYCD3* expression was able to regenerate shoots from callus in cell culture without addition of exogenous cytokinin, suggesting that *CYCD3* is a direct target of cytokinin and mediates the cell proliferation promoting effects of cytokinin in the meristem (Dewitte et al., 2007). Furthermore, cytokinin levels were unchanged in the *cycd3;1-3* mutant, while cell proliferation in the shoot meristem was defective resulting in reduced meristem size in the *cycd3;1-3* mutant that was reminiscent of the *lonely guy* (*log*) loss of function phenotype in rice and the *CKX* overexpressor phenotype in *Arabidopsis* (Kurakawa et al., 2007; Werner et al., 2003). In addition, *CYCD3* is target of the growth promoting factor *ANTEGUMENTA* (*ANT*) which is a direct target of the auxin-inducible gene *ARGOS*, suggesting that *CYCD3* not only promotes cell proliferation downstream of cytokinins, but also downstream of auxin (Hu et al., 2003; Dewitte et al., 2007).

Interestingly, expression array data and qRT-PCR results suggested that *CYCD3;3* is directly up-regulated upon ectopic JAG activation but also up-regulated in the *jag*-2 loss of function mutant. One possible explanation for this expression pattern is provided by the global ChIP-Seq and expression array: Among the core targets of JAG, several members of the *LONELY GUY* (*LOG)* family, which increase the levels of bioactive cytokinins (Kuroha et al., 2009), were found to be ectopically expressed in the *jag-1* loss of function mutant, while the cytokinin-degrading enzyme *cytokinin oxidase/dehydrogenase* (*CKX6*) showed decreased expression levels in the *jag-1* loss of function mutant. Together these changes may lead to increased levels of bioactive cytokinin in the *jag* loss of function mutant and consequently induce ectopic *CYCD3* expression. Similarly, changes in auxin signaling (see Chapter 8) in the *jag* mutant could change *CYCD3* levels. Another explanation for the ectopic expression of *CYCD3* in the *jag* loss of function mutant could be a compensatory response to the ectopic expression of *KRPs* observed in the *jag* loss of function mutant. In this respect, Cheng et al. (2013) found that mRNA levels of *CYCD3;2* and *CYCD3;3* were down-regulated in the *krp1/2/4/5/7* quintuple mutant.

Furthermore, two members of the *P-type cyclin* family, *(CYCP) CYCP 3;1* and *CYCP 4;1* were identified as directly repressed upon JAG-GR activation in the expression array and in an independent qRT-PCR experiment. In addition, *CYCP 3;1* but not CYCP *4;1* showed increased mRNA levels in the *jag-2* mutant compared with the wild-type (Figure 6.1.C-F). *CYCPs* are a highly conserved but only recently discovered group of cyclins in plants (Torres Acosta et al., 2004). In *Arabidopsis thaliana,* seven *CYCPs* have been identified and all have been shown to bind to *CDKA;1* in a yeast two-hybrid assay. *CYCPs* have been shown to be expressed in the shoot apex and early leaf primordia (Torres Acosta et al., 2004). Motifs within the *CYCP* sequences share high similarity with *PHO80* proteins in budding yeast which are involved in phosphate signaling, but no evidence has been found for this function in plants and their function remains unclear (Torres Acosta et al., 2004).

Because my expression profiling experiments suggested strong regulation of *CYCP3;1* by JAG, I investigated the genetic interaction between these two genes by generating a double loss of function mutant. However, the *cycp3;1 jag* double mutant did not show any developmental or morphological changes compared to the *jag-1* single mutant (data not shown). I next aimed to investigate whether *CYCP3;1* and *CYCP4;1* have redundant

functions, because both genes have similar expression domains and were directly repressed by JAG. Therefore, I aimed to generate a triple *cycp3;1, cycp4;1 jag-1* mutant. However, attempts to generate a triple mutant by crossing have been unsuccessful so far, most likely because *CYCP3;1(AT2G45080)* and *CYCP4;1(AT2G44740)* are located in close vicinity within a distance of 150 kb on chromosome 2 and may therefore be strongly linked. It must also be noted that I have not yet investigated the mRNA levels of *CYCP3;1* and *CYCP4;1* in mutants to verify that they are indeed mRNA null.

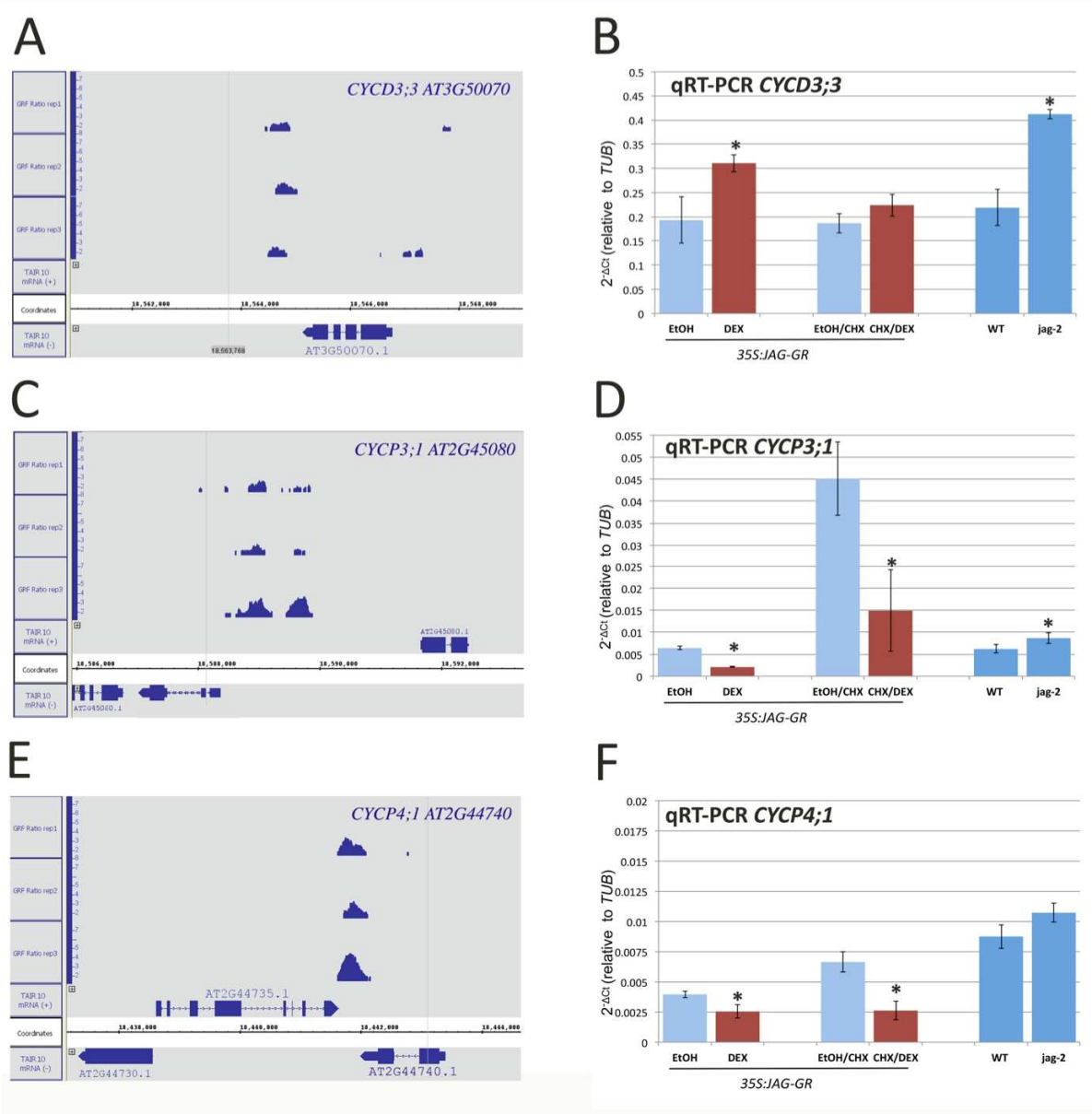

Figure 6.1. ChIP-Seq peaks detected in each replicate within 3 kb upstream and 1.5 kb downstream of the coding sequences and qRT-PCR in inflorescence apices of *35S::JAG-GR* plants, wild-type, and *jag-2* mutant plants.

(A, C, E) Visualisation of read enriched regions mapping to the TAIR10 Arabidopsis reference genome (x-axis) using the Integrated Genome Browser (Nicol et al., 2009), ChIP-Seq peak score values (y-axis) based on the ratios of normalised reads between JAG-GFP and control samples were calculated for every single nucleotide position using CSAR software (Muiño et al., 2011a), the maximum score value within the candidate peaks was used to test for significance of the enrichment; ChIP-Seq peaks detected in each replicate within 3 kb upstream and 1.5 kb downstream of the coding sequences for the *CYCD3;3*

locus on chromosome 3, the CYCP3;1 locus and CYCP4;1 locus on chromosome 2. (B, D, F) Expression levels (relative to the *TUB4* constitutive control) of *CYCD3;3*, CYCP3;1 and CYCP4;1; mRNA measured by qRT-PCR in inflorescence apices of *35S::JAG-GR* plants 4h after mock treatment (light blue) or treatment with dexamethasone 10 µM (red); CHX indicates samples from plants that were also treated with cycloheximide 10 µM or untreated wild-type (WT) and *jag-1* plants (dark blue); bars show the mean and standard deviation of three biological replicates; asterisks indicate statistically significant differences (unpaired two-sample Student's *t*-test, $p < 0.05$) between dexamethasone-treated samples and corresponding controls or between the wild type and *jag-2*.

6.3. JAG directly represses *KRP2* and *KRP4*

6.3.1. *KRP* genes are strong candidates to mediate the effects of *JAG* on cell cycle progression

My ChIP-Seq and array experiments also revealed that JAG directly represses *KRP2* and *KRP4,* which are members of the plant-specific protein family of *Kip-related proteins* and show sequence similarity to a conserved domain in the three *KIP/C*IP proteins *CiP p21, KIP p27 and p57* in mammals. The mammalian *CIP/KIP family* are cyclin-dependent kinases inhibitors (CKI) that negatively regulate the G1 to S-phase transition and are involved in checkpoint control during cell cycle progression and in exit from proliferation phase preceding differentiation (reviewed by Denicourt and Dowdy, 2004; Besson et al., 2008). In *Arabidopsis*, seven members of the KRP protein family have been characterized as low molecular weight proteins of 24 kD and 31 kD for KRP2 and KRP4, respectively (De Veylder et al., 2001). Similar to their mammalian counterparts, all seven members have been shown to particularly bind *CDKA;1* and members of the G1/S-phase specific D-type cyclins in a yeast two-hybrid assay (de Veylder et al., 2001; Zhou et al., 2002a). All members of the KRP protein family share a conserved CDK-interacting domain at the C-terminus (Torres Acosta et al., 2011).

Association of KRPs with cyclin/CDKs complexes has been shown to destabilise the ATP binding site in CDKA and consequently inhibit its dephosphorylation, which is required to activate CDKA to phosphorylate RBR at the transition from G1 to S-phase. RBR is a repressor of the E2F/DP transcription factor complex that promotes the transition from G1 to S-phase by promoting the expression of genes required for S-phase entry and DNA replication. Coexpression of a dominant positive allele of the plant *CDKA;1* which caused premature cell proliferation with decreased cell sizes in yeast, with KRP2 and KRP4 resulted in enlarged yeast cells owing to cell cycle arrest, providing evidence that KRPs can inhibit CDKA activity and cell cycle progression *in vivo* (de Veylder et al., 2001). In addition, it has been shown that CDKA activity was decreased *in planta* upon ectopic expression of *KRP1* (Wang et al., 2000). Consistently, CDKA activity measured *in planta* by a histone H1 phosphorylation assay was gradually increased in *krp* double, quadruple and quintuple mutants. By contrast, *CDKA* expression levels were only slightly increased in the quintuple mutant, providing further evidence that KRPs inhibit CDKA activity at the level

of phosphorylation rather than at transcriptional level (Cheng et al., 2013). In line with the increase in CDKA phosphorylation activity, an increase of phosphorylated RBR1 levels and an increase in expression levels of genes promoted by the E2F pathway were observed in the quintuple mutant. In addition, five mitotic cyclins were upregulated in the *krp* quintuple mutant while the G1 to S-phase associated *CYCLIN D3;2-3* were down regulated (Cheng et al., 2013).

Furthermore, it has been shown that all members of the *Arabidopsis* family including *KRP4* and *KRP2* are under post-translational control and interacted with FBL17, a mediator of proteosomal degradation, in a BiFC experiment in tobacco leaves (Zhao et al., 2012). Zhou et al. (2003) showed that in *ICK1* the N-terminal domain is needed for protein instability. Co-expression assays performed in tobacco leaves showed that the presence of FBL17 protein reduced the fluorescence signal, particularly of KRP4-GFP and KRP7-GFP fusion proteins, and to a lesser degree of KRP2-GFP fusion protein (Zhao et al., 2012). It has been shown that FBL17 is a direct transcriptional target of *E2FA* and is under direct control of *RBR1*, suggesting that KRP degradation is under transcriptional control of E2F and RBR1 and a key step at the G1 to S-phase transition.

In wild-type plants, *KRP2* was most highly expressed in flowers, while *KRP4* was expressed in the mitotically active tissue of flowers and leaves (de Veylder et al., 2001; Ormenese et al., 2004). Tissue-specific expression profiling confirmed that *KRP2* and *KRP4* are expressed in young flowers, particularly in petals, and that *KRP2* is specifically expressed in stems (Torres Acosta et al., 2011). While no clear morphological changes were observed in single, double and triple mutants, the *krp1/2/4/5/7* quintuple mutant showed a significant size increase in seeds, cotyledons, leaves and petals, with reduced cell sizes and higher cell density than in the wild type. Together, this suggested that KRPs have a dosage-dependent effect on CDKA activity and act redundantly to repress cell proliferation and to affect mature organ size and shape (Cheng et al., 2013).

Wang et al. (2000) were the first to report on the effects of ectopic expression of *ICK1* (*KRP1*) under the *35S* promoter on mature organ size and shape. Lateral organs such as leaves and floral organs were reduced in size. Wang et al. (2000) described the floral phenotype for the *ICK1* overexpressor, “flowers stayed closer and were at the same level or below the inflorescence apex” and “the flowers appeared like a compact cluster when viewed from the top”, a description reminiscent of the *jag* loss of function mutant,

particular in L-*er* background. Wang et al. (2000) further speculated that this close appearance might be caused by reduced growth of the inflorescence stem and the pedicels. In respect to the petal phenotype of the *KRP1* overexpressor Wang et al. (2000) reported that sepals, petals and stamen were shorter and reduced in overall size and "petals were narrower with serrations along the top edge". In addition, ectopic expression of *KRP2* under the *35S* promoter resulted in smaller serrated leaves and "sepals and petals modified in size" that appeared green (De Veylder et al., 2001).

In leaves of *KRP2* overexpressing lines, kinematic analysis revealed that cell proliferation rates were severely reduced and endoreduplication was inhibited resulting in 10-fold fewer but larger cells with lower ploidy levels than in the wild type, while the temporal pattern of organ development and onset of expansion and differentiation was unchanged (de Veylder et al., 2001). In addition, Verkest et al. (2005) specified that weak over-expression of *KRP2* inhibited mitotic CDK-cyclin complexes while endoreduplication was unaffected. Moreover, inhibition of the mitotic cell cycle in lines weakly over-expressing KRP2 appeared to trigger onset of endoreduplication, increasing the number of cells with higher ploidy levels compared to cells in wild-type leaves (Verkest et al., 2005). In a similar way, KRP1 has been shown to bind to CYCD3 and overexpression of *KRP1* caused dwarfed plants with a reduced number but enlarged cells (Wang et al., 2000). This observation was further corroborated by Roeder et al. (2010) who found that mild overexpression of *KRP1* under the epidermal *ATML1* promoter in sepal primordia resulted in an increased number of cells exiting mitotic cell proliferation earlier than in the wild type, resulting in increased number of giant cells with increased ploidy levels compared to wild-type sepals (Roeder et al., 2010).

While no lines with ectopic expression of *KRP4* under the *35S* promoter were recovered (De Veylder et al., 2001), tissue-specific ectopic expression of *KRP4* under the *ATLM1* promoter resulted in reduced numbers of cells with increased final cell sizes in the epidermis of all lateral organs (Bemis and Torii, 2007). Interestingly, epidermis-specific ectopic expression of *KRP1* and *KRP4* caused reduced organ sizes in all lateral organs. For example, floral organs of the *KRP1* and *KRP4* showed prematurely opened floral buds because of distorted sepals, a phenotypic feature reminiscent of the *jag* mutant. Petals appeared slightly shorter and narrower but kept their white appearance in the lobe region suggesting that there was no defect in conical cell type formation (Bemis and Torii,

2007). In sepals, Bemis and Torii (2007) observed that non-giant cells increased to abnormally large sizes upon epidermal specific ectopic expression of *KRP1* and *KRP4,* while Roeder et al. (2010), who investigated the effect of epidermal layer-specific ectopic expression of *KRP1* in a live-imaging approach, observed an increase in the number of giant cells. In summary, work on *KRPs* has provided evidence that they are key cell cycle inhibitors and that ectopic expression of *KRP* has an effect on final cell number, final cell sizes and final organ sizes and shapes.

The observations described above indicated that the interaction between JAG and KRP genes was likely to be functionally relevant. For this reason, I aimed to confirm that JAG directly represses *KRP2* and *KRP4* in the context of floral organogenesis using ChIP followed by q-PCR, qRT-PCR and RNA *in situ* hybridization. Furthermore, I aimed to investigate the expression domains of *KRP2* and *KRP4 in vivo* using GFP- and GUS-reporter constructs in wild-type and *jag* loss of function mutant background. *KRP2* overexpressing lines have narrower, serrated leaves and show defects in floral organ development with partial male sterility (de Veylder et al., 2001 and Zhou et al., 2002), similar to *jag* loss of function mutants. Therefore, I speculated that ectopic *KRP2* expression in the *jag* mutants might be at least partially the cause for the similar growth defective phenotypes. I further hypothesized that generating a double loss of function mutant would rescue the wild-type phenotype in flowers. By generating *krp2 jag* and *krp4jag* double and *krp2 krp4 jag* triple loss of function mutants, I aimed to investigate whether repression of *KRPs* by JAG is required for wild-type floral organ development.

6.3.2. Results

6.3.2.1. *KRP2* and *KRP4* are direct targets of JAG

The cell cycle inhibitors *KRP2* and *KRP4* have been identified as directly down-regulated targets of JAG in the overlap of the ChIP-Seq data and the global expression profiling data (see Chapters 2 and 3). In the ChIP-Seq experiment, two DNA binding sites with significant enrichment have been identified near the genomic region of *KRP2*, with one maximum peak score located 1.4 kb upstream of the transcriptional start of *KRP2* and the other maximum peak score located 1.2 kb downstream of the stop codon (Figure 6.2.A). For *KRP4,* one significantly enriched DNA binding site was identified 0.3 kb downstream of the stop codon (Figure 6.3.A).

To further confirm the significantly enriched DNA binding sites for *KRP2* and *KRP4*, I performed an independent ChIP experiment using anti-GFP antibodies for immunoprecipitation of the JAG-GFP protein – DNA complex in *jag-2* plants complemented with the *pJAG:JAG-GFP* construct and in L-*er* wild-type plants serving as a negative control. ChiP was followed by qPCR using oligonucleotides designed in close vicinity to the identified maximum peak scores (KRP2 -1616, KRP2 +1342, and KRP4 +295). For both DNA binding sites near the genomic region of *KRP2* and for the DNA binding site 0.3 kb downstream of the stop codon of *KRP4* a significant enrichment was observed in immuno-precipated DNA from *pJAG:JAG-GFP jag-2* inflorescences in comparison to immunoprecipitated DNA from wild-type inflorescences, when normalised to the input DNA of the samples (Figure 6.2.B and 6.3.B).

As a further control of the DNA binding specificity of JAG, I performed qPCR using oligonucleotides that amplified a region within 3 kb upstream of the start codon of *KRP2* and *KRP4,* but were at least 0.5 kb distant from the peaks assigned by ChiP-Seq (KRP2 -159 and KRP4 -1691). In addition, the DNA binding site 1.3 kb upstream of the transcriptional start of *KRP2* was confirmed using anti-GR antibodies for immuno-precipitation of ectopic JAG-GR protein–DNA complexes in wild-type plants harbouring the DEX-inducible *35S:JAG-GR* construct. In this experiment, ectopic JAG-GR was activated by DEX treatment and control plants harboring the *35S:JAG-GR* were treated with ethanol. To confirm the enrichments with q-PCR oligonucleotides KRP2 -1616 and KRP2 -159 were used (Figure 6.4.).

6.3.2.2. JAG represses *KRP2* and *KRP4*

To further confirm that JAG not only binds to the genomic regions near the *KRP2* and *KRP4* loci, but also transcriptionally regulates them, I performed qRT-PCR and RNA *in situ* hybridisation experiments. In the expression-array experiment, *KRP2* and *KRP4* were found to be significantly repressed (FDR<0.01) upon ectopic JAG-GR activation with a $\log_2$ ratio of -1.44 and -0.84 respectively (see Chapter 2). To confirm the global expression profiling data, I performed qRT-PCR on inflorescence apices tissue of wild-type plants harbouring the *35S:JAG-GR* construct. For ectopic JAG activation, the plants were subjected to a DEX treatment or ethanol-control treatment and incubated for 4 hours.

Because the Kip-related protein family consists of seven members *KRP1-KRP7* (De Veylder et al., 2001), I compared the expression levels of all seven protein family members in floral apices by qRT-PCR (Figure 6.5.A). Firstly, I found that *KRP2* and *KRP4* have significantly higher expression levels in floral apices compared with the other five members of the *KRP* family (*KRP1*, *KRP3* and *KRP5-7*). Furthermore, the qRT-PCR results confirmed that *KRP2* and *KRP4* expression levels were decreased upon ectopic JAG-GR activation. In addition, I observed significant up-regulation of *KRP2* mRNA levels in the *jag-2* mutant compared with wild type (p-value <0.05). By contrast, up-regulation of *KRP4* was not significant between the *jag-2* loss of function mutant and the wild type (p-value <0.05) (Figure 6.5.B). Interestingly, in the micro-array experiment, neither *KRP2* nor *KRP4* were found to be significantly differentially expressed between wild type and *jag-1* loss of function background. In addition to *KRP2* and *KRP4*, *KRP7 (At1g49620)* was identified as a direct target in the ChIP-Seq experiment (see Chapter 3). However, *KRP7* did not show any significant differences in the expression array experiments and could not be confirmed by qRT-PCR, possibly because of very low expression levels in the inflorescence apices.

In summary, these data further supported that *KRP2* is directly repressed by JAG in floral apices and that the repressor function of JAG is clearly reflected in ectopic expression in the *jag* loss of function background. By contrast, *KRP4* is directly repressed by JAG but was not significantly differently expressed between wild type and *jag* loss of function mutants. In this respect, JAG might repress *KRP4* in a very specific temporal and spatial context and therefore its repressor effect might be diluted when sampling whole inflorescence apices. Or, *KRP4* might be redundantly repressed by other genes controlling organ growth in floral apices.

A good candidate to function redundantly with JAG is the single C_2H_2 zinc finger transcription factor *NUBBIN/JAG-LIKE* (*NUB/JGL*) (Ohno et al., 2004; Dinneny et al., 2004; Norberg et al., 2005; Dinneny et al., 2006). *NUB* shares 34% sequence similarity with *JAG* and has been characterised as the closest homolog to *JAG* (Dinneny et al., 2004). Double homozygous *jag nub* mutants show severely reduced and serrated sepals and petals, and are sterile. To investigate whether *NUB* acts redundantly with *JAG* to control *KRP2* and *KRP4,* I performed qRT-PCR on cDNA derived from inflorescence apices of *jag-1* and *nub* single mutants, the *jag-1 nub* double mutant (homozygous for both loss of function

mutations) and wild type, all in *Col-0* background. While mRNA levels of *KRP2* were further increased in the *jag-1 nub* double loss of function mutant compared to the *jag-1* single mutant (Figure 6.6.A), no significant change was observed for *KRP4* expression levels in the *jag-1 nub* double mutant (Figure 6.6.B). This suggests that *KRP2* but not *KRP4* is at least in part under control of NUB. Therefore, JAG and NUB act redundantly to repress *KRP2* but not *KRP4*. In addition, no significant changes in mRNA levels were observed between the *nub* single loss of function mutant and wild type, further supporting the observation that particularly *JAG* acts as a strong repressor of *KRP2*.

To investigate whether loss of *KRP2* function would rescue the severe phenotype of the *jag-1 nub* double mutant, I generated *the jag-1, nub, krp2-3* (the *krp2-3* allele will be introduced in more detail below) triple mutant in *Col* background. Similarly to the phenotype of the *jag-1 krp2-3* double mutant, discussed in more detail below, the *jag-1 nub krp2-3* triple mutant showed a partial but significant rescue of distal petal width and smoother petal margins in comparison with the *jag-1 nub* double mutant (Figure 6.7.A-F) (no measurements taken). However, overall organ size was still significantly smaller in the triple loss of function mutant compared to the *jag* single loss of function mutant and loss of KRP2 function did not rescue the sterility in the double homozygous *jag nub* mutant. Interestingly, *krp2-3 jag-1 nub triple* mutant showed significantly elongated pedicels and thicker stems with increased internode length compared with the *jag-1 nub* double loss of mutant (Figure 6.7.A-D), suggesting that KRP2 has a function in pedicel and inflorescence stem development. This finding is supported by the expression of *KRP2* in stem tissue (Torres Acosta et al., 2011). In the same context, Bemis and Torii (2007) reported that plants ectopically expressing *KRP1* and *KRP4* under the epidermis- specific *ATML1* promoter produced inflorescences with short pedicels and shorter siliques due to reduced cell numbers in these organs. However, I have not observed any obvious differences in pedicel length and stem thickness in the *krp2-3 jag* mutant, suggesting that this phenotype could be caused by the specific interaction between *NUB* and *KRP2*. Measurements of pedicel length, internode length and stem thickness of the *jag-1 nub*, *krp2-3 jag-1*, *krp2-3 jag-1 nub* double and triple mutants would shed further light into this phenotype.

6.3.2.3. Effects of JAG on the expression patterns of *KRP2* and *KRP4* during early organogenesis

In summary, the combination of ChIP experiments and the expression array analysis, both confirmed by independent qPCR experiments using L-*er* and Col ecotype background, provided me with consistent evidence that JAG represses *KRP2* and *KRP4* in inflorescence apices. However, the sampled inflorescence apices consisted of a mixture of floral buds at different developmental stages with an array of different tissues (meristems, perianth and reproductive organs). In the next step, I aimed to investigate the spatial and temporal pattern of *KRP2* and *KRP4* expression in floral organogenesis in wild-type background. Furthermore, I aimed to investigate the expression domains of ectopic *KRP2* and *KRP4* expression in the *jag* mutant background.

I performed *RNA in situ* hybridisation using DIG-labeled probes for *KRP2* and *KRP4* on *jag-2* mutant and wild-type inflorescences. Both, the *KRP2* probe (594 nt) and the *KRP4* probe (553 nt) were designed to avoid the C-terminal region, which has been reported to be highly conserved between the seven members of the Kip-related protein family (de Veylder et al., 2001). For *KRP2,* a strong signal was observed in inner deeper layers of the inflorescence meristem and the floral meristem for both *jag-2* and wild-type flowers (Figure 6.8.A-B). Furthermore, in some buds a signal was detected in early sepal primordia emerging from the floral meristem particularly at the adaxial side in *jag-2* mutant flowers compared to wild-type buds of similar developmental stage. For *KRP4,* I detected a faint spotty signal that was difficult to interpret and I did not observe any significantly obvious differences in probe signal between flowers of the *jag-2* loss of function mutant and the wild type (Figure 6.8.C-D), which was consistent with the qRT-PCR results for *KRP4*. Similar to my experiment, Bemis and Torii (2007) used RNA *in situ* hybridization with a similar probe to detected expression of *KRP4* in inflorescence tissue and observed a faint signal throughout the shoot apical meristem, the inflorescence meristem, the floral meristem, young floral organ primordia, suggesting very low abundance for the *KRP4* mRNA. However, for my experiment that aimed to reveal differences in expression pattern for *KRP2* and *KRP4* between the *jag-1* mutant compared with wild type, I had to conclude that RNA *in situ* hybridisation did not help to localise the expression domains of *KRP4*, and only in part, helped to localise the expression domains of *KRP2.* Even though I

observed ectopic *KRP2* expression in the adaxial side of early sepal primordia, these results were not clearly visible in all floral buds.

For this reason I aimed to observe *KRP2* and *KRP4* expression domains *in vivo* with reporter lines. I generated fluorescent reporter lines for KRP2 and KRP4 . The *pKRP2:KRP2-GFP* included the complete genomic sequences from 3.65 kb upstream of the start codon to 1.33 kb 3' of the stop codon, including all coding sequences and introns, with the 700 bp GFP cDNA fragment inserted in frame at the end of the KRP coding sequence. In contrast, the *KRP4* reporter consisted of a 1.3 kb promoter region, a truncated genomic region reduced to the first intron and exon, with the conserved C-terminal CDK interacting domain deleted (De Veylder et al., 2001), fused to the *CYPET* cyan fluorescent protein cDNA sequence (700 bp) and a 1.3 kb 3' region. With this construct I aimed to disrupt the CDK-binding function of the gene in order to exclude any interference with the endogenous KRP4 function while retaining signals for protein-protein interactions, nuclear localization, and degradation.

The *pKRP2:KRP2-GFP* reporter lines showed good expression levels in seedling roots, with the GFP signal being clearly nuclear-localised (Figure 6.9.). In the inflorescence, a strong nuclear GFP signal was observed in the deeper cell layers of inflorescence meristems and floral meristems of *jag-1* mutant (Figure 6.10.A) and wild-type plants (Figure 6.10.B) harboring the *pKRP2:KRP2-GFP* construct, consistent with the signal observed in the *RNA in situ* hybridization experiment. While, in early floral stages (until stage 3-5, according to Smyth et al., 1990), KRP2-GFP was detected in the deeper layers of the floral meristems, in later stages (from stage 6 onwards according to Smyth et al., 1990) KRP2-GFP was detected in the sepal primordia in wild-type and *jag-1* plants (Figure 6.10.C-H). In addition, KRP2-GFP was also observed in the apical region of the central hollow tube forming the future gynoecium, which was prematurely exposed in *jag-1* mutant flowers compared to the wild type flower where the sepals tightly enclose the inner whorls and did therefore not allow access for confocal imaging.

As seen for *pKRP2:KRP2-GFP*, the *pKRP4:KRP4x-CYPET* also showed clear signal in seedling roots (Figure 6.9.). By contrast, no *KRP4x-CYPET* signal was observed in the inflorescence tissue of wild-type plants (data not shown). In this context, Jakoby et al., (2006) who investigated subcellular localization of the KRP1 protein, reported that KRP1 has several NLS signals, one of which is located within the CYCD and CDK binding domains

at the C-terminus of the protein. Deletion of the C-terminal located nuclear localization signal (NLS) excluded KRP1-YFP from the nucleus, suggesting that by deleting the complete C-terminus I not only deleted the CDK interacting function but possibly also deleted an important nuclear localization signal.

The expression patterns of KRP2 and KRP4 were further investigated by crossing GUS-reporter lines for *KRP2* and *KRP4* (gifts from Lieven De Veylder) into the *jag-1* mutant background. The KRP2:GUS signal was consistent with the expression pattern observed in the lines harboring the *pKRP2:KRP2-GFP* construct*:* KRP2-GUS appeared not to be expressed in the youngest floral buds, but was detected in sepal and petal primordia at later developmental stages (Figure 6.11.). In the *jag-1* mutant background, the GUS signal was stronger and appeared to extend into the basal regions of the petals, while in the wild type it appeared to be restricted to the margins. In both backgrounds, the KRP2:GUS signal was strong in the developing style and stigma and faded away before anthesis. In addition, KRP2:GUS expression was detected in the pedicel, which was particularly strong in the *jag-1* background compared to the wild type (Figure 6.11.). No KRP4:GUS signal could be detected in the inflorescence tissue even though presence of the construct was confirmed by early GUS expression in seedling roots (data not shown), suggesting that KRP4:GUS signal was too weak to be detected in floral organs.

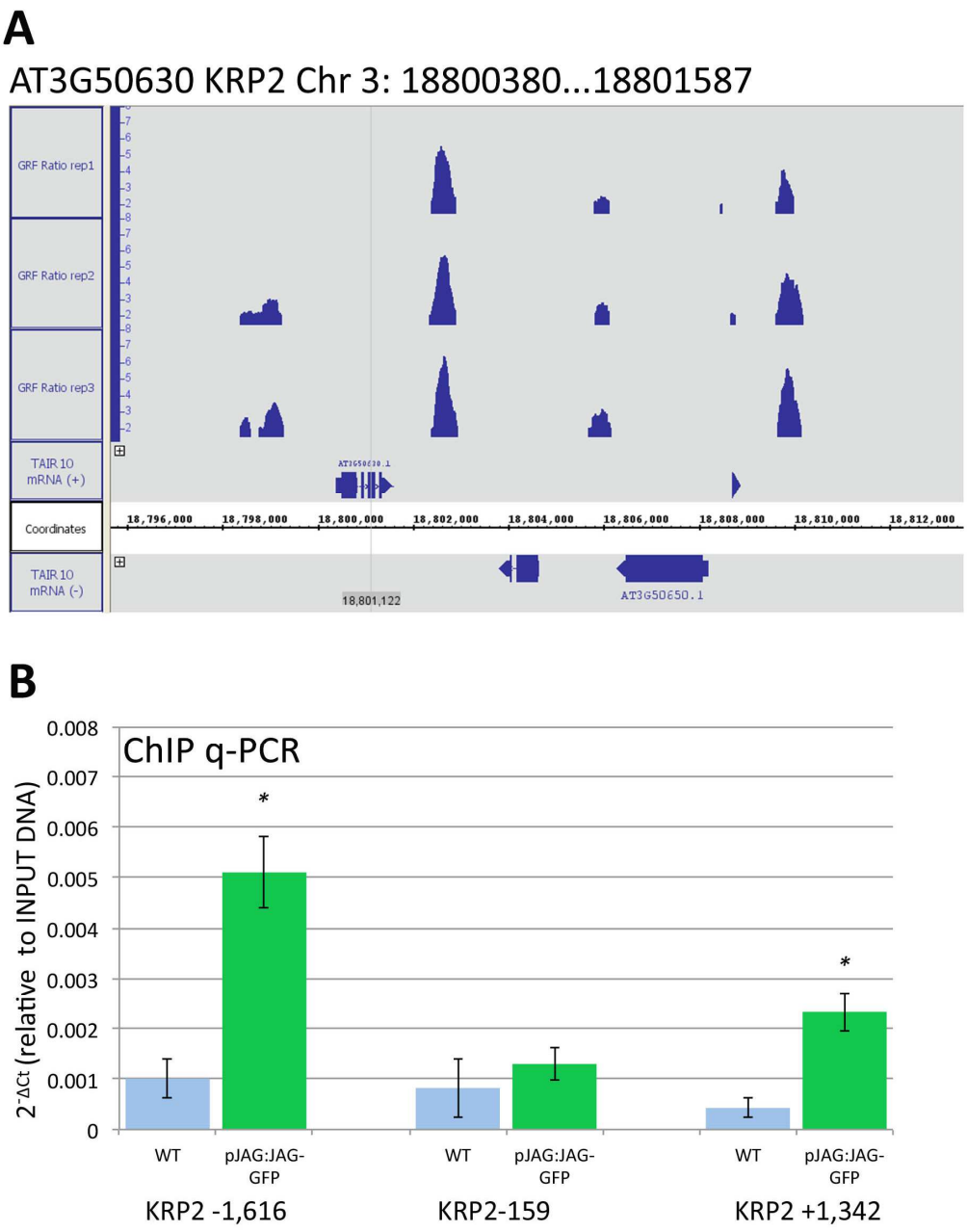

Figure 6.2. Endogenous JAG-GFP directly binds upstream and downstream of the *KRP2* locus. (A) Visualisation of read enriched regions mapping to the TAIR10 Arabidopsis reference genome (x-axis) using the Integrated Genome Browser (Nicol et al., 2009), ChIP-Seq peak score values (y-axis) based on the ratios of normalised reads between JAG-GFP and control samples were calculated for every single nucleotide position using CSAR software (Muiño et al., 2011a), the maximum score value within the candidate peaks was used to test for significance of the enrichment; ChIP-Seq peaks detected in each replicate within 3 kb upstream and 1.5 kb downstream of the coding sequence for the *KRP2* locus

on chromosome 3. (B) Binding of JAG-GFP to the upstream and downstream region of *KRP2* confirmed by ChIP-qPCR; target sequences 1.6 kb upstream of the transcriptional start of *KRP2* and 1.3 kb downstream of the stop codon, including a control region 0.16 kb upstream of the *KRP2* transcriptional start; bars show the mean and standard deviation of three biological replicates; numbers below the bars indicate the left border of the q-PCR amplicon relative to the coding sequence; asterisks indicate significant difference to the negative WT control ($p < 0.05$, Student's *t*-test).

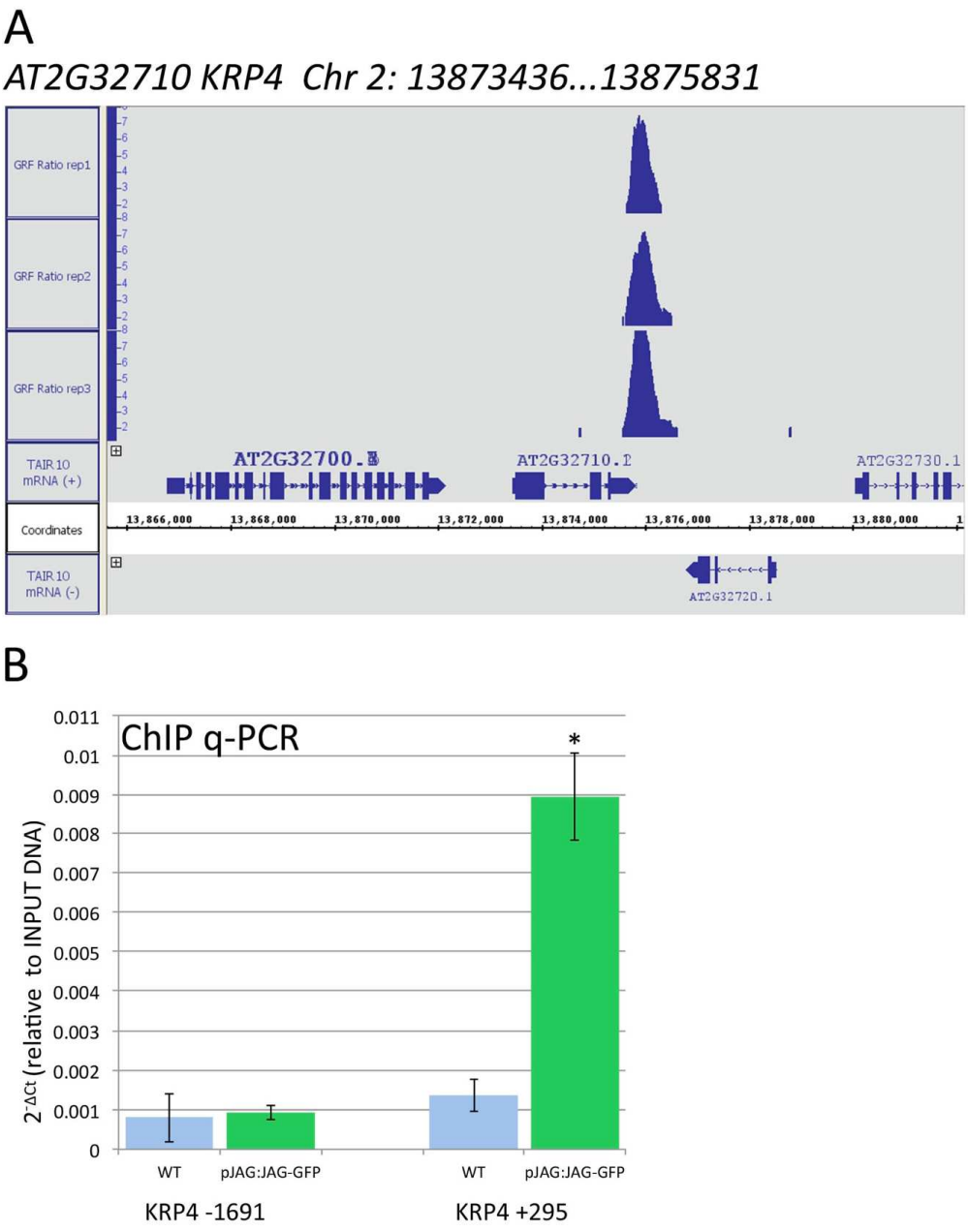

Figure 6.3. Endogenous JAG-GFP directly binds downstream of the *KRP4* locus.

(A) Visualisation of read enriched regions mapping to the TAIR10 Arabidopsis reference genome (x-axis) using the Integrated Genome Browser (Nicol et al., 2009), ChIP-Seq peak score values (y-axis) based on the ratios of normalised reads between JAG-GFP and control samples were calculated for every single nucleotide position using CSAR software (Muiño et al., 2011a), the maximum score value within the candidate peaks was used to test for significance of the enrichment; ChIP-Seq peaks detected in each replicate within 3 kb upstream and 1.5 kb downstream of the coding sequence for the *KRP4* locus on chromosome 2. (B) Binding of JAG-GFP to the downstream region of *KRP4* confirmed by ChIP-qPCR; target sequences 0.3 kb downstream of the KRP4 stop codon and a control region 1.7 kb upstream of the *KRP4* transcriptional start; bars show the mean and standard deviation of three biological replicates; numbers below the bars indicate the left border of the q-PCR amplicon relative to the coding sequence; asterisks indicate significant difference to the negative WT control ($p < 0.05$, Student's *t*-test).

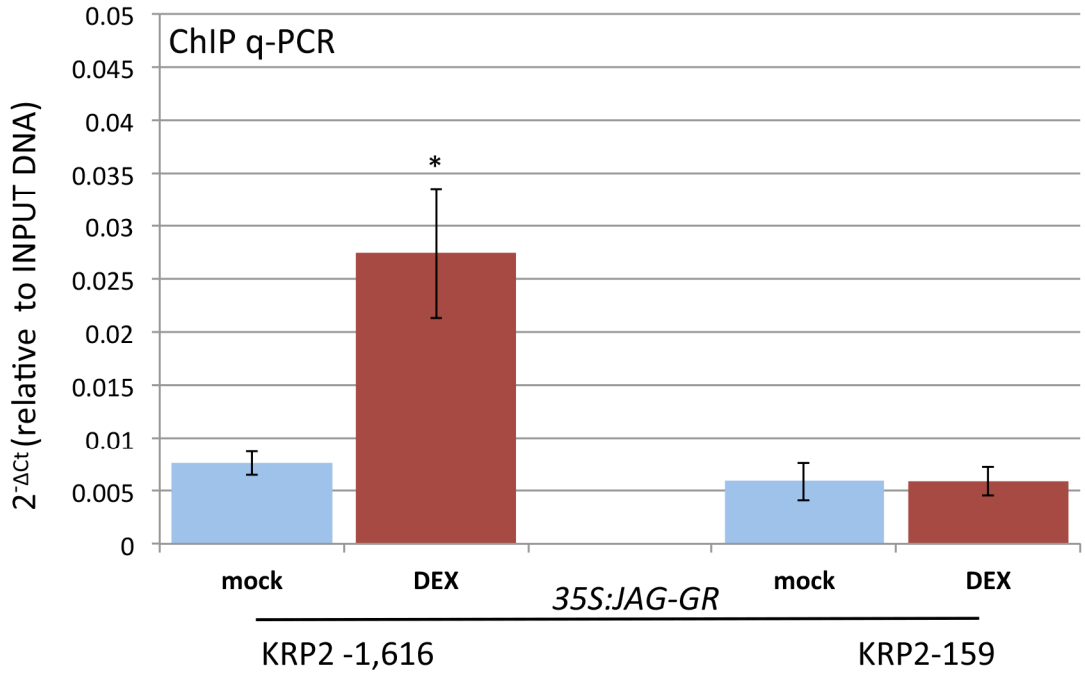

Figure 6.4. Ectopic JAG-GR binds to the promoter of *KRP2*. Chromatin immunoprecipitation (ChIP) using anti-GR antibodies and inflorescence apices of *35S::JAG-GR* plants 4 h after mock treatment (light blue) or treatment with dexamethasone 10 µM (red); target sequences 1.6 kb and control sequence 0.16 kb

upstream of the *KRP2* transcriptional start; bars show the mean and standard deviation of three biological replicates; numbers below the bars indicate the left border of the q-PCR amplicon relative to the coding sequence; asterisks indicate significant difference to the mock control ($p < 0.05$, Student's *t*-test).

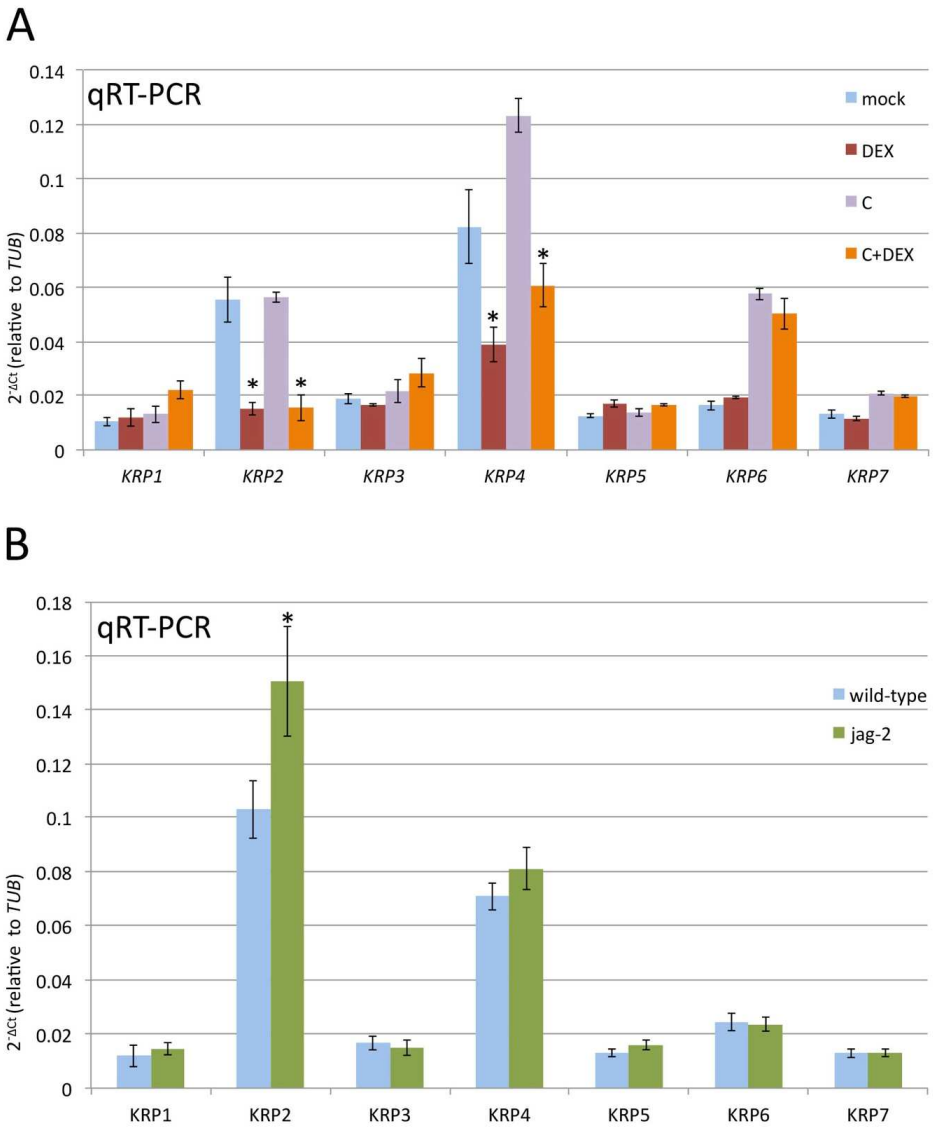

Figure 6.5. Expression analysis by qRT-PCR for the seven members of the KIP-related protein family. JAG represses *KRP2 and KRP4*. Expression levels for *KRP1-KRP7* (relative to the *TUB4* constitutive control); (A) in inflorescence apices of *35S::JAG-GR* plants 4h after mock treatment (light blue) or treatment with dexamethasone 10 µM (red); mock treatment in the presence of cycloheximide 10 µM (lilac), DEX-treatment in the presence of cycloheximide (orange); (B) in inflorescence apices of wild-type (blue) and *jag-2*

inflorescences (green); bars show the mean and standard deviation of three biological replicates; asterisks indicate statistically significant differences (unpaired two-sample Student's *t*-test, $p < 0.05$) between dexamethasone-treated samples and corresponding controls or between the wild type and *jag-2*.

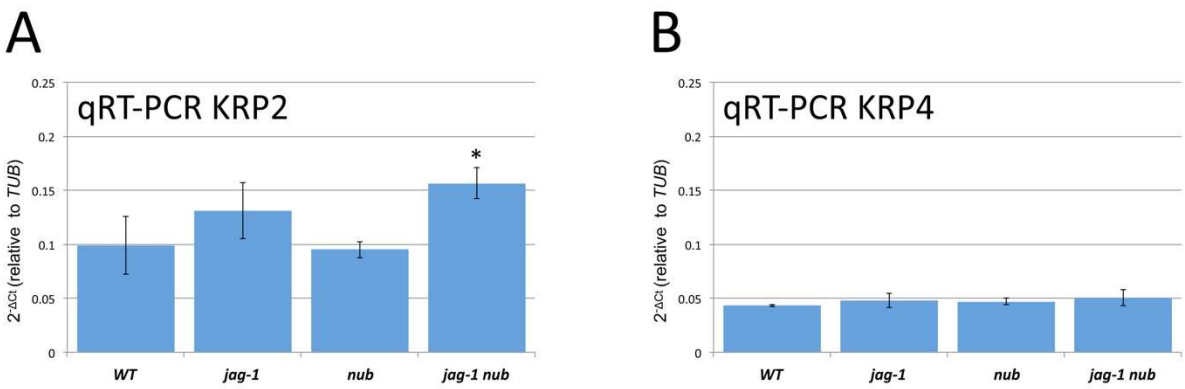

Figure 6.6. Expression analysis by qRT-PCR for *KRP2* and *KRP4* in *jag-1* and *nubbin* loss of function mutant background. Expression levels for (A) *KRP2* and (B) *KRP4* (relative to the *TUB4* constitutive control) in inflorescence apices of *jag-1* and *nub* single mutants and the *jag-1 nub* homozygous double mutant compared to wild type; bars show the mean and standard deviation of three biological replicates; asterisks indicate statistically significant differences (unpaired two-sample Student's *t*-test, $p < 0.05$) between the mutants and wild type.

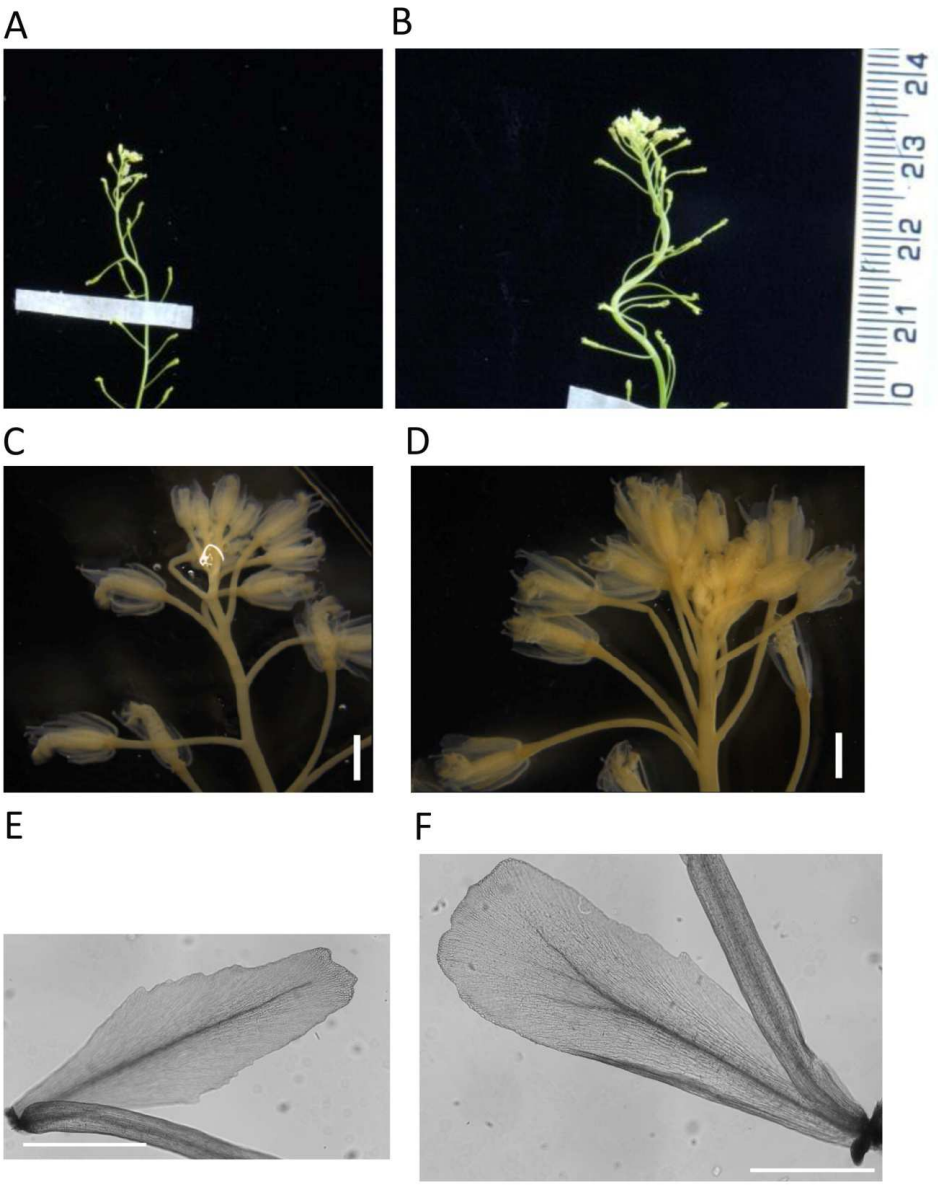

Figure 6.7. The *krp2-3 jag-1 nub* triple loss of function mutant shows in part rescue of distal organ growth of floral organs, elongated pedicels and increase in pedicel and inflorescence stem thickness. Scale bars: Ruler on the right applies for (A) and (B); (C-D) 1 mm, (E-F) 500 µm;

Inflorescence phenotype of (A, C) the homozygous *jag-1 nub* double loss of function mutant compared to the (B, D) homozygous *jag-1 nub krp2-3* triple loss of function mutant with elongated pedicels and increased stem width. (E-F) Petal of the homozygous *jag-1 nub* double mutant (E) compared to the *jag-1 nub krp2-3* triple mutant which shows a broader distal lobe area with smoother distal margins. Petals were imaged using the light microscope DM6000 with 10X magnification as described below.

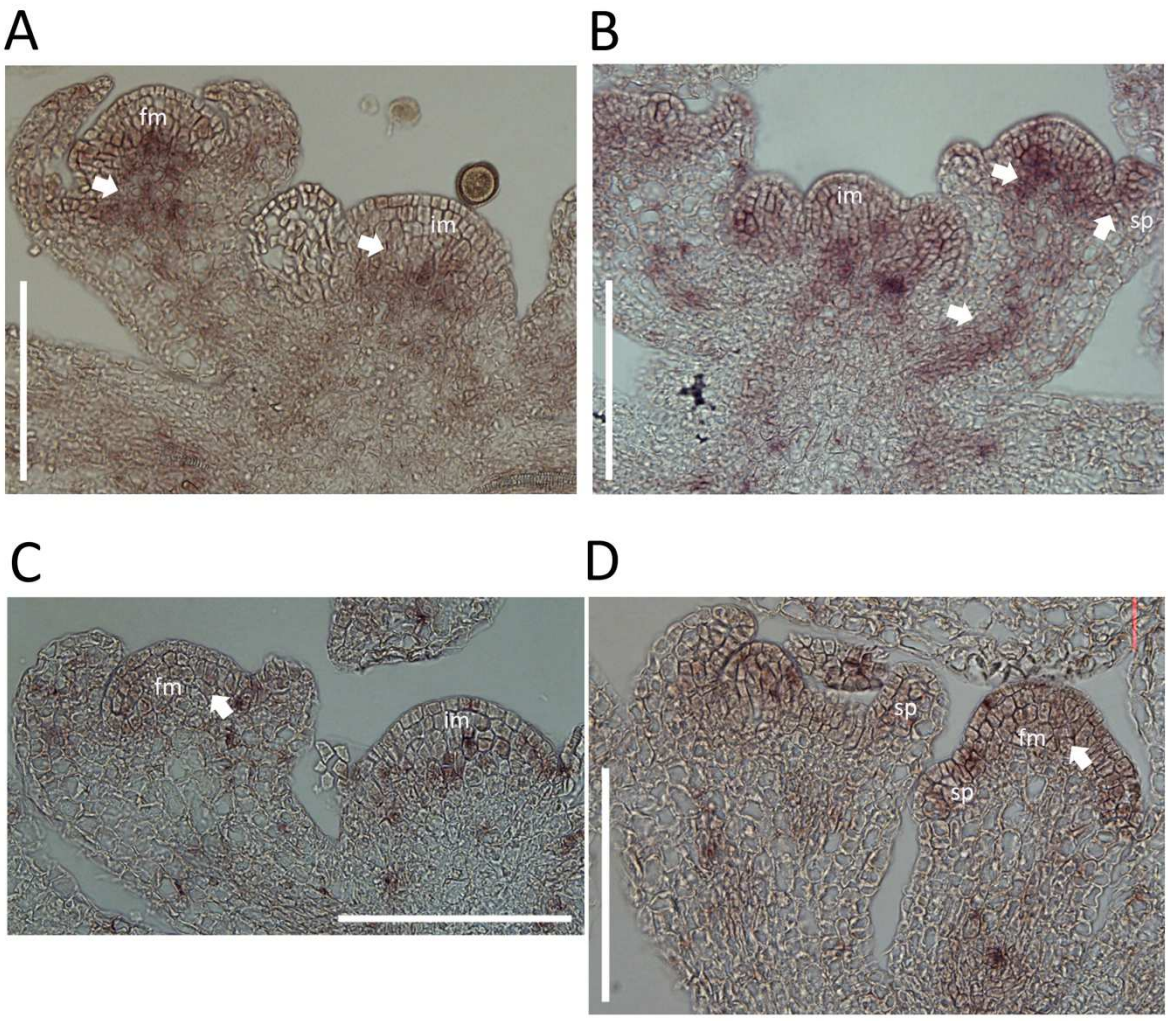

Figure 6.8. *RNA in situ* hybridization showing expression domains of KRP2 and KRP4 in wild type and *jag-2* inflorescences. Inflorescence meristem: im; floral meristem: fm; sepal primordium: sp; Scale bars: 100 µm.

(A-B) Sections through wild-type (A) and *jag-2* (B) inflorescence apices hybridised with *KRP2* antisense probe; arrows indicate KRP2 expression in deeper layers of the inflorescence meristem and in the pedicel; in *jag-2* sepal primordium arrow indicates KRP2 signal in the adaxial side.

(C-D) Sections through wild-type (C) and *jag-2* (D) inflorescence apices hybridized with *KRP4* antisense probe; arrows indicate KRP4 expression in the epidermal and subepidermal layers of the inflorescence and floral meristem.

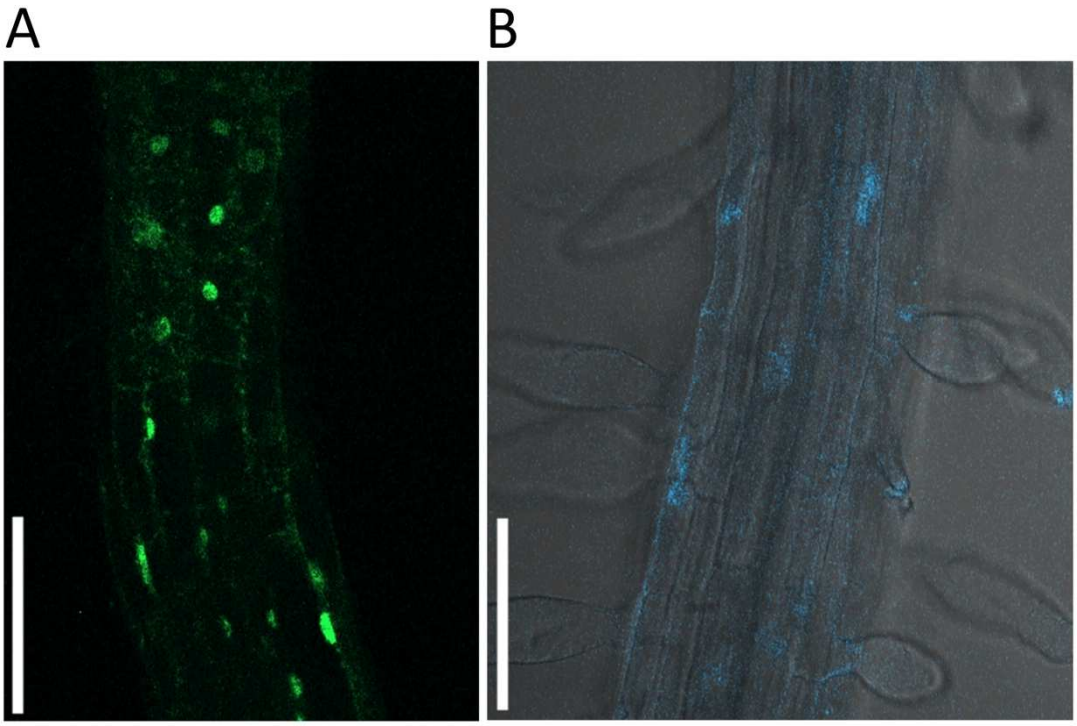

Figure 6.9. Expression of KRP2-GFP and KRP4X-CYPET in wild-type seedlings harboring the *pKRP2:KRP2-GFP* and *pKRP4:KRP4X-CYPET* constructs. Scale bars: 100 µm; (A) KRP2-GFP expression in the proliferation and elongation zone of roots of 10-day old seedlings; (B) KRP4X-CYPET expression in the differentiation zone of roots of 10-day old seedlings.

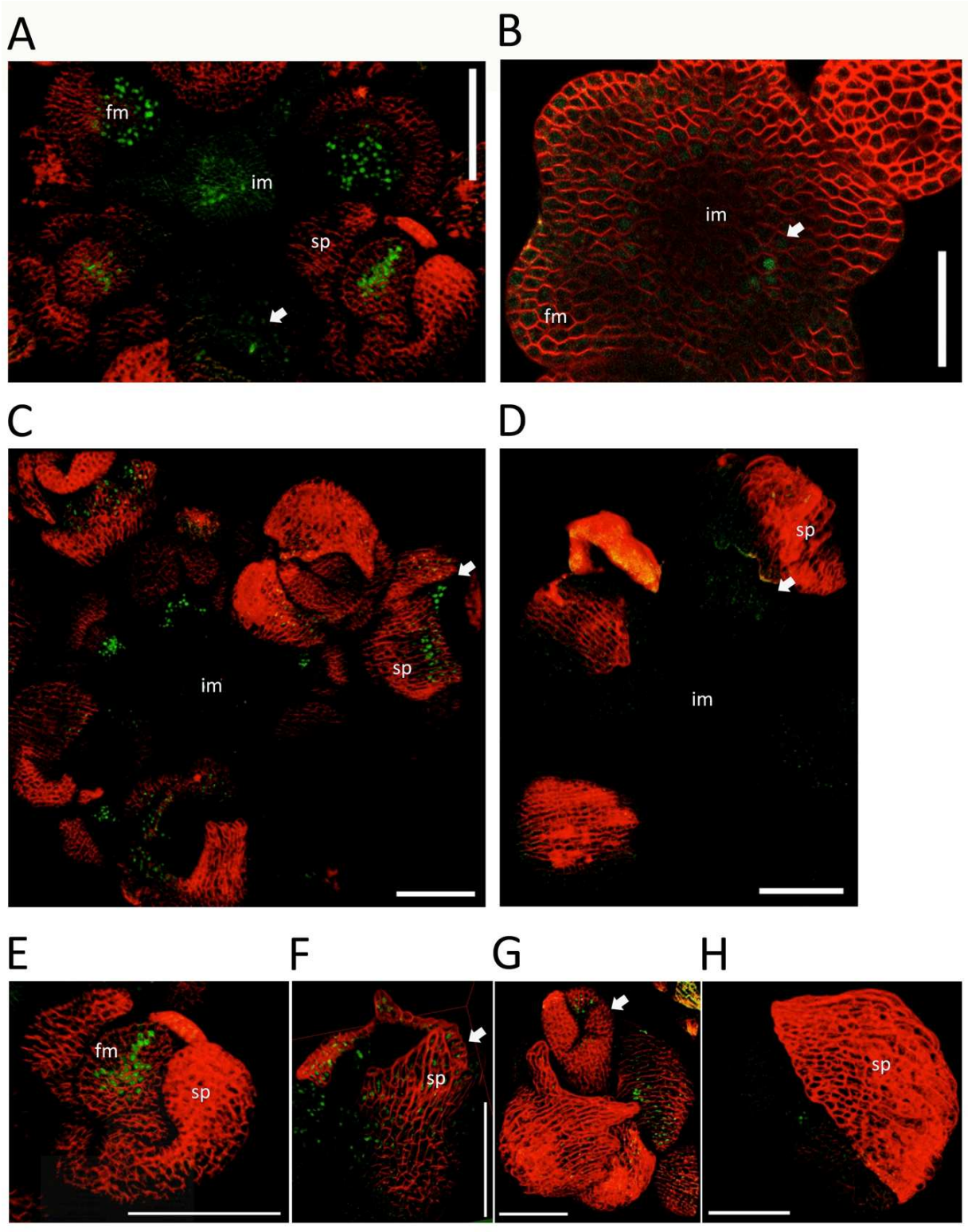

Figure 6.10. KRP2-GFP expression in inflorescences of wild type and jag-1 harboring the pKRP2:KRP2-GFP reporter construct. Inflorescence meristem: im; floral meristem: fm; sepal primordium: sp; Scale bar (A, C-H): 100 µm, (B): 50 µm; 3D projections of confocal stacks showing inflorescences of (A, C) *jag-1* and (B, D) wild type with the inflorescence

meristem (im) in the center, surrounded by developing floral buds; (A-B) arrows indicate that KRP2-GFP is localized in the deeper layers of the inflorescence meristem and the floral meristem; (C,D) arrows indicate that KRP2-GFP is localized in the sepals from stage 5 onwards; (E-G) KRP2-GFP is expressed in the floral buds of *jag-1;* (E) in floral meristem, (F) in sepals, (G) in the distal region of the tube forming the gynoecium; (H) KRP2-GFP is expressed in floral buds of wild type, however wild-type sepals cover the inner whorls reducing the accessibility for confocal imaging; 3D projections of the confocal stack generated in Fiji (Schmid et al., 2010).

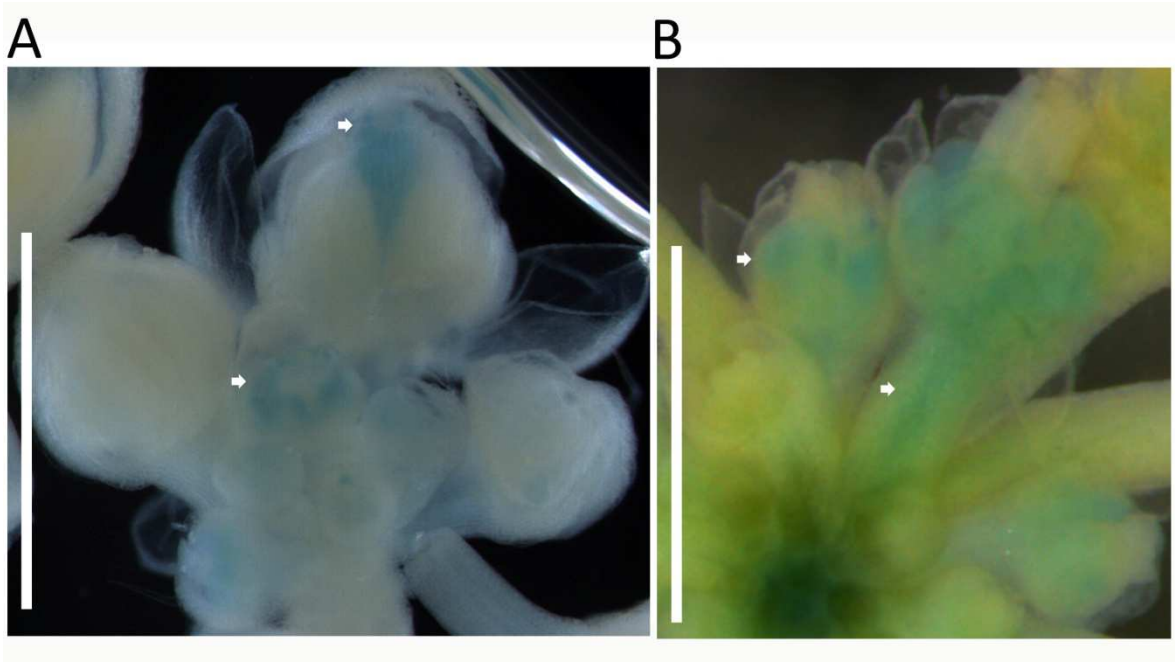

Figure 6.11. Ectopic KRP2 expression in *jag-1* inflorescences. Scale bars: 500 µm; (A) KRP2:GUS signal in wild type inflorescence; arrows indicate expression in the distal margins of the petal primordia and in the gynoecium; (B) KRP2:GUS signal in *jag-1* inflorescence; arrows indicate strong expression throughout petal primordia and strong expression in the pedicel.

6.3.2.4. *krp2* and *krp4* mutations partially restore mature organ growth and shape

In the next step, I aimed to investigate the functional relevance of the repression of *KRP2* and *KRP4* by JAG. Lines ectopically expressing *KRP2* under the *35S* promoter have narrower, serrated leaves and show defects in floral organ development with partial male sterility (de Veylder et al., 2001 and Zhou et al., 2002), similar to *jag* loss of function mutants. In addition, it has been shown that ectopic expression of *KRP4* in the epidermal layer caused similar growth defects in floral organs (Bemis and Torii, 2007). Therefore, I hypothesised that ectopic *KRP* expression in the *jag* mutants might be the cause for growth defects in the *jag* mutant background. In this case, loss of *KRP2* and/or *KRP4* function in the *jag* loss of function mutant background might at least in part rescue floral organ outgrowth.

To test whether repression of *KRP2* or *KRP4* was required to promote floral organ growth, I compared the shape and size of mature organs in plants with different combinations of the *jag-1*, *krp2-3* and *krp4-1* mutations with the wild-type *Col-0* control. Therefore, I generated the double mutant lines *krp2-3 jag-1* and *krp4-1 jag-1* and the *krp2-3 krp4-1 jag-1* triple mutant, all in *Col-0* background. Both, the *krp2-3* and the *krp4-1* single mutant are T-DNA insertion lines identified from the SALK T-DNA insertion mutant collection. The loss of function allele *krp2-3* (SALK 130744, first described by Sanz et al., 2011) has an insertion in the first exon and the loss of function allele *krp4-1* (SALK 102417) has an insertion in the second exon. The *krp4-1* allele has recently been described as a loss of function allele by Cheng et al. (2013). In addition, I confirmed by qRT-PCR using oligos 537 bp downstream of the start codon with an amplicon spanning exon 1 and exon 2, that *krp4-1* is a loss of function allele (Figure 6.12.).

As reported by Cheng et al. (2013), both single *krp* loss of function mutants did not show any obvious macroscopic differences in development, overall plant architecture, or inflorescence phenotype compared to wild-type *Col-0* (Figure 6.13.A-C). By contrast, in the *jag-1* mutant, reduced growth often results in exposed carpels and stamens in young buds (Figures 6.13.D and 6.14.A, F), and mature sepals and petals are shorter and narrower than in the wild type. In the *jag-1* loss of function mutant background, loss of *KRP2* or *KRP4* function caused a partial rescue of the inflorescence phenotype, in particular, in respect to sepal and petal outgrowth. The developing floral buds in both double mutants and in the triple mutant had a tightly closed appearance compared with

the loosely open appearance of the developing floral buds in the *jag-1* loss of function mutant (Figures 6.13. and 6.14.). This suggested that there was rescue of sepal outgrowth to a degree that enabled sepals to enclose the developing floral organs of the inner whorls as observed in wild-type floral buds. In both *krp2-3 jag-1* and *krp4-1 jag-1* double mutants and in the *krp2-3 krp4-1 jag-1* triple mutant, sepal and petal outgrowth were in part recovered, including the white appearance of wild-type petals (Figure 6.14.E,J). However, full wild-type growth was clearly not recovered.

In order to quantify the partial recovery of sepal and petal outgrowth, I imaged petals and sepals of flowers at full anthesis under 10X magnification. Flowers were fixed and cleared in a 15-70% ethanol series and imaged using a 10X objective with bright field tiling settings. I imaged open flowers that were at anthesis with the petals clearly visible, the long anthers reaching the stigma that was fully covered with stigmatic papillae as described by Smyth et al. (1990). I measured maximum length of sepals, maximum width of petals, and total area of sepals and petals (Figure 6.15.). In a wild-type flower at full anthesis, sepals are on average 1.98 mm long with an average total area of 1.02 mm^2. In comparison, *jag-1* sepals are 1.33 mm long with an average total area of 0.45 mm^2, showing that *jag-1* sepals are on average smaller than half the size of wild-type sepals. The *krp2-3 jag-1* and *krp4-1 jag-1* double mutants showed a significant increase in average sepal length of 1.50 mm and 1.60 mm and an average total sepal area of 0.63 mm^2 and 0.76 mm^2, respectively. The increase in sepal size was even more pronounced in the triple mutant where sepals were on average 1.71 mm long with an average total area of 0.84 mm^2.

I also observed significant differences in petal size. While wild-type petals are on average 0.88 mm wide with an average total area of 1.67 mm^2, jag petals are on average 0.462 mm wide with an average total area of 0.81 mm^2, so *jag-1* petals are about half the size of wild-type petals. Petals of the *krp2-3 jag-1* and the *krp4-1 jag-1* double mutant were on average 0.58 mm and 0.65 mm wide with an average total petal area of 1.02 $mm^2$and 1.16 mm^2, respectively. The *krp2-3 krp4-1 jag-1* triple mutant showed a similar increase in maximum petal width (0.71 mm) and average total petal area (1.25 mm^2). Apart from a significant increase in petal size, I observed a change in petal shape. While wild-type petals fan out to form paddle shaped lobes, *jag-1* petals have narrow pointy distal tips (Dinneny et al., 2004; Ohno et al., 2004; Sauret et al., 2013). As a result, petals

of *jag-1* are often broader near the base than in the pointy distal region. In comparison, petals of both double mutants *krp2-3 jag-1* and *krp4-1 jag-1,* and the triple mutant *krp2-3 krp4-1 jag-1* fanned out to a broader distal region (Figure 6.14. F-J).

In addition to the *krp4-1* allele in *Col* background, I used the *krp4-2* allele in L-*er* background that was identified as *GT1143* (gene trap line) by Sundaresan et al., (1995).

The *krp4-2* allele has an insertion in the second exon and qRT-PCR using oligos 537 bp and 1599 bp downstream of the KRP4 start codon confirmed that *krp4-2* is a loss of function allele (Figure 6.16.). The rescue in petal shape was particularly obvious in the *krp4-2 jag-2* double loss of function mutant compared to *jag-2* single mutant (Figures 6.17. and 6.18.). While the *jag* loss of function mutation in L-*er* background causes strong serrations in the distal petal tip, petals of the *jag-2 krp4-2* double mutant had significantly smoother margins in addition to a broadened distal region (Figure 6.18.).

6.3.2.5. Loss of KRP2 and KRP4 in *jag* mutants rescues conical cells in the lobes of petals

In wild-type petals, the adaxial epidermis of the lobe region is composed of uniform conical cells with regular cuticular ridges. By contrast, the epidermal cells in the adaxial distal tip of *jag-1* petals are flat, elongated, and have irregular cuticular ridges, resembling cells found near the base in wild-type petals (Dinneny et al., 2004; Ohno et al., 2004). Because, the *krp2-3 jag-1*, the *krp4-1 jag-1* double mutants and the *krp2-3 krp4-1 jag-1* triple mutant showed a rescue in petal size and shape, particularly in the distal regions, I further investigated whether the cell types in the adaxial epidermal layer were rescued in comparison to the *jag-1* single loss of function mutant.

To compare the cell types, I imaged petals of flowers at full anthesis using cryo-scanning electron microscopy (Cryo-SEM). In comparison to the *jag-1* single loss of function mutant (Figure 6.19.B, I observed a rescue of the conical cells with regular cuticular ridges in the distal lobe regions of the *krp2-3 jag-1*, *krp4-1 jag-1* and in the *krp2-3 krp4-1 jag-1* triple mutant (Figure 6.19.C-E, I-K). In order to quantify the extent of recovery, I measured the lobe area that was composed of conical cells in petals that were cleared in ethanol. In this experiment, wild-type Col petals had a total area of 2.32 mm2 and conical cells covered 1.33 mm^2, which corresponded to 56% of the total petal area. In the *krp2-3 jag-1*, the *krp4-1 jag-1*, and the *krp2-3 krp4-1 jag-1* petals had total areas of

1.32 mm^2, 1.47 mm^2, and 1.46 mm^2, respectively. In the *krp2-3 jag-1*, the *krp4-1 jag-1*, *and the krp2-3 krp4-1 jag-1* conical cells covered on average 0.11 mm², 0.29 mm², and 0.26 mm² in the distal lobe area, which corresponded to 8.50%, 20%, 18% of the total petal area, respectively (Figure 6.19.F). In comparison, conical cells were absent from the pointy and narrow lobe region of *jag-1* petals, an observation previously reported by Dinneny et al. (2004) and Ohno et al. (2004). Thus, as previously observed for overall petal growth, the area of the petal epidermis composed of conical cells showed a statistically significant increase in the *krp2/4 jag-1* double and triple loss of function mutants compared to the *jag-1* single mutant, but did not reach the area seen in the wild-type controls in any of the double or triple mutant combinations.

In sepals, Roeder et al. (2010) showed that mild overexpression of *KRP1* resulted in an increase in giant cell formation in sepals. In my experiment, SEM images did not reveal any obvious changes in final cell size distributions in the sepals of the single *krp2-3* or *krp4-1 and the double krp2-3 krp4-1* double loss of function mutants compared to the wild type (Figures 6.20.E-G and 6.21.E-G). Moreover, I did not observe an increase of giant cell formation in the sepals of *jag-1* loss of function mutant (Figures 6.20.A and 6.21.A). On the contrary, epidermal cells in the *jag-1* sepals appeared to be more uniform in size with fewer extreme cell size differences between neighbouring cells as observed in the wild-type sepal (Figure 6.21.E; Roeder et al., 2010). In addition cells appeared less bulgy and less lobed in the *jag-1* single mutant. Interestingly, lobes of epidermal cells have been described as a means to resist tension and rupture when neighboring cells grow at different growth rates (Asl et al., 2011), which would be in line with the uniform cell sizes observed in the *jag* sepals. No obvious changes in cell shape and cell sizes were observed in the sepals between *jag-1* and the *krp2-3 jag-1*, *krp4-1 jag-1* and *krp2-3 krp4-1 jag-1* double and triple mutants (Figures 6.20.A-D and 6.21.A-D).

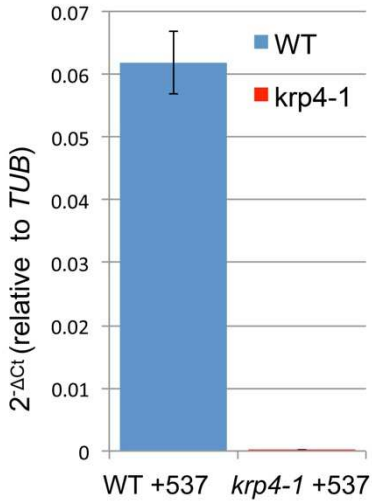

Figure 6.12. Transcript levels of *KRP4* in the *krp4-1 Col* mutant shown by qRT-PCR. Numbers on the horizontal axis below the bars correspond to the left border of the amplified region relative to the coding sequence; bars indicate mean and standard deviation of three biological replicates.

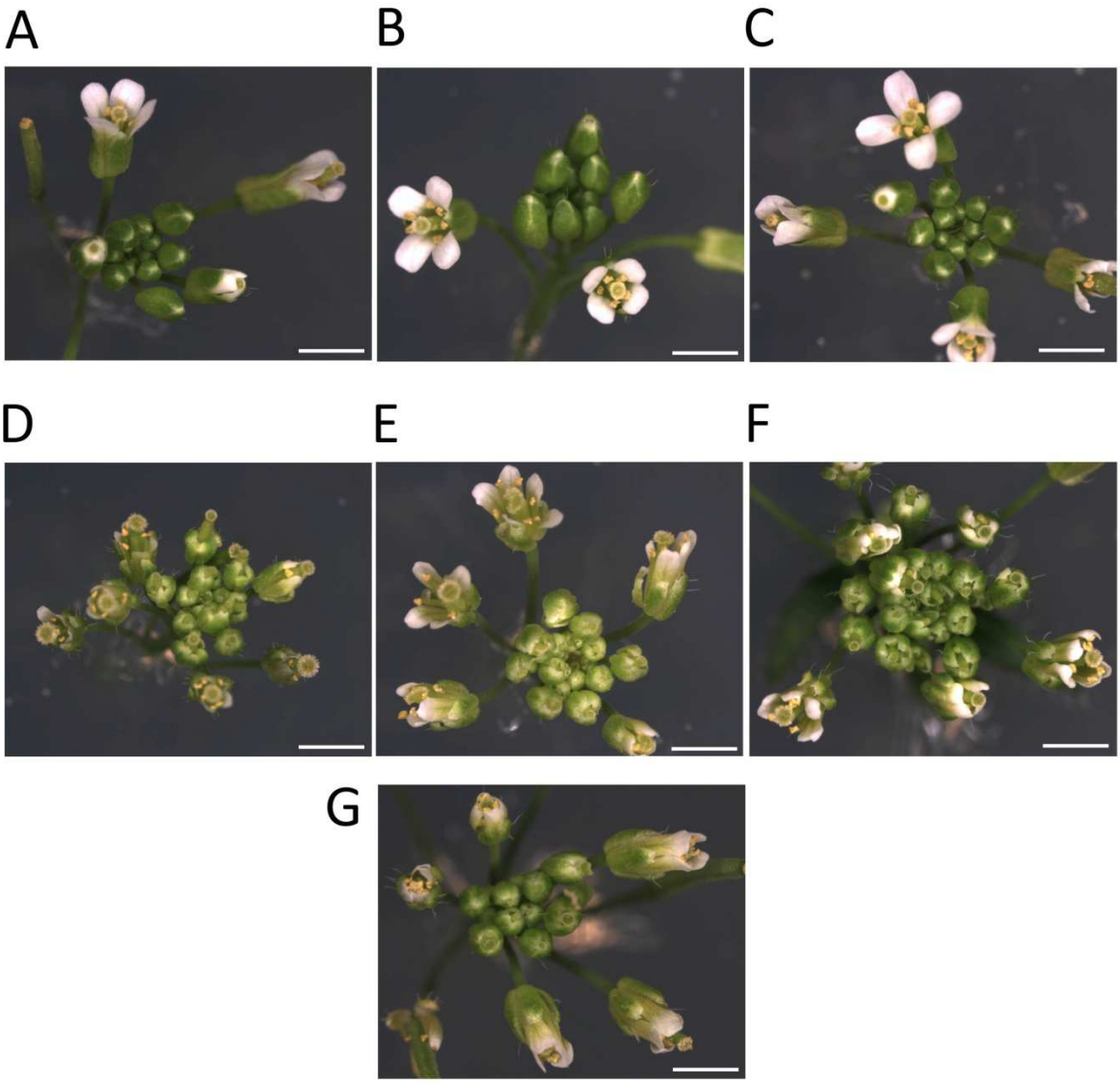

Figure 6.13. Partial rescue of *jag* organ growth defects by *krp2* and *krp4* mutations.

Scale bars: 1 mm; (A-E) Top view of inflorescences of wild type (A), *krp2-3* (B), *krp4-1* (C), *jag-1* (D), *krp2-3 jag-1* (E), *krp4-1 jag-1* (F) and *krp2-3 krp4-1 jag-1* (G); note that sepals fail to completely enclose the buds in *jag-1*, but this defect is partially suppressed by the *krp2* and *krp4* mutations.

Figure 6.14. Partial rescue of flower phenotype by loss of KRP2 and KRP4 in *jag-1* background. Scale bars: 1 mm; Representative early floral buds in the inflorescence center of *jag-1* (A), *krp2-3 jag-1* (B), *krp4-1 jag-1* (C), *krp2-3 krp4-1 jag-1* (D) and wild-type control (E); note the open floral buds with prematurely protruding gynoecium in *jag-1* and its partial rescue in the double and triple mutants; Representative mature flowers of *jag-1* (F), *krp2-3 jag-1* (G), *krp4-1 jag-1* (H), *krp2-3 krp4-1 jag-1* (I) and wild-type control (J); note the defective sepal and petal growth in *jag-1* and the partial recovery of growth and the recovery of whitish petal appearance in the *krp2-3 jag-1*, *krp4-1 jag-1* and in the *krp2-3 krp4-1 jag-1* mutant.

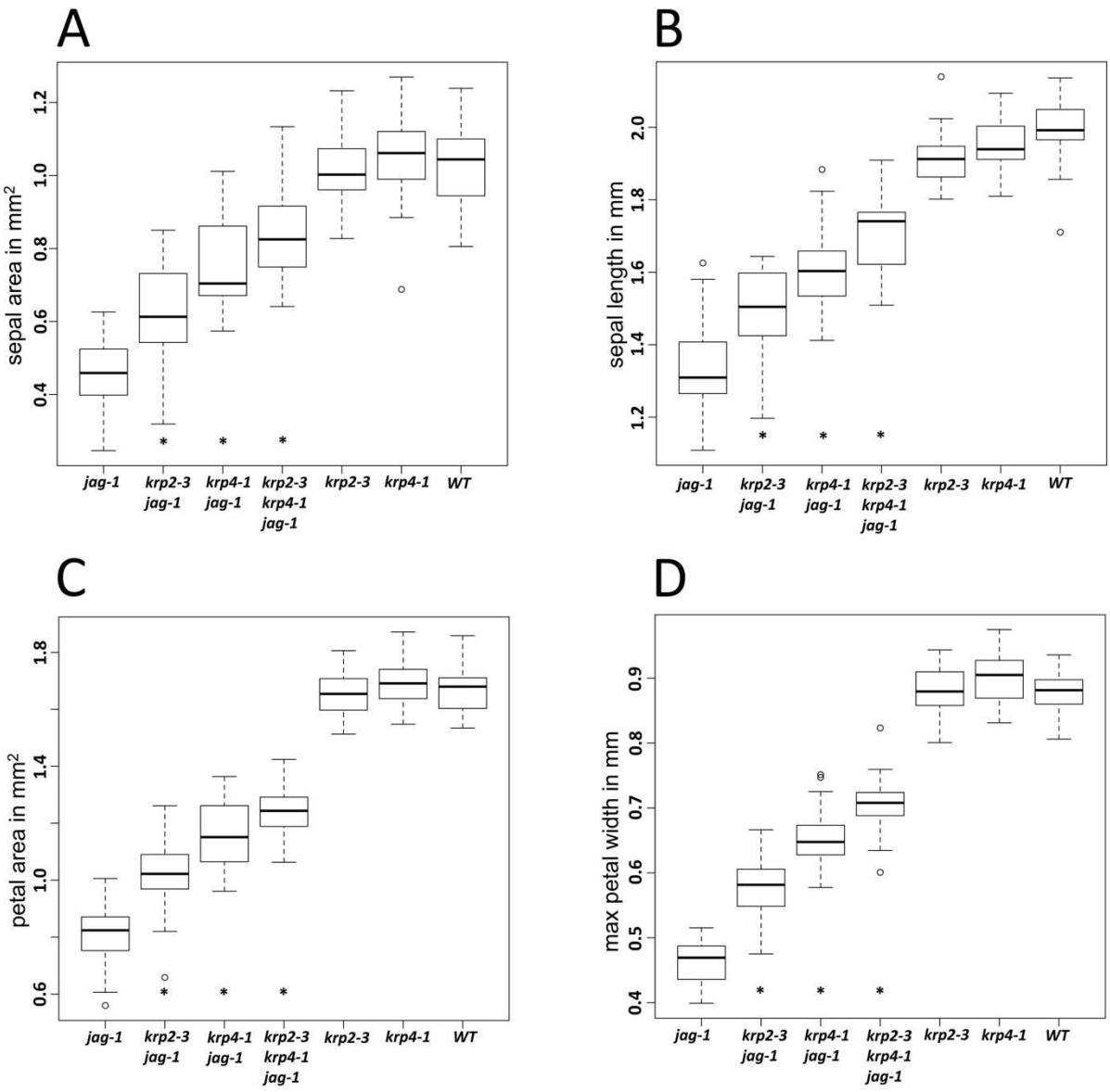

Figure 6.15. Quantification of the rescue of sepal and petal outgrowth upon loss of KRP2 and KRP4 function in the *jag-1* mutant background. (A-D) Distribution of sepal area (A), sepal length (B), petal area (C) and maximum petal width (D) for the genotypes indicated; box plots show median (thick line) second to third quartiles (box), minimum and maximum range (dashed line) and outliers (single points). Asterisks for the double and triple mutants indicate that the mean is significantly different from *jag-1* (Student's *t*-test, $p<0.05$).

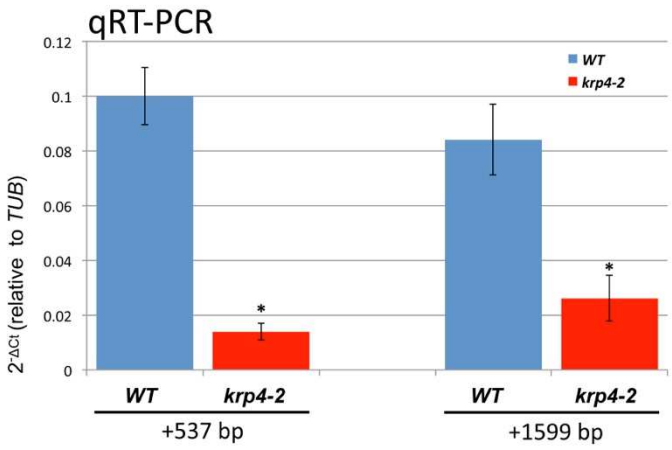

Figure 6.16. Transcript levels of *KRP4* in the *krp4-2* L-*er* mutant shown by qRT-PCR. Numbers on the horizontal axis below the bars correspond to the left border of the amplified region relative to the coding sequence; bars indicate means and standard deviations of three biological replicates.

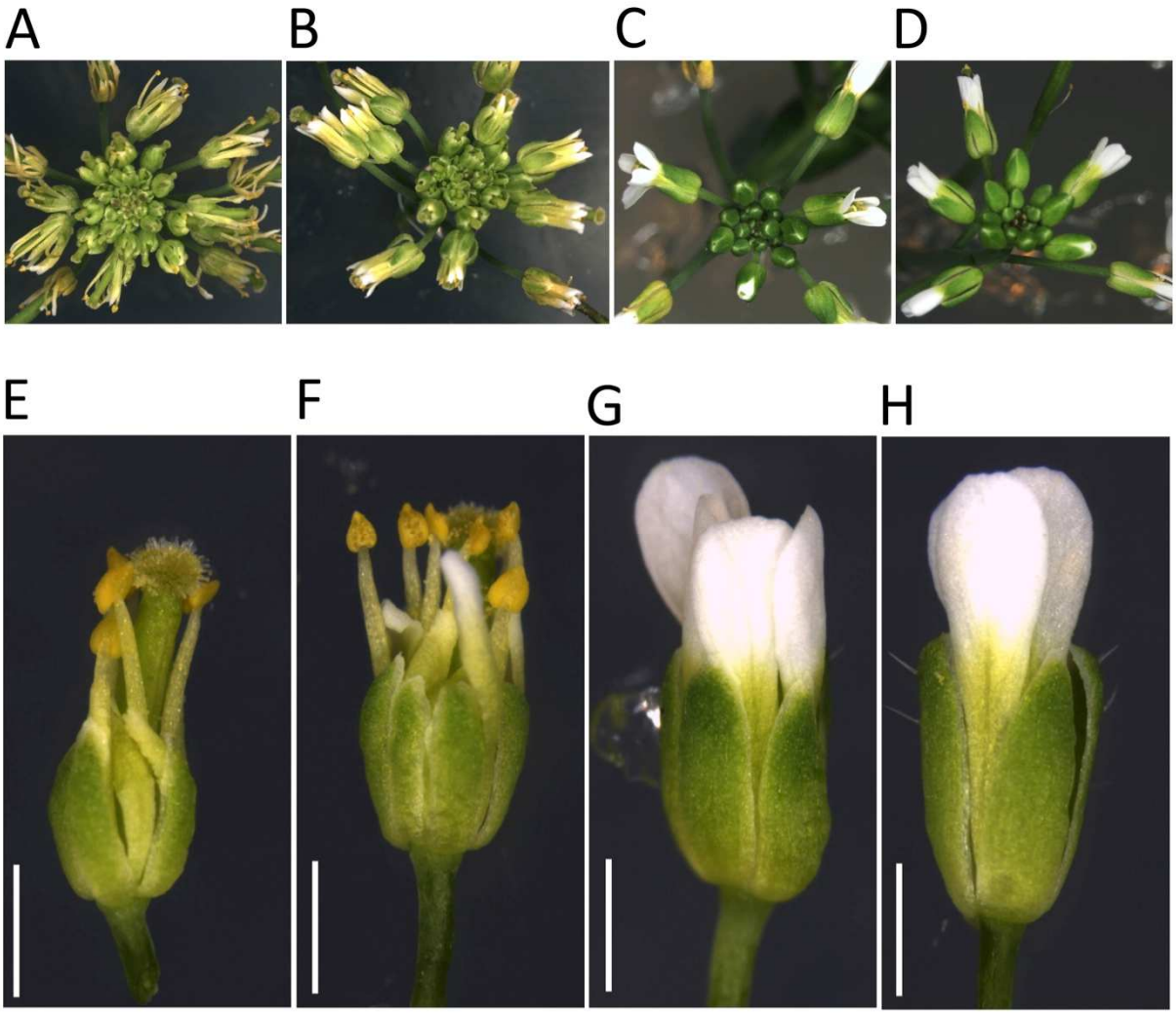

Figure 6.17. Rescue of the floral organ defects in the *krp4-2 jag-2* double mutant.

(A-D) Top view of inflorescences of *jag-2* (A), *krp4-2 jag-2* (B), *krp4-2* (C), and wild-type control (D); bars: 1 mm. (E-H) Representative mature flowers of *jag-2* (E), *krp4-2 jag-2* (F), *krp4-2* (G), and wild-type control (H); note the severe defects in petal growth in *jag-2* and the partial recovery of growth in the *jag-2 krp4-2* double mutant; bars: 1 mm.

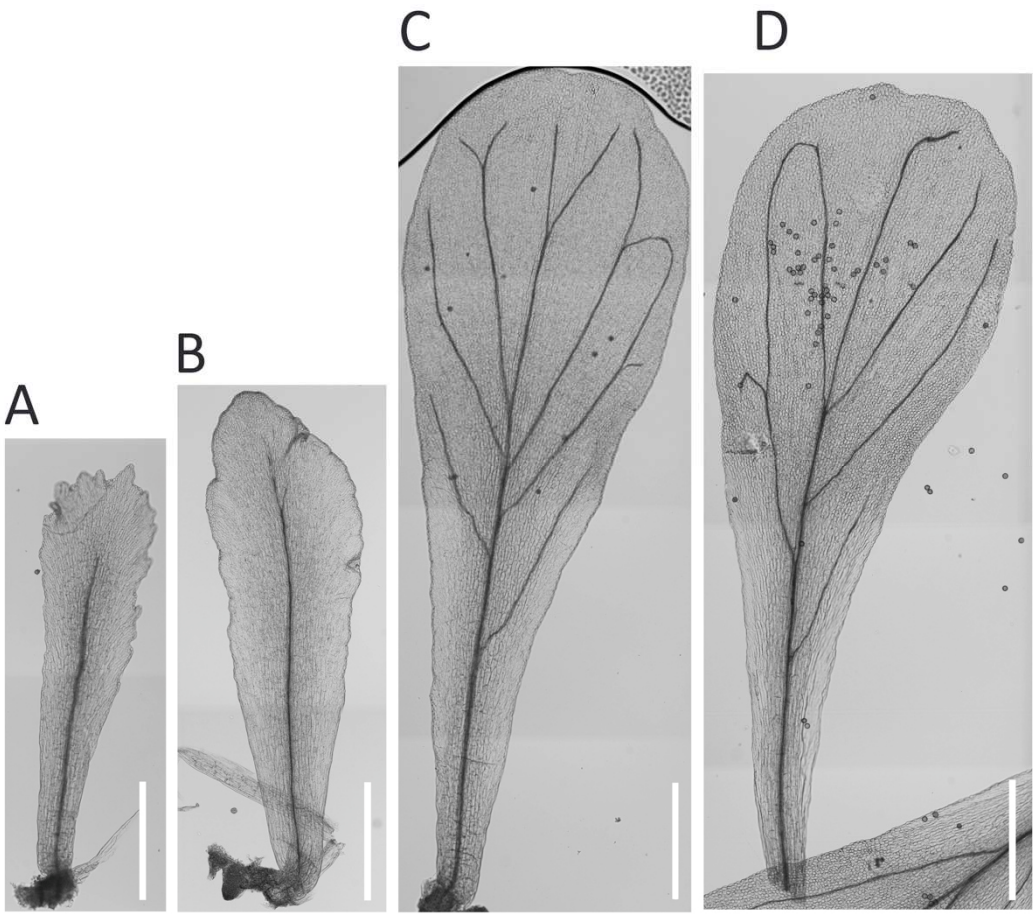

Figure 6.18. Rescue of floral organ defects in the *krp4-2 jag-2* double mutant.

Scale bars: 500 µm; Representative petal from mature flowers, cleared in 70% ethanol and imaged with 10X magnification using the Leica DM6000; petals of *jag-2* (A), *krp4-2 jag-2* (B), *krp4-2* (C) and wild type (D); note the severe serrations of the petal margins which are specific for the *jag* loss of function mutation in L-*er* background; in the *krp4-2 jag-2* double mutant petals have smoother margins.

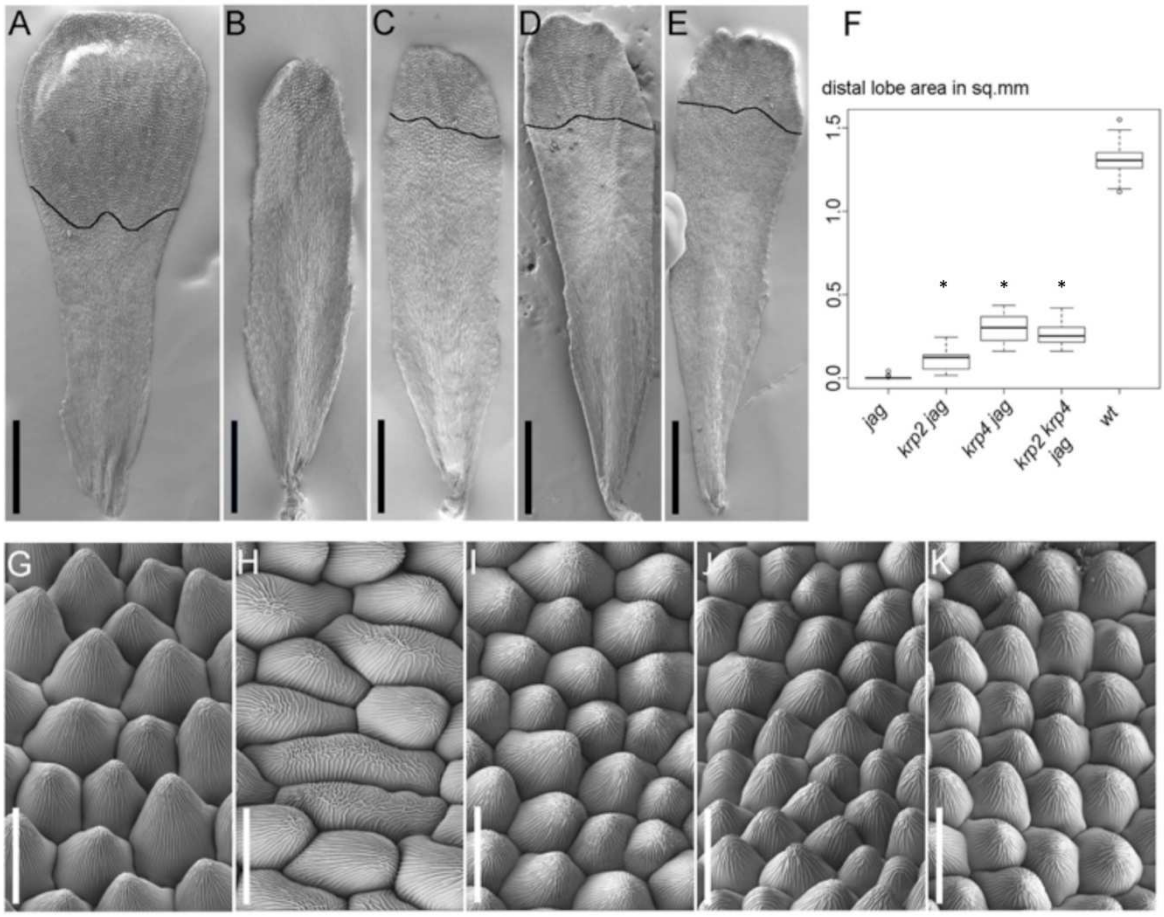

Figure 6.19. *krp2* and *krp4* mutations recover epidermal cell morphology in *jag* petals. Scanning electron micrographs of mature petals (A-E) and conical cells in the distal petal region (G-K) from wild-type Col (A, G), *jag-1* (B, H), *jag-1 krp2-3* (C, I), *jag-1 krp4-1* (D, G), *jag-1 krp2-3 krp4-1* (E, H); bars: 500 µm (A-E); Scanning bars: 20 µm (G-K); the black lines across the distal region of the petals shows the boundary of the distal petal lobe, where conical epidermal cells are seen; (F) Area of distal petal lobe for the genotypes indicated; box plots show median (thick line) second to third quartiles (box), minimum and maximum range (dashed line) and outliers (single points). Asterisks for the double and triple mutants indicate that the mean is significantly different from *jag-1* (Student's *t*-test, *p-value*<0.05).

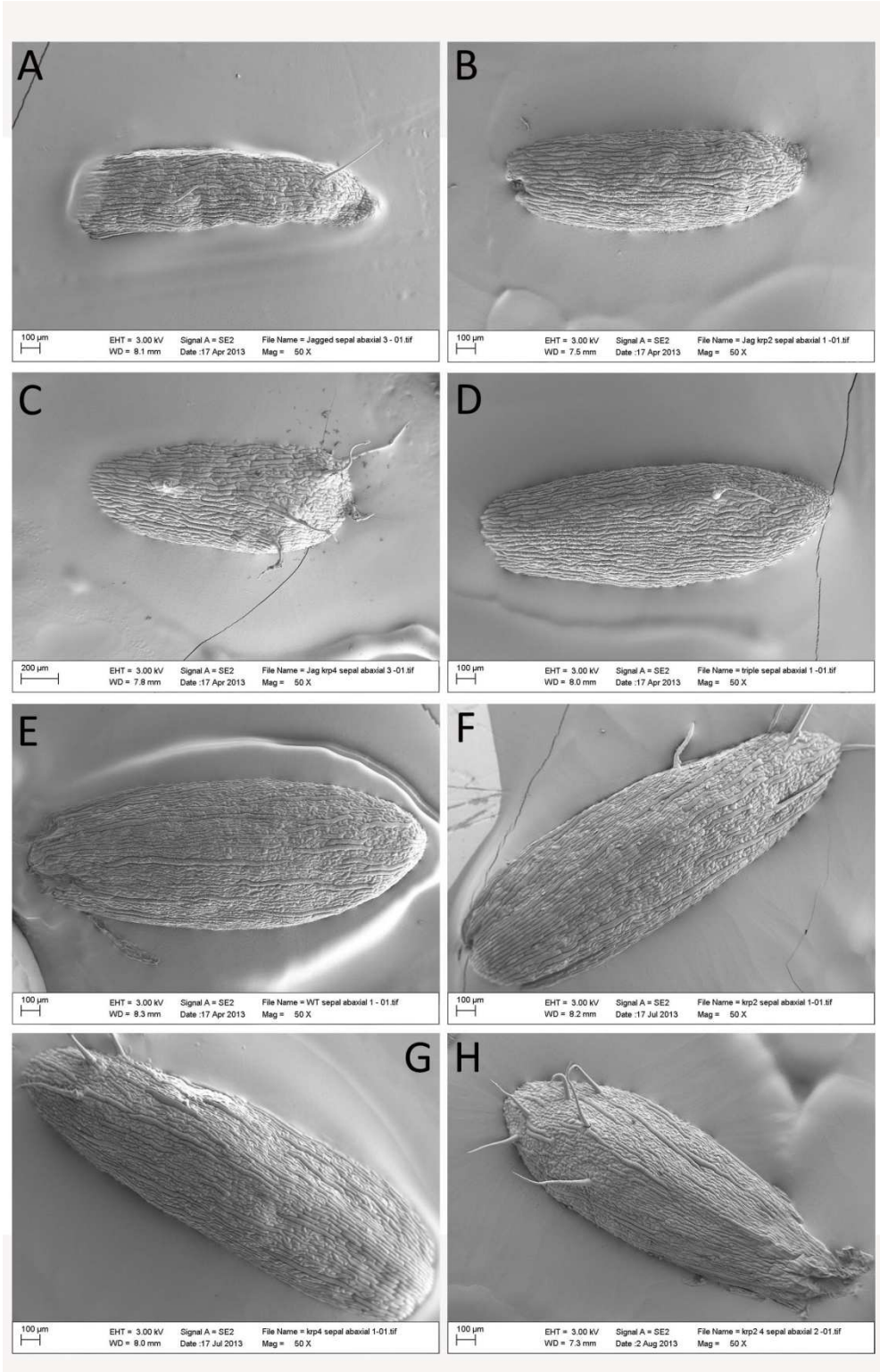

Figure 6.20. *krp2* and *krp4* mutations do not recover epidermal cell morphology in *jag* sepals. Scale bars: 100 µm (A-H): Scanning electron micrographs of mature sepals from *jag-1* (A), *krp2-3 jag-1* (B), *krp4-1 jag* (C), *jag-1 krp2-3 krp4-1* (D), wild type (E), *krp2-3* (F), krp4-1 (G), *krp4-1 krp2-3* (H);

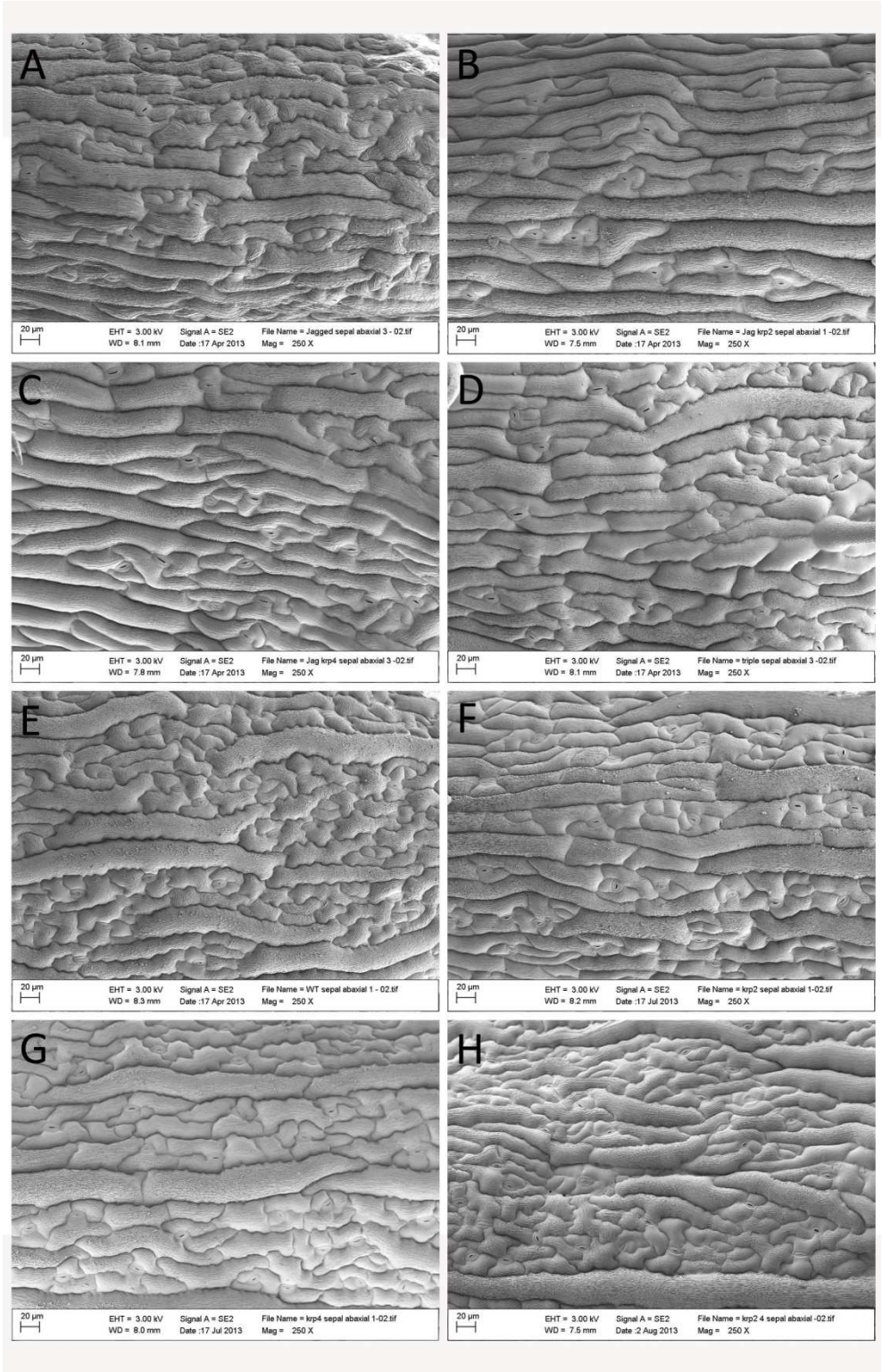

Figure 6.21. *krp2* and *krp4* mutations do not recover epidermal cell morphology in *jag* sepals. Scale bars: 20 µm (A-H): Scanning electron micrographs of mature sepals from *jag-1* (A), *krp2-3 jag-1* (B), *krp4-1 jag* (C), *jag-1 krp2-3 krp4-1* (D), wild type (E), *krp2-3* (F), krp4-1 (G), *krp4-1 krp2-3* (H);

6.4. Discussion

Here I showed that JAG directly targeted several regulators of the core cell cycle at the transition from G1 to S-phase. In particular, I confirmed that JAG directly represses *KRP2* and *KRP4*, two members of the Kip-related protein family. Furthermore, I showed that loss of KRP2 and KRP4 function independently caused significant morphological changes in mature floral organs in the *jag* mutant background. Together, these findings reveal novel functions for two members of the KRP family.

Until now, high functional redundancy has been reported for the seven members of the KRP family, which complicated functional analysis based on loss of function mutants. For example, all seven KRPs have overlapping expression domains in tissues competent to undergo mitotic divisions (Menges et al., 2005, Verkest et al., 2005, Ormenese et al., 2004). Moreover, it has been repeatedly confirmed in pairwise interaction assays but also in a global screening approach using co-purification by tandem affinity purification technique with KRP proteins as baits that all seven KRPs show the same protein binding specificities for CDKA and D-type cyclins (De Veylder et al., 2001; Wang et al., 2000; Van Leene et al., 2010). Consistently, single mutants have been reported to not show any significant growth or morphological differences (Cheng et al., 2013), with the exception of the *krp2-1* and *krp2-3* single mutants that showed an increase in lateral root initiation (Sanz et al., 2011). However, it has been shown that the krp1/2/4/5/7 quintuple loss of function mutant had an effect on final organ sizes and shapes (Cheng et al., 2013), confirming that loss of the cell cycle inhibitory function of KRPs affects organogenesis in a dosage-dependent manner.

In contrast to the effects of single loss of function mutants, several studies on ectopic expression of single members of the KRP family have revealed clear morphological effects. For example, ectopic expression of *KRP1* (*ICK1*), *KRP2*, and *KRP4* under different promoters resulted in reduced, greenish floral organs with narrower and shorter sepals and petals and carpels protruding prematurely from young floral buds (Wang et al., 2000; Zhou et al., 2002; De Veylder et al., 2001; Verkest et al., 2005; Bemis and Torii et al., 2007; Ferjani et al., 2013). Therefore, it has been well established that ectopic expression of *KRPs* has an effect on final organ size and shape. My work puts these ectopic effects into the regulatory context of floral organ development and relates it to the function of the

growth promoting transcription factor JAG. Consistently, the floral phenotypes described for the *KRP* overexpressors are reminiscent of the *jag* loss of function phenotype. I showed that loss of KRP2 and KRP4 function in the *jag* mutant background at least in part rescued overall organ outgrowth, suggesting that ectopic expression of *KRPs* are at least in part the cause for the *jag* mutant phenotype of reduced sepal and petal outgrowth.

Interestingly, loss of function of either KRP2 or KRP4 caused partial rescue of organ growth, but mutation of both *KRP* genes in the triple *krp2 krp4 jag* mutant did not show any clear additive effects or significantly increased rescue. This suggests that KRP2 and KRP4 do not play equivalent and dosage-dependent roles downstream of JAG, but instead are required together to produce the inhibition of organ growth seen in the *jag* mutant. In addition, the rescue of organ growth in the triple mutant was not complete. Since JAG also directly targeted genes involved in cell expansion and cell growth, it could be that once cell cycle progression is de-repressed other growth-related factors become limiting. On the other hand, the limiting component could still lie within the regulatory network of the core cell cycle machinery. For example, expression profiling experiments have revealed that *CYCD3;3* is ectopically expressed in the *jag* mutant background even though *CYCD3;3* is a directly up-regulated target of ectopically activated JAG, suggesting that other factors may cause ectopic *CYCD3;3* expression in the *jag* loss of function background.

It could be speculated that ectopic expression of *KRPs* in the *jag* mutant background are the cause for elevated *CYCD3;3* levels as part of a regulatory feedback loop. In this context, Cheng et al. (2013) observed that *CYCD3* was down-regulated in the krp1/2/4/5/7 quintuple mutant. It has previously been shown that KRP2 interacts with CYCD2 in the root and promotes the nuclear localization of CYD2-CDKA complexes promoting lateral root initiation (Sanz et al., 2011). Therefore, it would be interesting to investigate whether *CYCD3;3* expression levels are responsive to loss of KRP function in the *jag* mutant background. In addition, it would be interesting to test whether the in part rescue of overall organ outgrowth is dependent on *CYCD3*;3 function by crossing the *cycD3;3* or *cycD3;1-3* mutant into the *krp2/krp4 jag* loss of function mutant background.

The genetic interactions between *jag* and *krp2/4* mutations, combined with the direct repression of KRP2 and KRP4 shown by the combined ChIP-Seq and JAG-GR experiments, predict that KRP2 and KRP4 should be ectopically expressed in the *jag* mutant. However, I

could only show this conclusively for KRP2. By using the *KRP2:KRP2-GFP* and the KRP2:GUS reporter lines, I observed that *KRP2* appeared not to be expressed in early floral organ primordia, but was expressed in the distal margins of sepals and petals of the wild type from stage 5 onwards. In particular, the KRP2:GUS signal was stronger and extended from the distal margins through the whole petal in the *jag-1* mutant background compared with wild-type. This expression pattern is in accordance with the functional analysis of the *KRP2* overexpressor by De Veylder et al. (2001) who followed the development of a leaf primordium of the first two true leaves over time using kinematic analysis (De Veylder et al., 2001; Asl et al., 2011). Interestingly, at day 5 after organ initiation, total organ area, cell numbers and average cell sizes of leaf primordia were comparable between the wild type and the *KRP2* overexpressor. By contrast, at day 21 after organ initiation, leaves of the KRP2 overexpressor were only 25% of the total leaf area of a wild type mature leaf and had ten times fewer but enlarged cells, suggesting that in leaf primordia, KRP2 function restricts cell proliferation rate and/or the timing of proliferation phase and exit from cell proliferation between day 5 and day 21 of development. In respect to these two possible functions, kinematic analysis further revealed that in both lines proliferation phase lasted until day 9 and was marked by a severe decrease in cell division rates, suggesting that strong ectopic KRP2 expression does not affect the timing of cell proliferation to expansion and differentiation phase. By contrast, during cell proliferation phase, cell cycle duration calculated as the inverse of the cell division rate (cells/cell/hour) was double as long in the KRP2 overexpressor line with average 43 hours compared with the cell cycle duration of 20 hours in the wild type leaf (De Veylder et al., 2001).

However, in weak overexpression lines of KRP2 it was shown that endoreduplication was promoted over mitotic cell proliferation causing premature exit from mitotic cell proliferation (Verkest et al., 2005). In this context, it was suggested that high CDKA and CDKB levels are required for mitosis and that their regulation by KRP2 decides whether a cell enters mitosis or endoreduplication. Verkest et al. (2005) found that KRP2 is targeted for proteasomal degradation via CDKB, and KRP2 protein levels are stabilised in a dominant negative *cdkb1* line. It was shown that KRP2 only reduces the kinase activity of CDKA, not of CDKB, suggesting that CDKB can control CDKA activity by fine tuning KRP2 levels. This interaction provided an explanation to the question why in plants with strong

ectopic expression of *KRP1* and *KRP2* entry into S-phase and subsequent mitosis was blocked, while upon milder ectopic expression entry into S-phase was possible but subsequent mitosis was blocked leading to an increase in endoreduplication (Verkest et al., 2005; Weinl et al., 2005). Verkest et al. (2005) suggested that CDKB promotes *KRP2* degradation in order to maintain high CDKA levels that are required for mitotic cell divisions. In the case of endoreduplication, CDKB levels drop leading to stabilized KRP2 that can inhibit CDKA levels to a degree where entry into S-phase is still promoted but entry into M-phase is inhibited. Together, this suggested that KRP2 acts in a dosage-dependent manner and may have a function in restricting proliferation rate but may also regulate the timing of cell cycle exit and onset of endoreduplication. Premature exit from cell proliferation would be in line with the reported premature decrease in the cell proliferation marker histone H4 in petals of the *jag-1* mutant (Dinneny et al., 2004).

In respect to these findings by De Veylder et al. (2001) and Verkest et al. (2005), the recovery of the conical cells in the double and triple loss of function mutant could be explained in two ways. On the one hand, it is possible that conical cell morphology is affected by the rates and direction of tissue growth during the stage when conical cells differentiate. In this case, rescue of conical cell morphology in *jag-1* would be an indirect consequence of the partial rescue of organ growth caused by the de-repression of cell proliferation in *krp2-3* and *krp4-1* mutations. In line with this, it could be hypothesised that the elongated cells in the distal lobe of *jag* loss of function petals compared to small tightly packed conical cells could be the effect of ectopic KRP2 expression inhibiting cell proliferation. On the other hand, the altered morphology of epidermal cells in *jag-1* petals could result from a defect in cell differentiation, suggesting that *KRP*2 and *KRP4* may also affect the balance between cell cycle progression and cell differentiation during floral organ growth. In order to further investigate these hypotheses quantification of final cell sizes in sepals and petals would be needed in addition to the qualitative information about shapes and final cell sizes already provided by the bright field microscopy and SEM images. In addition, flow cytometry and clonal analysis could be used in order to further investigate the effects of KRP2 in respect to changes in the timing of onset of differentiation and cell cycle exit.

In summary, this work revealed that JAG directly represses the cell cycle inhibitors KRP2 and KRP4 and therefore directly controls entry into S-phase and cell cycle

progression. Because loss of KRP2 and KRP4 function caused a partial but significant rescue of floral organ outgrowth in the *jag* loss of function mutant, it can be concluded that de-repression of cell cycle inhibition during early organogenesis is required for floral organ outgrowth according to the developmentally programmed size and shape. These results are also consistent with the idea that the growth of plant tissues is actively restrained below the levels that would be physiologically possible. This idea was initially proposed as an adaptive response, during which growth is restrained by members of the DELLA family which act as transcriptional repressors of gibberellin-mediated signalling in response to environmental stress (Achard et al., 2006). In this respect, it is interesting that DELLA proteins have also been shown to regulate KRP2 expression (Achard et al., 2009). In relation to the role of KRPs in floral organogenesis, it can be hypothesised that in addition to a potential role in modulating growth in response to environmental conditions, localised release of a growth restraint imposed by the KRP CDK inhibitors may be used to generate the differential tissue growth required for morphogenesis.

Chapter 7 - JAG regulates cell size homeostasis by repressing Kip-related cell cycle inhibitors

7.1. Introduction

Based on the significant rescue of organ outgrowth observed in the mature floral organs of the *krp2/4 jag* double and triple loss of function mutants, I further investigated whether loss of KRP2 and/or KRP4 function could also rescue the *jag* loss of function phenotype in early emerging primordia as observed in Schiessl et al. (2012; note that imaging data presented in the paper were not obtained by me, therefore I cited the paper whenever imaging results were concerned; also note that the imaging protocol presented in the paper differed from the imaging protocol used in this chapter). Previous work has shown that JAG modulates the coordination of cell volume and entry into S-phase at early stages of sepal outgrowth and KRPs have been reported to control the cell cycle at the G1 to S-phase transition. Therefore, I investigated whether the effect of JAG on cell size homeostasis could be mediated by repressing *KRP2* and/or *KRP4* and whether loss of KRP function in the wild-type and *jag* mutant background has an effect on cell size homeostasis.

In order to test this hypothesis, a previously adapted imaging protocol was used that combined the DNA synthesis marker 5-ethynyl-2′-deoxyuridine (EdU) with the cell wall marker propidium iodide (PI) (Salic and Mitchison et al., 2008; Truernit et al., 2008; Schiessl et al., 2012). While incubation with the DNA synthesis marker allowed me to monitor cells that had been in S-phase during the three-hour incubation with EdU, the cell wall marker propidium iodide was used for high resolution imaging in deep tissues to analyse the geometry of cells after 3D cell segmentation (see details in Materials and Methods).

In preparation for this protocol, I dissected inflorescence apices and removed floral buds older than stage 5, cut the stem and let the apices recover for 48 hours on germination medium. For the last three hours of recovery, I transferred the dissected inflorescence apices to germination medium supplemented with 10 µm EdU (Figure 7.1.A-C). Because EdU is an analogue of the nucleotide thymidine, all cells that underwent DNA replication during the three-hour incubation, incorporated EdU into the freshly

synthesized DNA strands. Then, the incorporated EdU was labeled with the fluorophore ALEXA 488 by click chemistry, which involves a cycloaddition catalysed by copper in the presence of the reducing agent ascorbic acid (Salic and Mitchison et al., 2008). Subsequently, I performed a modified pseudo-Schiff-propidium iodide (mPS-PI) reaction (Truernit et al., 2008) to stain the cell walls with propidium iodide, followed by a clearing of the floral apices with chloral hydrate, which allowed high-resolution imaging of the cell walls in the floral buds. In detail, I imaged the emerging sepal primordia in stage 3 buds, which are readily accessible for imaging. Both signals were detected using a Zeiss 510 Meta confocal microscope with excitation laser light at 488 nm and emission filters set to 572-625 nm to detect the propidium iodide signal (false color red in the images) and 505-600 nm to detect the nuclear localised EdU signal (false color green in the images) (Figure 7.1.D). I used Fiji to display images and to generate 3D projections and orthogonal views, and BIOIMAGE XD (Kankaanpaa et al., 2012) for 3D cell segmentation (Figure 7.1.E). Furthermore, custom scripts were developed to automatically determine cell volumes and cell positions relative to the meristem summit and to primordium boundaries in order to locate cells in the meristem or primordium, to attribute cell layers, to detect artifacts of under and over-segmentation, and to select cells with EdU labeling from non-EdU labeled cells.

Combining the cell volume data with the EdU labeling results allowed a comparison of cell size distributions for the cells that had or had not undergone S-phase in different tissues, for example the floral meristem and sepal primordia of wild type and *jag* mutant background (Figure 7.1.F).

7.2. Results

7.2.1. JAG modulates cell size homeostasis in sepal primordia

In the floral meristem of wild-type and *jag* mutant plants, where *JAG* is not expressed, the median size of cells that had undergone S-phase (EdU-positive cells) during a three-hour incubation with the cell cycle marker EdU was significantly larger than that of cells that had not undergone S-phase (EdU-negative cells) (p-value < 0.05 unpaired Wilcoxon signed rank tests), with a clear divide in size between these two cell populations. This

confirmed previous observations based on a smaller number of cells selected manually, instead of using the automated script employed here (Schiessl et al., 2012).

In addition, I observed that cells that had not undergone S-phase were significantly smaller in the floral meristems of the *jag-2* loss of function mutant compared to the EdU-negative cells in the wild-type control, while there was no significant cell size difference between the EdU-positive cells in the floral meristem of *jag-2* and wild type (Figures 7.2. A-B and 7.3. A-B (red boxplots); 7.6.) This was also observed when comparing the *jag-1* allele and the corresponding wild-type control in L-*er* background (Schiessl et al., 2012). In contrast, however, the size of EdU-negative cells was not significantly different between *jag-1* and wild type in *Col* background (Figure 7.4.A-D (red boxplots)). Considering that *JAG* is specifically expressed in the emerging primordia and absent from floral meristems, these results suggest that *JAG* had a non-cell autonomous effect on cell growth in the meristem specifically for cells that have not undergone S-phase without altering the size at which meristem cells entered S-phase. This effect required modifier genes present in the L-*er* accession, but not in *Col* background.

In wild-type sepal primordia, the median cell size did not differ significantly between the EdU-positive and EdU-negative cells (p-value <0.05 unpaired Wilcoxon signed rank test), suggesting that entry into S-phase and cell volume were uncoupled. In addition, cells of wild-type sepal primordia showed an increase in heterogeneity of cell volumes (Figures 7.2.A (blue boxplots) and 7.3. A-B; Schiessl et al., 2012). In contrast, the median cell size of EdU-positive cells was significantly larger than that of EdU-negative cells in *jag* mutant sepal primordia. While the cell sizes of EdU-positive cells were comparable between *jag-2* and wild-type primordia cells, *jag-2* primordia had smaller EdU-negative cells than the wild type, resulting in the significant difference in cell volumes between cells having and not having undergone S-phase in the *jag-2* mutant (Figures 7.2.B; 7.3.A-B (blue boxplots); Schiessl et al., 2012). This difference was further enhanced by the fact that cell sizes remained uniform in *jag* sepal primordia compared to the more heterogeneous cell sizes in wild-type primordia. This suggested that entry into S-phase and cell volume remained coupled in the cells of *jag* mutant sepal primordia. In this respect, these cells behaved similarly to cells in the meristems of wild type and *jag* mutant, where *JAG* is not expressed. Together these results provided evidence that JAG is required for the transition from a meristematic to primordium growth in emerging sepals

and that JAG changes the way cell growth and cell cycle are coordinated during this transition.

7.2.2. Ectopic *JAG* caused cells to enter S-phase at smaller cell sizes in the meristem

To further investigate the function of JAG in modulating the coordination of entry into S-phase and cell volume, I tested whether ectopic expression of JAG in the meristem is sufficient to cause the loss of coordination observed in the wild type sepal primordium in the presence of *JAG*. For this, I used wild-type plants harboring the *35S:JAG-GR* construct (as described in Chapter 2) and activated ectopic JAG-GR by incubating the dissected floral buds in germination medium supplemented with 10 µM DEX for 45h prior to the incubation with 10 µM EdU and 10 µM DEX for 3h.

Activation of ectopic JAG-GR in the floral meristem caused cells to enter S-phase at an inappropriately small median cell volume of 136 µm³ compared to the meristem cells in the mock-treated plants that entered S-phase at a median cell volume of 174 µm³. By contrast, median cell volumes of the EdU-negative cells only decreased slightly in the meristem cells of DEX-treated *35S:JAG-GR* plants compared with the EdU-negative cells in the meristem of the mock-treated plants with 133 µm³ and 146 µm³, respectively (Figure 7.7.; Schiessl et al., 2012). These results showed that cells in the meristem are physiologically capable of entering S-phase at smaller cell sizes than they actually do in the context of the wild-type meristem and that ectopically activated JAG pushed cells into S-phase at smaller cell sizes, suggesting that a factor that acts similarly to a cell size threshold restricts cells to enter S-phase at abnormally small cell sizes in the meristem and that ectopic JAG can override this mechanism until an appropriate cell size is achieved.

7.2.3. Loss of *KRP4* in *jag* mutants affects coordination of cell size and entry into S-phase

To test whether repression of *KRP* genes mediates the effect of *JAG* on S-phase entry, I analysed how the loss of *KRP2* and *KRP4* function affected the relation between cell volume and DNA synthesis, both in wild-type and in *jag* mutant backgrounds.

In comparison to their wild-type controls, both *krp4* single mutants *krp4-2 L-er* (Figure 7.2.C, red boxplots) and *krp4-1 Col* (Figure 7.4C, red boxplots) showed a significant

decrease in meristem cell volumes for both EdU-positive and EdU-negative cells. For example, in the *krp4-2* single mutant the median cell volume for EdU-positive and EdU-negative cells was 139.60 µm³ and 113.09 µm³, respectively. By contrast, in the wild-type L-*er* control the median cell volume for EdU-positive and EdU-negative cells was 172.3 µm³ and 136.88 µm³, respectively. Because the cell volumes were uniformly reduced in the meristems of the *krp4* single mutants, the difference between cells having undergone S-phase and cells not having undergone S-phase remained comparable between the *krp4* mutants and their corresponding wild-type controls. In the sepal primordia the reduction in cell volumes was not significant between both *krp4* single mutants and the corresponding wild-type controls (Figures 7.2. A, C (blue boxplots); 7.3.A-B; 7.4.A, C (blue boxplots), 7.5.), consistent with the idea that KRP4 function is repressed by JAG in emerging primordia (see Chapter 6). In conclusion, *KRP4* appeared to modulate cell size specifically in the meristem, but *krp4* mutant meristems retained coordination between cell size and entry into S-phase as observed in the wild-type meristems, showing that *KRP4* is not essential to couple cell cycle with cell size.

Combining the loss of *JAG* and *KRP4* function in the *jag-2 krp4-2* L-*er* and in the *jag-1 krp4-1 Col* double loss of function mutants caused a similar reduction in the volumes of the EdU-positive and EdU-negative meristem cells as observed in the *krp4-2* L-*er* single mutant, with a median cell volume of 144.42 µm³ and 125.06 µm³ (Figures 7.2.A-D (red boxplots); 7.3.A-B; 7.4.A, C, D, G (red boxplots); 7.5.).

In sepal primordia, the loss of *JAG* and *KRP4* function in the *krp4-2 jag-2 L-er* and in the *krp4-1 jag-1 Col* caused an increase in the volume of EdU-negative cells while EdU-positive cells remained at similar small cell volumes as observed in the meristem of the *krp4* single and *krp4 jag* double mutants. As a result of the increased size of EdU-negative cells in sepal primordia of the *jag-2 krp4-2* double mutant, the difference in cell volumes between EdU-positive and EdU-negative cells reverted to levels comparable to the wild-type primordia. That loss of *KRP4* function in the *jag-1* mutant background changed the sizes specifically of cells not undergoing S-phase in the sepal primordia was an unexpected result, because *KRPs* have been characterized to interact with CDKA/CYCLIN D complexes to control the G1/S phase transition (Figures 7.2. A-D (blue boxplots); 7.3. A-B; 7.4. A,C,D,G (blue boxplots); 7.5.).

Using bootstrapping, the 95% confidence intervals for the differences in cell sizes between EdU-positive and EdU-negative cells (Figure 7.6.) were calculated, which confirmed that the difference between median cell volumes of EdU-positive and EdU-negative cells is significantly diminished in the sepal primordia of the *krp4-1 jag-1* double mutant compared to the *jag-1* single mutant. This suggested that the loss of *KRP4* function rescued the uncoupling of entry into S-phase and cell volume in the *jag* mutant background.

In contrast to the *krp4* mutants, I did not observe any significant changes in cell volumes of meristem and primordia cells or differences between volumes of cells having and not having undergone S-phase for the *krp2-3* loss of function allele in wild-type or *jag-1* background (Figure 7.4.B, E). The result that KRP2 did not have a significant effect on the coordination between cell volume and cell cycle in the epidermal layer of the meristem of early stage 3 sepal primordia is in line with the observation that *KRP2* is not expressed in these tissues (Chapter 6, Figures 6.10. and 6.11.). In conclusion, analysis of the single loss of function mutants suggested that *KRP4*, but not *KRP2*, plays a role in the regulation of cell size homeostasis, particularly in the epidermal layer of the meristem.

7.2.4. Loss of KRP2/KRP4 did not visibly rescue the growth defects in early sepal primordia

In respect to the question whether changes in cell size homeostasis have an effect on overall rescue of bud morphology, I did not observe any rescue of organ outgrowth in early sepal primordia of the *krp2/4 jag* double and triple mutants. This suggests that the changes in cell size homeostasis do not affect organ growth, or that the short time between primordium emergence and the stages analysed here (stage 3) may not be sufficient for changes in organ growth to unfold (Figure 7.8.). Interestingly, the only obvious morphological change observed between the *jag-1* single mutant and particularly the *jag-1 krp2-3 krp4-1* triple loss of function mutant was an increase of the intersepal zones appearing as gaps between emerging sepal primordia (arrow, Figure 7.8.D).

In summary, my experiments showed that *KRP4*, but not *KRP2*, is involved in the modulation of cell size homeostasis in the floral meristem and during early sepal organogenesis. In addition, the loss of KRP4 function in the *jag* loss of function mutant

background rescued the uncoupling of S-phase entry and cell volume as observed in the wild-type primordium, suggesting that ectopic KRP4 may be the cause for the meristem-like co-ordination between cell size and entry into S-phase observed in *jag* mutant sepal primordia. Therefore, it can be speculated that JAG directly represses *KRP4* in order to mediate the changes in cell size homeostasis that are required when sepal primordia emerge from the floral meristem in the wild type.

7.3. Discussion - *KRP4* mediates the role of *JAG* on the coordination between cell growth and cell cycle

Using a quantitative 3D imaging approach, I found that the effects of JAG on modulating cell size homeostasis during the transition from meristem to primordium growth behavior are mediated by repression of *KRP4,* but not *KRP2.* Therefore, this work provided insight into how cell size homeostasis is directed by a growth regulator during early organogenesis. My results are consistent with the idea that *KRP4* is involved in a mechanism that links cell cycle progression to a critical minimum cell size threshold.

7.3.1. KRP4 modulates cell size homeostasis

Several live-imaging studies and kinematic analyses have estimated that in leaves and floral organs, wild type primordium cells divide on average every 20 hours (De Veylder et al., 2001; Roeder et al., 2010; Asl et al., 2011; Schiessl et al., 2012). Induction of synchronised cell cycle re-entry in root pericycle cells that were arrested in G1-phase showed that it took no longer than 4 hours until the late S-phase markers and markers for S-phase to G2-phase were expressed, and no longer than 6 to 12 hours until the G2 to M phase marker *CYCB1;1* was fully expressed, and the first cells had undergone cytokinesis (Himanen et al., 2002). According to these observations, it can be estimated that cells progress through S-phase within about 3-4 hours and that cells progress through G2 and cytokinesis within 6 hours. Although progression through the cell cycle is likely to vary between cell types, the available data suggest that plant cells in growing tissues spend almost half the time of cell cycle duration in G1-phase. In respect to the quantitative 3D imaging experiment, these findings suggested that cells that were labelled with the DNA synthesis marker EdU (EdU-positive cells) after a 3-hour incubation period were

predominantly in S-phase or G2 phase, with exception of some cells that had been labelled during late S-phase and may already have undergone cytokinesis and thus represented newly divided daughter cells. Cells that had not been labelled with EdU may have spent the three-hour incubation period entirely in G1-phase, or G2-phase or may have undergone cytokinesis and therefore represent newly born daughter cells in G1-phase.

In respect to cell growth during cell proliferation, work in budding yeast has provided evidence that proliferating cells predominantly grow in G1-phase. It was hypothesised that during S-phase and M-phase resources need to be focussed on DNA replication and rearrangement of cellular components, to finally separate the new daughter cells (Goranov et al., 2009). This is in line with my observations in the wild-type floral meristem, where EdU-negative cells were significantly smaller than cells that had entered S-phase, suggesting that most EdU-negative cells represented newly divided daughter cells that had to increase considerably in size before entering S-phase. In addition, both groups of cells, the EdU-negative cells and the EdU-positive cells were very uniform in size. Together, this suggested that cell size and cell proliferation are tightly coordinated and that there is a strong dependency of cell size on entry into S-phase in the meristem.

Strong dependency of entry into S-phase on cell size has previously been observed in budding yeast, where it has been identified as a mechanism to maintain cell size homeostasis and to generate uniform cell sizes over several generations (reviewed by Jorgensen and Tyers, 2004). Provided that growth predominantly happens in G1-phase (Goranov et al., 2009) and cell divisions are symmetric, a newly divided yeast daughter cell has to double in size before undergoing S-phase, in order to maintain cell size homeostasis. In budding yeast, the mechanism to maintain cell size homeostasis has been characterised as a critical size threshold involving a rate-limiting and unstable activator that activates a series of events that lead to DNA replication, also refered as “Start”, as soon as a certain minimum size threshold is achieved. Several candidates, for example the *G1 cyclin CLN3*, have been suggested to represent such a rate-limiting unstable activator that accumulates in G1 phase and is involved in a signalling cascade that triggers “Start”, depending on a minimum cell size (reviewed by Jorgensen and Tyers, 2004; Figure 7.9.A).

Coordination between cell cycle progression and cell size has also been established in multicellular organisms, for example, a cell sizing mechanism operating at G1-S phase has

been reported in mammalian cell culture cells, although the molecular mechanism remains unknown (Tzur et al., 2009). In the *Arabidopsis* meristem, it has been shown that the application of aphidicolin and hydroxyurea, two compounds that block DNA synthesis, resulted in inhibition of growth, while inhibition of mitosis by application of the microtubule-depolymerising compound oryzalin did not inhibit cell growth and led to endoreduplication and increased cell sizes (Grandjean et al., 2004). This suggested that there is a dependency of cell growth on DNA synthesis, whereas cell growth is not dependent on mitotic division. However, it has been speculated that in multicellular organisms these basic cell-autonomous dependencies between cell cycle progression and cell growth may be modulated or overridden in a temporal and spatial context by developmental regulators, in order to allow organ patterning by differences in local tissue growth and cell proliferation rates (reviewed by Jorgensen and Tyers, 2004; Marshall et al., 2012).

Specifically in plants, critical cell size thresholds have not been identified yet. However, it can be hypothesised that in the meristems, where cell proliferation serves the purpose of giving rise to a population of stem cells with uniform cell sizes, a critical size threshold would be useful as a mechanism to maintain cell size homeostasis (Figure 7.9.B).

Furthermore, it could be speculated that in order to accommodate the growth behaviour observed in organ primordia with increased in cell proliferation rates and cell growth rates, and an increase in cell size heterogeneity (Roeder et al., 2010; Schiessl et al., 2012), a cell size threshold would need to be altered or even removed (Figure 7.9.C).

In the work presented here, it appeared as there was a critical size threshold in place in the wild-type meristem that prevented smaller cells from entering S-phase. Because EdU-positive cells were only found in a very narrow size range, it appeared that all cells that reached this critical size uniformly entered S-phase and progressed through the cell cycle. Interestingly, when JAG was ectopically activated in the meristem by using the DEX-inducible *35S:JAG-GR* line, cells entered S-phase at signficantly smaller cell sizes, while the EdU-negative cells decreased in size only slightly, suggesting that cell size homeostasis was maintained but entry into S-phase was shifted to smaller cell sizes. Therefore, if there was a critical size threshold in place in the meristem, ectopic JAG would be able to modulate or even override the mechanism that delays entry into S-phase until a certain cell volume is achieved.

A similar cell size distribution for EdU-positive and EdU-negative cells with cells entering S-phase at smaller cell sizes than in wild-type meristems was also observed in the meristem of the *krp4* single mutant (and also in the *krp4 jag* double mutant), suggesting that ectopic JAG in the meristem may have repressed *KRP4* and therefore have caused a similar cell behaviour as in the *krp4* loss of function mutants. Together, this suggested that changes in *KRP4* expression levels can shift the cell size at which cells enter S-phase. Furthermore, KRP4 function was required for the meristem-like coordination between cell size and cell cycle as observed in *jag* mutant primordia. In comparison, the *krp4 jag* double mutant showed a loss of coordination between these two processes similar to wild-type sepal primordia. Together, this supported the idea that *KRP4* may be involved in setting or responding to a critical cell size threshold in the meristem and *jag* sepal primordia. In the meristem context, it would be interesting to further investigated whether shifting cell size homeostasis by ectopic *JAG* expression has an effect on overall inflorescence meristem and floral meristem size and shape, and on the number of flowers and floral organs initiated.

With the recently gained knowledge that JAG directly represses KRPs and directly activates *CYCD3;3*, one could speculate that ectopic expression of JAG, on the one hand promoted *CYCD3* and on the other hand repressed *KRP4*, generating a situation favorable for cells entering S-phase in the meristem of DEX-treated *35S:JAG-GR* plants. Both genes, *KRP4* and *CYCD3* would be good candidates to be part of a critical size threshold mechanism in plant meristems. Protein levels of KRPs and D-type cyclin have been shown to be under post-translational control via the proteasomal degradation pathway, (Verkest et al., 2005; Ren et al., 2008; Zhao et al., 2012), suggesting that their protein levels can be reset in newly divided daughter cells, a prequisite for a critical size thresholds as described by Jorgensen and Tyers (2004).

Repression of KRP4 by JAG-GR (see Chapter 6) would be expected to promote CYCD function and consequently facilitate entry into S-phase in the meristem of DEX-treated *35S:JAG-GR* plants. However, it has previously been shown that KRPs not only interact with CYCD/CDK complexes to inhibit them, but also to promote the complex formation between D-type cyclins and CDKA and to promote nuclear localisation of these complexes (Sanz et al., 2011). This suggested that *KRPs* have a dual function: On the one hand *KRPs* play a crucial role in preparing for G1/S-phase entry by promoting nuclear localisation of

CYC-D/CDKA complexes, but on the other hand, *KRPs* are also able to tightly inhibit the G1/S-phase transition. This dual role where *KRP4* tightly inhibited entry into S-phase but at the same time promoted the preparation for entry into S-phase would be one way to explain the cell size distributions I have observed in the sepal primordia of the *krp4 jag2* and *krp4 jag1* double mutants in comparison to the corresponding *jag* single mutants. In the double loss of function mutants, loss of coordination between cell volume and entry into S-phase appeared to be restored, similar to wild-type sepal primordia, with no significant difference in cell sizes of EdU-positive and EdU-negative cells, predominantly because EdU-negative cells increased in size concomitant with an increase in cell size heterogeneity. But how would the loss of a cell cycle inhibitor cause a cell size increase in cells that have not undergone S-phase? One explanation would be that KRP4 promotes the activity of a factor that promotes entry into S-phase. Therefore, at high KRP4 levels entry into S-phase would be tightly controlled but also highly promoted once the tight control is released, leading to narrow size ranges for EdU-positive and EdU-negative cells as observed in the wild-type meristem and in the sepal primordia of the *jag* loss of function mutant (Figure 7.10.A). By contrast, in the primordium of the double loss of function mutant, loss of KRP4 would loosen the tight control on S-phase entry but at the same time attenuate the activity of the factor that promotes entry into S-phase. As a result, cells would be able to enter S-phase at smaller but also larger cell sizes and cells would not appear to be uniformly pushed into S-phase as soon as they reach the critical size threshold (Figure 7.10.B). Consequently, EdU-negative cells, provided they are predominantly in G1 phase, would be allowed to grow larger before entering S-phase, which would explain the concomitant increase in cell size and cell size heterogeneity (Figure 7.8.B). In line with this hypothesis, Cheng et al. (2013) found that mRNA levels of *CYCD3;2* and *CYCD3;3* were down-regulated in the *krp1/2/4/5/7* quintuple mutant.

Another explanation for the cell size increase of EdU-negative cells could arise from the fact that loss of KRP4 function could promote premature entry into S-phase, but not the subsequent progression from G2-M phase. It has been shown by Dewitte et al. (2003) that ectopic expression of *CYCD3* in cell culture cells leads to accumulation of cells in G2-phase, because the transition of cells entering from G1 to S-phase is accelerated but progression from G2 to M-phase is an independent and separable step. It could be hypothesised that loss of *krp4* function has a similar effect on cell cycle progression,

where an increased number of cells enters S-phase at smaller cell sizes, but G2 to M phase transition remains unaffected and is the limiting factor. With the imaging approach used in this project these cells would be detected as larger EdU-negative cells together with the smaller EdU-negative cells in G1-phase, resulting in an increase in median cell volumes and cell size heterogeneity for the EdU-negative cells. Thus it could be speculated that in a wild-type primordium, JAG moderately represses *KRP4* to a level that allows uncoupling of cell size and entry into S-phase, resulting in an increase of cell size heterogeneity in the pool of EdU-negative cells comprising of cells in G2-phase, M-phase and newly divided daughter cells in G1-phase.

It is also worth noting that my q-RT PCR results have shown that *CYCD3;3* is up-regulated in the *jag* loss of function mutant. Consequently, loss of *KRP4*, which antagonises the G1/S phase promoting function of *CYCD3*, would even have accelerated entry into S-phase in the sepal primordia of the *krp4 jag* double loss of function mutant, unless the ectopic expression of CYCD3 was caused by ectopic KRP4 expression. Interestingly, Bemis and Torii (2007) reported that ectopic expression of *KRP4* under the epidermis-specific promoter *AtML1* did not have an effect on cell proliferation rate or final cell size in the meristem, while it caused severe reduction in cell number and signficant cell enlargment in primordium cells. On the one hand, the effects of ectopic KRP4 expression may be diminished as a net effect of the meristem-specific cell behavior, with undifferentiated cells of the stem cell pool exhibiting slow growth rates, slow proliferation rates and not undergoing post-mitotic cell expansion compared to cells in lateral organs, which exit cell proliferation phase, expand and differentiate. On the other hand, Bemis and Torii (2007) suggested that in the meristem, ectopic *KRP* expression might be counteracted by the *CLV*-*WUS* and cytokinin signaling pathway, which tightly regulates maintenance of stem cell homeostasis and meristem size. In this context, Dewitte et al. (2007) have shown that *CYCD3;1-3* play a major role in regulating the size of the shoot apical meristem. Meristems of the *cycd3;1-3* triple mutant consisted of fewer cells and were reduced in size. Furthermore, it was shown that *CYCD3* acts downstream of cytokinins to promote cell proliferation in the meristem.

Against this background, my experiments provided evidence that there is a strict cell size threshold in place for meristem cells entering S-phase, and that KRP4 plays a key role in maintaining this cell size threshold. Therefore, it could be speculated that ectopic *KRP4*

expression adds *KRP4* to an already highly saturated system with high *CYCD3* levels promoting entry into S-phase and high *KRP4* levels counteracting premature entry into S-phase as part of a size threshold mechanism. This could be further amplified if *KRP4* promoted CYCD3 activity. However, I have not investigated the transcript levels of *CYCD3* in the *krp4 jag* double loss of function mutant, which would provide a preliminary insight into whether KRP4 can promote *CYCD3* expression at transcript level.

In summary, even though the two hypotheses for the function of KRP4 appear to oppose each other, they can be considered as variations of the same regulatory mechanism involving the dosage-dependent balance between S-phase promoting factors, most likely D-type cyclins in complex with CDKA, and KRPs as their inhibitors. In this respect, mathematical models have been developed that proposed that in the plant cell cycle, negative regulatory feedback loops involving CYCD/CDKA complexes and *KRPs* could be sufficient to ensure stable and unidirectional progression through the cell cycle. For example, Dissmeyer et al., (2010) proposed a mathematical model in which cell cycle progression has been described as a function of CDKA activity, with cyclins being the activating components and KRPs being the key inhibitors in a system that acts like a bistable switch, giving rise to two steady states of CDKA activity. For example, in G1-phase CDKA activity is maintained at a low steady state due to high KRP levels; with increasing activation of CYCD/CDKA;1 complexes, the system becomes unstable and switches to the G1 to S-phase transition. Intermediate levels of CDKA activity are rapidly overcome by a double feedback loop, where CDKA;1 in complex with D-type cyclins promotes the degradation of its KRP inhibitors, resulting in a steady state with low KRP levels and high CDKA-CYCLIN D levels in S-phase (Dissmeyer et al., 2010).

Recently, the model described above has been extended to include post-translational degradation of KRPs via the FBL17- mediated proteasomal pathway. Zhao et al. (2012) who, in particular, studied entry into S-phase in the context of cell divisions during male and female gametogenesis and suggested that entry into S-phase is predominantly regulated by a module comprising *CYCD/CDKA;1, RBR, E2F, FBL17* and *KRPs*. *RBR1* represses *FBL17,* which targets KRP proteins for proteasomal degradation, but also represses *E2FA,* which promotes *FBL17*. To promote the transition from G1 to S-phase, CDKA;1 phosphorylates RBR1, in order to release E2FA from RBR1 repression and to promote *FBL17* expression via *E2F* activation and direct de-repression by *RBR1*. In the

case of high KRP activity causing reduced CYCD/CDKA;1 activity, entry into S-phase might not only be impaired because of reduced RBR1 phosphorylation (and thus persisting repression of E2F), but also because of enhanced direct repression of FBL17 by RBR1, which would be needed to target KRPs for proteasomal degradation.

In this context, it would be interesting to include the regulatory effects of developmental regulators such as *JAG* and *ANT*, which have been shown to directly regulate several key components of this negative regulatory feedback loop at transcriptional level, in order to model the impact of these regulators on cell cycle progression. In addition, data on cell behavior in regard to S-phase entry and cell volume could be integrated into already existing models of cell cycle regulation, which would provide further explanations for the data arising from my imaging experiments and improve or extend existing models. Furthermore, it would be interesting to investigate whether the effects of loss of KRP4 are functionally linked to CYCD3 function. It would be of particular interest to test whether the function of *KRP4* in cell size homeostasis is dependent on *CYCD3* by repeating the quantitative 3D imaging experiment using combined EdU/PI staining in *krp4 jag cycd3* mutants. In order to confirm the function of KRP4 in regulating cell size homeostasis in the meristem and in early organogenesis, it would be interesting to complement the *krp4* single mutant with a fully functional *pKRP4:KRP4* construct including the 3 kb promoter region and the 1.45 kb 3' region downstream of the stop codon. In addition, inducible ectopic *KRP4* expression or tissue-specific ectopic *KRP4* expression, for example under the strong floral promoter *AP1* or the lateral organ specific promoter *ANT*, would allow us to further investigate the effects of KRP4 function on cell size homeostasis during cell proliferation in the meristems and lateral organ primordia.

In addition to the static data obtained from the pseudo-Schiff propidium iodide staining combined with EdU labeling, dynamic data on cell size and entry into the different phases of the cell cycle would also help to reveal the effects of KRP4 on the cell cycle regulation and cell size homeostasis with high resolution. In order to investigate whether entry into S-phase is accelerated in the *krp4* loss of function mutants and if so, whether this has an effect on G2/M-phase transition, a *CYCB1;1-GFP* reporter construct could be introduced into the *jag* and *jag krp4* loss of function mutant background to mark cells undergoing G2/M-phase. Furthermore, it would be of particular interest to be able

to follow KRP4 expression *in vivo*, even though this has been proven difficult during this project. This difficulty is in line with the observations of several authors attempting to detect KRPs at transcript or protein level by *in situ* hybridisation or Western Blotting (Jakoby et al., 2006; Bemis and Torii, 2007; Torres Acosta et al., 2011) and confirms that some KRP transcripts and proteins have low endogenous abundance. For example, Wang et al., (2000) could not detect *ICK1* in Western Blots in the wild type, although blocking the 26S proteasome pathway with the drug MG132 resulted in an increased signal. Therefore, future efforts to detect *KRP4* expression could focus on generating a reporter line with multimeric 3X-GFP to increase signal brightness. Considering post-translational modifications and fast proteasomal degradation of KRPs (Zhao et al., 2012), a fully functional *pKRP4:KRP4-mCherry* reporter line could be generated, with m-Cherry having been reported to have faster protein folding properties compared to GFP (reviewed by Schmid and Neumeier, 2005).

7.3.2. Does KRP2 have a function in cell size homeostasis?

In *krp2* mutants, quantitative 3D imaging, combining the cell wall marker PI with the DNA synthesis marker EdU, did not reveal any significant effects on cell size homeostasis in the epidermal cells of the floral meristem and in early sepal primordia. This observation is in line with the expression pattern I observed for *KRP2* using a p*KRP2:KRP2-GFP* fusion line: KRP2-GFP was expressed in the deeper layers of the inflorescence meristem, close to the site of emerging floral primordia, and in the central deeper layers of the floral primordia, but was not found in the epidermal layers of meristems. Although KRP2-GFP is eventually expressed in the epidermal layer of sepal primordia, this only occurs from stage 5 onwards (Chapter 6). Therefore, *KRP2* expression did not coincide with the developmental stage and tissues imaged in this experiment.

However, two independent experiments following leaf primordia development by De Veylder et al., (2001) and by Ferjani et al., (2013) provided strong evidence that *KRP2* does have a function in modulating cell size homeostasis, when studied in the context of *KRP2* overexpression and in slightly later stages of organogenesis compared with my experiment. De Veylder et al., (2001) observed that in the wildtype the average cell size of proliferating cells remained constant between day 5 to day 9 of leaf primordia

development, suggesting that cell division and cell growth were balanced and cell size homeostasis was maintained during the cell proliferation phase of wild-type leaf primordia formation. By contrast, in the KRP2 overexpressor line, cell sizes had already increased during the proliferation phase, indicating that cell division was slower than the expansion rate. These findings have recently been supported by Ferjani et al. (2013) who used a kinematic analysis of cotyledons and first leaves of *KRP2* overexpressing lines to show that cell sizes increased by two-fold, compared to cell sizes in the wild type during proliferation phase. This result implies that *KRP2* has at least an effect, if not a direct function, in the coordination of cell proliferation and cell size in proliferating cells.

In this context, it has to be noted that several other mutants impaired in cell proliferation, for example the *an3* mutant, responded with an increase in cell expansion during post-mitotic cell expansion, but not during the proliferation phase (Ferjani et al., 2013). Interestingly, in the *KRP2* overexpressing lines, the increase in cell size during proliferation phase was linked to increased activity of vacuolar-type H+ ATPases. It has been shown that ectopic expression of *KRP2* in the *det3-1* mutant background with reduced V-ATPase activity (see also Chapter 8) resulted in a reduction in cell number, but in cell sizes similar to the wild type, suggesting that the increase in cell size observed in the *KRP2* overexpressor is dependent on the activity of vacuolar-type ATPases. In contrast, this dependency on DET3 function has not been observed in the *an3-4* and *fugu* loss of function mutant backgrounds (Ferjani et al., 2013). This work revealed that KRPs and V-ATPases are key players in the coordination of cell volume and cell proliferation during early organogenesis. In line with the work by Ferjani et al. (2013), JAG not only directly targeted *KRP2* and *DET3* but also several additional genes associated with V-ATPases and plasma membrane-located ATPases (Chapter 8), suggesting that modulating the activity of ATPases could be a common regulatory pathway to coordinate cell volume in relation to cell proliferation during the early mitotic phase of organ development.

In conclusion, to further investigate the function of *KRP2* on cell size homeostasis and the link to vacuolar ATPases, the effects of *KRP2* on 3D cell geometry would have to be followed at the site of expression, either in the deeper layers of the floral buds or in sepal primordia later in development, which is very challenging with the imaging and 3D segmentation techniques currently used. In the future, flow cytometry and detection of

fluorescent cells could also be used to determine the nuclear content of cells that express KRP2-GFP under its endogenous promoter.

7.3.3. Does *JAG* have a non-cell autonomous effect on cell sizes in the meristem?

Using quantitative 3D imaging, I observed that EdU-negative cells were significantly smaller in the sepal organ primordia but also in the floral meristem of the *jag* single mutant in comparison to EdU-negative cells in the wild-type. Because *JAG* is not expressed in floral meristems, this suggested that *JAG* has a non-cell autonomous effect on growth of cells in G1-phase in the meristem but without altering the size at which meristem cells entered S-phase. Provided that most EdU-negative cells are in G1-phase, reduced cell sizes would suggest that *jag* mutant cells grow slower. Because the sizes of EdU-positive cells appeared to be comparable to the EdU-positive cells in the wild type meristem, a decrease of cell proliferation rate in the meristem of the *jag* single mutant may be expected – live imaging would help to address this question. It could also be speculated that the cell non-autonomous effect of loss of JAG function could be caused by the fact that primordia cells still behave like meristem cells and therefore may interfere with the signaling pathway that determines the size of the stem cell population, namely the *WUSCHEL/CLAVATA* signaling pathway which could result in reduced growth and proliferation rates of meristem cells.

Another possibility is that elevated cytokinin levels in the organ primordia of the *jag* single mutant could be the signal that mediates the non-cell autonomous effect of JAG on meristem cell growth. Global expression profiling combined with ChIP-Seq revealed that JAG directly represses several members of the *LONELY GUY (LOG)* family (see Chapter 2 and 3), which increase the levels of bioactive cytokinin (Kurakawa et al., 2007). In particular, *LOG1* has been shown to be ectopically expressed in the *jag* loss of function mutant in an independent qRT-PCR experiment (Chapter 8). In addition, JAG directly activates *CKX6*, a member of the cytokinin degrading protein family (Werner et al., 2003). Together, this would result in high cytokinin levels in the primordia of the *jag* loss of function mutant compared to wild-type primordia, which could act as a non-cell autonomous signal.

The fact that the effects of *JAG* in the meristem were only significant in the L-*er* background provides additional, indirect support for the involvement of cytokinin. It has

been shown that mutating all three members of the *ERECTA* (*ER*) family changed the way the shoot apical meristem responded to increased cytokinin levels (Uchida et al., 2013). Exogenous cytokinin application did not cause any obvious changes in meristem size or shape in the wild type. By contrast, it caused severe changes in meristem size and shape in the *er erl1 erl2* triple mutant: The meristem expanded in size, formed ectopic structures and consisted of an increased number of smaller cells. In addition, organogenesis was impaired, with an increase in leaf primordia developing into leaves of aberrant shapes. In summary, it was suggested that members of the *ER* family buffer the response to cytokinin in respect to the *WUS/CLV3* regulatory feedback loop to maintain stem cell homeostasis (Uchida et al., 2013). To further investigate the effect of the *er* loss of function mutation on the cell non- autonomous effect of JAG in the meristem, the first step would be to cross the *jag-1* allele in *Col* to the *erecta* mutation in *Col* background and to confirm whether this causes changes in the cell sizes of EdU-negative cells compared to meristem cells in the *jag* mutant in *Col* background.

7.3.4. Does modulating cell size homeostasis have an effect on overall organ growth?

Results from this work suggest that *KRP4* links cell cycle to cell growth at the cellular level. The roles of *KRP* genes in both cell size homeostasis and in overall organ growth (Chapter 6) raised the question whether both processes are causally linked or separable processes. No obvious rescue in overall primordium development was observed in 3D projections of early floral buds of the *krp4 jag* double mutants compared with the *jag* single mutants. Therefore, my current data do not support a causal link between changes in cell size homeostasis and overall organ size. One explanation could be that the short time between primordium emergence and the stages analysed here (1-2 days) may be insufficient for changes in organ growth to unfold. It should also be considered that suppression of the *jag* growth defects by the *krp* mutations was not complete, therefore additional targets of *JAG* are likely required for full organ growth. It is possible that when cell cycle progression is accelerated by loss of *KRP* function, other cellular processes remain limiting for early primordium growth in the *jag* mutant.

Considering that KRP4 and KRP2 interact with CDKA and D-type cyclins, which primarily control entry into S-phase, both *KRPs* could affect cell growth and cell size through the length of G1 or by tuning the threshold volume at which S-phase can be initiated.

Assuming that proliferating cells increase in size predominantly in G1 (Goranov et al., 2009), reducing the proportion of time spent in G1 could influence overall cellular growth, and consequently tissue growth during cell proliferation phase. In the *jag* loss of function mutant, decreased growth rates have been observed (Schiessl et al., 2012), which may increase the significance of the time spent in G1 and of a minimum cell size checkpoint, in comparison to wild-type primordia, which show accelerated growth.

Furthermore, whether modulating cell size homeostasis in early stages of organogenesis has an effect on mature organ size and shape may depend on how long cells stay in proliferation phase and on the ability to expand post-mitotically, both of which vary between different tissues and organs. In this context, KRP2 has been suggested to play a role in exit from cell proliferation and onset of endoreduplication, two key processes that have been suggested to be key drivers of final organ size and shape and final number of cells and final cell size, in particular, in leaves and sepals (De Veylder et al., 2001; Verkest et al., 2005; Roeder et al., 2010; Asl et al., 2011). In the case of KRP2, which has been shown to have an effect on cell size homeostasis (Ferjani et al., 2013), it would be interesting to further investigate whether significant differences in overall organ outgrowth become apparent at the onset of *KRP2* expression in stage 5 sepal primordia.

To uncover the mechanisms by which KRPs could affect organ growth, it is also important to consider roles other than entry into S-phase. For mammalian CKIs, it has been shown that they have diverse functions essential for cell and tissue homeostasis. Mammalian CKIs have been shown to affect transcriptional regulation, cell fate determination, cell migration and cytoskeleton rearrangements. It has been suggested that these multiple functions of mammalian CKIs could be achieved by phosphorylation events and protein-protein interactions that would lead to conformational changes in the CKIs and affect their subcellular localisation, affinities and protein stability (reviewed by Besson et al., 2008). It has been shown that CIP/KIP participate in the assembly of active cyclin/CDK complexes and may therefore also be able to promote cyclin/cyclin-dependent kinase complexes, suggesting that promoting or inhibitory effects of CIP/KIP on the cell cycle might be dependent on the cellular context and cofactors (reviewed by Besson et al., 2008). Furthermore, it has been shown that all three members of the CIP/KIP family are able to interact with the Rho signaling pathway, suggesting that CIP/KIP play a role in the cytoskeletal rearrangements during cell divisions (reviewed by Besson et al., 2008).

In plants, there has not been evidence for similar additional functions of the KRPs yet. KRPs phosphorylation sites have also been identified (De Veylder et al., 2001; Torres Acosta et al., 2011) and suggest unknown regulatory inputs, as seen for animal CIP/KIP. However, it has recently been proposed that KRP5 binds to DNA and that the punctuated nuclear expression pattern of KRP5 is related to its association with heterochromatin (Jegu et al., 2013). Using ChIP-Seq, Jegu et al. (2013) showed that DNA pull-downs with KRP5 predominantly consisted of transposable elements and about 25% protein coding reads, suggesting that KRP5 can bind to heterochromatin and euchromatin. GO analysis on the enriched DNA binding sites close to protein coding regions revealed enrichment for cell wall modifiying genes such as extensins. It was hypothesized that binding to heterochromatin may facilitate chromatin decondensation and promote endoreduplication, further suggesting that KRP5 may connect endoreduplication with cell elongation. Future investigations will shed light on possible additional functions of KRPs in modulating cell cycle progression, the endocycle and cell expansion.

In summary, quantitative, 3D analysis of cell geometry and DNA synthesis revealed that repression of *KRP4* was the main cause of changes in cell size homeostasis induced by *JAG* during organ primordium emergence. Therefore, this work provided insight into the mechanisms by which a growth regulator modulates cell size homeostasis during development of a multicellular organism.

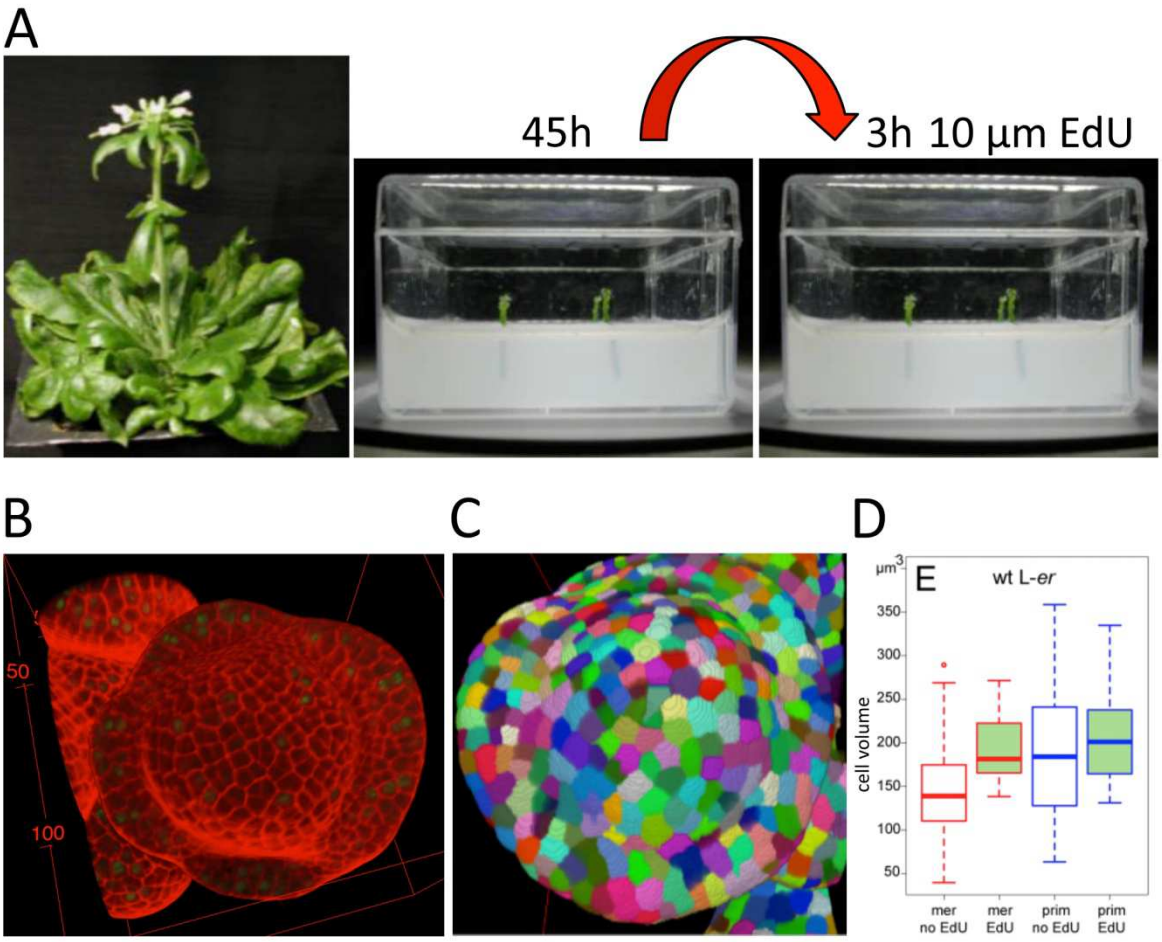

Figure 7.1. Quantitative 3D imaging of floral buds combining the S-phase marker EdU with the cell wall marker propidium iodide. (A) Dissection of inflorescence apices, recovery on germination medium for 45 h, transfer to germination medium supplemented with 10 µm EdU for 3 h; (B) 3D projection of a z-stack where the red channel (cell wall image) and the green channel (nuclear-localised EdU signal) are merged generated in Fiji; (C) 3D projection of the 3D segmented cell wall image generated using BIOIMAGE XD software (Kankaanpaa et al., 2012), (D) for quantitative image analysis custom scripts were developed to automatically determine cell volumes and cell positions relative to the meristem summit and to primordium boundaries in order to locate cells in the meristem or primordium in the L1 cell layer and to select cells with EdU labelling from non-EdU labelled cells; this resulted in tissue specific cell size distributions for EdU-labelled (EdU-positive) and non-EdU labelled (EdU-negative) cells.

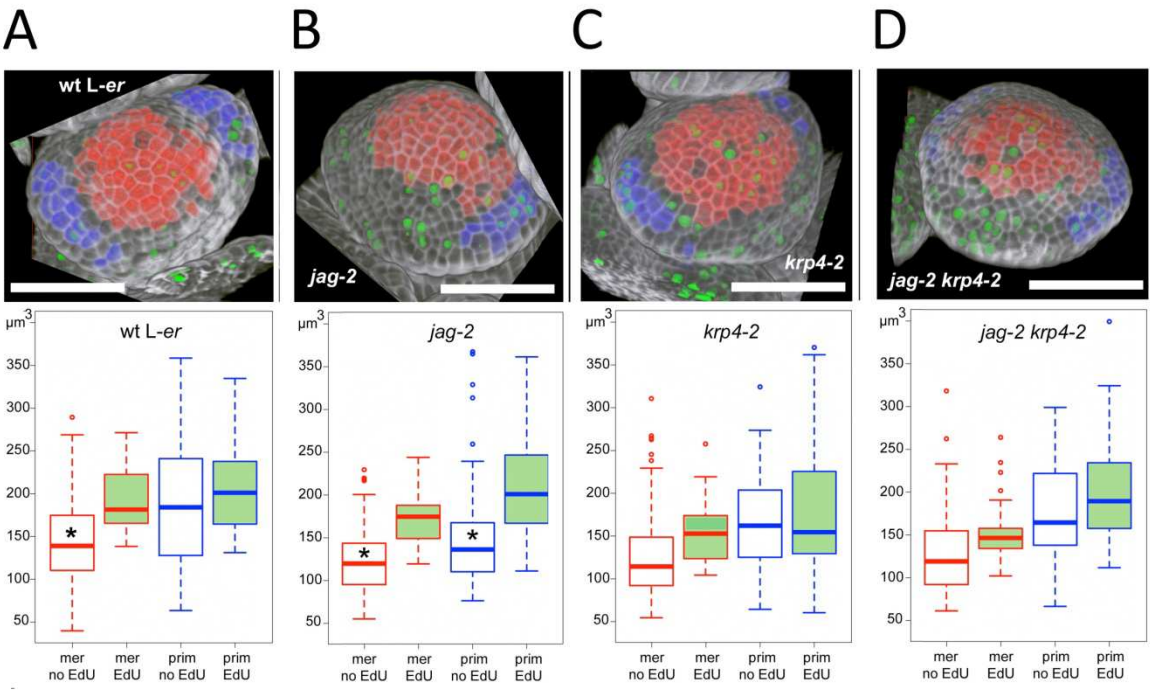

Figure 7.2. *KRP4* is required for the defective coordination between cell volume and S-phase entry in the *jag* mutant.(A-D) representative floral buds from wild-type (A), *jag*-2 (B), *krp4*-2 (C), and *jag-2 krp4*-2 (D) plants with the corresponding cell size distribution boxplots below; Scalebars: 50 µm; the images are 3D reconstructions from stacks of confocal images of pseudo-Schiff propidium iodide (mPS-PI) stained buds (Truernit et al., 2008) overlapped with images produced by 3D segmentation, selection of correctly segmented meristem (red) and primordium (blue) cells, and detection of EdU-labelled nuclei (green); Box plots represent combined cell volumes from at least three independent buds each from wild-type (A), *jag*-2 (B) *krp4*-2 (C),and *jag-2 krp4*-2 (D) plants; the boxplots show median (thick line) second to third quartiles (box), minimum and maximum range (dashed line) and outliers (single points) for meristem (red) and primordium (blue) cells marked with EdU (green) or not (white); black asterisks indicate that the median cell volumes of EdU-positive and EdU-negative cells are significantly different (with *p*-values calculated for the null hypotheses that median volumes are equal for EdU-positive and EdU-negative using the Wilcoxon two-tailed signed-rank test).

A

Differences between EdU-positive and EdU-negative cells in L-*er* background

tissue EdU/no EdU labelling	meristem EdU	meristem no EdU	primordium EdU	primordium no EdU
WT L-*er* median	**175.692**	**139.392**	**200.7632**	**183.7264**
p-value EdU x no EdU		0.00007792		0.129
***krp4-2* L-*er* median**	**153.16**	**114.7262**	**154.148**	**161.7044**
p-value EdU x no EdU		0.0002092		0.759
***jag-2* L-*er* median**	**174.82**	**120.03**	**200.375**	**135.713**
p-value EdU x no EdU		3.014E-09		7.169E-07
***krp4-2 jag-2* L-*er* median**	**147.036**	**119.6405**	**189.2435**	**164.2395**
p-value EdU x no EdU		0.0001091		0.04686

B

Differences between genotypes in L-*er* background

tissue EdU/no EdU labelling	meristem EdU	meristem no EdU	primordium EdU	primordium no EdU
p-values WT x *jag-2*	0.152	0.00000243	0.84	0.000386
p-values WT x *krp4-2*	0.00111	0.0000019	0.0976	0.0578
p-values *jag-2* x *jag-2 krp4-2*	0.00227	0.553	0.428	0.00476

Figure 7.3. Summary of cell size distributions for EdU-positive and EdU-negative cells in floral meristems and sepal primordia of wild type, *krp4-2*, *jag-2*, and *krp4-2 jag-2* in L-*er* background. (A) Summary of median cell sizes in µm³; *p*-values were calculated for the null hypotheses that median volumes are equal for the EdU-positive cells and EdU-negative cells, Wilcoxon two-tailed signed-rank test); (B) Summary of *p*-values for the null hypotheses that median volumes are equal in the pair-wise comparison of genotypes (wild type x *jag-2*, wild type x *krp4-2*, and *jag-2 x jag-2 krp4-2*) for meristem or primordium cells, EdU-negative or EdU-positive cells using the Wilcoxon two-tailed signed-rank test).

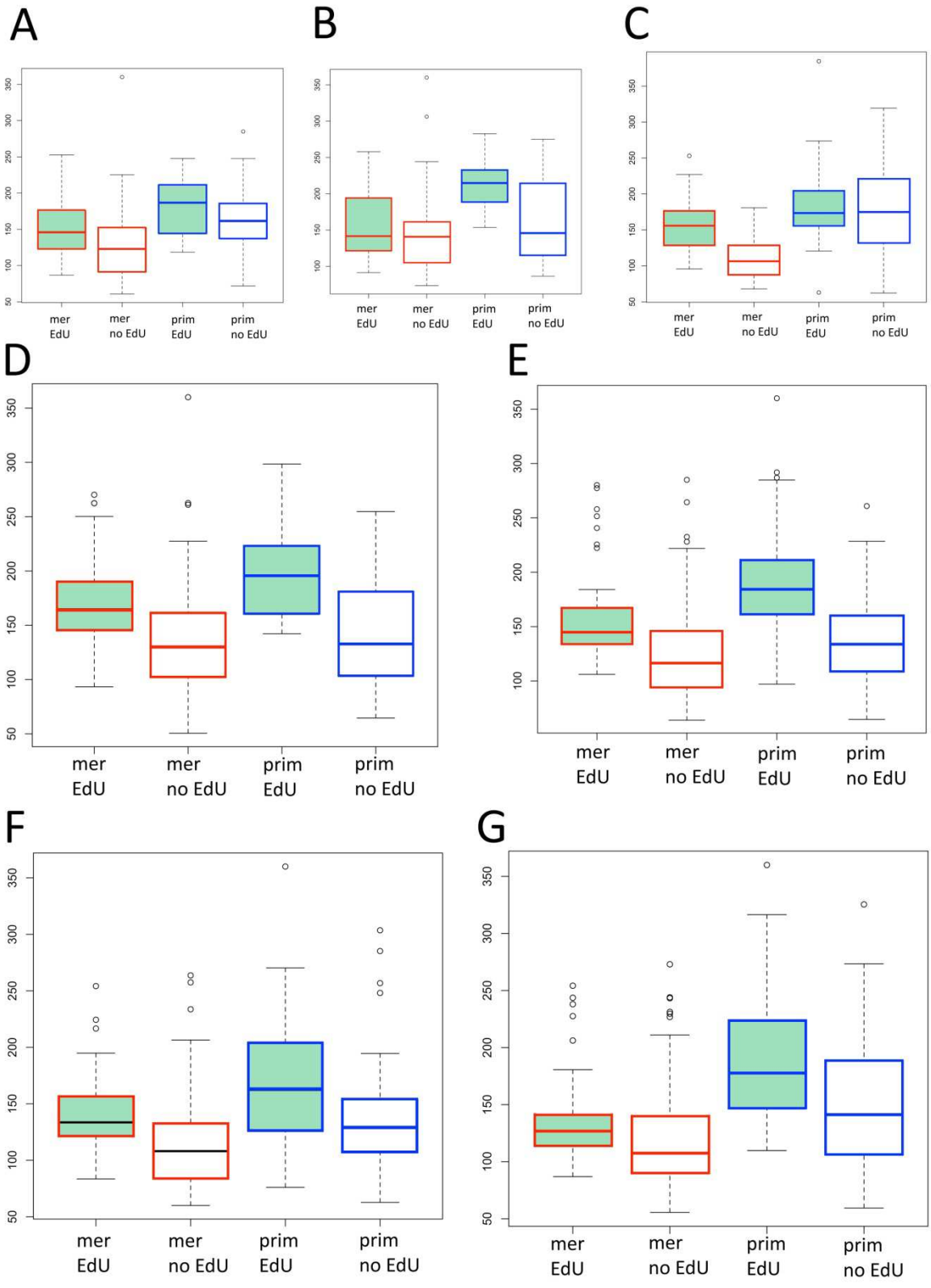

Figure 7.4. Cell size distributions for EdU-positive and EdU-negative cells in the floral meristem and early sepal primordia for combinations of the *jag-1, krp2-3, krp4-1* loss of function genotypes in *Col* background. Combined cell volumes from at least three

independent buds each from wild-type (A), *krp*2-3 (B), *krp4*-1 (C), *jag*-1 (D) *krp2-3 jag-1* (E), *krp4-1 jag* (F), and *krp3-2 krp4-1 jag* (G) plants; the box plots show median (thick line) second to third quartiles (box), minimum and maximum range (dashed line) and outliers (single points).

Differences between EdU-positive and EdU-negative cells in *Col* background

tissue EdU/no EdU labelling	meristem EdU	meristem no EdU	primordium EdU	primordium no EdU
WT *Col* median	**176.127**	**128.01**	**181.306**	**161.946**
p-value EdU x no EdU		0.003819		0.2888
***krp4-1 Col* median**	**155.751**	**106.189**	**173.0295**	**175.1105**
p-value EdU x no EdU		0.0002096		0.8687
***jag-1 Col* median**	**170.464**	**138.13**	**176.85**	**126.517**
p-value EdU x no EdU		0.00000265		0.000000141
***krp4-1 jag Col* median**	**134.26**	**104.689**	**159.86**	**130.58**
p-value EdU x no EdU		0.000002112		0.004657

Figure 7.5. Summary of cell size distributions for EdU-positive and EdU-negative cells in floral meristems and sepal primordia of wild type, *krp4-1*, *jag-1*, and *krp4-1 jag-1* in *Col* background. (A) Summary of median cell sizes in µm³; *p*-values were calculated for the null hypotheses that median volumes are equal for the EdU-positive cells and EdU-negative cells, Wilcoxon two-tailed signed-rank test.

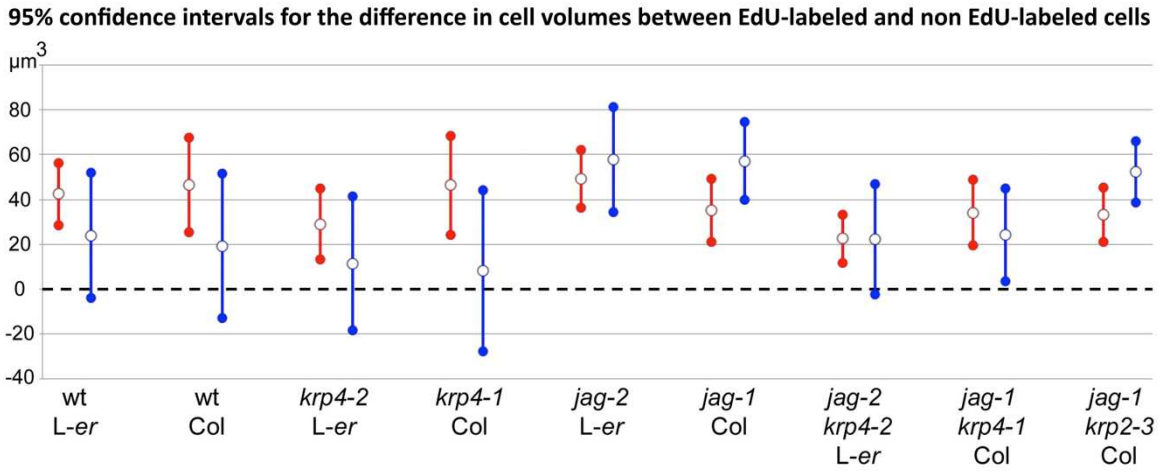

Figure 7.6. 95% confidence intervals for the differences in cell volumes between EdU-labeled and non-EdU labeled cells. 95% confidence intervals calculated by bootstrapping, ordinary bootstrap with 999 replicates, non-parametric, for the difference in volumes (in

µm³) between EdU-positive and EdU-negative cells in the meristem (red bars) or primordia (blue bars) of buds with the genotypes indicated.

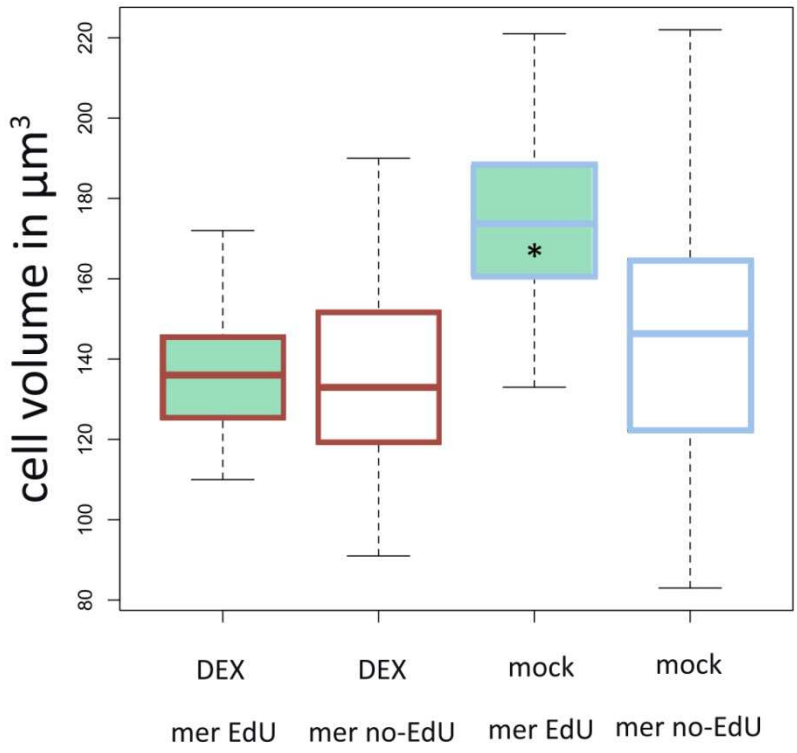

Figure 7.7. Cell size distribution for EdU-positive and EdU-negative cells in the floral meristem of DEX-treated (dark red) and mock-treated (light blue) plants. Boxplots show median (thick line), second to third quartiles (box), minimum and maximum range (dashed line) and outliers (single points); black asterisks indicate that the median cell volumes between EdU-positive and EdU-negative cells are significantly.

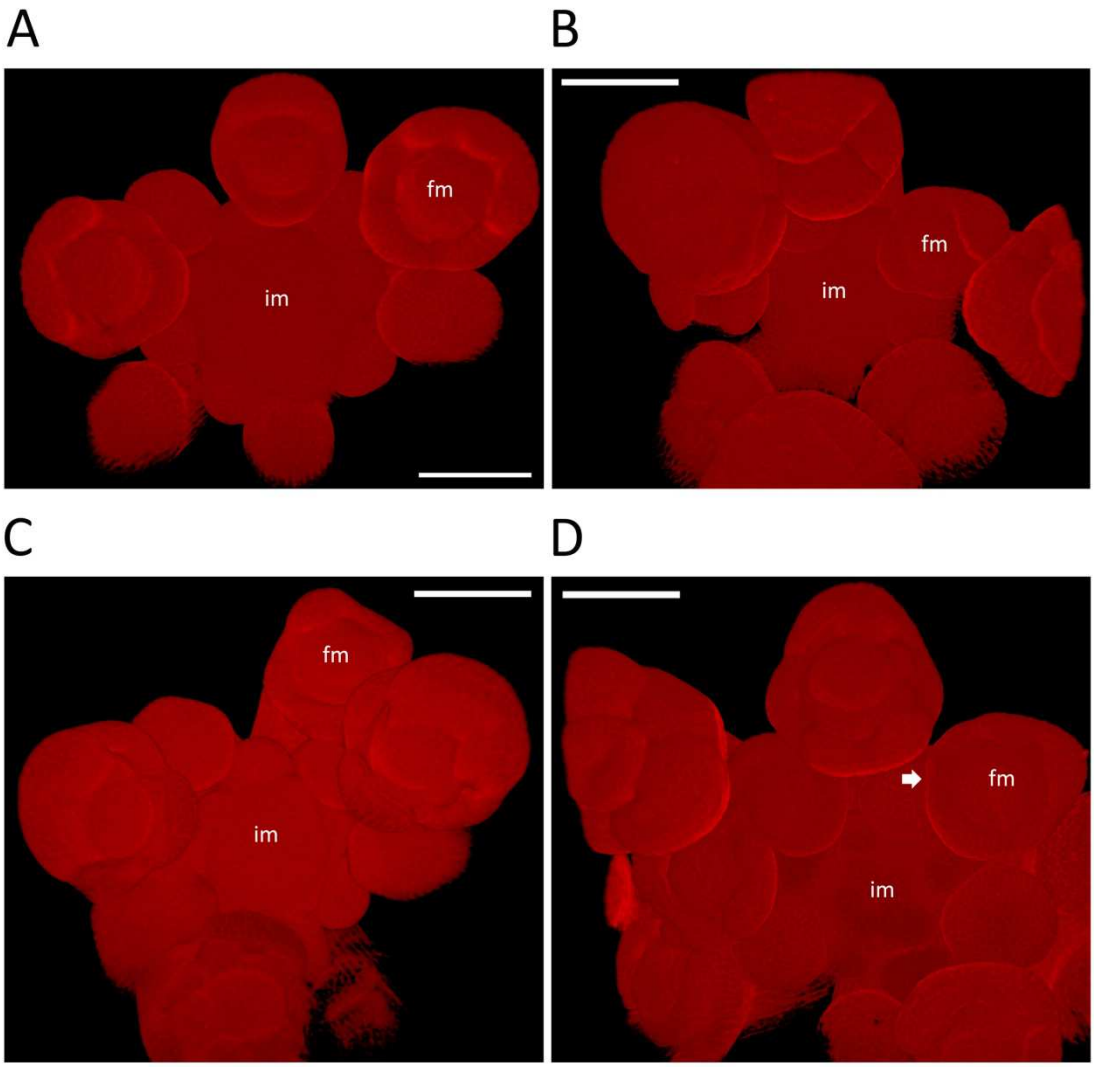

Figure 7.8. Loss of KRP2 or KRP4 function did not rescue the morphology of the *jag*-1 sepal primordia. Scalebars: 50 µm; (A-D) images are 3D reconstructions from stacks of confocal images of pseudo-Schiff propidium iodide (pS-PI) stained inflorescence apices (Truernit et al., 2008); *jag-1* (A), wild type (B), *krp4-1 jag-1* (C*), krp2-3 krp4-1 jag-1* (D), arrow indicates the increased intersepal zone.

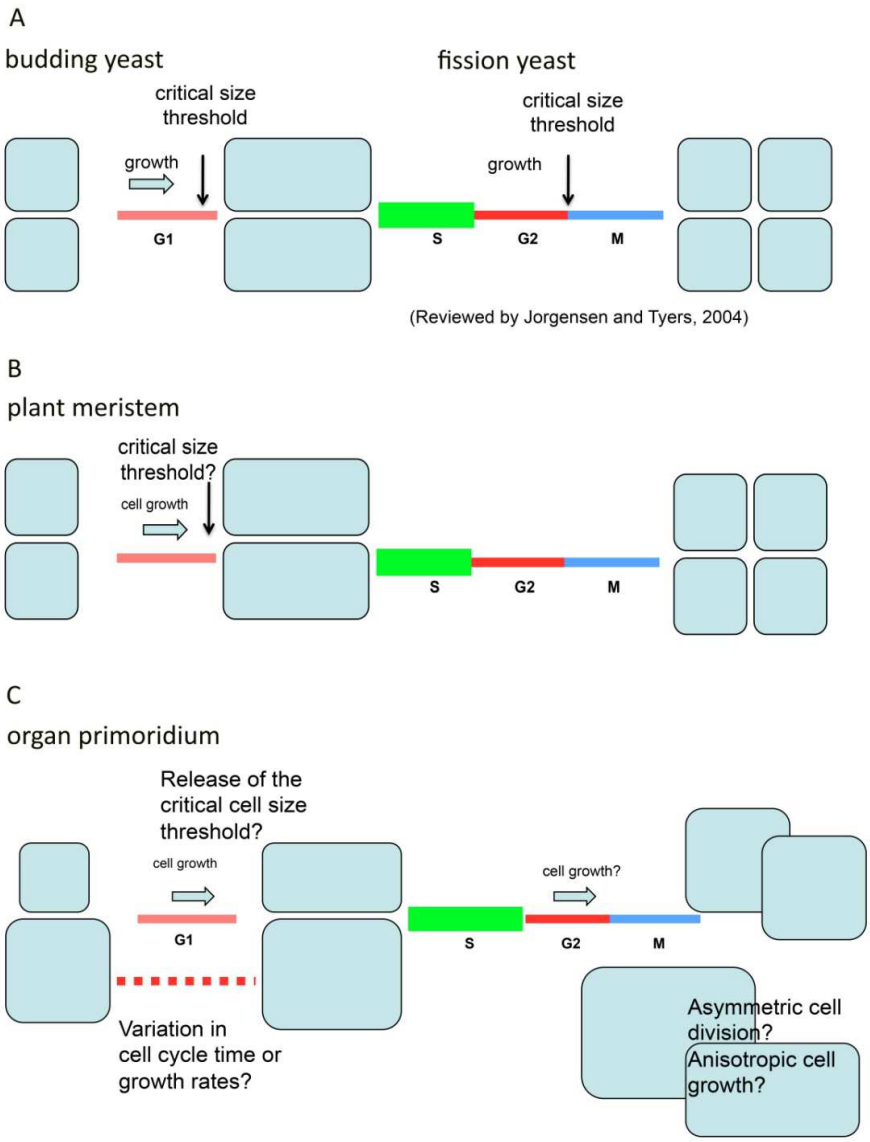

Figure 7.9. Coordination of S-phase entry and cell growth.

(A) Dependency of S-phase entry on cell size in *Saccharomyces cerevisiae* (budding yeast) with a minimum cell size threshold in place at the transition from G1 to S-phase that ensures cell size homeostasis over generations, in addition a cell cycle progression checkpoint at the transition from G2 to M-phase has been identified for *Schizosaccharomyces pombe* (fission yeast), reviewed by Jorgensen and Tyers (2004); (B) hypothesis that a minimum cell size threshold could be in place in plant meristems to regulate the uniform cell sizes in the stem cell pool; (C) hypothesis that a minimum cell size threshold would need to be repressed in order to accommodate the changes in growth behavior during the transition from meristem to primordium growth behavior with increased cell proliferation rates, cell growth rates and increase of cell size

heterogeneity (Schiessl et al., 2012); increase in cell size heterogeneity could, for example, be generated by local variations in growth rates and in cell proliferation rates, asymmetric divisions, and anisotropic cell expansion.

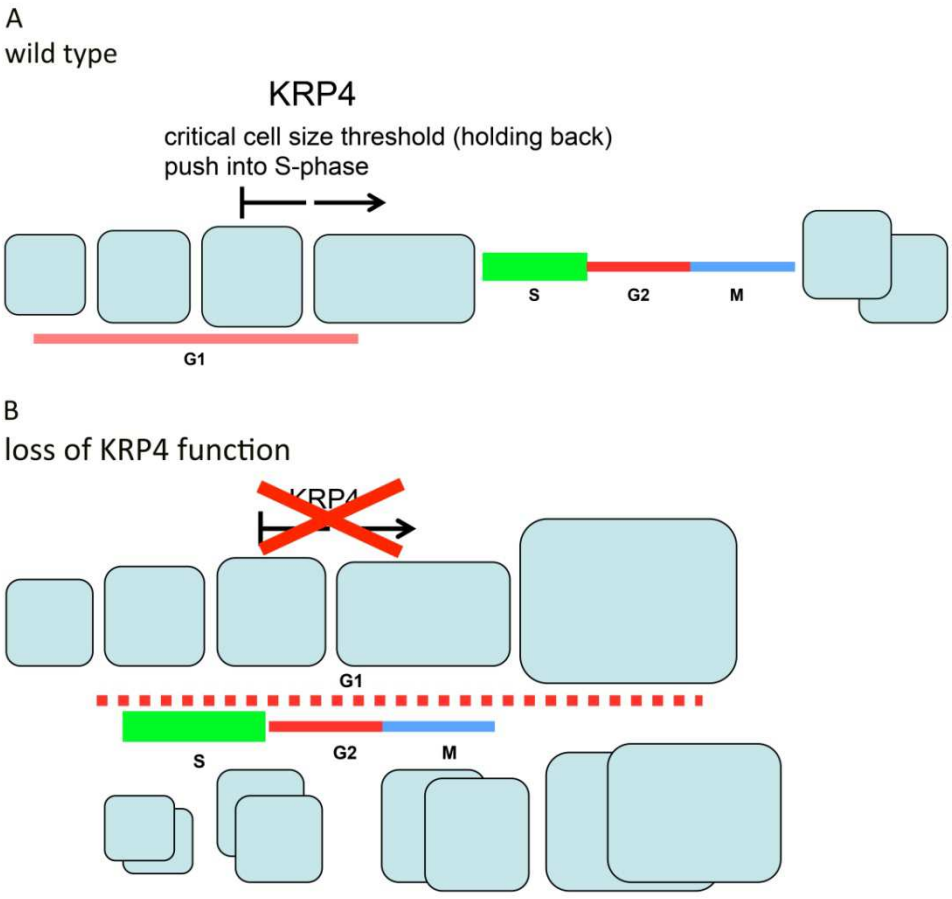

Figure 7.10. Putative dual function of KRP4 promoting and promoting preparation for entry into S-phase.

(A) In the wild type meristem, high KRP4 levels could have a dual function during cell proliferation, where KRP4 inhibits entry into S-phase until a certain minimum cell size threshold is reached but concomitantly promotes entry into S-phase once the certain cell size threshold is reached, this would explain the very narrow cell size distribution pattern observed in the wild type meristem, where cells as soon as they reach a certain cell size appear to be pushed into S-phase. (B) Accordingly, loss of KRP4 function would allow cells to enter S-phase at smaller and larger cell sizes and hence coordination between entry into S-phase and cell size would be decreased and allow for increase in cell size heterogeneity of cells undergoing and not undergoing S-phase.

Chapter 8 - Novel direct candidates of JAG obtained from combined analysis of ChIP-Seq and global transcriptome data

8.1. Introduction

In the previous chapters, I have shown that JAG as a transcriptional growth regulator targets several processes during organ primordia formation: At organ level, JAG mediates the transition from a meristematic to a primordium cell behaviour, it restricts boundary-specifying genes and is involved in organ patterning along the proximal-distal axis. At cellular level, JAG promotes cell growth, growth anisotropy and cell proliferation. To promote organ outgrowth and organ patterning, these processes have to be coordinated in a spatial and temporal context. In this respect, gene ontology (GO) analyses for the 1,634 ChIP-Seq target genes and for the 495 genes that were directly targeted and differentially expressed upon ectopic JAG activation (Chapters 2 and 3) revealed enrichments for hormone-related processes and growth-related processes in the cell wall and at the cell wall - plasmamembrane interface.

Here, I introduce and discuss novel interesting candidate genes that are directly and indirectly regulated by JAG, which I did not have the opportunity to investigate further during this project, but which will provide future leads to answer key questions of plant morphogenesis, for example, how anisotropic growth and differences in local tissue growth rates are regulated by transcriptional growth regulators such as *JAG* and how local tissue growth rates are coordinated within a developing organ by cell-cell communication and non-autonomous intercellular signals.

8.2. JAG directly targets genes involved in cell expansion-related processes

8.2.1. JAG directly targets regulators of cell turgor pressure during cell expansion

During cell expansion, the balance of turgor pressure and cell wall extensibility controls the increase in cell volume (Schopfer, 2006). At the core of these processes are plasma membrane located ATPases that actively translocate protons from the cytosol to the apoplast by hydrolising ATP. Thereby, ATPases generate a gradient in H+ concentration across the plasma membrane, resulting in a pH gradient and a charge gradient which

leads to apoplast acidification of up to 2 pH value units and a negative membrane potential of -120 to -160 mV in the cytosol compared to the apoplast (reviewed by Sze et al., 1999). On the return of protons into the cytoplasm, ions and metabolites such as sucrose and amino acids can be actively transported in and out of the cytoplasm against their concentration gradients and electrochemical gradients via symporters and antiporters.

The proton gradient also generates the force for the uptake of calcium and potassium via channels specific to these cations (reviewed by Sze et al., 1999). In particular, during cell expansion, high turgor pressures are achieved by influx of potassium and calcium cations leading to osmotic uptake of water into the cytosol (Rodriguez-Navarro et al., 2000). The higher the membrane potential, the higher is the driving force for cation uptake into the cytosol and subsequently the generated turgor pressure. At the same time, ion influx into the cytosol causes a decrease in membrane potential and a depolarisation of the membrane, which needs to be counteracted by increased translocation of protons. In this process, plasma membrane-located ATPases are the only means to maintain and to regulate the negative electrochemical potential inside the cytosol compared to the apoplast and therefore, turgor pressure and cell expansion are highly dependent on the activity of plasma membrane ATPases. In addition, these ATPases cause the acidification of the apoplast and hyperpolarisation of the plasma membrane that is associated with cell wall swelling and cell wall relaxation during cell expansion (reviewed by Wolf et al., 2012).

In *Arabidopsis*, a gene family of eleven members encodes *plasma membrane ATPases* (*AHAs*). *AHA1* and *AHA2* have been reported to function as the predominant and most ubiquitous ATPases in *Arabidopsis* (Haruta et al., 2010). In my experiments, I found that JAG directly down-regulated *AHA2* (Figure 8.1.A-B) and directly bound to *AHA1*. Both single mutants were more sensitive to external conditions that require enhanced proton transport in order maintain the electrochemical potential. For example, *aha2* seedlings showed reduced hypocotyl elongation in the presence of high external potassium and high external pH values compared to the wild type (Haruta and Sussman, 2012). Under optimal growth conditions, no differences in growth and development were observed between the *aha2* single mutant and wild type, suggesting that *aha1* and *aha2* act redundantly to maintain proton homeostasis.

Interestingly, *AHA1* transcript levels were not increased in the *aha2* single mutant and the compensation was rather due to increased activity of the remaining ATPases (Haruta et al., 2010; Haruta and Sussman, 2012), providing evidence that post-translational modifications play a major role in regulating ATPase activity (reviewed by Sze et al., 1999; Haruta et al., 2010; Haruta and Sussman, 2012). For example, plasma membrane ATPases contain an autoinhibitory domain at their C-terminus with several phosphorylation and dephosphorylation sites for activation and deactivation by kinases and phosphatases. In response to phosphorylation and dephosphorylation, a 14-3-3 protein associates with the C-terminal region of ATPases and promotes ATPase activity (reviewed by Sze et al. 1999; Haruta and Sussman, 2012). In this context, JAG also directly down-regulated the calcium-responsive serine-threonine kinase *PKS5*/*CIPK11* (Figure 8.1.D) which is a member of the calcium signalling network of *calcineurin B-like* (*CBL*) and *CBL interacting kinases* (*CIPK*) that read out local calcium concentration signatures at the plasma membrane and at the tonoplast (reviewed by Weinl and Kudla, 2009). *PKS5/CIPK11* negatively regulates *AHA2* activity by phosphorylating the binding site of 14-3-3 protein in the C-terminal region of the AHA2 protein. In line with these findings, loss of function *pks5* seedlings are more tolerant to high external pH values compared to wild type because of increased ATPase activity leading to increased proton extrusion (Fuglsang et al., 2007).

Furthermore, a reduction of proton pumps in the *aha1* and *aha2* mutants was compensated by up-regulation of K+ transporters, suggesting that a decrease in membrane potential can be compensated by increasing the density of potassium ion transporters (Fuglsang et al., 2007). In this respect, JAG directly up-regulated the K^+ transporter *AKT2* (Figure 8.1.C), which has been reported to function in potassium uptake in the plasma membrane of leave mesophyll cells and in guard cells (Dennison et al., 2001; Szyroki et al., 2001). However, the potassium transporter AKT2 is not only expressed in mesophyll leaf cells but also in flower stems and sepals, and has been shown to act as a phloem potassium channel. Sucrose is loaded into the sieve element/companion cell complex via proton/sucrose symporters and *ATK2* maintains the K^+ dependent membrane potential in the phloem and prevents membrane depolarisation in response to sucrose loading. By using ^{14}C-labelled CO_2, it was shown that in the *akt2* mutant, the loading of sucrose into the phloem and the subsequent transport to sink tissues such as the flower was impaired. Accordingly, the *akt2* loss of function mutant

produced fewer leaves and fewer and shorter inflorescence stalks as the wild type (Deeken et al., 2000; Deeken et al., 2002). Also connected to the control of potassium transporters, JAG directly up-regulated *CBL9* (FDR 0.05), which interacts with *CIPK23* to promote the activity of the potassium transporter *AKT1*. It has been shown that the *cbl9 cbl1* double mutant is as sensitive to low potassium availability as the *akt1* mutant (Cheong et al., 2007; Xu et al., 2006).

Another gene family targeted by JAG and implicated in Ca^{+2} and proton transport are the *RAPID ALKALINISATION FACTORS-LIKE* genes (*RALFLs*) *RALFL4* and *RALFL21,* which encode small polypeptide signalling molecules (Pearce et al., 2001). In particular, *RALFL4* was up-regulated upon JAG-GR activation and down-regulated in the *jag-2* mutant in the qRT-PCR experiment (Figure 8.1.E, F). The *RALFL* family in Arabidopsis consists of 34 members (Olsen et al., 2002) and it has been shown that they locate to the apoplast once they have been proteolytically processed by subtilases (Escobara et al., 2003; Srivastava et al., 2009). Little is known about the signalling mechanism of RALFL polypeptides, however, Scheer et al. (2005) provided evidence that RALFLs can bind to proteins located in the plasma membrane. Ectopic expression of *AtRALFL1* was found to trigger a fast increase in cytosolic calcium concentration in an aequorin bioluminescence assay (Haruta et al., 2008) and it was suggested to mediate the response of proton ATPases. Furthermore, *AtRALFL23* has been shown to be repressed upon brassinolide treatment and ectopic expression of *ATRALFL23* diminishes the growth promoting effects of brassinosteroids and impairs elongation of the hypocotyls. Plants ectopically expressing *AtRALFL23* showed reduced acidification of the rhizosphere compared to wild-type seedlings when grown on medium supplemented with a pH indicator, suggesting that *AtRALFL23* represses extracellular acidification (Srivastava et al., 2009). In addition, ectopic expression of *AtRALFL23* resulted in overall shorter and bushier plants, suggesting that *AtRALFL23* is a growth inhibitor (Srivastava et al., 2009). These findings supported previous results obtained from exogenous application of tomato RALF polypeptide.

Exogenous application of tomato RALF to tobacco cell suspension culture caused rapid alkalisation of the medium and applied to *Arabidopsis* seedlings it caused growth arrest in the root meristem and elongation zone (Pearce et al., 2001). By contrast, silencing of *NaRALF* expression in tobacco by an inverted repeat construct inhibited the outgrowth of root hairs owing to an increase in apoplastic pH, slowed down apoplastic pH oscillation

and reduced ROS accumulation in the apoplast. The root hair phenotype was in part restored when the plants were grown on low pH medium and reproduced when wild-type plants were grown on medium with high pH (Wu et al., 2007), suggesting a role for *NαRALF* in maintaining apoplast acidification rather than alkalinisation. Most recently, it has been shown that ectopic expression of *RALF1* resulted in reduced cell sizes while silencing of *RALF1* resulted in increased cell sizes in the root. Furthermore, an antagonistic interaction between *RALF1* and the brassinosteroid signalling pathway has been proposed (Bergonci et al., 2014). In all cases, RALFs and RALFLs had strong effects on cell growth by mediating the pH in the apoplast and therefore might play a crucial role in mediating cell wall related growth processes. Also in respect to the processing of RALFLs, JAG directly targeted a subtilase (*At5g59130*) which is strongly expressed in sepals and floral tissue and is predicted to be located in the apoplast according to the BAR eFP browser (http://bar.utoronto.ca/efp/cgi-bin/efpWeb.cgi). *At5g59130* was strongly repressed upon ectopic JAG expression.

In addition to plasma membrane located ATPases, V-ATPases are located in the vacuole membrane and in the endomembrane system. V-ATPases translocate protons from the cytosol to vacuoles and into the inside of the endomembrane vesicles, leading to acidification of these subcellular compartments and regulation of ion and solute fluxes. Furthermore, acidification of endomembrane vesicles influences protein-protein interactions, receptor-ligand binding properties, and catalyse biosynthesis processes. While plasma membrane ATPases are single polypeptides of 100 kD, V-ATPAses are 650 kD protein complexes consisting of multiple subunits and interacting molecules (reviewed by Sze et al., 1999). JAG directly targets several genes encoding subunits of V-ATPases, for example *isoform3 of the subunit VHA-a*, the *16 KDA PROTEOLIPID SUBUNIT 4* (*AVA-P4*), and *DET3* which encodes a *VACUOLAR ATP SYNTHASE SUBUNIT C* (*VHA-C*) that promotes hormone-induced cell elongation in hypocotyls (Schumacher et al., 1999). Furthermore, the *det3-1* loss of function mutant which shows a decrease in V-ATPase activity by 50% was dwarfed and the cell sizes of mesophyll cells in *det3-1* cotyledons and first leaves were reduced to about 50% of the wild type (Fukao and Ferjani, 2011). Interestingly, Ferjani et al. (2013) have recently shown that V-ATPase activity is needed to mediate the increased cell sizes caused by ectopic expression of the cell cycle inhibitor KRP2 (first described by De Veylder et al. (2001) and shown here to be a key JAG target

gene; see Chapters 6 and 7). In the *det3-1* mutant background ectopic expression of the cell cycle inhibitor KRP2 resulted in reduced cell numbers but cell sizes similar to wild type. However, none of the V-ATPase genes mentioned above showed significant differences in gene expression in response to changes in JAG function in the expression array experiment.

Still in respect to VHA-C that functions in the assembly and disassembly of functional V-ATPases (Hong-Hermesdorf et al., 2006), JAG directly down-regulated *WITH NO LYSINE K3* (*WNK3*/*ZIK3*), a member of the serine-threonine kinase family *WITH NO LYSINE K* (*WNK*). While no information is available about the biological function of *WNK3*, *WNK8* has been shown to directly bind and phosphorylate VHA-C in *in vitro* assays (Hong-Hermesdorf et al., 2006). However, WNK3 did not interact with VHA-C in the yeast two-hybrid assay (Hong-Hermesdorf et al., 2006) and its function remains elusive.
While up-take of calcium via antiporter to the endomembrane compartments is mediated by the proton gradients generated by V-ATPases, release of calcium from endomembrane compartments is mediated by calcium channels, which are sensitive to the signalling molecule myoinositol 1,4,5-triphoshpate. Interestingly, JAG directly down-regulates *INOSITOL(1,4,5)P3 5-PHOSPHATASE II*, which dephosphorylates myoinositol 1,4,5-triphoshpate (Figure 8.1.G). Loss of function mutant plants have increased levels of myoinositol 1,4,5-triphoshpate and cytosolic calcium, which for example, leads to premature pollen germination (Wang et al., 2012), hypersensitivity to ABA in seed germination (Gunesekera et al., 2007) and decreased GA signalling (Fleet et al., 2009), suggesting an important role in calcium and hormone regulated developmental processes. In addition, JAG directly targeted the tonoplast located calcium/proton exchanger *CAX3* which has been shown to regulate apoplast acidification and auxin influx by promoting plasma membrane located proton ATPases, suggesting that extracellular and intracellular ion and proton homeostasis are regulated by the coordinated function of proton ATPases and transporters located at the vacuole and in the plasma membrane (Cho et al., 2012). Furthermore, JAG directly targeted a *type IIA (SERCA-type) Ca^{++} ATPase* and indirectly activated *ACA4*, a tonoplast located Ca^{++}-ATPase involved in the accumulation of calcium in the vacuole (Geisler et al., 2000).

In the context of the vacuole, JAG directly down-regulated the vacuole-located *GLYCINE RICH PROTEIN 5* (*GRP5*) (Figure 8.1.H) which has been shown to promote cell elongation in root cells and dark grown hypocotyls. GRP5 over-expressing lines have longer roots, larger leaves and elongated inflorescence stems while loss of function mutants have shorter roots, smaller leaves and reduced stem heights compared to the wild type. However, the biological function of this gene remains to be elucidated. Using a GUS reporter line driving several minimal promoter constructs, Mangeon et al. (2010) mapped the promoter region that is responsible for expression of *GRP5* in leave epidermis, inflorescence stems and reproductive organs to between 164 and 288 bp upstream of the transcriptional start of GRP5. Interestingly, JAG binds to the *GRP5* promoter 140-170 bp (max peak score in all three replicates) upstream of the transcriptional start, suggesting that GRP5 expression in the leaf and inflorescence are under direct transcriptional control by JAG, possibly via the previously described promoter region.

8.2.2. JAG directly targets genes involved in cell wall relaxation and cell wall loosening

Cell wall acidification to pH 4.5-6 activates members of the expansin family, which play a major role in cell wall relaxation and subsequent wall extension. It has been suggested that expansins weaken non-covalent hydrogen bonds between cellulose microfibrils and the hemicellulose matrix and allow matrix polymers and cellulose microfibrils to slide apart. This dissociation of wall polymers generates space and increases the surface area within the wall, paving the way for cell wall degrading enzymes such as glycosylases, galactosidases, pectin lyases, and galacturonases. Expansins mediate a fast wall relaxation response that does not weaken the mechanical strength of the cell wall. In early experiments, exogenous expansin application to tomato shoot meristems caused ectopic organ primordia formation (Fleming et al., 1997). Loss of function and ectopic expression of expansins have been shown to have very immediate effects on cell size and organ size, suggesting that expansins may be a good targets to exert growth regulatory functions (Cho and Cosgrove, 2000). In petunia, ectopic expression of the petunia *EXPANSIN1* (*PhEXPA1*) gene caused an increase in leaf and petal area due to increase in cell sizes and premature branching from axillary meristems (Zenoni et al., 2011). In my experiments, JAG regulated several members of the *αEXPANSIN* protein family. For example *EXPANSIN*

A15 is a direct target of JAG while *EXPANSIN A3*, *A4* and *A5* are indirectly down-regulated upon ectopic JAG activation and *EXPANSIN A9* is indirectly up-regulated upon JAG activation.

In addition to expansins that target the non-covalent links between hemicelluloses and cellulose microfibrils, modifications of pectins play a crucial role in cell wall hydration. Pectin homogalacturonan polymers are synthesised in the endomembrane system and excreted to the cell wall as highly methylated compounds. Pectin demethylesterases (PMEs) remove methyl groups from the homogalacturonan polymers, leave a free carboxyl group and release methanol and a proton (Wolf et al., 2009). Subsequently, the removal of the methyl group can lead to association of water molecules that facilitates hydration of the cell wall, cell wall loosening and degradation of pectins. *Pectin methylesterases* are inhibited by *pectin* methylesterase inhibitors (*PMI*s). Using monoclonal antibodies that specifically detect demethylesterified pectins, Peaucelle et al. (2008) showed that demethylesterified pectins were predominantly observed in incipient and early flower primordia in contrast to the central dome of the meristem where predominantly methylesterified pectins were found. Ectopic expression of a *pectin methylesterase inhibitor* (*PMI*) resulted in a decrease of demethylesterification at the site of incipient floral primordia in the inflorescence meristem and at incipient organ primordia in floral meristems. In addition, primoridia formation was inhibited, which resulted in a pin-like inflorescence meristem in the PMI over-expressor line (Peaucelle et al., 2008). In addition, site specific exogenous application of pectin demethylesterases caused bulging and ectopic development of floral primordia at the site of application, suggesting that demethylesterification is not only essential, but also sufficient for *de novo* primordia formation and outgrowth, and similar results were obtained when over-expressing *PME5* (Peaucelle et al., 2008). Using atomic force microscopy Peaucelle et al. (2011) confirmed that the degree of pectin demethylesterification correlated with the increased elastic response of cell walls observed at the sites of incipient organ primordia and in emerging primordia compared to the central meristem dome. Furthermore, meristem cells of the *PME5* over-expressor showed the same elasticity profile as wild type primordia cells and in the *PMEI* over-expressor primordia cells had the same elasticity profile as wild type meristem cells (Peaucelle et al., 2011), suggesting that cell wall elasticity mediated by pectin demethylesterification marks the transition from meristem

to primordia cell behaviour. JAG weakly bound to and activated pectin methylesterase (At5g62360) and indirectly activated four members of the *pectin methylesterase inhibitor family* (*PMI*). In addition, JAG directly bound to *QUASIMODO* (Figure 8.2.A) which is a pectin methyltransferase located in the Golgi Apparatus, and *pectin methylesterase PCRA* was indirectly repressed by JAG.

Both pectin methylesterases and expansins have been suggested to change the physical and chemical properties of cell wall polymers and render them more accessible for cell wall degrading enzymes such as polygalacturonases and members of the *XYLOGLUCAN ENDOTRANSGLUCOSYLASE /HYDROLASE (XTH)* protein family. *XTHs* can cleave and re-ligate glycosidic bonds in the *backbone* of xyloglucan hemicelluloses. Owing to their function they are involved in cell wall loosening, integration of new cell wall material and cell wall stiffening. It has been shown that the effect of *XTHs* depends on the length of the xyloglucan chains that are ligated into the cell wall matrix. While incorporation of long xyloglucan chains had a growth inhibitory effect, incorporation of small oligosaccharides promoted cell expansion in pea stems (Takeda et al., 2002). JAG directly repressed *XYLOGLUCAN ENDOTRANSGLUCOSYLASE/HYDROLASE 28 (XTH28* (Figure 8.2.B), which has been reported to have a specific function in the elongation of cells in the stamen filament. In the *xth28* loss of function mutant, filaments failed to elongate to the length of the stigma impairing self-fertilisation (Kurasawa et al., 2009). Furthermore, *XTH6*, *XTH7* and *XTH9* were identified as direct targets by ChIP-Seq but showed only weak peaks. In addition, two xylosidases were among the direct targets of JAG, which showed only weak peaks in the ChIP-Seq and no differential expression in the array experiment.

However, several *xylosidases*, *glucosidases* and *galactosidases* were found to be indirectly up-regulated, suggesting that these genes encoding enzymes that can cleave hemicelluloses are promoted by JAG. Furthermore, three *pectin lyase-like* genes, which are predicted to have polygalacturonase activity, were directly and one indirectly down-regulated by JAG, for example the expression of the direct target *pectin lyase* (*At5g63180*) in response to gain and loss of JAG function was confirmed by qRT-PCR (Figure 8.2.C-D).

8.2.3. JAG directly targets genes involved in the plant redox system

In respect to the redox state in the apoplast, JAG directly targeted the promoter region of gene *At5g21100* (Figure 8.2.E), which encodes one of the three putative apoplast-located ascorbate oxidases identified in the *Arabidopsis* genome (Yamamoto et al., 2005). *Ascorbate oxidase* (*At5g21100*) showed a strong decrease in expression levels upon ectopic JAG activation in the expression array experiment and is highly expressed in sepals and petals according to the BAR eFP browser (http://bar.utoronto.ca/efp/cgi-bin/efpWeb.cgi). The single loss of function mutant showed reduced stem height and had increased tolerance to salt owing to reduced ascorbate oxidase activity that resulted in decreased hydrogen peroxide accumulation compared to wild type (Yamamoto et al., 2005). Ascorbate functions as a soluble antioxidant and is the major component of the redox buffering capacity in the apoplast. Therefore, the effect of reactive oxygen species on downstream signalling cascades and cell wall cross-linking processes is dependent on the pool of reduced ascorbate in the apoplast (Smirnoff et al., 2000). Ascorbate oxidases oxidise ascorbate to mono-dehydroascorbate and reduce the antioxidant pool in the apoplast. In this respect, it was shown that ectopic expression of ascorbate oxidase in tobacco seedlings drastically decreased the pool of reduced ascorbate in the apoplast and it was suggested that reducing the pool of ascorbate can have similar effects on the redox state of the apoplast as the generation and release of reactive oxygen species (Pignocchi et al., 2003). Pignocchi et al. (2003) showed that auxin promoted expression of ascorbate oxidase, which led to a decrease in the redox buffering capacity of the apoplast. On the other hand, Pignocchi et al. (2006) showed that ectopic expression of ascorbate oxidase in tobacco seedlings caused a decreased response to auxin treatment and an increased response to gibberellic acid treatment, suggesting that the effect of auxin on growth is dependent on a pool of reduced ascorbate. Furthermore, it has been shown that an increase in ascorbate oxidase expression repressed the expression of a calcium channel (Pignocchi et al., 2006). Moreover, data obtained from synchronised cell suspension culture suggested that ascorbate and its oxidised product mono-dehydroascorbate may function in the control of cell cycle progression (Kato and Esaka, 1999). Together, these observations suggest that *ascorbate oxidase* (*At5g21100*) could be a key target to modulating cell growth-related processes in the apoplast.

In addition, JAG directly targeted *SKU5* and several members of the *SKU5-SIMILAR* (*SKS*) family (*SKS4*, *At4g22010*; *SKS5*, *At1g76160*, (Figure 8.2.F); *SKS17*, *At5g66920*) and directly activated *SKS18* (*At1g75790*), which are multicopper oxidase-like proteins and are related to ascorbate oxidases and ferroxidases (Sedbrook et al., 2002; Jacobs and Roe, 2005). *SKU5* is expressed in expanding young tissue of roots, leaves and flowers. Biochemical assays revealed that the *SKU5* protein is glycosylated, anchored to the plasma membrane and associated with the cell wall. Using a *SKU5-GFP* fusion reporter line, it was further confirmed that SKU5 associates with the plasma membrane and surrounds the cell outlines (Sedbrook et al., 2002). Interestingly, in the elongation zone of the root, brighter signals were observed along the longitudinal axis and at three-cell junctions (Sedbrook et al., 2002), suggesting that *SKU5* could play a role in longitudinal cell expansion. However, no difference in cell length and width was observed between root cells of the *sku5* mutant and the wild type. In the *sku* loss of function mutant, the roots and hypocotyls show axial rotation of cell files and the roots skew and coil to the left when grown on the surface in tilted agar plates or when touching the bottom of a plate but not when growing in media, suggesting that roots skew most likely in response to touch. Another member of the *SKS* family, *SKS6* has been shown to play a role in the formation of leaf veination (Jacobs and Roe, 2005). However, the biological functions of *SKU5* and members of the *SKS* family remain to be elucidated.

Furthermore, JAG directly targets two members of the *microRNA 398* family, *miR398B* and *miR398C*, which target the mRNA transcripts of two *copper/zinc dismutases* (*SOD*), the cytosolic *CDS1* and the chloroplast located *CDS2*, which can detoxify superoxide radicals to hydrogen peroxide and water (Sunkar et al., 2006), and a chaperone protein required for copper delivery (*CCS1*) (Bouchè, 2010). Interestingly, *miR398* is highly expressed in roots, stem and cauline leaves, moderately expressed in adult rosette leaves but not detectable in floral tissue with the exception of the anthers (Sunkar et al., 2006), suggesting that there are tissue specific differences in *miR398* expression that might reflect developmental processes. Consequently, mRNA transcripts of the dismutases *CDS1* and *CDS2* were most abundant in floral tissue (Sunkar et al., 2006). From this expression pattern it can be inferred that JAG rather down-regulates than up-regulates *miR398* and therefore may promote detoxification of superoxide radicals and attenuate the effects of reactive oxygen species (ROS). Furthermore, it has been shown that *miR398* was

transcriptionally repressed in response to environmental oxidative stress while the abundance of *CDS1* and *CDS2* mRNA transcripts increased specifically because of repressed post-transcriptional silencing rather than induction of *de novo* transcription of these genes (Sunkar et al., 2006). Furthermore, it was shown that plants harbouring a *CDS2* with a mutated *miR398* recognition site and therefore increased CDS2 mRNA levels showed lower rates of chlorophyll degradation and accumulated lower levels of anthocyanin than the wild type when exposed to high light stress (Sunkar et al., 2006). This suggested that *miR398* negatively regulates the superoxide scavenging capacity by targeting the copper/zinc dismutases *CDS1* and *CDS2*.

8.2.4. JAG targets genes involved in biosynthesis and deposition of cell wall material

After cell wall extension, new material needs to be synthesised and deposited at the extended wall. While the precursors of matrix polymers such as hemicelluloses and pectins are synthesised in the Golgi apparatus and transported to the cell wall in vesicles, cellulose synthase complexes migrate in the plasma membrane and cellulose microfibrils are synthesised at the plasma membrane - cell wall interface. It has been suggested that the cellulose synthase complex is guided by cortical microtubule arrangements, which orchestrate location of insertion, orientation and density of cellulose microfibrils (reviewed by Cosgrove, 2005; Wolf et al., 2012).

CELLULOSE SYNTHASE 3 (*CESA3*) and *CESA6* are direct targets of JAG but show no differences in expression, while *CESA5* is indirectly down-regulated. *CESA3* and *CESA6* have been reported to form cellulose synthase complexes with *CESA1* to synthesis the primary cell wall. The *cesa3* loss of function mutant showed pollen grain deformations while the *cesa6* mutant showed mild defects in cell elongation (Persson et al., 2007).

In addition, JAG directly and indirectly repressed ten out of thirty members of the *CELLULOSE SYNTHASE LIKE* family (*CSLs*) (Richmond and Somerville, 2000), while none of them was activated upon ectopic JAG-GR activation (Figure 8.3.A-D). *CSLs* function as glucomannan synthases and as xyloglucan synthases (Liepman et al., 2007; Goubet et al., 2009). In particular, members of the *CSLA* group are involved in the biosynthesis of the hemicellulose components mannan and glucomannan, which are found in primary cell walls but are also a major component in secondary cell walls to reinforce stems. Interestingly, *CSLA* genes are highly abundant in floral organs, for example *CSLA1* and

CSLA10 are most abundant in sepals and petals (Liepman et al., 2007). Interestingly, these two genes were also found to be differentially expressed in response to changes in JAG function (Figure 8.3.B-D). In addition, it was suggested that glucomannans might function as developmental signals, for example, the *clsa7* mutant is embryo-lethal but can be rescued by ectopic expression of *CSLA9* (Goubet et al., 2009).

In the context of cell wall polymer modifications, three members of the *TRICHOME BIREFRINGENCE-LIKE* protein family (*TBL*) were directly target by JAG: *TBL25*, *TBL37*, and *TBL42*. *TBL37* was directly down-regulated by JAG (Figure 8.3.E-F) while *TBL25 showed* no significant differences in expression and *TBL42* was not present on the expression array chip. The TBL family consists of 46 members in *Arabidopsis* and is named after the first identified mutant *tbr* that showed defects in the crystallinity of the cellulose in trichomes and linked the family to cellulose biosynthesis processes (Bischoff et al., 2010). In addition, it has been shown that TBL proteins harbour a putative O-acetyl transferase domain and are involved in O-acetylation of specific xyloglucan and pectin cell wall polymers in the Golgi apparatus (Gille et al., 2011; reviewed by Gille and Pauly, 2012; Bischoff et al., 2010a). For example, in the *tbl3* loss of function mutant the amount of pectin acetyl esterifcation was decreased while pectin methylesterifaction was increased, suggesting that *TBL3* may function in maintaining the acetyl esterification in pectins and hemicelluloses (Bischoff et al., 2010a). In enzymatic assays, it has been shown that the higher the degree of O-acetylation in cell wall polymers, the less accessible are they for enzymatic degradation most likely because of conformational changes in the non-covalent interactions of the cell wall polymers. The O-acetylation of cell wall polymers mediated by TBL proteins is antagonised by acteylesterases that remove acetyl groups from xyloglucan and pectins (reviewed by Gille and Pauly, 2012). Interestingly, JAG directly activated *pectinacetylesterase At3g05910* while pectinacetylesterase *At2g46930* was indirectly activated.

8.2.5. Overview: what is the functional relevance of JAG targeting genes involved in cell expansion?

Here, I introduced target genes of JAG that are involved in cell expansion and growth-related cell wall processes. For example, JAG directly and indirectly targeted several genes that have been reported to play a role in turgor-driven cell expansion and growth-related cell wall modifications. These candidates provide further support for the results obtained by the quantitative 3D live imaging approach which revealed that JAG mediates the transition from meristem to primordium cell behaviour by promoting both an increase in cell proliferation rates and cell growth rates in early organ primordia (Schiessl et al., 2012). Using quantitative 3D analysis of cell geometry, we observed that proliferating cells in early sepal primordia have a narrow size range between 100 - 350 µm³ (Schiessl et al., 2012; Chapters 7 and 8). In contrast, it has been shown that cells that have exited proliferation expand in size up to 100- to 1000-fold and more, predominantly by vacuolar-driven cell expansion (Marshall et al., 2012). Images obtained from electron transmission electron microscopy showed that meristem cells and early primordia cells do not have large central vacuoles neither in the *jag* loss of function mutant nor in the wild type (Schiessl et al., 2012), further confirming that during cell proliferation phase, cytoplasmic cell growth is the predominant process by which cells increase in size. Furthermore, combining quantitative 3D analysis of cell geometry with an S-phase marker (see Chapter 7) revealed that JAG has an effect on the size at which cells enter S-phase and therefore modulates cell size homoestasis during cell proliferation phase in developing organs.

Since JAG promotes growth and cell proliferation and regulates the coordination of these two processes, it can be speculated that JAG promotes growth in a very tightly controlled way that is advantageous for increased cell proliferation rates and overall tissue growth rates, besides regulating cell proliferation at the entry into S-phase (see Chapter 7). Conversely, JAG may suppress processes that result in massive cell expansion and cell differentiation.

In this respect, it could be speculated that JAG promotes cell expansion but concomitantly needs to tightly control processes that lead to high turgor pressure on the one hand and extreme cell wall extensibility, on the other hand. This hypothesis is supported by the fact that JAG down-regulates the plasmamembrane ATPase *AHA2* and directly repressed *INOSITOL (1,4,5)P3 5-PHOSPHATASE II* which leads to enhanced levels

of the signalling molecule myoinositol 1,4,5-triphosphate and possibly to enhanced calcium signalling. Furthermore, JAG attenuates the effects of reactive oxygen species by increasing the antioxidant pool in the apoplast and by promoting the ROS scavenging mechanisms. For example, JAG directly repressed the apoplastic ascorbate oxidase that promotes growth and is upregulated upon exogenous auxin treatment (Pignocchi et al., 2003). In addition, JAG was found to directly and indirectly repress several members of the expansins, xyloglucan endotransglucosylases, and pectin lyases. By contrast, JAG was found to directly and indirectly activate pectin methylesterase inhibitors that promote cell wall stiffening.

In addition, quantitative 3D live imaging revealed that JAG promotes a shift to anisotropic growth. In this context, it can be speculated that JAG not only tightly controls expansion rates but also promotes localised cell wall extensibility to facilitate oriented growth. In this context, *JAG* directly and indirectly represses ten out of thirty *CSLs* genes, which are involved in the biosynthesis of mannan and glucomannan which have been shown to reinforce cell walls and thus counteract flexible and extensible cell walls. Similarly, JAG directly repressed *TBL37*, which has been suggested to be involved in O-acetylation of xyloglucans, a process that attenuates enzymatic degradation of cell wall polymers and also results in reinforced cell walls. By contrast, TBL antagonising acteylesterases were directly and indirectly up-regulated by JAG.

In summary, these candidates provide leads for future work on how JAG mediates the transition from isotropic meristem-like cell expansion to anisotropic primordium-like cell expansion with increased cell expansion rates. However, there are several challenges in respect to studying cell wall-related proteins in more detail. Firstly, cell wall-related proteins belong to large families, which appear to have redundant functions. Therefore, only few single loss of function mutants with phenotypes have been identified for genes belonging to these families, making reverse genetics approaches difficult. Secondly, cell-wall related genes are ubiquitously expressed in all plant cells therefore specific spatial and temporal expression differences may be diluted and are hence difficult to detect using quantitative qRT-PCR and or RNA *in situ* hybridisation. Thirdly, in the case of cell wall-related proteins, the transcriptome analysis will only be of limited use, because cell wall-related proteins undergo complex post-translational modifications and it will therefore be difficult to assess the activity of individual cell wall related proteins *in vivo*.

For example, cell wall-related proteins such as the pectinmethylesterases and pectinmethylesterase inhibitors are produced in the Golgi Apparatus, transported by vesicles to the plasma membrane – cell wall interface and excreted into the cell wall during this process they undergo several post-translational modifications. In addition, it has been shown that the activity of many cell-wall related proteins is dependent on pH-value and substrate affinities.

One initial approach to the role of cell wall modifying genes downstream of JAG would be to generate fluorescent marker or GUS reporter lines. In particular, fluorescent reporter lines would be useful to follow the subcellular localisation of cell wall proteins by live-imaging comparing meristems and early organ primordia in wild-type and *jag* loss of function mutants. Furthermore, it would also be interesting to find out whether these genes play particular roles in proliferating cells compared to expanding and differentiating cells. P*ectin lyase At5g09730*, the *cellulose synthase-like CLS01A*, *TBL37*, and the *SKS5* gene that showed very high and consistent enrichments in the ChIP-Seq experiment and showed differential expression in the array and in the qRT-PCR experiments would be promising candidates for preliminary reporter line experiments. Furthermore, it would be interesting to investigate whether the single loss or gain of function mutants have effects in meristem organisation and early organogenesis using quantitative 3D analysis of cell geometry. In this context, Peaucelle et al. (2008) found that an increase in cell wall elasticity occurred first in subepidermal layers in incipient organ primordia, only later when the bulge and crease had formed, elasticity increased in the epidermal layer. This observation was consistent with their *PME*5 expression data, suggesting that subepidermal layers contribute to final organ size and shape. For the quantitative 3D imaging approach used in this project, I focussed on cells in the epidermal layer. In future projects with a focus on cell growth, quantitative 3D analysis of cell geometry should include subepidermal layers. In order to further investigate the effects of JAG on cell wall acidification and calcium signalling, apoplast pH-sensitive biosensor marker lines as described by Gjetting et al. (2012), calcium imaging techniques and ROS quantification techniques could be used. Furthermore, in order to investigate the effects of candidate genes on the mechanical properties of the cell wall, atomic force microscopy as described by Peaucelle et al. (2008) could be used.

8.3. JAG directly targets genes involved in hormonal pathways

8.3.1. Introduction

The GO terms “hormone synthesis” and “hormone responses” were also found to be enriched in the combined ChIP-Seq and expression array analysis (Chapters 2 and 3), suggesting that one of the key functions of JAG is to orchestrate hormone-mediated cell communication that is required for both tissue patterning and tissue growth. Because morphogenesis requires the coordinated behaviour of all cells within a growing organ but gene regulatory networks act at cellular level, biochemical and biomechanical signalling pathways are needed for cell-cell communication within tissues and between tissues of an organ. Therefore, the interactions between developmental regulators and the plant hormones, predominantly cytokinin, auxin, gibberellins, and brassinosteroids, but also crosstalk between the plant hormone pathways, play a major role during floral organogenesis in coordinating stem cell maintenance, organ initiation, and patterning and outgrowth of organs (reviewed by Veit, 2009; Besnard et al., 2011; Depuydt and Hardtke, 2011).

In line with the crosstalk of these four plant hormones and their close interaction with the gene regulatory network directing morphogenesis, JAG directly and indirectly targeted genes involved in the biosynthesis, conversion, degradation, perception and signal transduction of cytokinins, auxin and gibberellins, of which the most promising candidates are described and discussed in more detail below. These candidates provide evidence that JAG not only promotes growth at a cellular level but also regulates coordination of growth within tissues and thus links organ growth with organ patterning and therefore plays an integrative role in the gene regulatory network of floral organ morphogenesis.

8.3.2. JAG directly targets genes involved in the biosynthesis and degradation of cytokinins

During plant development, cytokinins promote proliferation of undifferentiated cells in the central zone of the shoot apical meristem and sustain the duration of cell proliferation in early organ primordia, for example by promoting the activity of the D-type cylcin *CYCD3;1* (Holst et al., 2011; Dewitte et al., 2007). JAG directly targeted several members of the *LONELY GUY* (*LOG*) family, which catalyse the last step in the biosynthesis of bio-active cytokinin. There are nine members of the *LOG* family in *Arabidopsis,* which have been shown to have overlapping functions. Therefore, functional analysis has mainly been done in rice which has one *LOG* gene (Kuroha et al., 2009; Tokunaga et al., 2012). In rice, *LOG* is expressed in the shoot apical meristems but absent from incipient leaf primordia. The strongest expression has been observed in subepidermal layers of the distal tip of floral meristems. In rice, loss of LOG function leads to early termination of the inflorescence meristem and to flowers with reduced organ number, caused by a decrease of cell proliferation in the meristems (Kurakawa et al., 2007).

In *Arabidopsis*, *LOG4* has been shown to be expressed in the epidermal layer of the meristem dome and has been suggested to function in the proximal/distal patterning of the meristem where it acts in the *WUS – CLV* pathway to locate the *WUS* domain (Chickarmane et al., 2012). Several members of the *LOG* family are expressed in inflorescences. While *LOG1* is expressed in early floral buds, *LOG3* is expressed in the developing style, *LOG5* and *LOG8* are broadly expressed in young floral buds and in pedicels and sepals of mature flowers. *LOG1*, *LOG5* and *LOG8* are also expressed in the pro-vascular and vascular tissue of leaves and in the stem. Over-expression of *LOG* genes resulted in increased cell proliferation and meristem activity in the leaf vascular tissue (Kuroha et al., 2009). I found that JAG directly binds to *LOG1*, *LOG3*, *LOG6* and *LOG8* (Figure 8.4.A, C). The direct targets *LOG3* and *LOG8* did not respond to ectopic *JAG-GR* activation in the expression array and *LOG6* was not present on the ATH1 array. Using qRT-PCR, I confirmed that *LOG1* and *LOG5* are repressed upon ectopic JAG-GR activation and both are ectopically expressed in the in the *jag-1* mutant (Figure 8.4.B-C).

Another link to cytokinin was that JAG directly activated *cytokinin oxidase/dehydrogenase* (*CKX6*) (Werner et al., 2003), which is involved in cytokinin degradation. Ectopic expression of the *CKX3* gene under the organ primordium-specific

ANT promoter (*ANT:CKX3*) resulted in significantly smaller lateral organs with severely reduced numbers of cells owing to premature cell cycle exit (Holst et al., 2011). This suggested that cytokinins have a crucial role in sustaining the duration of cell proliferation during early organogenesis. Interestingly, ectopic degradation of cytokinins in floral organ primordia had an effect on the number of floral buds initiated at the flanks of the inflorescence meristem, suggesting that ectopic degradation of cytokinins in the primordia has a non-cell autonomous effect on meristem organisation (Holst et al., 2011).

In addition, *CKX5* and the SOB five-like gene *SOFL1* are direct targets of JAG but were not represented on the ATH1 array. *SOFL1* and *SOFL2* have been shown to promote catalysis of biosynthetic intermediates of bio-active cytokinin and are highly expressed in vascular tissue of developing leaves and in flowers (Zhang et al., 2009). Together, these expression patterns suggest that JAG functions to keep cytokinin levels low. In particular in the context of the *LONELY GUY* family, it would be interesting to investigate whether ectopic JAG expression results in premature termination of the inflorescence meristem by assessing the number of floral organs produced in the milder and stronger *AP1>JAG* lines and in repeatedly with DEX treated *35S:JAG-GR* plants. On the other hand, it would be interesting to test whether ectopic cytokinin activity in the *jag loss* of mutant has a non-cell autonomous effect on meristem organisation. This is of particular interest in respect to my findings that meristem cell sizes are smaller in the *jag* loss of function mutant compared with wild type meristem cells even though *JAG* is not expressed in the meristem (Chapter 7)

8.3.3. JAG directly targets genes involved in biosynthesis, localisation and signalling of auxin

Auxin plays a crucial role in organ initiation and promotes organ outgrowth and organ patterning during organogenesis. In particular, establishment of polarised, oriented tissue growth and organ patterning processes depend on local concentration gradients of auxin, which require localised auxin distribution. In the acidic apoplast, auxin is present in its protonated form IAAH and can passively pass the plasma membrane and enter the cytosol. In addition, auxin is actively transported by influx carriers such as members of the *AUX1/LAX* family. In the cytoplasm with a neutral pH-value, IAAH deprotonates to polar IAA^-, which cannot passively exit the cytoplasm via the plasmamembrane. Therefore,

transport of cytoplasmic auxin is dependent on efflux carriers of the PIN protein family, which are the main components of polar auxin transport. In particular, in the shoot apical meristem polarised PIN1 localisation is required to generate auxin maxima that position the incipient primordia (Benkova et al., 2003; Reinhardt et al., 2003; reviewed by Besnard et al., 2011; Ljung, 2013).

In this context, JAG directly repressed the protein-serine/threonine kinase *PINOID* (*PID*), which functions in the dynamic subcellular localisation of PIN auxin efflux carriers (Figure 8.5.A-D). For dynamic polarised subcellular PIN localisation, PIN proteins continuously cycle between the plasmamembrane and endosomal membrane compartments via endosomal vesicles along actin filaments (Geldner et al., 2001). In this context, PID phosphorylates PIN proteins and promotes PIN sorting to a transport pathway that promotes PIN localisation at the apical side of cells (Michniewicz et al., 2007; Kleine-Vehn et al., 2009). Furthermore, PID interacts with the calcium-binding calmodulin protein TOUCH3 (TCH3) that has been described to respond to mechanical stimuli. *PID* and *TCH3* are both responsive to auxin and have overlapping expression patterns in floral buds. In vitro binding assays showed that the interaction between PID and TCH3 is calcium-dependent. Auxin causes high levels of free calcium in the cytosol and calcium has been shown to negatively regulate PID activity *in vivo*. For example, phopshorylation activity of PID was enhanced in the presence of calmodulin and calcium influx inhibtors, suggesting that TCH3 fine-tunes the auxin response by repressing PID activity in a calcium-dependent manner (Kleine-Vehn et al., 2009). In this context, it has been suggested that auxin and the signals derived from mechanical forces in the cell wall during organ growth could be coordinated via PID and its interaction with the mechanosensitive TCH3 protein (Besnard et al., 2011). Interestingly, the plasmamembrane located SKU5 protein has been described to be touch-sensitive and may be involved in oriented growth. In this context, it would be interesting to investigate any functional links between these genes.

In the inflorescence meristem below the tip of the dome, PIN1 is localised apically in the epidermal cells in the wild type, while in the *pid* mutant PIN1 is located to the basal plasma membrane (Friml et al., 2004). *PID* is most abundantly expressed in flowers, suggesting that PID-mediated PIN localisation plays a major role in floral organ development. PID is expressed in defined groups of cells in the periphery of the

inflorescence meristem that mark the incipient floral primordia. In stage 3 flowers and in stage 5 flowers *PID* is expressed at the adaxial flanks of the floral meristem and transiently expressed in developing floral organ primordia. Furthermore, *PID* is expressed in the vasculature of the flower stalk and the pedicels, and in the vasculature of the style (Christensen et al., 2000; Benjamins et al., 2001). The *pid* loss of function mutant has a pin-like inflorescence, only a few aberrant flowers develop with reduced number of sepals, no stamen and a trumpet shaped pistil, but increased number of petals that are enlarged (Christensen et al., 2000; Figure 8.5.C).

Loss of function *pid* mutant seedlings frequently have three cotelydons, while the *pin1 pid* double mutant seedlings fail to produce cotyledons and have a radial symmetric appearance. In the *pid pin* mutant the boundary specifying genes *CUC1 and CUC2,* and the meristem maintenance gene *STM* are ectopically expressed preventing organ primordia formation. Loss of either *STM* or *CUC1* and *CUC2* in the *pin1 pid* double mutant restored outgrowth of the two cotyledons, suggesting that *PIN1* and *PID* generate an auxin maxima that restricts *CUC1, CUC2* and *STM* to the organ boundaries (Furutani et al., 2004). Together, the ChIP-Seq, expression array and qRT-PCR results showed that *PID* is down-regulated upon ectopic JAG expression (Chapters 2 and 3). The *pid jag-2* double loss of function mutant in L-*er* background showed additive effects with *jag*-like petals in an otherwise *pid*-like inflorescence (Figure 8.5.C). However, the numbers of petals appeared to be reduced and the petals appeared to be less serrated in the *pid jag-2* double mutant (reduction in petal number and changes in petal shape and size have not been quantified yet).

Regarding the localisation of PIN efflux carrier proteins in petals, Sauret et al., (2013) showed that in early petal primordia the *DR5* marker is expressed in the distal tip and extends to a broader distal domain, where it is maintained over time-course of petal development, to only narrow down and disappear when petals reach maturity. Correspondingly, the auxin efflux carrier *PIN1* localises to the distal side of epidermal cells along the midline of the proximal/distal axis. However, fairly early in petal primordia development, *PIN1* proteins started to point divergently towards the distal petal margins. At later stages in petal development *PIN1* shows strong expression near the petal margins, with no particular polar localisation, and is strongly expressed in the pro-vascular tissue. Towards petal maturity, *PIN1* expression faded and *PIN3* expression

became stronger in the epidermis of the distal margin, with *PIN3* molecules pointing away from the margins. By contrast, in the *jag* mutant petal the *DR5* marker could not be detected in early primordia and at later stages *DR5-GFP* was only detected in discontinuous patches along the distal margin. In addition, the *PIN1-GFP* and *PIN3-GFP* signals were both reduced in the *jag* mutant at all developmental stages and showed a narrow localisation pattern in the distal tip. Consistent with the *PIN3-GFP* results, my expression array analysis showed that *PIN3*, but not *PIN1*, showed significantly lower expression levels in the *jag-1* mutant compared with wild type, suggesting that *PIN3* is indirectly transcriptionally activated by JAG.

In contrast to the *jag* mutant, in the *AP1>JAG* line with ectopic *JAG* expression the DR5 marker was extended downwards along the lateral margins of the petals almost to the transition to the petiole (Sauret et al., 2013). Based on this observation combined with the PIN localisation and DR5:GUS activity in the *jag* mutant, it can be hypothesised that JAG is required to repress *PID* expression in order to allow PIN orientation divergent from the strict apical orientation promoted by *PID*. It would be interesting to investigate whether there are differences in the orientation of *PIN1* proteins in the *jag-1* mutant compared to wild type, however PIN1-GFP and PIN3-GFP proteins were only weakly expressed in *jag-1* and could therefore not be detected at this early stages of development in the imaging experiment of Sauret et al. (2013). It could also be hypothesised that ectopic expression of *PID* prevents the PIN proteins from basal orientation in the inner provascular and vascular tissue and therefore causes defects in vascular tissue formation, as observed in the *jag* loss of function mutant sepals and petals, where the vasculature is often reduced to the midvein and vascular strands fail to form loops (Dinneny et al., 2004; Ohno et al., 2004; Chapter 6). However, apart from an increase in secondary inflorescences, no particular flower phenotype has been described for the *35S:PID* yet (Benjamins et al., 2001; Christensen et al., 2000).

It has been previously shown that *PTL* influences the dynamics of auxin distribution in the incipient petal primordia with the *DR5* marker being disrupted in the petal founder cells of the *ptl* mutant. In the *pin ptl* and *pid ptl* double mutants the number of petals is reduced compared to the single auxin efflux carrier mutants, suggesting that the increase in petal number in the efflux carrier loss of function mutants is dependent on *PTL* function. *PTL* also had an effect on *PIN1* and the influx carrier *AUX1*. However, the effect

of ectopic expression of *PTL* on auxin dynamics and the dependency of *PTL* on *PID* function has not been investigated yet. Here, it could be hypothesised that the reduction in the number of petals I have observed in the *pid jag2* double mutant could be the consequence of changed auxin dynamics owing to ectopic expression of *PTL* in the *jag* loss of function mutant (Chapter 5). In a first step to test this hypothesis, *PIN1* and *PID* expression, and in particular *PIN1* localisation would have to be investigated during petal initiation in stage 3 to stage 5 buds in the context of ectopic *PTL* expression and compared to the localisation in the *jag* loss of function and gain of function mutant. In addition, this approach would also further elucidate whether ectopic *PTL* expression in the petal margins is the cause for disrupted auxin dynamics in later stages of petal development as proposed by Sauret et al., (2013).

In addition to the connections to auxin transport discussed above, JAG appears to regulate auxin metabolism and responses. For example, JAG directly up-regulated *CYTOCHROME P450 79B3* (*CYP79B3)* which catalyses the conversion of tryptophan to indole-3-acetaldoxime, one of the first steps in auxin biosynthesis (Zhao, 2010). Furthermore, several members of the *AUXIN-INDUCED PROTEIN* family (*IAA) such as IAA13, IAA18* and *IAA26*, which repress transcription of auxin responsive genes, and members of the *AUXIN RESPONSIVE* family (*ARF*), such as ARF*18* and ARF*8*, were directly targeted by JAG. Additionally, several members of the *SMALL AUXIN UP RNA* (*SAUR*) family such as *SAUR15*, *SAUR27* and *SAUR28* were directly and *SAUR68* was indirectly repressed by JAG. Members of the *SAUR* family rapidly respond to auxin and several members have been associated with cell expansion (*SAUR19, SAUR63*) (Spartz et al., 2012; Chae et al., 2012).

In some cases, JAG appeared to regulate auxin responses indirectly, through microRNAs. For example, JAG targeted *miR167*, which controls *ARF6* and *ARF8,* both of which play a role in floral organ development (Chapter 4). Also related to the control of miRNA functions, JAG directly repressed *AGONAUTE 7* (AGO7), which specifically forms complexes with *miR390* that guide the cleavage of *TAS3* precursor *tasiRNAs* (Hunter et al., 2003). In a further link to auxin-related miRNA function, JAG directly targeted *mir393B*, which in turn targets all members of the TAAR clade auxin receptors (*TIR1, AFB1, AFB2* and *AFB3*) (Si-Ammour et al., 2011). The TAAR clade is a component of the SKP/CULLIN/F-BOX ubiquitin ligase complex that targets IAA proteins for proteasome-dependent

degradation (Kepinski and Leyser, 2005; Mockaitis and Estelle, 2008). Mutant seedlings of *mir393b* show elongated hyponastic leaves, a phenotype that was also observed in the *ago7* mutant and is shared by mutants with auxin hypersensitivity (Si-Ammour et al., 2011).

The *TAS3*-derived *tasiRNAs* mentioned above have been reported to target *ARF3* (*ETTIN*) and *ARF4*, which play a major role in the adaxial/abaxial patterning in leaf development (Fahlgren et al., 2006; Hunter et al., 2006). In this context, JAG also directly represses the auxin-responsive homeodomain leucin zipper (HD-Zip) Class II gene *HAT2* (Figure 8.5.D-E) which has been identified as a direct target of *REVOLUTA* and *KANADI*, the two key players of adaxial/abaxial patterning in early organ primoridia (Reinhart et al., 2013). HAT2 was directly activated by the adaxial patterning gene *REV* and down-regulated upon ectopic expression of *KAN* (Reinhart et al., 2013), suggesting that *HAT2* is involved in promoting adaxial patterning. Ectopic expression of *HAT2* under the *35S* promoter resulted in seedlings with elongated hypocotyls, which was attributed to increase of cell elongation rather than cell proliferation, and smaller leaves with elongated petioles (Sawa et al., 2002).

In summary, JAG targeted multiple genes involved in auxin transport, signalling and response pathways, suggesting that JAG could promote organ growth, in particular oriented growth and local tissue growth rates required for organ patterning, through auxin mediated growth pathways.

8.3.4. JAG directly targeted genes involved in gibberellin biosynthesis and signalling

Gibberellins play a major role in promoting plant growth and development, for example, they promote seed germination, vegetative plant growth, stem elongation, floral development and fruit patterning. Mutants deficient in GA biosynthesis or signalling are in general dwarfed and late flowering. Gibberellins function as inhibitors of the DELLA proteins, which are growth-inhibitor proteins that can bind to transcription factors and DNA. The relief of the DELLA repression by gibberellins is mediated by the GA-GID-DELLA complex, which targets DELLA proteins for proteasome-dependent degradation and thus promotes growth (reviewed by Achard et al., 2009; Davière and Achard, 2013).

My ChIP-seq and array data revealed multiple links between JAG and gibberellin metabolism. For example, JAG directly down-regulated *GIBBERELLIN 20-OXIDASE 2*

(GA20ox2) (Figure 8.6.C) (FDR <0.05) and indirectly down-regulated *GA20ox1,* two genes that play a key role in the biosynthesis of bioactive gibberellins, generating C19 gibberellins, which are further converted to bioactive gibberellins by *GA3ox1* (Rieu et al., 2008). In addition, JAG indirectly down-regulated *GA3ox1,* which catalyses the final step in the conversion to bioactive gibberellins and has been shown to be expressed at the base of developing floral buds, in elongating stamen and in the distal tip of developing sepals (Mitchum et al., 2006). Furthermore, JAG directly up-regulated *GIBBERELLIN 2-OXIDASE 1* (*GA2ox1)* that is involved in the degradation of bioactive gibberellins and is most abundantly expressed in flowers (Figure 8.6.A- B). The five *GA2ox* genes identified in *Arabidopsis* negatively regulate shoot elongation and inflorescence length and in the *ga2ox* quintuple mutant an increase in the number of stem and inflorescence internodes and flowers was observed (Rieu et al., 2008a). In addition, JAG also targeted *GA2ox8*, which was not represented on the expression array chip. In contrast to *GA2ox1-5*, which cleaves C19 gibberellins, *GA2ox7* and *GA2ox8* cleave C20 gibberellins and have therefore been suggested to negatively regulate the abundance of C20 precursors for the biosynthesis of bioactive gibberellins.

Furthermore, the *ga2ox7/8* double mutant shows elongated hypocotyls, suggesting that *GA2ox7* and *GA2ox8* negatively regulated the levels of bioactive gibberellins. In this context, it has been suggested that GA homeostasis is maintained by feedback and feed forward regulation at different levels of GA biosynthesis and degradation (Nemhauser et al., 2006; Rieu et al., 2008 and 2008a). For example, the *ga2ox* quintuple mutant that has increased levels of GA showed reduced levels of genes involved in GA biosynthesis, for example *GA20ox1* and *GA3ox1* (Rieu et al.,2008 and 2008a). Furthermore, *GA2ox8* has been shown to be up-regulated upon exogenous GA application, while *GA2ox1* has been shown to be down-regulated (Schomburg et al., 2003). In summary, my data suggest that JAG represses the biosynthesis of bioactive GA while promoting degradation of bioactive GA.

In addition, JAG also targeted several genes involved in gibberellin signalling pathways: JAG directly up-regulated *GID1b* and indirectly up-regulated *GID1c*, two of the three GA receptor homologs of *GA INSENSITIVE DWARF 1* (*GID1 a-c*). The triple mutant *gid1a-c* has been shown to be insensitive to exogenous application of GA, while the wild type showed

enhanced growth in response to exogenous GA application. The *gid1a-c* triple mutant fails to elongate the stem and showed reduced cell expansion in leaves and roots.

Furthermore, *the gid1 a-c* was delayed in flowering under long-day conditions and showed growth defects in floral organs: pedicels failed to elongate and petals and stamen arrested in stage 10 of development. In addition, stamen filaments failed to elongate and less pollen could reach the stigma, a phenotype similar to the *xth28* mutant (Kurasawa et al., 2009). In the *gid1a-c* triple mutant, GA levels were significantly higher than in the wild type and the GA biosynthesis gene *GA3-ox1* was upregulated. Furthermore, application of GA to wild-type seedlings reduced the transcript levels of *GA3ox1* but not in the *gid1a-c* triple mutant. Together, this suggests that defective GA signalling is compensated by an increase in GA biosynthesis, in line with the observations that GA homeostasis is maintained by an auto-regulatory feedback loop involving genes that function in biosynthesis and degradation of GA (Nemhauser et al., 2006; Rieu et al., 2008 and 2008a). The fact that the *gid1a-c* triple mutant was still viable and produced seeds suggested that there are additional receptors mediating response to GA. For example, the members of the *GAMYB* family have been identified to mediate GA responses in particular in pollen development and seed germination, a role in floral transition and direct binding to the *LFY* promoter was suggested (Achard et al., 2004).

Furthermore, JAG directly targeted *BRG1* and directly repressed *BRG2*, two out of four members of the *BOTRYTIS SUSCEPTIBLE 1 INTERACTOR* (*BOI*) and *BOI-RELATED GENE* (*BRG*) family (Figure 8.6.D-F). *BOIs* are RING domain proteins, which can function as E3 ligases in the ubiquitination process that leads to proteasomal degradation. ChIP experiments showed that BOI can directly bind to promoter regions of known direct targets of DELLA proteins, suggesting that BOIs and DELLAs interact to transcriptionally repress a specific subset of GA-responsive genes (Park et al., 2013). In the *boi* quadruple mutant, responses to GA signalling were enhanced, resulting in early flowering and decreased chlorophyll content, while *35S:BOI* lines showed repressed GA signalling with delayed flowering and increased chlorophyll content in leaves, suggesting that *BOIs* function similar to *DELLAs* in repressing GA responses. GA promotes early flowering, in particular under short-day conditions, by promoting *LFY* expression. In the boi quadruple mutant, *LFY* expression was increased, as observed in the *della* mutant. Conversely, in the *BOI* overexpressor *LFY* was repressed, suggesting that *DELLA*s and *BOIs* act

redundantly to regulate *LFY*. By contrast, *SOC1* did respond to changes in BOI expression but not *DELLAs*, suggesting that *DELLAs* and *BOIs* act redundantly to regulate *LFY* but independently to regulate *SOC1* (Park et al., 2013). However, the *boi* quadruple mutant showed hypocotyl length similar to wild type and the *gai-1* boi quatruple mutant showed same hypocotyl length as the single *gai-1* mutant suggesting that BOIs are not required for hypocotyl elongation.

Finally, as described above for auxin responses, JAG also appeared to target gibberellin responses indirectly through miRNAs. JAG directly targeted *miR159A* (*At1g73687*) and *miR159B* (*At1g18075*) two related micro RNAs that are cleaved to 21 nucleotide long micro RNAs, in contrast to *miRJAW* (*At4g23710*), which is cleaved to 20 nucleotide long micro RNAs and targets *CIN-like TCP* genes but also targets MYB domain transcription factors (Palatnik et al., 2003). It has been shown that *miR159A* and *miR159B* specifically target *MYB33* and *MYB65*, which are members of the *GAMYB-like R2R3 MYB* domain transcription factor family (Allen et al., 2007). *MYB33* and *MYB65* play a specific role in anther development and formation of the aleurone tissue in seed germination, and are completely repressed by *miR159A/B* in vegetative tissue. In the *mir159ab* double mutant, *MYB33* and *MYB65* were up-regulated in vegetative tissue. Leaves of the *mir159ab* were smaller and consisted of mesophyll cells double the size compared to wild-type with cell number per area unit reduced to 50%, suggesting that ectopic expression of *MYB33* and *MYB65* inhibited cell proliferation in leaves. Because this phenotype was also observed in the *KRP2* over-expressor by de Veylder et al. (2001), Alonso-Peral et al. (2012), tested the expression levels of all seven members of the *KRP* family and revealed that *KRP7* was up-regulated in the *mir159ab* mutant, however, loss of KRP7 function did not rescue the *mir159ab* mutant phenotype in the triple loss of function mutant (Alonso-Peral et al., 2012).

An additional layer of regulation is added to the gibberellin signalling pathway by close functional and molecular interation with the brassinosteroid signalling pathway, as observed during hypocotyls elongation in particular in response to light (Tanaka et al., 2003; Gallego-Bartolome et al., 2012). Transcriptional regulation in response to brassinosteroids is mediated by the transcription factor family of *BRASSINAZOLE RESISTANT1* (*BZR1*) and its homologs (Ryu et al., 2007). It has recently been shown that the DELLA protein GAI interacts with BZR1 and interferes with its promoter binding

activities using yeast-two hybrid and BiFC assays. Furthermore, using a heat shock-inducible construct of the negative dominant gai-1 mutation, Gallego-Bartolome et al. (2012) showed that ectopic induction of the DELLA protein GAI interfered with BRZ1-mediated gene expression, suggesting that DELLA proteins act via the BRZ1 pathway, which was also further confirmed by reverse genetics. In this context, JAG directly up-regulated *BRZ1-homolog3* (*BEH3*) (Figure 8.6.G-H).

In conclusion, JAG directly targeted multiple genes involved in gibberellin biosynthesis, degradation and signalling. I found that JAG activates the GA receptors *GID1b* and *GID1c* and *GA2ox1*, which degrade bioactive GA, while JAG negatively regulated the GA biosynthesis genes *GA20ox*1 and *GA20ox2* and GA3ox1 and two members of the *BRG* genes that repress GA responsive genes similar to *DELLA* genes. This would suggest that JAG promotes GA signalling by increasing the receptors and repressing the repressors of GA-responsive genes. From these regulatory functions, one could hypothesise that in the *jag* loss of function mutant GA signalling is decreased and repression of GA-responsive genes is increased, at least for the subset of BRG target genes. Consequently, this could be compensated by an increase in GA levels which could be the outcome of increased GA biosynthesis and a decrease of GA degradation owing to auto-regulatory feedback mechanisms, but also owing to the direct regulatory effects of JAG on genes involved in GA biosynthesis and degradation. Ultimately, this could lead to increased GA levels in the *jag* loss of function mutant, in line with my observations that loss of *jag* mutants show similar phenotypes as mutants with increased in GA levels: leaves and stems are pale green in colour, suggesting a decrease in chlorophyll content. Furthermore, *jag* loss of function mutant plants flowered at least 7-10 days earlier with fewer leaves compared to wild type plants, although the statistical significance has not been tested yet.

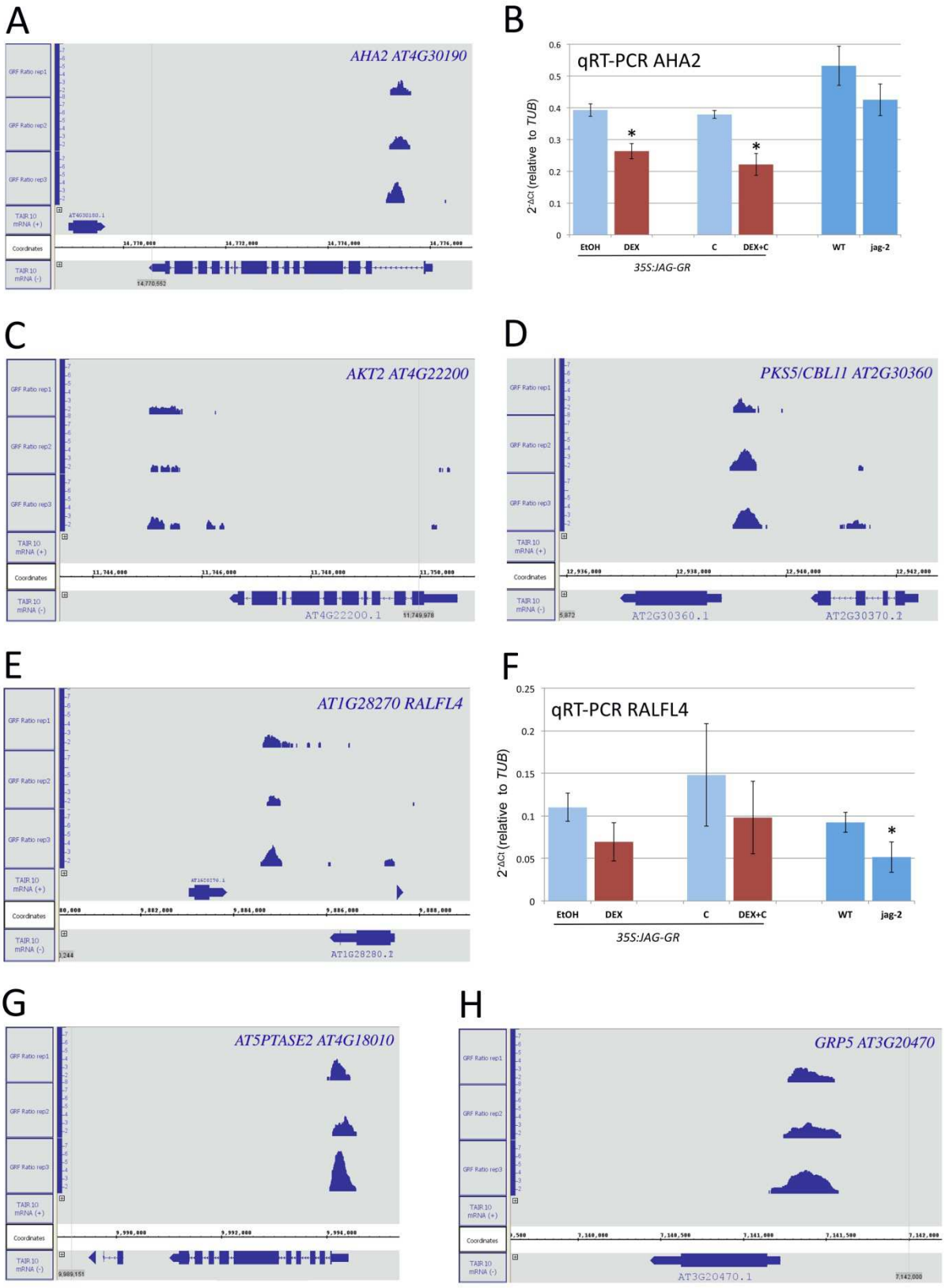

Figure 8.1. JAG directly and indirectly regulates genes involved in cell expansion.

(A, C-E, G-H) Visualisation of read enriched regions mapping to the TAIR10 Arabidopsis reference genome (x-axis) using the Integrated Genome Browser (Nicol et al., 2009), ChIP-Seq peak score values (y-axis) based on the ratios of normalised reads between JAG-GFP and control samples were calculated for every single nucleotide position using CSAR software (Muiño et al., 2011a), the maximum score value within the candidate peaks was used to test for significance of the enrichment; ChIP-Seq peaks detected in each replicate within 3 Kb upstream and 1.5 Kb downstream of the coding sequences for the *AHA2*, *AKT2*, *PKS5*, *RALFL4. AT5PTASE2*, and *GRP5*. (B, F) Expression levels (relative to the *TUB4* constitutive control) of *AHA2* (B) and *RALFL4* (F); mRNA measured by qRT-PCR in inflorescence apices of *35S::JAG-GR* plants 4h after mock treatment (light blue) or treatment with dexamethasone 10 µM (red); CHX indicates samples from plants that were also treated with cycloheximide 10 µM; or untreated wild-type (WT) and *jag-2* plants (dark blue); bars show the average and standard deviation of three biological replicates; asterisks indicate statistically significant differences (unpaired two-sample Student's *t*-test, $p < 0.05$) between dexamethasone-treated and mock-treated samples and between the untreated wild type and *jag-2* (dark blue bars) (compared in a separate independent experiment).

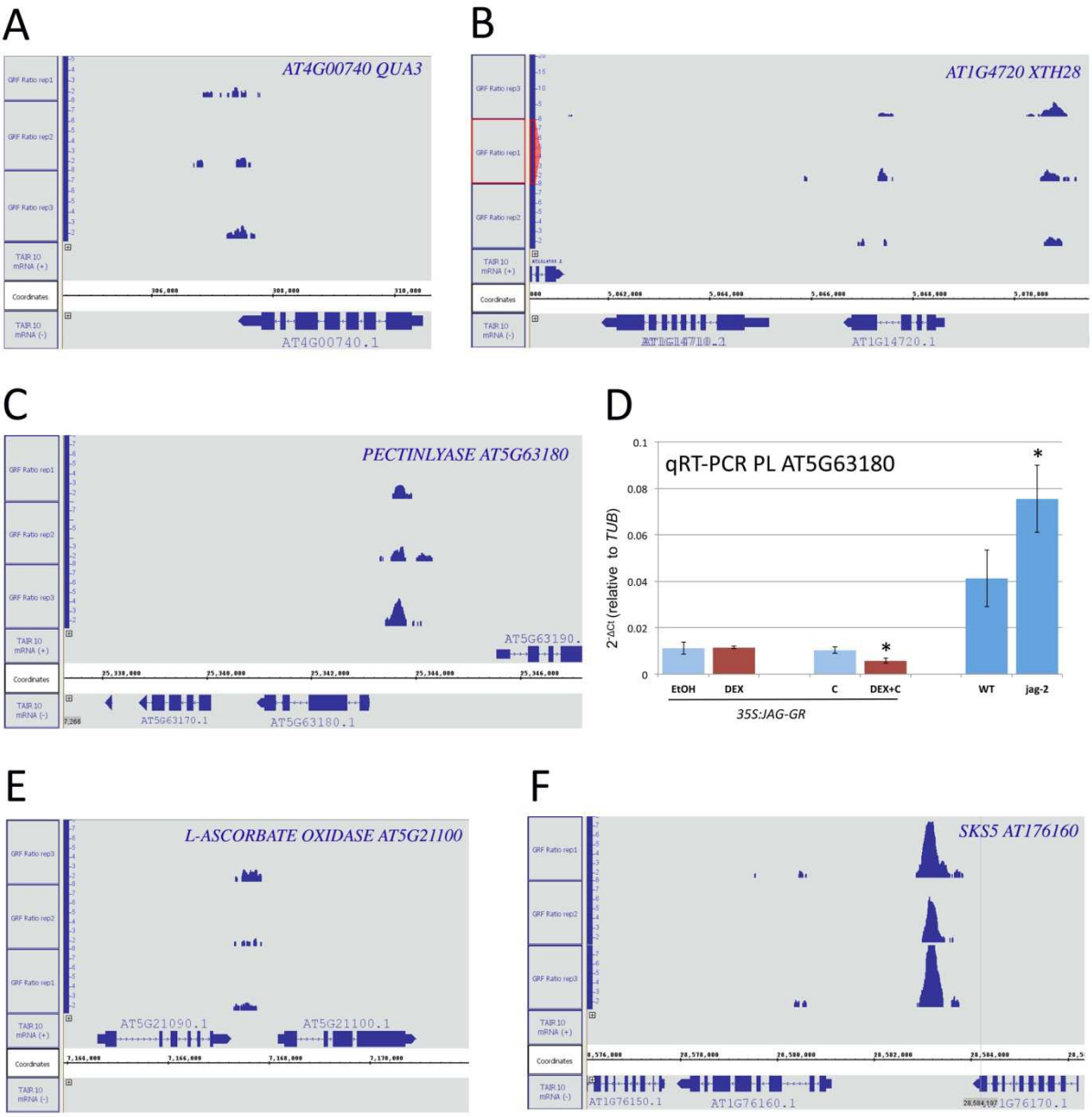

Figure 8.2. JAG directly and indirectly regulates genes involved in cell wall-related and apoplast processes.

(A-C, E-F) Visualisation of read enriched regions mapping to the TAIR10 Arabidopsis reference genome (x-axis) using the Integrated Genome Browser (Nicol et al., 2009), ChIP-Seq peak score values (y-axis) based on the ratios of normalised reads between JAG-GFP and control samples were calculated for every single nucleotide position using CSAR software (Muiño et al., 2011a), the maximum score value within the candidate peaks was used to test for significance of the enrichment; ChIP-Seq peaks detected in each replicate within 3 Kb upstream and 1.5 Kb downstream of the coding sequences of *AT4G00740*

(QUASIMODO3), *XTH28*, pectinlyase (*AT5G63180)*, *L-ASCORBATE OXIDASE AT5G21100*, and *SKS5* (*AT1G76160*). (D) Expression levels (relative to the *TUB4* constitutive control) of pectinlyase (*AT5G63180)*; mRNA measured by qRT-PCR in inflorescence apices of *35S::JAG-GR* plants 4h after mock treatment (light blue) or treatment with dexamethasone 10 µM (red); CHX indicates samples from plants that were also treated with cycloheximide 10 µM; or untreated wild-type (WT) and *jag-2* plants (dark blue); bars show the average and standard deviation of three biological replicates; asterisks indicate statistically significant differences (unpaired two-sample Student's *t*-test, $p < 0.05$) between dexamethasone-treated and mock-treated samples and between the untreated wild type and *jag-2* (dark blue bars).

A

direct targets	
At5g03760	CELLULOSE SYNTHASE LIKE A9 (CSLA09)
At5g16190	CELLULOSE SYNTHASE LIKE A11 (CSLA11)
At5g22740	CELLULOSE SYNTHASE-LIKE A2 (CSLA2)
At4g16590	CELLULOSE SYNTHASE-LIKE A1 (CSLA01)
At4g24000	CELLULOSE SYNTHASE LIKE G2 (CSLG2)
At4g31590	CELLULOSE-SYNTHASE LIKE C5 (CSLC05)
At3g07330	CELLULOSE-SYNTHASE LIKE C6 (CSLC06)
indirect targets	
At1g24070	CELLULOSE SYNTHASE LIKE A10 (CSLA10)
At1g55850	CELLULOSE SYNTHASE LIKE E1 (CSLE1)
At3g28180	CELLULOSE-SYNTHASE LIKE C4 (CSLC04)

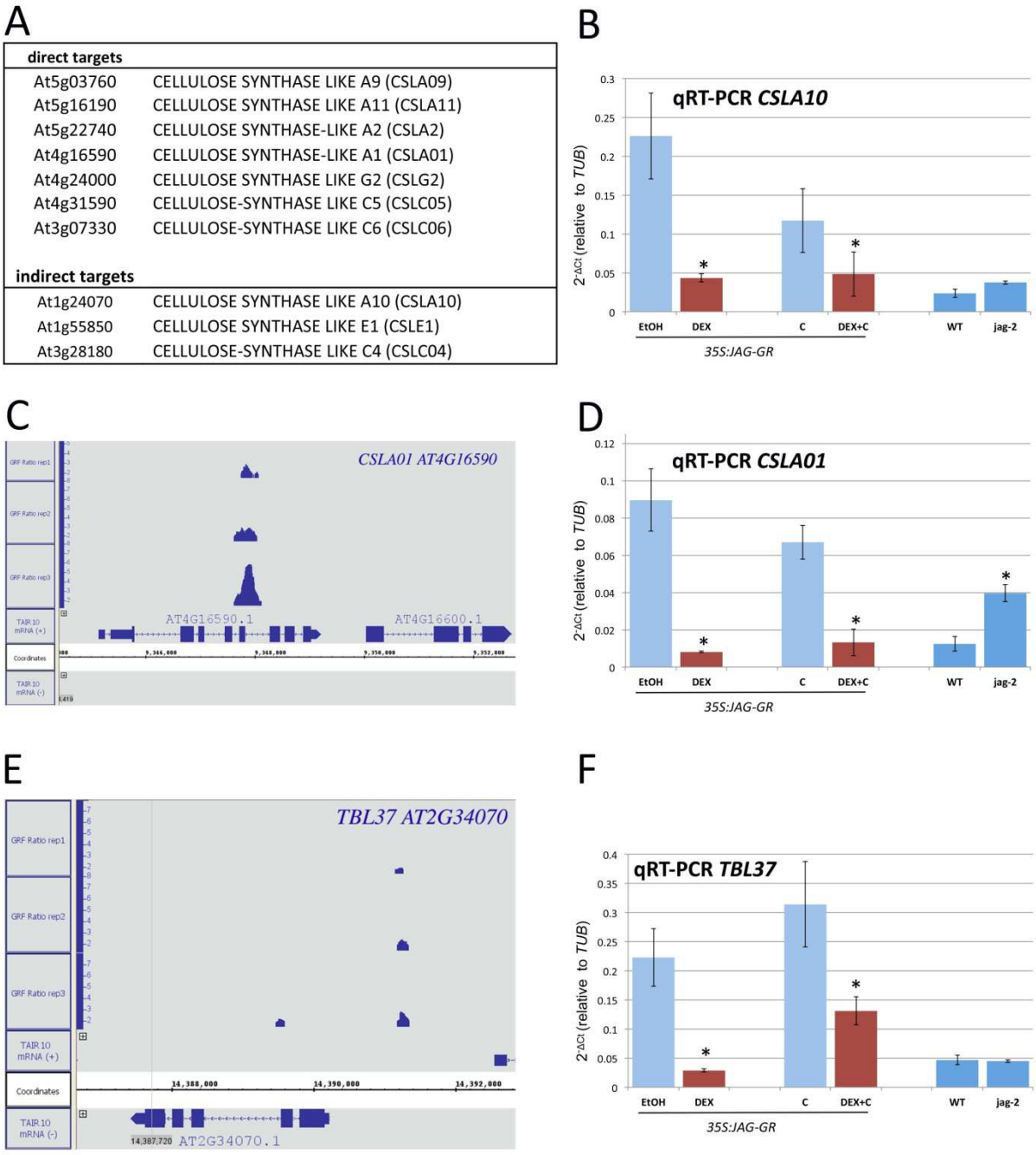

Figure 8.3. JAG directly and indirectly regulates cell wall-related genes.

(A) Overview of directly and indirectly repressed members of the *CELLULOSE SYNTHASE-LIKE* family. (B-D) Expression levels (relative to the *TUB4* constitutive control) of *CSLA10* (B) and *CSLA01* (D); mRNA measured by qRT-PCR in inflorescence apices of *35S::JAG-GR* plants 4h after mock treatment (light blue) or treatment with dexamethasone 10 µM (red); CHX indicates samples from plants that were also treated with cycloheximide 10 µM; or untreated wild-type (WT) and *jag-2* plants (dark blue); bars show the average and

standard deviation of three biological replicates; asterisks indicate statistically significant differences (unpaired two-sample Student's *t*-test, $p < 0.05$) between dexamethasone-treated and mock-treated samples and between the untreated wild type and *jag-2* (dark blue bars); (C) Visualisation of read enriched regions mapping to the TAIR10 Arabidopsis reference genome (x-axis) using the Integrated Genome Browser (Nicol et al., 2009), ChIP-Seq peak score values (y-axis) based on the ratios of normalised reads between JAG-GFP and control samples were calculated for every single nucleotide position using CSAR software (Muiño et al., 2011a), the maximum score value within the candidate peaks was used to test for significance of the enrichment; ChIP-Seq peaks detected in each replicate within 3 Kb upstream and 1.5 Kb downstream of the coding sequences of CSLA01; (E-F) ChiP-Seq peaks and expression levels (as described above) detected for *TBL37*, a member of the the *TRICHOME BIREFRIGENCE-LIKE* family.

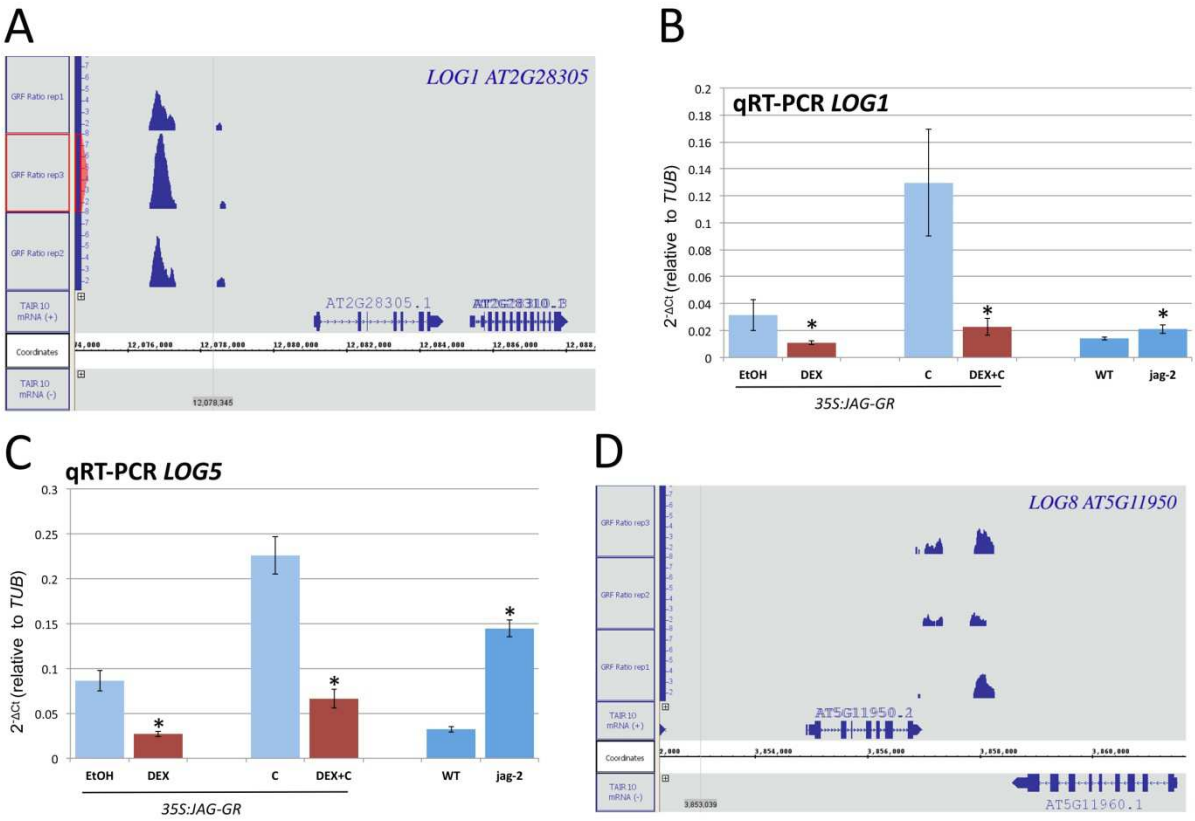

Figure 8.4. JAG directly targeted several members of the cytokinin activating LONELY GUY family. (A, D) Visualisation of read enriched regions mapping to the TAIR10 Arabidopsis reference genome (x-axis) using the Integrated Genome Browser (Nicol et al., 2009), ChIP-Seq peak score values (y-axis) based on the ratios of normalised reads between JAG-GFP and control samples were calculated for every single nucleotide position using CSAR software (Muiño et al., 2011a), the maximum score value within the candidate peaks was used to test for significance of the enrichment; ChIP-Seq peaks detected in each replicate within 3 Kb upstream and 1.5 Kb downstream of the coding sequences of *LOG1* and *LOG8. AT5PTASE2*, and *GRP5*. (B, C) Expression levels (relative to the *TUB4* constitutive control) of *LOG1* (B) and *LOG5* (C); mRNA measured by qRT-PCR in inflorescence apices of *35S::JAG-GR* plants 4h after mock treatment (light blue) or treatment with dexamethasone 10 µM (red); CHX indicates samples from plants that were also treated with cycloheximide 10 µM; or untreated wild-type (WT) and *jag-2* plants (dark blue); bars show the average and standard deviation of three biological replicates; asterisks indicate statistically significant differences (unpaired two-sample Student's *t*-test, $p < 0.05$) between dexamethasone-treated and mock-treated samples and between the untreated wild type and *jag-2* (dark blue bars).

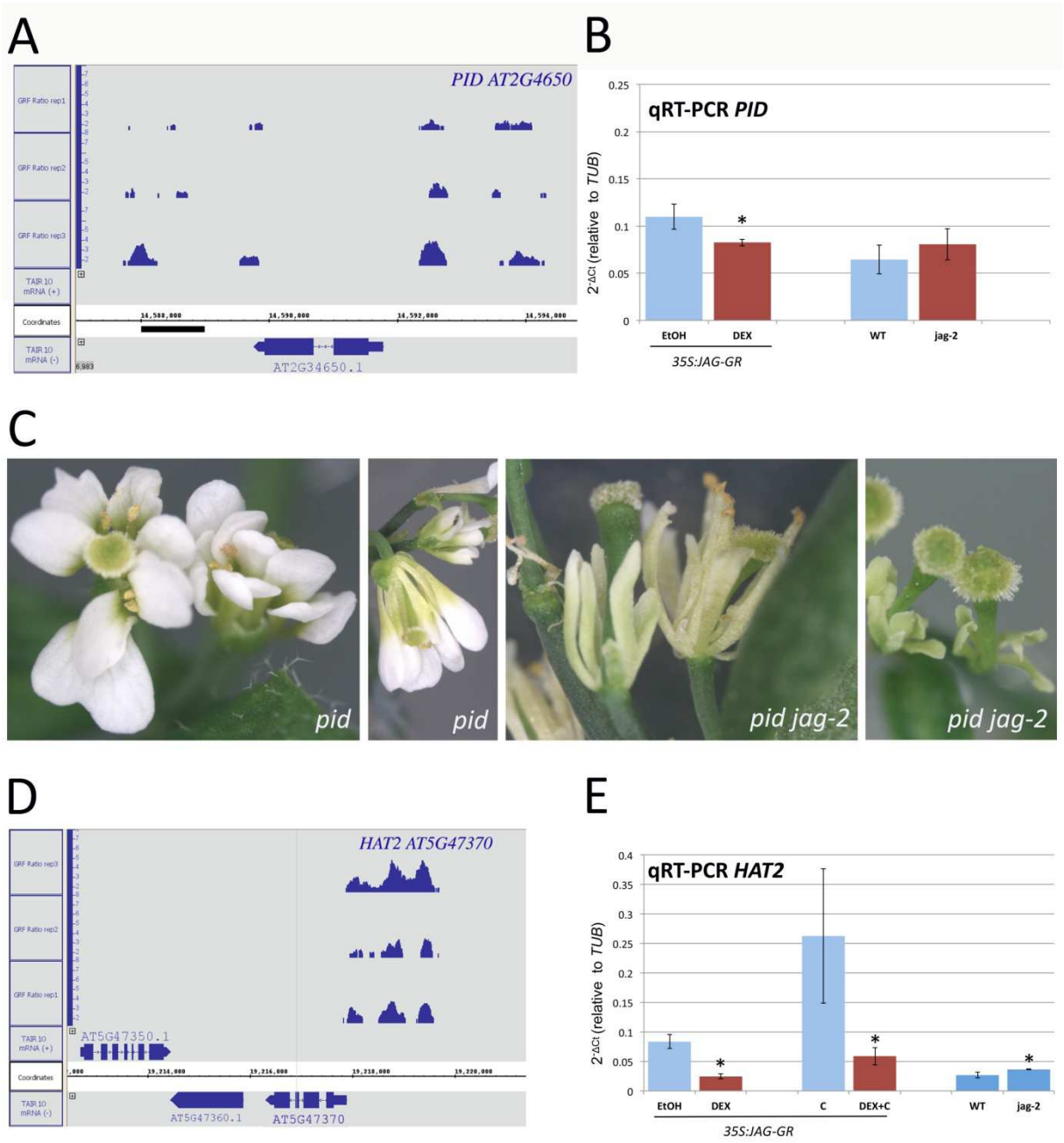

Figure 8.5. JAG directly targeted PINOID, a gene involved in polar auxin transport , and the auxin-responsive gene HAT2. (A, D) Visualisation of read enriched regions mapping to the TAIR10 Arabidopsis reference genome (x-axis) using the Integrated Genome Browser (Nicol et al., 2009), ChIP-Seq peak score values (y-axis) based on the ratios of normalised reads between JAG-GFP and control samples were calculated for every single nucleotide position using CSAR software (Muiño et al., 2011a), the maximum score value within the candidate peaks was used to test for significance of the enrichment; ChIP-Seq peaks detected in each replicate within 3 kb upstream and 1.5 kb downstream of the coding

sequences of *PID* and *HAT2*. (B, E) Expression levels (relative to the *TUB4* constitutive control) of *PID* (B) and *HAT2* (C); mRNA measured by qRT-PCR in inflorescence apices of *35S::JAG-GR* plants 4h after mock treatment (light blue) or treatment with dexamethasone 10 µM (red); CHX indicates samples from plants that were also treated with cycloheximide 10 µM; or untreated wild-type (WT) and *jag-2* plants (dark blue); bars show the average and standard deviation of three biological replicates; asterisks indicate statistically significant differences (unpaired two-sample Student's *t*-test, $p < 0.05$) between dexamethasone-treated and mock-treated samples and between the untreated wild type and *jag-2* (dark blue bars). (C) Inflorescences of the *pid* single loss of function mutant (right) and the *pid jag2* double loss of function mutant (left) with additive effects of narrower, smaller petals, both in L-*er* background.

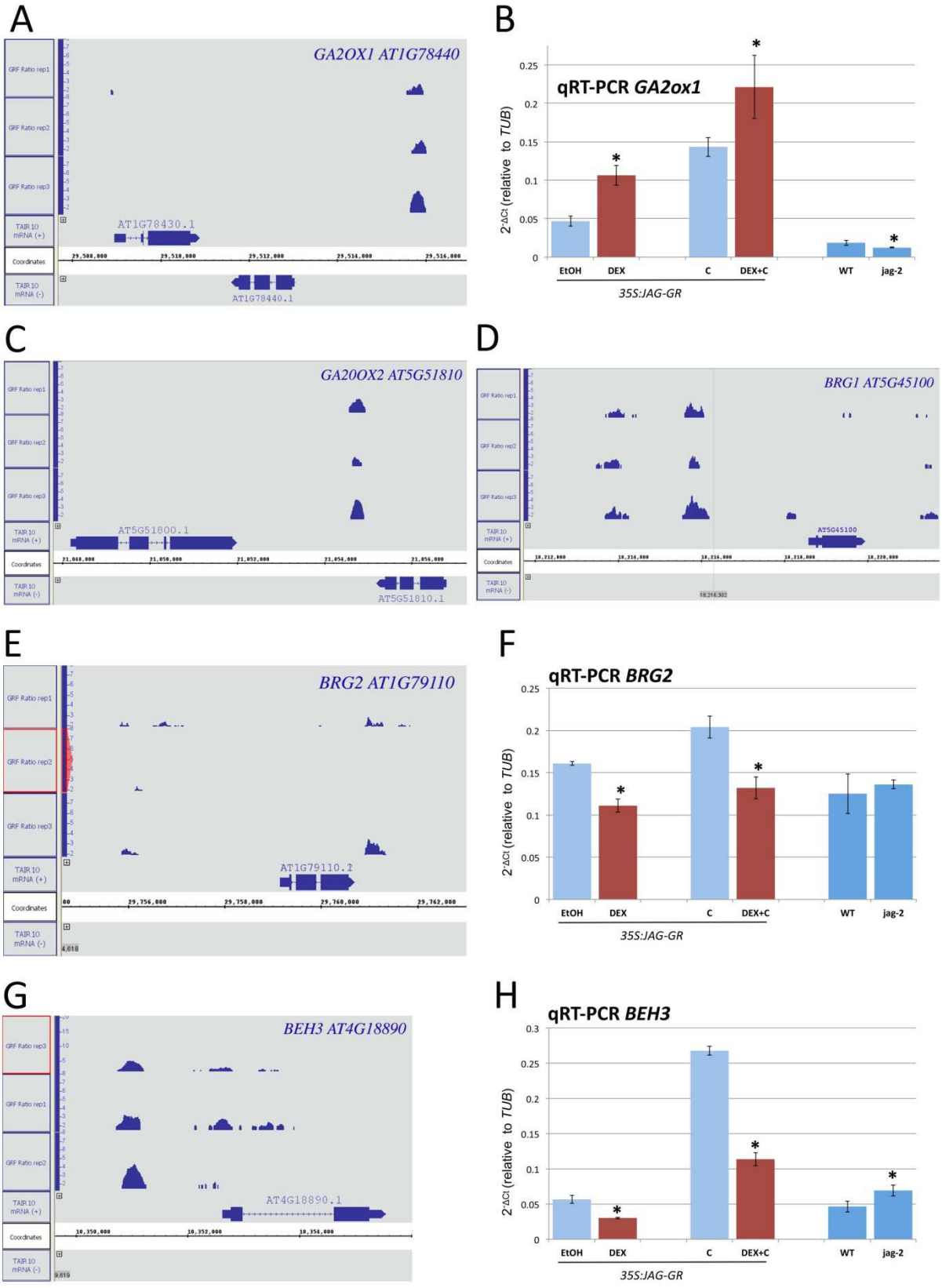

Figure 8.6. JAG directly targeted genes involved in gibberellins biosynthesis and degradation and brassinosteroid signalling. (A, C-E, G) Visualisation of read enriched

regions mapping to the TAIR10 Arabidopsis reference genome (x-axis) using the Integrated Genome Browser (Nicol et al., 2009), ChIP-Seq peak score values (y-axis) based on the ratios of normalised reads between JAG-GFP and control samples were calculated for every single nucleotide position using CSAR software (Muiño et al., 2011a), the maximum score value within the candidate peaks was used to test for significance of the enrichment; ChIP-Seq peaks detected in each replicate within 3 kb upstream and 1.5 kb downstream of the coding sequences of *GA2OX1, GA20OX2, BRG1, BRG2, BEH3*. (B, F, H) Expression levels (relative to the *TUB4* constitutive control) of *GA2OX1* (B), *BRG2* (F) and *BEH3* (H); mRNA measured by qRT-PCR in inflorescence apices of *35S::JAG-GR* plants 4h after mock treatment (light blue) or treatment with dexamethasone 10 µM (red); CHX indicates samples from plants that were also treated with cycloheximide 10 µM; or untreated wild-type (WT) and *jag-2* plants (dark blue); bars show the average and standard deviation of three biological replicates; asterisks indicate statistically significant differences (unpaired two-sample Student's *t*-test, $p < 0.05$) between dexamethasone-treated and mock-treated samples and between the untreated wild type and *jag-2* (dark blue bars).

Chapter 9 - General Discussion

9.1. JAG is required to produce fully functional organs

How organs develop to species-specific size, shape and function during postembryonic development in plants still harbours many unsolved questions. In plants, morphogenesis is based on the processes of cell proliferation and cell growth, which have to be coordinated within tissues and at organ level. However, it remains unclear how these processes are coordinated, whether developmental regulators target both processes in parallel or whether they regulate them singly and generate dependencies between them. Moreover, only few developmental regulators within the gene regulatory network of organ growth and morphogenesis have been functionally characterised in detail.

The single C_2H_2 zinc finger transcription factor *JAG* has been identified to play a key role in organogenesis, based on the severe phenotype in the loss of function mutants. Floral organs are narrower, shorter and have serrated margins, therefore they fail to reach the final species-specific size and shape. In addition, in the *jag* loss of function mutant sepals fail to enclose the inner developing whorls and defects in pollen development result in partial male sterility in *jag* mutants. From this it can be concluded that *JAG* plays a key role during organ initiation and subsequent distal growth to produce fully functional flowers. Here, I aimed to reveal the molecular mechanisms and genetic interactions by which *JAG* mediates its growth promoting functions.

During this project, I used quantitative 3D imaging to investigate JAG-dependent changes in cell behaviour and I used global expression analysis and genome-wide analysis of JAG DNA-binding sites to find downstream targets of JAG. Reverse genetics and reporter lines were used to confirm that the identified molecular interactions were genetically and functionally relevant. The global expression profiling, analysis of genome-wide DNA binding sites and quantitative 3D analysis of cell geometry combined with the S-phase marker EdU enabled me to identify downstream targets of *JAG* and to explore the cellular effects of these interactions on cell size homeostasis. This resulted in a step by step discovery of functionally relevant direct interactions between JAG and its target genes, in particular the cell cycle inhibitors of the KRP family. Furthermore, data obtained

during this project has been used to validate a mathematical model explaining polarity during petal growth (Sauret et al., 2013).

9.2. JAG provides a molecular link between organ patterning and tissue growth

Data obtained during this project revealed that the transcription factor JAG directly links the genetic pathways of organ patterning, tissue growth and morphogenesis. JAG directly repressed genes involved in meristem development, such as *CLV1* and the TALE proteins *BEL1* and *SAW2,* and the floral primordium identity gene *LFY.* These interactions are is in line with the findings from the quantitative 3D imaging approach, which showed that *JAG* is required for the transition from meristematic to primordium behaviour. The fact that sepal primordia still emerged and were physically distinguishable from the meristem in the *jag* mutant revealed that the changes in cell behavior that underpin primordium growth are genetically separable from those required for primordium emergence (Schiessl et al., 2012). Furthermore, *JAG* directly repressed several organ boundary specifying genes such as *PTL* and *HAN,* suggesting that growth-restricting boundary genes need to be repressed in order to promote tissue growth.

In respect to organ patterning and organ polarity, *JAG* directly repressed *BOP2* and directly bound to *BOP1*. *BOP1/2* are expressed in the basal region of lateral organs, where they are involved in the regulation of organ growth and morphogenesis along the adaxial-abaxial and proximo-distal axes and antagonise *JAG* (Norberg et al., 2005; Jun et al., 2010). In the leaf it has been shown that ectopic expression of *JAG* and loss of *BOP* function result in the same phenotype of ectopic leaf blade growth in the petiole region, suggesting that *BOP1/2* promote petiole growth behaviour and *JAG* promotes leaf blade growth, both acting as cell autonomous transcriptional regulators within exclusive domains. By contrast, *JAG* did not appear to interact with *FILAMENTOUS FLOWER (FIL)* a member of the *YABBY* transcription factor family that functions redundantly in adaxial/abaxial organ patterning, with the *fil jag* double mutant showing additive effects (Ohno et al., 2004).

Mutual antagonism between cell autonomous transcriptional regulators has been shown to be a common mechanism to link organ patterning and tissue growth. For example, the role of antagonising cell autonomous acting transcription factors linking

distal-proximal organ patterning and growth has been well established in the context of *Arabidopsis* ovule development. The antagonistic and in part synergistic interactions between *NOZZLE (NZZ)* and *BEL1*, *ANT* and *INNER OUTER (INO)* downstream of floral organ identity genes has been shown to determine the distal nucellus region bearing the megaspore, the central chalaza region, and the basal funiculus (Balasubramanian and Schneitz, 2000 and 2002). In the *nzz* mutant, the distal and central regions of the ovule are missing or reduced, similar to the *jag* loss of function mutant phenotype in leaves and perianth organs. Because the ovule consists of very distinctive regions along the proximal-distal axis, it was possible to precisely characterise the growth defects in the *nzz* mutant with the basal funiculus region being extended by increased cell proliferation at the expense of a missing or reduced central chalaza region and distal nucellus region (Balasubramanian and Schneitz, 2000 and 2002). Similarly, basal elongated cells appeared to replace the typical conical cells in the reduced distal lobe region of *jag* loss of function petals, possibly as a result of ectopic *BOP1/2* expression.

Similarly to *BOP1/2*, *NZZ* has been shown to be involved in establishing the abaxial/adaxial axis by repressing *INO*, suggesting that patterning of abaxial/adaxial and proximal/distal polarity are interconnected processes and under the control of the same transcriptional regulators. Based on its function linking patterning and growth, Balasubramanian and Schneitz (2000) referred to *NZZ* as a "floral organ-building" gene acting downstream of floral organ identity genes. In this context, Bencivenga et al. (2012) showed that *NZZ* and *BEL1* are required for auxin and cytokinin signalling during ovule development, showing that cell autonomously acting transcriptional regulators are interconnected with non cell autonomously acting plant hormones during organ patterning and organ growth (Bencivenga et al., 2012).

Another example of proximal-distal patterning mediated by the antagonistic interaction of transcription factors associated with auxin signalling is found during early embryogenesis. The earliest event of proximal-distal patterning is the asymmetric division of the zygote into an apical cell that gives rise to the pro-embryo and the larger basal cell the suspensor. After three to four rounds of cell divisons, the pro-embryo reaches the 8-cell/16-cell globular stage of the pro-embryo during which a basal and apical domain (a root pole and a shoot pole) are established that later give rise to the shoot and the root meristems. The pro-embryo is pre-patterned by a polar apical to basal auxin flux

mediated by the basal orientation of PIN auxin efflux carriers. While *PLETHORA* (*PLT*) transcription factors determine root fate, members of the *CLASS III HOMEODOMAIN-LEUCINE ZIPPER III* (*HD-ZIP III*) family (*REVOLUTA*, *PHABULOSA*, *PHAVOLUTA* and *INCURVATA*) are expressed in the central apical domain and have been shown to promote apical shoot fate during early embryogenesis. It has been shown that the *PLT* transcription factors are actively repressed in the apical domain by the transcriptional co-repressor *TOPLESS* (*TPL*) to allow the development of a shoot pole. On the other hand, expression of mutated *HD-ZIP III* genes that are resistant to *miR165*/*166* converted root poles into shoot poles in *plt* mutant background (Smith and Long, 2010). In addition to proximal/distal patterning, *HD-ZIPIII* transcription factors have a role in abaxial/adaxial patterning. When shoots are converted to roots the established abaxial/adaxial orientation in the apical domain is lost. Taken together, this further supports the idea that proximal/distal and abaxial/adaxial patterning converge in the embryo and during post-embryonic lateral organ development, and that transcriptional regulators such as *NZZ* and members of the *HD-ZIP III* are involved in both adaxial/abaxial and proximal/distal patterning, as suggested for *BOP1/2*.

Interestingly, the boundary specifying gene *HANABA TARANU* (*HAN*), which also interacts with *JAG* in a mutually antagonistic way (Zhang et al., 2013), has been shown to play an important role in establishing the boundary between the basal region of pro-embryo and the suspensor, the region where the root meristem initiates from (Nawy et al., 2010). In the *han* loss of function mutant the expression domain of *PLT1* shifted from the basal pro-embryo domain into the apical domain and several suspensor-specific genes were found in the basal region of the pro-embryo, suggesting that *HAN* as a boundary-specifying gene facilitates the apical/basal patterning by establishing a boundary between domains of different specification (Nawy et al., 2010). This further provides evidence for the importance of boundary specifying genes not only for organ separation, but also for establishing distinct domains during axial patterning.

Mutual antagonism of cell autonomous transcriptional regulators is also a well-established mechanism in animal development. For example in Drosophila limb development, the proximal/distal-distal axis is established by the non cell autonomously acting secreted signalling proteins Dpp and Wingless, which promote the cell-

autonomous homeodomain transcription factors *Distal-less* in the distal limb domain and *Homothorax* in the proximal body wall domain. It has been shown that these two domains exclude each other. Because animal cells can migrate, it has been shown that chimeric cells expressing *Distal less* in the proximal *Homothorax* expression domain migrate back to the distal domain and the other way around, thereby generating a boundary between the proximal *Homothorax* domain and the *Distal less* limb domain. Loss of *Distal less* function caused expansion of proximal structures at the expense of distal structures, which led to the hypothesis that basal proximal structures could be a default developmental pattern which requires distal regulators that superimpose distal organ patterns on top of a default basal organ pattern (Cohen and Jürgens, 1989; Wu and Cohen, 1999).

In animals, appendages such as wings and legs are patterned by gradients of secreted signalling molecules (morphogens) such as Dpp (Decapentaplegic) and Wingless. Several models have been proposed for how morphogen gradients can be translated into growth and morphogenesis. A key component of these models is the Hippo pathway, which transduces signals between receptors in the plasmamembrane and the nucleus to integrate cell division and growth with environmental and developmental cues. The Hippo pathway restricts cell proliferation, promotes apoptosis of excess cells and integrates the growth controlling Myc pathway to determine final organ sizes (Pan, 2010; Halder and Johnson, 2011; Neto-Silva et al., 2009). In plants, no comparable central pathway has been discovered yet that integrates and translates developmental and environmental cues into regulation of cell proliferation and cell growth. However, the signalling molecule auxin is a good candidate to link organ patterning and organ growth processes in plants. Auxin has been shown to regulate both cell cycle progression and cell expansion (reviewed by Perrot-Rechenmann, 2010). During early plant embryogenesis, inductive signalling in discrete domains of the developing pro-embryo has been shown to be dependent on local auxin gradients (Nawy et al., 2010). The mechanism to generate localised auxin maxima during organ initiation and subsequent organogenesis by polarly oriented PIN auxin efflux carriers has been well established (Benkova et al, 2003; Heisler et al., 2005; Sauret et al., 2013). In this context, my results showed that *JAG* directly repressed the *PIN* associated kinase *PINOID (PID). PID* functions in the apical localisation of PIN efflux carriers and therefore promotes a basal-apical auxin flux, which results in

auxin maxima in the distal area of developing leaves and petals (Friml et al., 2004; Kleine-Vehn et al., 2009; Sauret et al., 2013). Therefore JAG might function in apical-distal organ patterning by directly targeting oriented, polar auxin transport. In addition, JAG indirectly influenced auxin dynamics by repressing *PTL* (Sauret et al., 2013).

The interaction between *JAG* and *PID* could also be functionally relevant in anisotropic growth processes, as live imaging suggested that *JAG* promotes a shift from isotropic to anisotropic growth (Schiessl et al., 2012). In respect to anisotropic growth, several factors modifying the behaviour of microtubules and microfibrils have been identified, for example CLASP proteins and the WAVE protein complex (reviewed by Ivakov and Persson, 2013). However, except for the *GRF-interacting factor AN3*, which has been described to play a role in microtubule arrangement and specifically targets the cell wall protein *MERI5* (Kim et al., 2002), JAG did not appear to directly target genes involved in oriented microtubule arrangement and cellulose microfibril alignment. It is also possible that the main contributors for the shift from isotropic growth to anisotropic growth are found within the growth-related cell wall targets of JAG. For example, *JAG* controlled genes that are likely to participate at different stages of oriented cell wall extension, including apoplast acidification (*AHA2*, *PKS5, RALFL4*), apoplast redox system (*Ascorbate oxidase*) and putative cell wall modifying enzymes (pectin lyases, pectin acetylesterase, cellulose synthase-like). Several gene candidates with unknown or vague functions showed very strong enrichments of DNA binding sites and significant differences in expression levels. For example, *AT3G50650*, a member of the GRAS transcription factor with unknown function, *AT4G18010* a member of the *INOSITOL(1,4,5)P3 5-PHOSPHATASE II family* and *GLYCINE RICH PROTEIN 5* (*AT3G20470)* with functions in the vacuole, were all significantly down-regulated upon ectopic JAG activation and ectopically expressed in the *jag* mutant. In the future, exploring the function of these candidates may reveal new players in particular in the field of oriented cell wall extension during cell growth but also cell wall-related processes during cytokinesis.

Potentially related to cell-cell communication during developmental processes, JAG also directly targeted several micro RNAs that targeted genes involved in development. As mobile factors, microRNAs have been shown to move between cells within a tissue and between tissues to facilitate the coordination of processes within an organ. For example, *miR164* and *miR396* that target *CUC* genes and members of the *GRF* family, respectively,

mediate growth and cell differentiation in the developing leaf primordia (Hasson et al., 2011; Rodriguez et al., 2010; reviewed by Powell and Lenhard, 2012).

9.3. JAG modulates cell size homeostasis by directly repressing KRP4

Quantitative 3D analysis of cell geometry combined with the S-phase marker EdU revealed that JAG is required to uncouple entry into S-phase and cell size in the primordium (Schiessl et al., 2012). By contrast, in the *jag* mutant primordia, S-phase entry and cell size appear to be coupled, with cells entering S-phase at uniform cell sizes around 150 µm³. Because a similar cell behaviour was observed in wild-type and *jag* meristems it was concluded that JAG is required for the shift from meristem to primordium cell behaviour (Schiessl et al., 2012). In this context, it was speculated that JAG modulates cell size homeostasis to allow increased cell proliferation, cell growth rates and an increase in cell size heterogeneity during primordium emergence.

In addition, data obtained from this project revealed that ectopic activation of JAG in the meristem caused cells to enter S-phase at smaller cell sizes than 150 µm³. This suggested that JAG was able to override an S-phase constraint mechanism that might impose a minimum cell size threshold, preventing cells from entering S-phase at cell sizes below 150 µm³ but pushing cells into S-phase as soon as they reach the minimum threshold level. Similarly, loss of *KRP4* function in the wild-type and *jag* loss of function mutant background caused cells to enter S-phase at smaller cell sizes in the meristem. Because ectopic activation of *JAG* and loss of *KRP4* had similar effects on meristem cell behaviour, I hypothesised that *KRP4* plays a major role in the minimum cell size threshold mechanism observed in meristem cells and that ectopic JAG activation repressed KRP4 in this context. Ectopic expression of JAG and loss of KRP4 show that cells are physiologically capable to divide at smaller cell sizes than they do in the developmental context of the wild-type meristem, suggesting that constraint of S-phase entry is a mechanism to regulate cell division and cell growth in specific tissues.

In the sepal primordia of the *jag* loss of function mutant, loss of *KRP4* function caused uncoupling of S-phase and cell size similar to the uncoupling observed in wild-type primordia. This suggested that ectopic *KRP4* expression could be the main cause for the coupling of S-phase entry and cell size in the *jag* mutant primordia compared to wild-type

primordia. Or in other words, in order to uncouple entry into S-phase from cell size in the wild-type primordium, JAG is required to repress *KRP4*. In this respect, it can be speculated that it is predominantly the repression of *KRP4* mediated by JAG that is required to allow an increase in cell proliferation rates but also for the increase in cell growth rates and the increase in cell size heterogeneity observed in sepal primordia in comparison to the growth behaviour in the meristem. In this context, Grandjean et al. (2004) showed that meristem growth stopped specifically upon inhibition of entry into S-phase while cells continued to grow when mitosis was blocked. Furthermore, several experiments showed that constraining S-phase entry by ectopic expression of *KRPs* inhibits cell growth and leads to a dramatic decrease in final organ sizes (De Veylder et al., 2001; Verkest et al., 2005; Bemis and Torii, 2007; Roeder et al., 2010). Expression of KRP2 and members of the SIAMESE family has also been shown to be promoted by the DELLA proteins, which have been suggested to actively restrain plant growth below the physiological maximum capacity in response to environmental cues (Achard et al., 2009).

Regulators of S-phase entry also play important roles in animal development. In mice, growth and tumor development is restrained by the *KIP* protein *p27.* Loss of *p27* in mice resulted in an overall increase in body size and *p27* mice were more susceptible to develop tumors owing to increased cell proliferation. Interestingly, loss of *p27* rendered the mice more responsive to growth hormones, suggesting that releasing a cell cycle constraint also promotes growth in animals (Teixeira et al., 2000). *Kip 27* has been shown to be directly targeted by *FoxO*, a Forkhead transcription factor that acts downstream of the TOR signalling pathway and promotes cell cycle arrest in response to stress, suggesting that *p27* is also regulated in response to developmental and environmental cues (Schmidt et al., 2002).

At the whole-organ scale, loss of *KRP* function in the *jag* loss of function background caused a partial but significant rescue of growth. These findings suggested that the growth defects in the *jag* mutant are at least in part caused by ectopic expression of KRPs, but that additional targets of *JAG* are required for full organ growth. For example, JAG targeted genes involved in growth-related cell wall modification, which I did not have the opportunity to investigate during this project, but are promising candidates to be studied in the future.

It has been a strongly debated question, what effects the coordination of cell proliferation and cell growth have on final organ size (reviewed by John and Qi, 2008; Marshall et al., 2012). In this context, the roles of *KRP* genes in both cell size homeostasis and in overall organ growth raise the question of whether both processes are causally linked. We could not detect any significant changes in the morphology or size of primordia in *krp4* mutants, although the short time between primordium emergence and the stages analyzed here (1-2 days) may be insufficient for changes in organ growth to unfold. Because I did not observe any significant rescue during early stages of organogenesis, it remains an unanswered question whether the significant changes in cell size homeostasis caused by the interaction between *JAG* and *KRP4* during organ initiation have an effect on final organ size and morphology. In this respect, Roeder et al. (2010), who followed development of the sepal primordium during later stages of development, showed that variation in cell cycle duration, which is comparable to cell size variation at entry into S-phase provided that cells spend variable times predominantly growing in G1 phase, plays a major role in cell type specification and morphogenesis. Moreover, Roeder et al. (2010) showed that ectopic expression of *KRP1* and loss of *SMR1* in the *loss of giant cells from organs* (*lgo*) mutant had an effect on final cell size distribution, besides the effects caused by shifts in endoreduplication rates. Apart from underpinning tissue growth and overall organ growth, cell size variation determines the mechanical and physiological properties of cells (diffusion, volume to surface area ratio) and has been suggested to influence metabolism, gene expression and intercellular communication (reviewed by Marshall et al., 2012; Laskowski et al., 2008; Wu et al., 2010).

Previously, *KRPs* have been identified as putative targets of floral organ identity genes (Kaufmann et al., 2009; Wuest et al., 2012). However, no genetic and functional interactions between KRPs and developmental regulators have been established yet, apart from the direct molecular interaction between *JAG* and *KRPs* revealed here. For example, do meristem maintenance genes directly or indirectly promote *KRP4* expression together with *CYCD3* expression to tightly coordinate S-phase entry with cell size, as observed in the quantitative 3D imaging experiments? The antagonistic interaction between *KRPs* and *D-type cyclins* in fine tuning CDKA activity has recently been described as a double negative feedback loop in mathematical models that aimed to explain the regulation of cell cycle progression in plants (Dissmeyer et al., 2010; Zhao et al., 2012). In

this respect, it could be speculated that because of their crucial functions they could also be key targets of other developmental regulators to inhibit or to promote entry into S-phase and concomitant cell growth. Future global transcriptome analysis and analysis of genome-wide DNA binding sites of key meristem regulators and growth regulators will provide answers to this question.

Taken together, could *KRPs* and *D-type cyclins*, as core cell cycle regulators, be central integrators of environmental and developmental cues? For example, it has been shown that cytokinin signalling and the transcription factor *ANT* modulates *CYCD3* function (Mizukami and Fischer, 2000; Dewitte et al., 2007). Moreover, data obtained during this project revealed that *JAG* directly promotes *CYCD3* expression. It would be interesting to find out whether *ANT* directly targets *KRPs* to exert its cell proliferation and growth promoting functions. *KRPs* and *cyclins* have been shown to be regulated post-translationally by targeted ubiquitin-dependent proteasomal protein degradation (reviewed by Blomme et al., 2013). Hence, it could be speculated that some of the growth regulators identified to function in the degradation pathway such as *BIG BROTHER*, *DA1* and *DA2* may target *CYCD3* for degradation or indirectly promote protein stability of KRPs.

9.4. Coordinating cell division and cell size

It has been suggested that in order to coordinate cell division and cell size, the two processes would either have to be dependent on each other or be regulated in parallel (reviewed by Jorgensen and Tyers, 2004; reviewed by John and Qi, 2008; reviewed by Wartlick and Gonzalez-Gaitan, 2011; reviewed by Sablowski and Carnier Dornelas, 2013). In unicellular budding yeast and fission yeast, minimum cell size thresholds at the G1/S-phase transition have been described to generate such a dependency between cell size and entry into S-phase (Jorgensen and Tyers, 2004). Several experiments with mammalian cell culture cells have shown that cells double in size before they undergo division, suggesting that there is an intrinsic dependency of entry into S-phase on cell size in cells of multicellular organisms (reviewed by Grewal and Edgar, 2003). Similarly, entry into S-phase was blocked when cell growth was inhibited while cells continued to grow when

mitosis was inhibited (Grandjean et al., 2004), suggesting that there is an intrinsic dependency between entry into S-phase and cell growth in plants.

Even though components such as the G1/S phase cyclins of the Cln family have been identified to act downstream of a minimum cell size threshold in yeast, it still remains an unsolved question how cells measure their size. It has been suggested that parameters of cytoplasmic growth, most importantly rates of ribosome biogenesis and protein translation, would provide information about the cells' growth rates and nutrient states. In addition, it has been suggested that cell size sensing may directly rely on parameters of cell geometry. In fission yeast, it was proposed that the protein kinase *Pom1* located at the cell poles would inhibit the mitotic apparatus in the centre of the cells, thereby overcoming the inhibitory influence of signals from the cell poles (Moseley et al., 2009), but the putative function of *Pom1* in cell size sensing could not be confirmed in the loss of function mutants (Wood and Nurse, 2013). More recently, Rho1 signalling has been suggested to link membrane trafficking and membrane growth to progression into mitosis in fission yeast. Moreover, it has been shown that blocking membrane trafficking inhibited ribosome biogenesis, suggesting that this hypothesis would be in agreement with the proposed role of ribosome biogenesis in cell size thresholds (Anastasia et al., 2013). In this context, it was speculated that in plants, protein synthesis and cell wall integrity pathways could be linked and provide parameters for a cell size sensing mechanism (Sablowski and Carnier Dornelas, 2013).

In the meristem context, where cells enter S-phase at very narrow sizes, data obtained during this project suggested that the core cell cycle regulator *KRP4* is involved in a minimum cell size threshold. As soon as cells reach a certain cell size, they pass the checkpoint, and enter S-phase which results in a population of cells with uniform sizes over several rounds of divisions, similar to what has been reported for fission yeast and budding yeast. This was further supported by Grandjean et al. (2004), who observed that meristem cell sizes are very uniform in spite of heterogeneity in cell cycle length. It has been suggested by Jorgensen and Tyers (2004) that during organ growth and morphogenesis, the minimum cell size threshold would be modulated and overridden by developmental regulators to allow for local variations in cell size distributions that are required for final size, shape and function of organs. In this context, my data suggests that

JAG, by repressing KRP4, is one of these developmental regulators that are able to modulate and loosen a minimum cell size threshold.

On the other hand, it has been doubted whether individual cells in tissues of multicellular organisms have the need for intrinsic cell size monitoring at all. Unicellular yeast cells grow exponentially and in this context a minimum cell size threshold at the G1/S phase entry ensures uniformity in cell sizes over generations. By contrast, it has been shown that mammalian cells show linear growth behaviour with smaller and larger cells increasing in size at the same rate (reviewed by Grewal and Edgar, 2003; Conlon and Raff, 2003). It is not clear whether cell growth in plants is linear or exponential. If growth were linear, the relative increase in cell size decreases for larger cells and sizes would converge even if initial size of sister cells were different, therefore a size checkpoint would not be required to maintain uniform cell sizes. If growth were exponential, differences in the size of sister cells after division would be amplified and the maintenance of uniform cell sizes would require a cell size checkpoint, in particular in tissues with uniform cell sizes such as the meristem. By contrast, exponential growth in the organ primordia could be one explanation for the increase in cell size heterogeneity and overall increase in cell growth rates. It would take live imaging combined with 3D analysis of cell geometry with high temporal resolution to distinguish between linear and exponential cell growth.

In contrary to unicellular cells, cells of multicellular organisms have to coordinate their growth and division rates with neighbouring cells to ensure integrity and functionality of the tissue they are part of, which would require a continuous coordinated adjustment and modulation of minimum cell size thresholds or a complete release from them. Therefore it has been suggested that cell size homeostasis in multicellular organisms may be the balanced net effect of cell cycle inhibiting/promoting factors and growth promoting/inhibiting factors rather than the effect of cell size thresholds. In this way, cell size homeostasis could be modulated by several synergistically and antagonistically acting non-cell autonomous factors and cell-autonomously acting regulators with high local and spatial resolution. In respect to this hypothesis, *KRP4* as a regulator of the core cell cycle machinery could be one of the key targets of developmental regulators that would regulate growth and cell division in parallel to modulating cell size homeostasis. What appears like a minimum cell size threshold in the meristem could be the net effect of

different meristem-specific regulators that restrict entry into S-phase by targeting KRP4, while at the same time activating factors such as *CYCD3,* which promote entry into S-phase. It has been suggested by Sanz et al. (2011), that KRP2 may combine these regulatory mechanisms in a dual function, by promoting the formation and nuclear-localisation of *D-type cyclin*/*CDKA* complexes on the one hand and by inhibiting the same complexes on the other hand. In this context, JAG may not only be able to override a cell size threshold but actually be an active modulator of cell size homeostasis by repressing KRP4. Further work on KRP4 and JAG as an endogenous developmental repressor of KRP4 will shed light on the mechanisms KRP4 and JAG are involved in to modulate cell size homeostasis.

It has been a long-standing question whether promoting cell proliferation can drive growth and which of the two processes is directly targeted by developmental regulators. In relation to this question, it has previously been reported that constraining S-phase is a regulatory mechanism to restrict growth (Achard et al., 2009). Results from this project showed that the direct repression of KRP4 by JAG promoted overall organ growth by releasing the constraint on S-phase. Moreover, the interaction between *JAG* and *KRP4* reveals a molecular link between the control of the G1-S transition and developmental regulation of cell size homeostasis and cell growth, suggesting that localized release of a growth restraint imposed by the KRP CDK inhibitors can be used to modulate cell size homeostasis required for differential tissue growth behaviour during morphogenesis. Even though this result does not provide an answer to the question of whether cell division is a driver of growth, it provides evidence that restricting S-phase and thus cell proliferation is used to modulate growth during plant development.

In summary, this work contributed to answering the question of how growth regulatory genes coordinate cell growth and cell proliferation to produce organs of defined shapes and sizes. The direct links between *JAG* and organ patterning genes and cellular effectors of growth and cell proliferation give insight into the cellular processes targeted by regulatory genes to sculpt plant organs. Finally, the results of this project place JAG at the interface between gene regulatory networks that control organ identity and patterning, and core cellular functions required for growth and morphogenesis (Figure 10.1.).

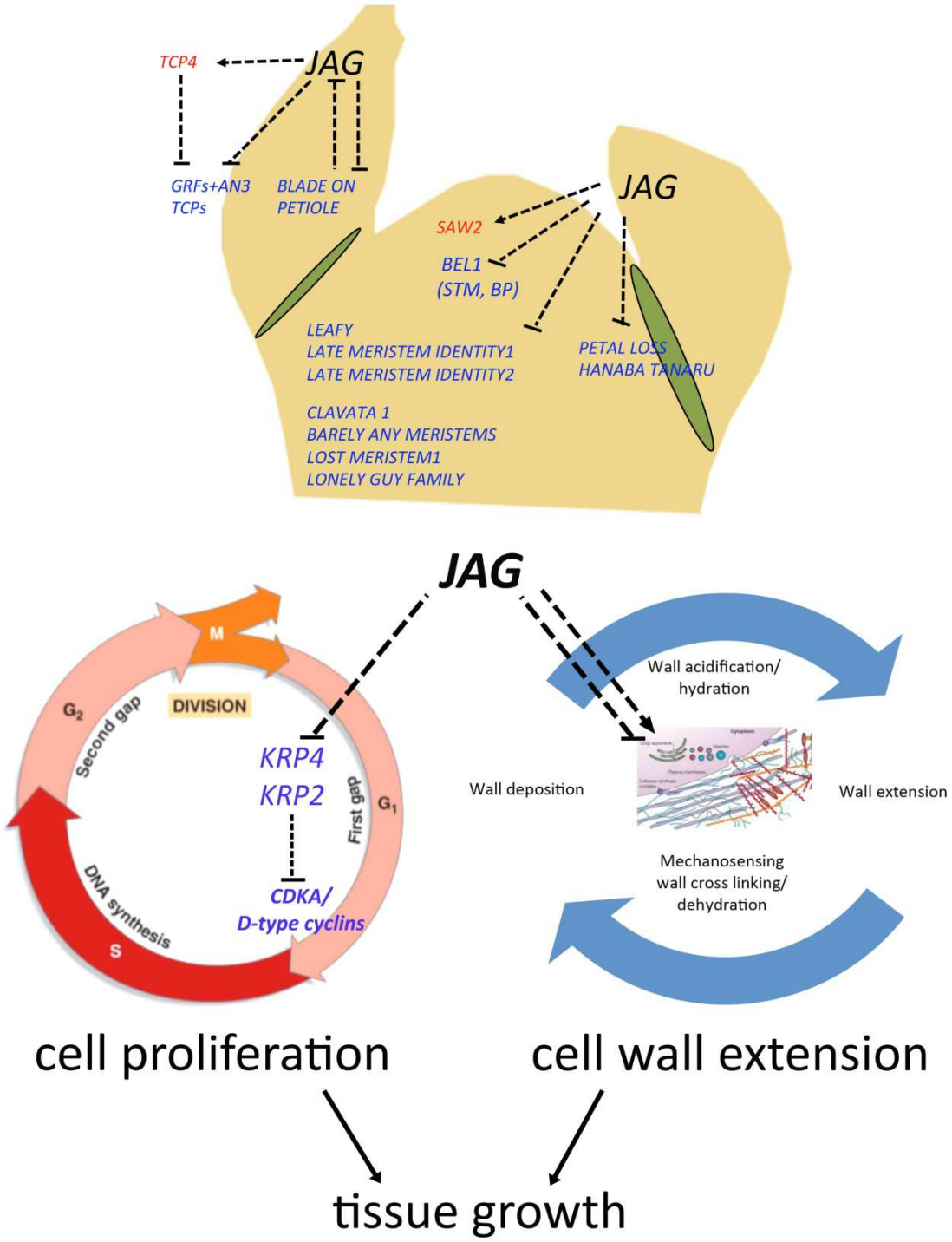

Figure 10.1 Overview of the gene candidates and functions that are targeted by JAG to promote tissue growth. This includes the repression of meristem organisation genes and boundary specifying genes, and the interaction with organ patterning genes and growth regulatory pathways. At cellular level, JAG promotes cell proliferation and cell growth and modulates the coordination of both processes by directly repressing KRP2 and KRP4, two regulators of the core cell cycle machinery and by directly targeting genes involved in cell wall-related growth processes.

Chapter 10 - Material and Methods

10.1. Plant material

10.1.1. Plant lines

Arabidopsis thaliana Landsberg-*erecta (*L-*er)* was used as wild type for the expression profiling, ChiP experiments and quantitative 3D imaging experiments*. Arabidopsis thaliana Columbia (Col)* was used as the wild type for imaging experiments.
The T-DNA insertion line *jag-1* was originally used in *Col* (Dinneny et al., 2004), and backcrossed three times into L-*er*. The EMS mutant *jag-2* in L-*er* background (Ohno et al., 2004) was identified to have a single nucleotide change (C/T) in the second exon that introduced a stop codon. The T-DNA insertion lines *krp2-3* and the *krp4-1* were identified from the SALK T-DNA insertion mutant collection and were used in *Col* background. The loss of function allele *krp2-3* (SALK_110338) has an insertion in the first exon and the loss of function allele *krp4-1* (SALK 102417) has an insertion in the second exon. The *krp4-2* allele (GT1143) was identified in L-*er* background from a transposable element gene trap mutant screen (Sundaresan et al., 1995).

10.1.2. Growth conditions

Fume sterilised seeds were germinated on growth medium (GM) (1 litre containing 1% glucose, 4.4 g Murashige and Skoog salts and vitamins (Duchefa), 3 ml of 0.85 M 4-morhpolineethanesulfonic acid (MES) buffer pH 5.7, adjusted to pH 5.7 with 1 M KOH, 0.9% agar added) and stratified for 48 h at 4 °C in the dark. Seeds were germinated under long day conditions (16 h light and 8 h dark) at 21° C. For seedlings grown on selection medium, 50 µg/ml Kanamycin, 100 µg/ml Gentamycin or 10 µg/ml Basta were added to the liquid but cooled down GM, according to the resistance. For JAG-GR activation in seedlings, seeds of plant lines harbouring the *35S:JAG-GR* construct were germinated on GM supplemented with 10 µM DEX and 0.01% ethanol.
Seedlings were transferred to JIC Arabidopsis Soil Mix Levington F2 compost with Intercept and grit at a 6:1 ratio. For all experiments, except quantitative 3D imaging experiments, plants were grown under long day conditions (16 h light and 8 h dark) at 18 °C day temperature and at 20 °C night temperature at 80% humidity. For quantitative 3D

imaging, plants were grown on JIC Arabidopsis Soil Mix at 16 °C under continuous light until flowering.

10.1.3. Seed sterilisation

10.1.3.1. Fume sterilisation of Seeds

Seeds (up to 500 µl) were filled into Eppendorf tubes and placed into an air-tight container with a beacon filled with 100 ml sodium hypochlorite (Sigma) in a flow hood. In order to produce chlorine fume 3 ml of hydrochloric acid 36% were added to the sodium hypochlorite and the desicator lid swiftly closed. Seeds were fume sterilised for 3 to 4 h.

10.1.3.2. Sterilisation of T0 transgenic seeds after floral dip transformation

Seeds harvested from floral dip transformation (Clough and Bent, 1998) were sterilised using Dichloroisocyanuric Acid Sodium Salt. Seeds (up to 500 µl) were filled into 2 ml Eppendorf tubes and 1 ml of Dichloroisocyanuric sterilisation solution was added. The Dichloroisocyanuric sterilisation solution was prepared in a volume of 20 ml containing 2.5 ml Dichloroisocyanuric stock solution 5% (1 g of salt dissolved in 20 ml of aqua dest), 10 ml ethanol 100% and 7.5 ml aqua dest). Seeds were incubated in the Dichloroisocyanuric sterilisation solution by gentle inversion for not longer than 12 min. Seeds were left to settle at the bottom of the Eppendorf tube for 1 min. Then, the solution was removed under the fumehood and seeds were washed twice with 1 ml ethanol 100%. After the last wash, seeds were left to dry under a sterile flow hood.

10.1.4. CTAB genomic DNA extraction

CTAB DNA extraction was used for genotyping and to obtain template DNA for cloning purposes. Plant tissue from young rosette leaves was collected in 1.5 ml Eppendorf tubes and snap-frozen in liquid nitrogen. Leave tissue was ground to fine powder in the 1.5 ml Eppendorf tubes using plastic pestles. Subsequently, 500 µl of CTAB-extraction buffer containing 100 mM Tris pH 8, 1.4M NaCl, 20 mM EDTA pH 8, 20 mg Hexadecyltrimethylammoniumbromide (CTAB)/ml buffer and 2 µl ß-mercaptoethanol/ml buffer were added to the ground frozen powder and homogenised briefly. Samples were incubated at 65 °C for 45 min. Samples were centrifuged at full speed for 10 min. The supernatant was transferred to a fresh tube, 500 µl of Chloroform:Isoamyl Alcohol 24:1

were added and the tubes inverted several times. Samples were centrifuged at full speed for 10 min and 500 µl of the supernatant were transferred into a fresh Eppendorf tube with 50 µl (1/10 of the supernatant volume) of 3M sodium acetate pH 5.6, 1 µl of glycogen and 500 µl (equal amount of the supernatant volume) of isopropyl alcohol added. For precipitation, samples were left at -20 °C for 20 min and subsequently centrifuged at full speed for 20 min. The DNA pellet was washed with 500 µl of 70% EtOH in a six-min centrifugation step and subsequently left to air-dry. The DNA pellet was re-suspended in 100 µl of water or TE buffer and stored at -20 °C for further use.

10.1.5. Genotyping

10.1.5.1. PCR genotyping

Genomic DNA obtained from CTAB DNA extraction was used as template to genotype plant lines by PCR. PCRs were performed in 50 µl-reactions (34.5 µl aqua dest, 2 µl genomic DNA, 5 µl 10x Taq Buffer (Roche), 1 µl 10 mM dNTPs, 0.5 µl Taq (home-made), 1 µl reverse oligo 10 µM diluted in water, 1 µl forward oligo 10 µM diluted in water. For genotyping a touch-down PCR programme was used with the following PCR programme parameters: 94 °C for 3 min as an initial denaturation step, followed by a denaturation step at 94 °C for 30 sec, annealing step for 30 sec starting from 65 °C in the first cycle, reduced by 1 °C in each following cycle down to 55 °C, followed by an extension step at 72 °C for 1 min, after the touchdown 25 cycles with annealing temperature 55 °C followed and a final elongation step at 72 °C for 10 min. The oligonucleotide combinations used for genotyping are summarised in the list below. In order to genotype SALK and SAIL T-DNA insertion lines, the primer design software tool from the SALK institute http://signal.salk.edu/tdnaprimers.2.html was used. To genotype the EMS mutant *jag-2* the primer design software tool dCAPS Finder 2.0 (Neff et al., 2002) was used.

10.1.5.2. Genotyping Oligonucleotides

T-DNA insertion line *jag-1*

jag-1 mutant allele

JL202 CATTTTATAATAACGCTGCGGACA

N0681 GGATCCAACTCAGAGCGAGTGATGATCTTG

Product size: estimated 1200 bp

JAG wild type

OJD126 TTAGTTTCCACACGCAGAGAGAG

OJD127 TCATGTGGCCACCAAGAGCTTG

Product size: estimated 500 bp

EMS mutant line *jag-2*

dCAPS (derived cleaved amplified polymorphic sequence) marker

jag2EMS-F CAGAACTTGAGTGAACAAAGTC,

jag2EMS-R AGCCCTCGAGGAAGGTTCT,

Product size 279 bp, when digested with SalI, WT digested – 30 bp,

mutant remained undigested

GABI-Kat line NUBBIN

nub (GK-244A08-014390)

T-DNA pAC161 CCCATTTGGACGTGAATGTAGACAC

GABI-Kat(OJD 153-R) AAGACAGCGGAGGATAAAGATATG

Product size: 500 bp

NUB wild type

ZINF3-F (OJD 154-L) GAGGGTTTAGAGAGAAGCAAAC

GABI-KAT(OJD 153-R) AAGACAGCGGAGGATAAAGATATG

Product size: 763 bp

SALK lines (WT=LP+RP, mutant=SALK_LB1+RP)

SALK_LB1 GCGTGGACCGCTTGCTGCAAC T

***KRP2*, *ICK2* (AT3G50630) SALK 130744**

krp2-1_LP ACGCGAGCTAGAGACTCTCTAGTAGA

krp2-1_RP TGGATTCAATTTAACCCACTCG

Product size: 1106 bp (wild type), 545-845 bp (*krp2-1* mutant)

KRP2, ICK2 **(AT3G50630) SALK_110338**

krp2-3_LP CGGTTAGGAGAAGAGAACGAG

krp2-3_RP TCGAAGTTGTACTTCTCCATGA

Product size: 1096 bp (wild type), 432-732 bp (*krp2-3* mutant)

KRP4, ICK7 **(AT2G32710) SALK_102417**

krp4-1_LP TGGTTAAAATTGAAACTGGCG

krp4-1_RP CCTGGTAGTGGTTGTTCGTTC

Product size: 1087 bp (wild type), 464-764 bp (*krp4-1* mutant)

CYC-P4;1**(AT2G44740) SALK_118728**

cycp4;1_LP TCACTAGTGTCATGGTCGCTG

cycp4;1_RP TGCTCTGCACATGTTCTTTTG

Product size: 1201 bp (wild type), 592-892 bp (mutant)

SAIL lines (WT=LP+RP, mutant=SAIL_LB1+RP)

SAIL_LB1 GCCTTTTCAGAAATGGATAAATAGCCTTGCTTCC

CYCLIN P3;1 **(AT2G45080) SAIL_764_C11**

cycp3;1_LP 5'CTTTCGAAACTCACAACGCTC3'

cycp3;1_RP 5'AAATCGCTAGGGAATCCATTG3'

Product size: 1199 bp (wild type), 537-837 bp (mutant)

KRP4, ICK7 **(AT2G32710) GT1143 (insertion in first intron)**

Gene trap transposable element with GUS-reporter (Sundaresan et al. 1995)

GT1143_F TGGAGGTGAATCCTCTATTGC (ATG+74 bp)

GT1143_R ATCAAACTGCATGGTGTGGA (ATG+612 bp)

Ds5I_R GGTAGTCGACGAAAACGGAACG

Product size: 546 bp (wild type), estimated 900-1000 bp (mutant)

10.2. Generating transgenic lines

10.2.1. Cloning of constructs

All cloning strategies were based on classic restriction digest and ligation cloning. Inserts were amplified using Phusion DNA polymerase, HF buffer supplemented by $MgCl_2$ using a touchdown PCR protocol (initial denaturation step for 98 °C for 5 min, followed by a denaturation step at 98 °C for 30 sec, annealing step for 30 sec starting from 65 °C in the first cycle, reduced by 1 °C in each following cycle down to 55 °C, followed by an extension step at 72 °C for 30 sec – 3 min according to amplicon length, after the touchdown 20-25 cycles with annealing temperature 55 °C followed and a final elongation step at 72 °C for 10 min. Amplicons were purified with Qiagen PCR purification kit according to the manufacturer's instructions and eluted in 25 µl elution buffer. For all restriction digests in all cloning steps restriction enzymes from Roche and New England Biolabs with incubation conditions according to the manufacturers' instructions were used. After restriction digest, inserts and plasmids were purified either by phenol purification and ethanol precipitation or separated on a 1% agarose gel, excised and purified using the QIAQUICK GEL EXTRACTION KIT (Qiagen). For phenol purification of restriction and ligation reactions, reactions were brought to a volume of 100 µl with aqua dest and 100 µl Phenol:Chloroform:Isoamyl Alcohol 25:24:1, saturated with 10 mM Tris pH 8.0, 1 mM EDTA (P2069, Sigma) were added and gently inverted. After a 10-min centrifugation step, the supernatant was transferred to a new Eppendorf tube for ethanol precipitation. For ethanol precipitation, reactions were supplemented with 1/10 of reaction volume 3M sodium acetate pH 5.6, 1 µl of glycogen and 2.5 of reaction volume of 100% ethanol. DNA was precipitated at -20C for 20 min and centrifuged at max speed for 20 min. The supernatant was discarded and the DNA pellet was washed with 300 µl ethanol 70% by centrifuging at max speed for 7 min. Subsequently, the DNA pellet was left to dry and re-suspended in 20-25 µl water. In order to calcµlate the amount of vector and insert for the ligations, amount and quality of insert and vector DNA was measured using a NanoDrop (Thermofisher). Ligations were performed using T4 Ligase (Roche) either overnight at 4 °C or for 8 h at 16 °C. Ligations were phenol-chloroform purified and ethanol precipitated and resuspended in 20 µl of water.

Vectors were dephosphorylated by shrimp alkaline phosphatase (Roche) following the manufacturers instructions. For initial cloning and subcloning steps, *Bluescript KS* conferring resistance to ampilicin/carbenicilin (100 µg/ml) was used. For plant transformation, final constructs were inserted into the binary vector *pPZP222* conferring resistance to Spectinomycin (100 µg/ml) in bacteria and Gentamycin (100 µg/ml) resistance in plants or into the binary vector *pCGN1547* conferring resistance in gentamycin (25 µg/ml) resistance bacteria and Kanamycin (50 µg/ml) resistance in plants. For all plant transformations the *Agrobacterium* strain *ASE* conferring resistance to Kanamycin (50 µg/ml) and Chloramphenicol (30 µg/ml) was used.

10.2.2. Electroporation of *E. coli* and *Agrobacterium*

Plasmid DNA was transformed into *Escherichia coli* strain *DH5α* for cloning purposes and into *Agrobacterium tumefaciens* strain *ASE* for stable plant transformation purposes using electro-competent cells. For transformation 50 µl of electro-competent cells were thawed on ice and between 2 µl and 5 µl of plasmid DNA derived from purified ligation reactions or mini-preps were added. The bacterial suspension was transferred to a pre-cooled transformation cuvette and placed into a Biorad Genepulser. For electro-transformation the following settings were applied using the Biorad Genepulser: Capacitance extender 250 µFD, Capacitance 25 µFD, Voltage 2.5 KV and Pulse Controller for *E.coli* at 200 Ω resistance and for *Agrobacterium* 400 Ω resistance with variable time constants. After electroporation, 900 µl of ice-cold SOC medium (10 ml LB medium supplemented with 200 µl 1M magnesium chloride, 200 µl 1M magnesium sulphate and 400 µl 20% glucose) were added to the cuvette and the bacteria suspension was transferred to a 1.5 ml Eppendorf tube. Subsequently, transformed *E. coli* were incubated at 37 °C for 1 h and transformed *Agrobacteria* were incubated at 28 °C for 1.5 h. Bacterial suspension (800 µl) were divided into 100 µl and 700 µl aliquot and spread on plates containing LB medium supplemented with antibiotics for selection. Plates were incubated at 37 °C overnight for *E.coli* and at 30 °C for 2 days for *Agrobacterium*. Single colonies were picked and transferred to 10 ml of liquid LB medium supplemented with antibiotics for selection. Liquid cultures were incubated in a shaker (200 rpm speed) at 37 °C and 28 °C for *E. coli* and *Agrobacterium*, respectively until liquid cultures reached log-phase.

Plasmid DNA was purified from *E.coli* cultures using Qiagen Miniprep Kit following the manufacturers' instructions.

10.2.3. Plant transformation

For plant transformation the floral dipping method (Clough and Bent, 1998) was used. Prior to transformation, presence of the binary vector was confirmed by colony PCR. 1 µl of liquid culture in 50 µl of water heat at 98 °C for 10 min. 1 µl of denatured diluted culture was used as a template in a 50 µl PCR reaction (1 µl of 10 µM dNTP mix, 1 µl of 10 µM oligo forward/reverse, 10X PCR-buffer and 0.5 µl home-made Taq-polymerase).
To grow *Agrobacterium* for transformation, 400 ml LB were inoculated with a 10 ml liquid culture in log-phase and incubated in a shaker at 28 °C to log-phase. To harvest the *Agrobacterium* cells, the liquid culture was centrifuged in a pre-cooled centrifuge at 3000 rpm for 20 min at 4 °C with centrifuge brakes blocked. The supernatant was discarded and the bacterial pellet was resuspended in 500 ml of ice-cold transformation media containing 25 g sucrose, 2.15 g MS salts plus vitamins adjusted to pH 5.8 with KOH suplemented with 150 µl Silwet L-77. For floral dip transformation, flowers (with siliques removed) were submerged into the bacterial suspension for 45 sec and subsequently transferred into plastic bags for 24 h and left in the dark. For seed collection, plants were grown in a containment glasshouse for 2 weeks. After 2 weeks plant were bagged and watering reduced.

10.3. Generating constructs

10.3.1. Construction of *p35S:JAG-GR*

JAG cDNA derived from wild type L*er* flowers was amplified from plasmid *pRS338* with primers 220901-F and 220902-R introducing a *BamHI* site at the start codon and a *BglII* site replacing the stop codon. The *p35S::JAG:GR* construct was generated following the cloning strategy described in Gallois et al. (2002) resulting in the Asp718-35S-BamHI-*JAG* cDNA-GR-nos-terminator-XbaI construct. The construct was transformed into L-*er* wild-type plants using the binary vector *pCGN1547* and *Agrobacterium* strain *ASE* by floral dip transformation (Clough and Bent, 1998). Plant line 22.11.3.27 was identified being homozygous with a single insertion for *p35S:JAG-GR* and showed ectopic expression

phenotype upon treatment of inflorescences with 10 µM dexamethasone (D1756, Sigma) in 0.1% EtOH. To confirm that the construct can complement the mutant phenotype, line 22.11.3.27 was crossed to *jag-2*.

10.3.2. Construction of *pJAG:JAG-GFP*

A 9.7 kb genomic fragment of *JAG* (location 25682925 – 25692696 antisense) was amplified from the transformation-competent artificial chromosome (TAC) clone *JATY67024* (Genome Enterprise Ltd) in two separate fragments. The fragment spanning the region 1.618 bp downstream of the stop codon was amplified using the primers 221001F and 221002R introducing a *KpnI* site at the 5'end and replacing the endogenous stop codon by an *NcoI* site and a stop codon 3 nucleotides downstream of the *NcoI* site. In a second PCR, a *PstI* site was introduced using primers 221001-F and 221003-R in order to clone the fragment into *pBluescript KS (-)* as a *KpnI* and *PstI* insertion.

For amplification of the fragment comprising the full-length genomic fragment of 1.623 bp and the regulatory sequence spanning 6.531 bp upstream the 5' UTR, primers 221004-F and 221005-R were used to introduce an *NcoI* site at the 5' end and a *BamHI* site at the 3'end. For in frame fusion of the two fragments via the *NcoI* site, the *pBluescript KS (-)* vector harbouring the 1.618 bp fragment was digested with *NcoI* and *BamHI* in order to take up the 5'fragment (8.141 bp). Subsequently, the joined fragment with final size of 9.7 kb was cloned into the binary vector *pPZP222*. The *pJAG::JAG:GFP* translational fusion was generated by insertion of the *sGFP S65T* fragment that was amplified with primers 221006F and 221007R introducing an *NcoI* site at both ends. The *pJAG::JAG:GFP* construct was transformed into *jag-2* using *Agrobacterium* strain *ASE* by floral dip transformation (Clough and Bent, 1998).

10.3.3. Construction of *KRP2:KRP2-GFP*

The construct for the *KRP2::KRP2-GFP* protein fusion was cloned and transformed into wildtype and *jag-1* loss of function background. The genomic fragment of *KRP2* (Chr3:18796861–18802701) including the promoter region (3647 bp), the genomic region (859 bp) were amplified as a single fragment from wild-type L-*er* genomic DNA introducing a *BamHI* at the 5' and an *NcoI* site at the 3' end replacing the stop-codon. The 3'end (1334 bp) was amplified introducing an XhoI followed by an *NcoI* site at the 5' end and a *KnpI* site at the 3'end. Both fragments were fused at the *NcoI* site in *pBluescript KS*

(-). In a second step, the *sGFP S65T* (Chiu et al., 1996) coding sequence was amplified introducing *NcoI* sites at both ends allowing in frame insertion into the *NcoI* site generated at the C-terminal end of the coding sequence of *KRP2*. In a third step, the *pKRP2::KRP2-GFP* construct was cloned into the binary vector *pCGN1547 conferring kanamycine resistance in plants*. Wildtype and *jag-1* plants of L-*er* and *Col-0* background were transformed.

10.3.4. Construction of *KRP4:KRP4x-CYPET* reporter construct

KRP4:KRP4x-CYPET line with the cyan fluorescent protein *CYPET* replacing the last intron and exon of *KRP4* genomic fragment at the C-terminus but retaining the 1.35 kb 3' end. The genomic fragment of *KRP4* (Chr2:13873436-13875831) including the promoter region (1338 bp), the genomic region including the first exon (578 bp), the first intron (871 bp), and 32 bp from the second intron were amplified as a single fragment of 2.819 bp total length from wild-type L-*er* genomic DNA. In this fragment restriction sites were introduced on either side, an *XbaI site* at the 5'end and a *BamHI* site at the 3', which allowed for subcloning into *pBluescript KS (-)* and final cloning into the binary vector *pCGN1547.* In order to join the 5' fragment with the 3' fragment and to allow for subsequent insertion of the *CYPET* construct, an *NcoI* site was introduced in frame in the second exon upstream of the *BamHI* site. The 3' fragment (1334 bp) starting 8 bp downstream of the genomic stop codon was amplified introducing an *NcoI* site at the 5'end and a *BamHI* site at the 3'end. In the next step, the 5' fragment was cloned into *pBluescript KS (-)* using the generated *XbaI* and *BamHI* restriction sites. Subsequently, the 3' fragment was inserted using the *NcoI* and *BamHI* sites. For the *CYPET* cyan fluorescent reporter protein, the *CYPET* (Genbank: AEH43768) coding sequence was amplified from the cloning vector *pBOB* (GenBank: JF927991.1 by Wachsman et al. (2011)), excluding the C-terminal ER localisation signal by introducing a stop codon at 783 bp. At both ends, *NcoI* sites were introduced, allowing for in frame insertion into the *NcoI* sites of the *KRP4* construct. In a final step, the *pKRP4::KRP4x-CYPET* construct was cloned into the binary vector *pCGN1547* conferring kanamycin resistance in plants. Wild-type and *jag-1* plants of L-*er* and *Col-0* background were transformed.

10.3.5. Cloning probes for RNA *in situ* hybridisation

To generate the templates for probe synthesis, *BEL-1* cDNA (1635 bp) was amplified from reverse transcribed RNA of L-*er* wild type inflorescence using primers BELBamHI-F and BELXbaI-R. The generated *BEL-1* cDNA and *BP* cDNA (995 bp) from glycerolstock 641 were cloned into *pBluescript KS(–)* as *BamHI-Xba* and *BamHI-EcoRI* insertions, respectively. For *STM*, the cDNA construct previously cloned into *pBluescript KS (-)* as *BamHI-XbaI* insertion by Gallois et al. (2002) was used.

To generate templates for probe synthesis, *KRP2* and *KRP4* cDNA was amplified from reverse transcribed RNA of L-*er* wild-type inflorescence using primers KRP2BamHI-F and KRP2XbaI-R, and KRP4BamHI-F and KRP4EcoRI-R, respectively. Both, the *KRP2* fragment (594 bp) and the *KRP4* fragment (553 bp) were designed to avoid the C-terminal region, which has been reported to be highly conserved between the seven members of the Kip-related protein family (de Veylder et al., 2001).

10.3.6. *JAG* cDNA with C-terminal poly-His tag fusion in *pEAQ-specialK*

In order to transiently express JAG in *Nicotiana benthamiana*, *JAG* cDNA was cloned into the *pEAQspecialK* vector (kindly provided by the lab of George Lomonossoff, JIC). The *pEAQ-specialK* vector system allowed for a poly-His tag fusion to the JAG protein on either terminus. To generate a C-terminal poly-His tag fusion, *JAG* cDNA was amplified from plasmid *pRS338* using primers P19CtNruI-F and P19CtXma-R that introduced *NruI* site at the 5' end and a *XmaI* site at the 3' end substituting the stopcodon. The fragment was cloned into *pEAQ-specialK* (Sainsbury et. al., 2009) as an *NruI-XmaI* insertion generating *JAG* cDNA fused to a C-terminal poly-His tag. Subsequently, the *pEAQ-specialK* vector containing the C-terminal poly-His tag sequence fused to the *JAG* cDNA was transformed into the *Agrobacterium* strain *LBA4404* (Sainsbury et al., 2009).

10.3.7. *JAG* cDNA with N-terminal poly-His tag fusion in *pRSETA*

In order to ectopically express *JAG* in the *E.coli* strain *BL21* and to purify the JAG protein by immobilised metal affinity chromatography, *JAG* cDNA was fused to an N-terminal poly-His tag downstream of the viral, IPGT inducible *T7* promoter using the vector system *pRSETA* (Invitrogen). For directional cloning, *JAG cDNA* was amplified from plasmid pRS338 using primers pRSETABamHI-F and pRSETAHindIII-R which introduced a *BamHI* and a *HindIII* restriction site at the 5' end and the 3' end, respectively.

Subsequently, the fragment was cloned into pRSETA plasmid as a *BamHI-HindIII* insertion resulting in JAG full-length cDNA with an N-terminal poly-His tag fusion. The plasmid was transformed into the *E.coli* strain *BL21* conferring resistance to chloramphenicol (35 ug/ml) and carbenicilin (50 ug/ml).

10.3.8. Cloning oligonucleotides

Construction of *p35S:JAG:GR*

220901-F CTGCGGATCCATGAGGCATGAGGAG

220902-R GGATAGATCTAGCGAGTGATGATCTTGAAAC

Construction of *pJAG::JAG:GFP*

221001-F TAGAGATTCGGGTACCTCACATAGTC

221002-R GCCCAT GGTTTAATAG

221003-R AGATCATCTGCAGCCCATGGTTTA

221004-F AACCATGGGCGAGTGATGATCTTG

221005-R GACTCTAATGGATCCG AGTTTATGCT

221006-F AAAACCATGGTTACTTGTACAGCTCGTCCAT

221007-R AAAACCATGGTGAGCAAGGGCGAGGAGCTG

Construction of *KRP2:KRP2-GFP*

5'KRP2BamHI-L AAAAGGATCCACTTGAGAAAGTGATCTGC

5'KRP2NcoI-R CATCGTCTTCACCATGGATTCAA

3'KRP2XhoNcoI-L TTAACTCGAGTCCATGGTGAAGACGATG

3' KRP2KpnI-R TTTTGGTACCTTCTCGCATCTTTGTGTTG

KRP2GFPNcoI-L AAAACCATGGGTGAGCAAGGGCGAGGA

KRP2GFPNcoI-R AAAACCATGGCTTGTACAGCTCGTCC

Construction of *KRP4:KRP4x-CYPET* reporter construct

5'Xba-F AAAAACCATGGGAGCAAGGGAGAGGAAC

5'NcoBamHI-R AAAAACCATGGTTAGTACAGTTCGTCCATG

3'Nco-F AAAACCATGGGGGGTTAATAGTTAAT

3'BamHI-R CCAAGGATCCATCAAAACAAGGCCATG

CYPETNcoI-F AAAACCATGGAAGACTAATCTTTTTCTC

CYPETNcoI-R AAAACCATGGTTAGTACAGTTCGTCCATG

Cloning probes for RNA *in situ* hybridisation

BELBamHI-F GATTAATCgGATCCAAGGGTT

BELXbaI-R CCTTGAGCCGTCtCTaGAGAC

KRP4BamHI-F TGGAGGTGGATCCTCTATTGC (=KRP4_cDNAENTRY-F)

KRP4EcoRI-R GTGTGAATTCCCTTGTGGTCCT (=KRP4_cDNAENTRY-R)

KRP2XbaI-R ATGGatcCGGTTAGGAGAAGAGAA

KRP2BamHI-F ACCAAGTGGCTCATCTTTCTaGAAA

Construction of *JAG* cDNA with C-terminal poly-His tag fusion in pEAQ-specialK

P19CtNruI-F TACCCTGCTCGCGAATGAG

P19CtXma-R GGACCCGGGGAGCGAGTGAT

JAG* cDNA with N-terminal poly-His tag fusion in *pRSETA

pRSETABamHI-F CTGCGGATCCAAGAGGCATG

pRSETAHindIII-R CACGCTCGAGTCAGAGCGA

10.4. Dexamethasone treatment for expression profiling

For JAG-GR activation, a 0.015% Silwet L-77 (De Sangosse) solution supplemented with 0.1% ethanol (control treatment), 10 µM dexamethasone (D4902, Sigma) with 0.1% ethanol, 10 µM dexamethasone, 0.1% ethanol and 10 µM cycloheximide (C7698, Sigma) or 10 µM cycloheximide, 0.1% ethanol (control treatment in the presence of cycloheximide) was pipetted into the centre of inflorescences of wild-type L-*er* plants harbouring the *35S:JAG-GR* construct in two rounds of applications with about 250 µl of solution each. In addition, for the *jag* loss of function mutant versus wild-type comparison in the expression array experiment, inflorescences of *jag-1* L-*er* plants were mock treated with a 0.015% Silwet L-77 (De Sangosse), 0.1% ethanol solution. After 5 h (for the expression array experiment) and 4 h (for qRT-PCR experiments) in daylight conditions, inflorescence apices (only unopened flower buds) of 12 plants were collected per sample in three biological replicates per treatment and snap-frozen in liquid nitrogen.

10.5. Global expression profiling using the Affymetrix gene chip ATH1

RNA extraction was performed using RNEasy plant mini kit (74904 QIAGEN) according to the manufacturer's instructions and eluted in 30 µl of RNAse free water. Amount and quality of the RNA were measured using a Nanodrop to ensure that the 260/280 ratio was above the minimum of 2 and not lower than 1.80 and the 260/230 ratio was between 2.00 and 2.20, according to the manufacturer's instructions (Thermo Fisher Scientific). Concentrations were adjusted if necessary to achieve the required aliquots of 100 ng/µl (1 µg of total RNA in 10 µl aliquots per sample), as recommended for chip hybridisation by the Nottingham Arabidopsis Stock Centre, UK. The RNA was reverse transcribed and cDNA was hybridized on the *Arabidopsis thaliana* Affymetrix gene chip ATH1 at the Nottingham Arabidopsis Stock Centre, UK; the raw data and experiment metadata are available at http://affymetrix.arabidopsis.info/, experiment ID: NASCARRAYS-605. To select genes with significant differential expression, raw expression values obtained from each hybridized chip were imported in an R session (http://www.r-project.org/). The probe-set to gene annotation *ath1121501cdf* was downloaded from Bioconductor (http://www.bioconductor.org/). Data was normalized using the package GCRMA (Gharaibeh et al., 2008) and differential expression was tested using a *t*-test statistic. False Discovery Rate (FDR) was controlled by the method described by Benjamini and Hochberg (1995) and implemented in the bioconductor package *multtest*. Probe-sets targeting more than one TAIR10 gene and genes associated with multiple probe sets were discarded from the analysis at this point. A gene was considered differentially expressed when FDR<0.01 and the absolute value of the log2 ratio was larger than 0.5.

10.6. Quantitative reverse transcription-polymerase chain reaction (qRT-PCR)

10.6.1. RNA extraction and DNAse treatment

RNA was extracted using the RNEASY PLANT MINI KIT (74904 QIAGEN) according to the manufacturer's instructions and total RNA was eluted in 50 µl of RNAse free water. Total RNA was DNaseI treated with AMBION DNA free (AM1906, Invitrogen). In order to obtain 2 µg of total RNA after DNAse treatment with DNA-free from AMBION, 5 µg of eluted

RNA/DNA elute were DNAse treated in a total volume of 30 µl with 3 µl of 10X buffer and 2 µl of DNAseI for 1 h at 37° C according to the manufacturer's instruction. After DNAse treatment samples were measured and checked for good quality using the Nanodrop with RNA settings, resulting in average RNA concentrations of 80-150 ng/µl.

10.6.2. Reverse Transcription using DNAse treated RNA

Subsequently, reverse transcription (cDNA synthesis) was performed using 2 µg of DNAse treated RNA resulting in a final volume of 80 µl of final cDNA template. For this, 2 µg of RNA were incubated with 3 µl of Oligo dT (12-18) with a concentration of 0.5 µg/µl (18418-012l, Invitrogen) and 3 µl of dNTP mix (A, T, G, C) 10 µM each (Roche), (RNAse free water was used to add up to a total volume of 50 µl) for 5 min at 65° C to anneal the oligos and placed on ice for 1 min. Subsequently, 12 µl of 5X First Strand Buffer (supplied with the Superscript III enzyme), 3 µl of RNasin RNAse inhibitor (N2111, Promega), 3 µl of 0.1 M DTT (supplied with the Superscript III enzyme), 10 µl of RNAse free water, and finally 3 µl of SuperScript III Reverse Transcriptase (Invitrogen 18080-044) were added to result in a total volume of 80 µl. For reverse transcription the reactions were incubated at 50° C for 50 min in a PCR machine with heated lid, followed by 15 min at 70° C for deactivation of the reverse transcriptase.

10.6.3. qRT–PCR using the LightCycler LC480 system

For quantification of transcript levels, qRT-PCR was performed in technical triplicates in the LightCycler 480 System using LIGHTCYCLER 480 SYBR GREEN I MASTER (04707516001, Roche) in a total reaction volume of 10 µl, containing 5 µl of LIGHTCYCLER 480 SYBR GREEN I MASTER, 2 µl of the forward and reverse oligo mix (5 µM), 1 µl of cDNA template, and 2 µl of PCR-grade water (Roche). The reaction was performed in an LC 480 qPCR-cycler (Roche) using a standard programme with 5 min at 95° C, 40 cycles of 10 sec at 95° C, 15 sec at annealing temperature (usually 60 °C) and 15 sec at 72 °C. After each cycle, the SYBR GREEN signal was measured. The 40 cycles were followed by a melting curve starting from 65 °C to 98 °C. Data was saved as .ixo file format and analysed using the LC480 software and Excel (Microsoft). Data were analysed by applying $2^{-\Delta Ct}$ method (ΔCt = Ct gene of interest – Ct *ref gene*), using *ACTIN*2 (ACT2-F, ACT2-R) or TUBULIN alpha 4 chain expression (TUB4-RT_1-F, TUB4-RT_1-R) for normalisation (Livak and Schmittgen,

2001). Unpaired two-sample Student's t test was used to test for significant differences in expression levels.

10.6.4. Designing and testing oligos for qRT-PCR

For designing oligos for expression analysis, the primer design tool "quantprime" http://quantprime.mpimp-golm.mpg.de/ was used. Oligos were diluted in PCR-grade water to 100 µM stock solutions as recommended by the supplier (Sigma). Working dilutions were prepared to contain the forward and reverse oligo in a concentration of 2.5 µM each. The amplification efficiency of qRT-PCR oligos was tested using a dilution series of the dilution factors 1, 0.5, 0.2, 0.1 and 0.06 of mixed cDNA templates of the cDNA templates to be tested, including a water/non-template control in three technical replicates. The amplification efficiency of qRT-PCR oligo pairs was generally tested at an annealing temperature of 60 °C. The LC480 software was used to generate standard curves and to calculate the slope (optimum -3.3), the oligo amplification efficiency (amplification factors between 1.85 and 2 (=100%) were considered as acceptable). In addition, it was checked that the melting curve gave one single clear peak and that the non-template controls did not give any signal.

10.6.5 List of qRT-PCR oligonucleotides (5' – 3')

ACT2-RT_F	ATGGAAGCTGCTGGAATCCAC
ACT2-RT_R	TTGCTCATACGGTCAGCGATG
TUB4-RT_F	CTGTTTCCGTACCCTCAAGC
TUB4-RT_R	AGGGAAACGAAGACAGCAAG
BEL1-RT_F	AGTGACAAACCCTACATCCA
BEL1-RT_R	CGTATGTCACAGCTTGGTTA
BP-RT_F	CATGTCTTCAGATGGTTTCC
BP-RT_R	AGTCAGAGAAGGTAGCGTTG
STM-RT_F	ACCTTCCTCTTTCTCCGGTTATGG
STM-RT_R	GCGCAAGAGCTGTCCTTTAAGC
CLV1-RT_L	AGCTTCCACGGCTACTCTAT
CLV1-RT_R	AGTACATGCCTAATGGAAGC
LMI1-RT_L	CGATGAGGTGAAGAAGCTGAGAGC

LMI1-RT_R	TGATGGTCCCGGCAGAGATTTG
SAW2-RT_L	GCCTGAACGCTCCGTTAATATCC
SAW2-RT_R	TATCAGCATCGCTTGGGTACGG
JAG-RT_F	ACATGAATCGCCACCGACAAGAG
JAG-RT_R	CGTTACGGTAGACCAATTGACGAG
PTL-RT_F	GAAGGAAAAAGAGGAGTTGG
PTL-RT_R	GTCAACTTCTCAAGCCAAAC
TCP4-RT_L	GCCGTCCTCTGCTTCCTCTATTTC
TCP4-RT_R	TGGAAGCTAGACAAGCCCTGAAAC
TCP3-RT_L	ACAAGCCGTCCTCTGCTTCATC
TCP3-RT_R	CATTCGAAGCGCCCTGGAATATG
TCP10-RT_L	ACACAGTCGTAGTTCCCGAGAC
TCP10-RT_R	TCCCGAACGTGTCGAAATGAGTC
GRF5-RT_L	CACTCAAGACTCGACAACTGGTAGC
GRF5-RT_R	GTTGTGTGTGTTGGTGCAGATCC
AN3-RT_L	CTTAGCGAATGCGCCGAGAATC
AN3-RT_R	ACCATCAACTCTCAAGGCAACCG
CYCD3;3-RT_L	TGTCTGCTTCTGCTTCAGTGTCG
CYCD3;3-RT_R	TGCTGCTCTTGCACTCTTCTCC
CYCP3;1-RT_L	TGCGAAAGTAGGAGGATTAG
CYCP3;1-RT_R	ACACACTCACATTCACATGC
CYCP4;1-RT_L	GTGATGAGAAGACGATGGAC
CYCP4;1-RT_R	CTTCTTGCTTCGTCGTTG
KRP1-RT_L	CCGCTACAACAACAATCTAA
KRP1-RT_R	AATCTGAGAGAGGAGGAGAAA
KRP2-RT_L	GACGATCGTGAAACAGAAAC
KRP2-RT_R	GGCGAGACTCTACATCTTCA
KRP3-RT_L	CGTTATCTTGTTCCCTTGTG
KRP3-RT_R	GCCTTGTAACTTTGTTGAGG
KRP4-RT_L	AAGCTTCAACAGGACCACAAGGG
KRP4-RT_R	GGGTTGTCATGATTTCAGGCCTTC
KRP5-RT_L	GTGTCAATCAATGTCAAACG

KRP5-RT_R	TATCACCACAAGCTTCTTCC
KRP6-RT_L	CTCTCTAGCTCCGAGAACAA
KRP6-RT_R	ACGACAACAGAAATGGAATC
KRP7-RT_L	GATCTGAAAATGGAAGACGA
KRP7-RT_R	CGCGTTATCTGAAGAAGAAG
AHA2-RT_L	ACATTGACGGCAGTGGTAACTGG
AHA2-RT_R	TTTGGCAAGTTCGAGGATCTGC
RALFL4-RT_L	AAATCCGTCAATGCAACCTACCC
RALFL4-RT_R	GATGCAACCTTGCCCGTTGATG
PL63180-RT_L	ACCATCAACTCTCAAGGCAACCG
PL63180-RT_R	CGCATCCTCGTGCTTTGTTACCTC
CSLA10-RT_L	GGACAGAGTGTTGGAGGTAA
CSLA10-RT_R	TGAAGCACAACTACGTGAAG
CSLA01-RT_L	TACTCTCTCGGGTAGTCCAA
CSLA01-RT_R	CCATAGATCAGGCCATAGAG
TBL37-RT_L	GCATTTCTCCCACTCACTACATGG
TBL37-RT_R	ACCACCTGGGTATGTTGATCCG
LOG1-RT_L	ATGTACCAAGGCATGAGAAG
LOG1-RT_R	GAGATTTCACAAGTGGGACT
LOG5-RT_L	TAGCAGCAGCGGAAAGAGAGAG
LOG5-RT_R	TCAATCTCCTCGTCACCAGCTC
PID-RT_L	AAGCCTCACATTTCTCTTGCATCG
PID-RT_R	ATCTGGCGGAAGAGAGGGAGAATC
HAT2-RT_1L	AACGTCGAGGAAGAAGCTCAGG
HAT2-RT_1R	AGCTAGCTTCTGTTTGGGATTGAG
GA2OXI-RT_L	AACGTTGGTGACTCTCTCCAGGTG
GA2OXI-RT_R	AACCCTATGCCTCACGCTCTTG
BRG2-RT_L	ACCTTGCTCAGACGAACGAAGC
BRG2-RT_R	CTTAACCTGCGCCAGAACATGC
BEH3-RT_L	AGCTGGTTGGACTGTAGAAGACG
BEH3-RT_R	TCCATTGGTTTGCATCCCTTGC

10.7. *RNA in situ* hybridisation

For probe synthesis, *BEL-1* cDNA (nt 442-2077) was amplified from reverse transcribed RNA of L-*er* wild type inflorescence using primers BELBamHI-F and BELXbaI-R. *BEL-1* and *BP* cDNA (from glycerolstock) was cloned into *pBluescript KS(–)* as *BamHI-Xba* and BamHI-*EcoRI* insertions, respectively. For *STM*, the construct previously generated by Gallois et al. (2002) was used. For digoxigenin labelling, the probes were *in vitro* transcribed from linearised plasmid using the DIG RNA Labelling KIT (11277073910, Roche) and T7 RNA Polymerase (881767, Roche). *In situ* hybridisation was performed as described in Fobert et al., (1996) and Gomez et al., (2005). For staining and signal detection, Anti-Digoxigenin-AP Fab fragments (11093274910, Roche) in combination with NBT/BCIP (11681451001 Roche) were used according to the manufacturer's instructions. As a mounting solution a drop of VectaMount AQ, H5501 (VECTOR LABORATORIES) was used. Images were obtained using the Leica DM 6000 microscope with bright field settings. Images were analysed in Fiji (http://fiji.sc).

10.8. GUS staining

Plant tissue (seedlings, leaves or inflorescences) was fixed in ice-cold 90% acetone on ice for 20 min. Subsequently, the acetone was replaced by a wash solution containing 50 mM phosphate buffer pH 7.2, 0.5 mM K3Fe(CN)6 (potassium ferricyanide) and 0.5 mM K4Fe(CN)6 (potassium ferrocyanide) to equilibrate the tissue. The wash buffer was replaced by staining buffer which contained 50 mM phosphate buffer pH 7.2, 0.5 mM K3Fe(CN)6 (potassium ferricyanide), 0.5 mM K4Fe(CN)6 (potassium ferrocyanide) and 2 mM X-Gluc (5-bromo-4-chloro-3-indolyl-beta-D-glucuronide) from a 100 mM stock solution dissolved in Dimethylformamide. For staining, the tissue was vacuum infiltrated, wrapped in tin foil to protect from light and incubated at 37 °C for 4 h – overnight, depending on the tissue and expression levels of the GUS reporter. To clear the tissue from chlorophyll, the tissue was washed in an ethanol series up to 70% EtOH and left overnight to clear at 4 °C.

Images were obtained using in a Leica 205A stereo microscope using reflective light mode (LED settings) or transmission light (with bright field - BF settings).

10.9. Infiltration of tobacco leaves with *Agrobacterium* for transient expression of JAG protein

Infiltration of tobacco leaves with *Agrobacterium* solution was performed following the standard operating procedure BC-GL-001-version 002 from 2010-09-21. As the first step, the *pEAQ-specialK* plasmid harbouring *JAG* cDNA with a C-terminal poly-His tag fusion was transformed into the electro-competent cells of the *Agrobacterium* strain *LBA4404* using electro-transformation and plated on LB plates supplemented with Rifampilicin (50 µg/ml) and Kanamycin (50 µg/ml). In preparation for the infiltration, 100 ml of MMA buffer were prepared with 8.9 ml aqua dest, 10 ml of 0.1 M MES pH 5.6, 1 ml of 1 M $MgCl_2$ and 100 µl of 0.1 M Acetosyringonge. Single colonies of the *Agrobacterium* strain *LBA4404* harbouring the *pEAQ-specialK* with JAG cDNA fused to C-terminal poly-His tag were picked to inoculate 10 ml of LB medium supplemented with Rifampilicin (50 µg/ml) and Kanamycin (50 µg/ml). The culture was incubated overnight at 28 °C in the shaker. The overnight cultures were centrifuged for 7 min at 4000 x g at room temperature and the supernatant was discarded. The pellets were gently resuspended in 10 ml MMA buffer and incubated for 1 h. To adjust the concentration of bacteria in the final infiltration solution to OD600=0.4, the OD600 in the 10 ml culture was measured in a photospectrometer and additional MMA buffer was added accordingly. With an average OD600=2, the 10 ml cultures were diluted 1:4 to 50 ml of infiltration solution. For infiltration, fully expanded young leaves with a diameter of 6-7 cm of 4-week old tobacco plants (in vegetative phase with 2-3 fully expanded leaves) were pierced with a sterile syringe needle on either side. Subsequently, a sterile plastic syringe was used to infiltrate the leaves with *Agrobacterium* solution at the wounded sites. In total, 10 tobacco plants were infiltrated in this experiment, 6 plants with the *Agrobacterium* harbouring the *JAG* cDNA construct, 2 plants harbouring the *HT-GFP* control plasmid as a positive control, and 3 plants harbouring the empty *HT* plasmid as a negative control.

10.10. Expression of recombinant JAG poly His tag protein in *E.coli*

10.10.1. Protein expression and Purification

For protein expression in *E.coli* strain *BL21*, bacteria were grown in freshly prepared SOB medium. The SOB medium was prepared in one litre volumes and contained 20 g tryptone/casein, 5 g yeast extract, 0.5 g NaCl and 186 mg KCl with pH 7 (measured but no adjustments needed). After autoclaving, 1 l of SOB was supplemented with 10 ml of sterile 1 M $MgCl_2$. To start a culture, single colonies of *E.coli* strain *BL21* harbouring *pRSETA* with JAG cDNA (glycerolstock 708) were used to inoculate 10 ml of SOB media supplemented with Chloramphenicol (35 µg/ml) and Carbenicilin (50 µg/ml). The liquid cultures were grown overnight at 37° C in a thermoshaker incubator. The 10 ml overnight cultures were transferred to flasks containing 500 ml of SOB medium supplemented with Chloramphenicol (35 µg/ml) and Carbenicilin (50 µg/ml).

The 500 ml cultures were incubated in the thermoshaker at 37° C for 2-3 h to reach approximately OD600=0.6. For induction of *JAG* expression, 5 ml of 100 mM Isopropyl β-D-1-thiogalactopyranoside (IPTG) (Sigma) stock solution (filter sterilised) were added to 500 ml liquid culture to reach a final concentration of 1 mM IPTG. After induction, the culture was grown for 4 h (4 h showed strongest protein band at 30 kDa in a preliminary time course experiment). The cells were harvested in a centrifugation step at 4.500 rpm for 20 min at 4° C. The pellet was resuspended in 25 ml of pre-cooled lysis buffer containing 20 mM Tris and 0.5 M NaCl supplemented with proteinase inhibitor mini complete EDTA free tablet (1 tablet/25 ml) (Roche). The suspension was transferred into 25 ml tubes Sorvall centrifugation tubes. For sonication, the 25 ml tubes were placed in an ice bucket and placed under a probe sonicator. Sonication was performed 3x for 20 sec at medium power level with 2 min intervals on ice. Subsequently, the sonicated suspension was centrifuged in the SORVALL centrifuge at 10.000 rpm for 20 min at 4° C. TALON metal affinity resin beads (900 µl/25 ml suspension) were pre-equilibrated by a 3-min centrifugation step at 2,400 rpm at room temperature, the supernatant was discarded and the beads were resuspended in 5 ml lysis buffer. The equilibration step was repeated once and beads were resuspended in 900 µl lysis buffer. After centrifugation, the supernatant (about 20 ml) was incubated with 900 µl pre-equilibrated TALON metal affinity resin beads on a wheel for 4 h at room temperature to bind the JAG poly-His tag

protein. Subsequently, the beads were washed with washing buffer (20 mM Tris, 0.5 M NaCl supplemented with 15 mM imidazole). For the initial washing step, beads were incubated with 10 ml washing buffer on a wheel for 10 min at room temperature, centrifuged for 5 min at 700 x g, and the supernatant discarded. The washing step was repeated once. Then, the supernatant was discarded and beads were resuspended in 5 ml washing buffer and 2 samples were fused to be loaded on a 2 ml gravity column (TAKARA, Clontech). The settled beads were washed with a minimum of 20 ml of washing buffer before applying one ml of elution buffer (washing buffer supplemented with 250 mM imidazole) for the final washing step. For elution, 10 ml of elution buffer were pipetted in 1 ml aliquots into the columns and the eluted protein was collected in 1.5 ml fractions into Eppendorf tubes, with the first fraction showing high background and additional bands and the later fractions showing low background. After elution, 30 µl aliquots of the crude protein fractions and 30 µl of un-induced bacterial culture (negative control) were supplemented with 4x NuPAGE LDS Sample Buffer (Invitrogen) and denatured by boiling for 5 min in order to be loaded on an SDS-PAGE gel for quality check. The fractions showing a clear band at 30 kDa were combined and concentrated 150-200 fold to a concentration of 70 µg/ml using Pierce Protein concentrators columns (Thermo Fisher Scientific) with 9 kDa and 20 kDa molecular weight cut off (MWCO) excluding low molecular weight proteins as an additional clean up step resulting in increased amounts of protein of the expected size of about 30 kDa. Using the concentrator columns, all centrifugation steps were performed at 3,000-4,000 x g at 4° C. Bradford reagent (Sigma) was used according to the manufacturer's instructions to determine the final protein concentrations against a dilution series of BSA protein.

10.11. SDS-PAGE Gel electrophoresis

For SDS-PAGE (Sodium dodecyl-sulfate polyacrylamide gel electrophoresis) gel electrophoresis, denaturing 10% polyacrylamide gels were used. For the separation gel (10%), 25 ml (2 gels using the BIORAD equipment) containing 11.25 ml aqua dest, 6.25 ml Tris 1M pH 8.8, 8 ml 30% acrylamide w/v ratio 29:1 (SEVERN BIOTECH LIMITED), 125 µl SDS 20%, 250 µl (APS (ammonium persulfate) 10% freshly prepared), 25 µl TEMED (Tetramethylethylenediamine) were prepared. The separation gel was poured and

covered with a 1 cm layer of butanol and left to polymerise. After polymerisation (45 min), the butanol layer was removed and the gel surface was rinsed with water. For the stacking gel, 7.5 ml (2 gels using the BIORAD equipment) containing 4.9 ml aqua dest, 1.9 ml Tris 1M pH 6.8, 1 ml acrylamide 30%, 37.5 µl SDS 20%, 75 µl APS (10% freshly made), and 15 µl TEMED were prepared. The stacking gel was poured, so that the combs could be set and left to polymerise. Gels were run in 1X running buffer with 0.1% SDS. Running buffer was prepared as a 10x stock solution containing 0.25 M Tris base (30.28 g), 14.4% w/v Glycine (144 g). To 1 litre of 1X running buffer, 5 ml of 20% SDS were added. To load the protein samples (25-35 µl), 7-9 µl of 4x NuPAGE LDS Sample Buffer (Invitrogen) were added and the samples were subsequently denatured at 95° C for 5 min and centrifuged for 1-2 min at max speed. As a sizemarker, 10 µl of Page Ruler Prestained Protein ladder (Thermo Fisher Scientific) were diluted to 30 µl and loaded with the denatured samples. Electrophoresis for 10% SDS-PAGE gels was performed at 100 Volt and 30 mA for 2 gels and 20 mA for a single gel for up to 3 h. For developing the protein bands the gels were removed from the glass plates and incubated in 10-15 ml of InstantBlue solution (Expedeon) on a shaker for 15-20 min at room temperature. Gels were scanned on a standard office scanner.

10.12. Protein extraction from plant material using Laemmlibuffer

For protein extraction from fresh plant material, Laemmlibuffer was prepared 4X and kept at -20 °C (10 ml containing 2 ml 1M Tris-HCl pH 6.8, 1 ml 0.5 M EDTA pH 8, 800 mg SDS, 4 ml 10% glycerol, 400 µl beta mercaptoethanol, 8 mg Bromophenol BLUE). Before use, the 4X Laemmlibuffer was diluted 1:1 with aqua dest. To obtain crude protein extracts from *Arabidopsis* flowers, 1-3 inflorescences were harvested into Eppendorf tubes and snap-frozen in liquid nitrogen. Frozen plant tissue was ground and 100 µl of 2X Laemmlibuffer were added per 1-3 inflorescences. Subsequently, the samples were boiled for 10 min, centrifuged for 2 min and the supernatant recovered. For Western Blots 5 µl of crude denatured plant extract were loaded per lane.

10.13. Western Blotting using anti-6xHis and anti-JAG antibodies

Western Blotting was performed in order to test the expression of recombinant JAG poly-His tag protein in *E. coli* prior to the protein purification experiment. For this experiment, anti-6X His tag antibodies raised in rabbit (Rb pAG to 6X His tag; ab9108, Abcam) were used as the primary antibody in a 1:1000 dilution in combination with a goat anti-IgG rabbit HRP (goat pAb to Rb IgG HRP; ab6721) antibody diluted 1:5000. In order to test the rat anti-JAG antibodies, dilutions of the recombinant JAG protein and crude plant extracts boiled in Laemmli-Buffer were used. For this experiment, the rat anti-JAG antibodies (raised by Eurogentec) were used as the primary antibody diluted 1:500 in combination with the secondary rabbit anti-Rat IgG HRP antibody (A5795, Sigma) diluted 1:5000. Both secondary antibodies were conjugated to the horse radish peroxidase in order to allow quantification based on chemiluminescence.
For Western Blotting, SDS-PAGE electrophoresis was performed as described above. Prior to the electrophoretic transfer, the separation of the proteins was briefly checked by applying Ponceau Red. For the electrophoretic transfer of the proteins from the gel to the Hybond C Extra Nitrocellulose membrane - 45 micron (GE HEALTHCARE LIFE SCIENCES), the gel was submerged in transfer buffer (1X running buffer without SDS) and a stack of sponges, filter paper, the membrane and gel was produced in the correct orientation with the transfer equipment to allow for blotting of the negatively charged proteins onto the membrane. The transfer stack was placed into the BIORAD gel tank and placed onto a magnetic stirrer. The transfer was performed with 100 Volt for about 3 h at 4° C. Subsequently, the membrane was briefly equilibrated in buffer solution containing 1X TBS pH 7.4 (with 10X TBS buffer containing 12.1 g Tris base, 81.80 g NaCl). For blocking, the membrane was incubated in 1X TBS supplemented with 0.1% TWEEN and 5% milkpowder (10 g in 200 ml) for 1 h on a slow shaker at room temperature. For incubation with the primary antibody, the membrane was transferred to 10 ml of blocking solution (1X TBS pH 7.4, 0.1% TWEEN, 5% milkpowder) supplemented 10 µl of 6X His tag antibody or 20 µl of the primary rat anti-JAG antibody to achieve a 1:1000 or 1:500 dilution of the primary antibody, respectively, and incubated overnight at 4° C on a slow shaker. The incubation was followed by several quick washes and 3 washes of 10 min each at the slow shaker at room temperature with 1X TBS, 0.1% TWEEN solution. Subsequently, the membrane was

incubated with the corresponding secondary antibody diluted 1:5000 (2 µl in 10 ml) in blocking buffer and the membrane incubated for 1 h on the slow shaker at room temperature. This incubation step was followed by several quick washes and 3 washes of 10 min each at the slow shaker at room temperature with 1X TBS, 0.1%. Subsequently, the membrane was briefly dried on filter paper and to detect the horseradish peroxidase signal of the HRP-conjugated secondary antibody, the chemiluminescent substrate SuperSignal West Pico (Thermo Scientific) was used according to the manufacturer's instructions. Subsequently, the membrane was used to expose an X-ray film.

10.14. Chromatin Immunoprecipitation using dexamethasone inducible *p35S:JAG-GR* in WT L-*er* background, anti-GR antibodies and DYNABEADS protein A beads

10.14.1. Dexamethasone treatment, harvest of the plant material and fixation

For the chromatin immunoprecipitation 300-500 mg (fresh weight) of inflorescence apices (inflorescence meristem, unopened flower buds up to stage 12) tissue was used per sample. In order to obtain this amount of tissue per sample, between 70 and 80 main inflorescences (with 0-3 siliques developed) of the DEX- inducible *p35S:JAG-GR* line were induced with 10 µM DEX with 0.1% EtOH and 0.1% EtOH as control treatment in three biological replicates as described in detail for expression profiling. Four hours after treatment, 70-80 inflorescence apices were harvested into a 50 ml falcon tube with wet filter paper and kept at room temperature for the time of harvest (1 h). Samples were fixed in 30 ml fixation buffer (0.4 M sucrose, 10 mM TRIS pH 8, 1 mM EDTA pH 8.5, 1% formaldehyde, 100 µM PMSF) by vacuum infiltration for 20 min on ice. Cross-linking was stopped by adding 0.1 M glycine to the fixation buffer and incubation for 10 min on ice. After two washes with sterile water the plant tissue was dry blotted, weighed, packed into tin foil envelopes and frozen in liquid nitrogen for grinding.

10.14.2. Lysis and Sonciation

Chromatin immunoprecipitation was performed according to a modified protocol by Morohashi et al., (2007). Tissue (300 mg – 500 mg fresh weight) was ground with mortar and pestle in liquid nitrogen at 4 °C and re-suspended in 700 µl of lysis buffer (50 mM HEPES, pH 7.5, 150 mM NaCl, 1 mM EDTA, 1% Triton X-100, 0.1% deoxycholate, 0.1% SDS, 100 µM PMSF, 10 mM sodium butyrate and 2 tablets (per 50 ml of buffer) protease inhibitor cocktail complete Mini, EDTA-free (11836170001, Roche). The re-suspended samples were sonicated to average 500 bp fragment size in a Bioruptur waterbath sonicator located at 4 °C (3 x 5 min medium power level with 30 sec on/30sec off cycles). After sonication, samples were centrifuged for 10 min full speed at 4 °C. The supernatant was transferred to a fresh tube for the immunoprecipitation steps.

10.14.3. Chromatin Immunoprecipitation

For preparation of the the Dynabeads Protein A beads, the beads were washed twice in 750 ul lysis buffer using a Dyna magnetic rack for separation of the beads from the lysis buffer. Subsequently, the beads were equilibrated in lysis buffer supplemented with 1 mg/ml BSA (Sigma) and 20 µg/ml sonicated salmon sperm (Sigma) for 2 h at room temperature on a rotating wheel. For pre-clearing of the lysate, 25 µl of equilibrated Dynabeads Protein A beads (100.02 D, Invitrogen) were added to the 600-700 µl of supernatant and incubated for 2 h at 4 °C on the rotating wheel. After incubation, the beads were separated from the lysate using the magnetic rack and discarded. To sample the input DNA, 1/10 of the pre-cleared lysate was retained and frozen for the de-cross-linking step. The cleared lysate was incubated with 2 µl anti-GR antibodies (AB3580, Abcam) per 100 µl lysate at 4 °C overnight on a rotating wheel. After overnight incubation, 15 µl of equilibrated Dynabeads Protein A beads were added per 100 µl lysate and incubated at 4 °C for 4 h on a rotating wheel. After incubation, the beads were washed with 700 µl lysis buffer, 700 µl lithium chloride buffer (1 mM EDTA pH 8, 0.25M LiCl, 1% sodium deoxycholate (Sigma) and 1% NP40 IGEPAL (Sigma)), and 700 µl TE-buffer (10 mM Tris pH 8, 1 mM EDTA pH 8). For each buffer a short wash (1 min on the rotating wheel) and a long wash (5 min on the rotating wheel) were performed using the Dynabead magnetic rack for separation of the wash from the beads. For elution of the cross-linked immunoprecipitate from the beads, 40 µl of freshly prepared elution buffer

(1% SDS, 0.1 M sodium carbonate NaHCO3, 0.25 mg/ml proteinase K were added to the beads after the last wash with TE-buffer.

10.14.4. Elution, De-crosslinking and DNA purification

The beads were subsequently incubated at 65 °C for 10 min. Beads were separated using the DYNABEADS magnetic rack and 40 µl of elute were collected in a 200 µl PCR tube. The elution step was repeated once to result in a total volume of 80 µl of elute. At this step the input samples were thawed and transferred to 200 µl PCR-tubes and supplemented with 50 µl of elution buffer to a total volume of 80 µl. For de-cross linking the samples were incubated at 65 °C overnight in a thermo-cycler with the lid-heat swiched on. Input DNA and immunoprecipitated DNA were extracted using PCR purification Kit (28104, Qiagen) following the manufacturer's instructions. Purified DNA was eluted in 50 µl Qiagen elution buffer and stored at -80 °C.

10.14.5. Quantification of enrichments

For quantification of the enrichment, 1 µl of the purified immunoprecipiated DNA and of the purified input samples was used per 10 µl PCR-reaction to perform q-PCR in technical triplicates using the LightCycler System LC480 (Roche) as described above. Enrichment of promoter regions was calculated from ΔCt values (Ct immunoprecipitated DNA – Ct input DNA) using $2^{-\Delta\Delta Ct}$ method (Livak and Schmittgen, 2001). Unpaired two-sample Student's t test was used to test for significant differences between DEX induced and EtOH control treated samples.

10.15. Chromatin Immunoprecipitation using *pJAG:JAG-GFP* complementing *jag-2* mutant background and anti-GFP µMACS MicroBeads

10.15.1. Harvest of the plant material and fixation

For the chromatin immunoprecipitation with *pJAG:JAG-GFP jag-2* L-*er* plants and wild-type L-*er* plants 1300-1500 mg (fresh weight) of inflorescence apices were used per sample. In order to obtain this amount of tissue per sample, between 160 and 180 main inflorescences (at the developmental stage of 0-3 siliques developed) were harvested per sample. In order to keep the harvesting time to less than an hour, 60 to 80 plants per

biological replicate were harvested into a 50 ml falcon tube with wet filter paper in three independent harvests. After each of the three harvests, samples were immediately fixed in 35 ml fixation buffer (0.4 M sucrose, 10 mM TRIS pH 8, 1 mM EDTA pH 8.5, 1% formaldehyde, 100 µM PMSF) by vacuum infiltration for 20 min on ice. Cross-linking was stopped by adding 0.1 M glycine to the fixation buffer and incubation for 10 min on ice. After two washes with sterile water the plant tissue was dry blotted, weighed, packed into tin foil envelopes and frozen in liquid nitrogen for grinding. The tissue of the three independent harvests was later pooled to 1 biological replicate at the grinding step.

10.15.2. Lysis and Sonication

Chromatin immunoprecipitation was performed according to a modified protocol by Kaufmann et al. (2009). Per sample, tissue of the three harvests (1300 mg – 1500 mg fresh weight in total) was pooled in a mortar ground with a pestle in liquid nitrogen at 4 °C. The ground tissue was resuspended in 25 ml of lysis buffer (M1) containing 10 mM sodium phosphate pH 7, 0.1 M NaCl, 1 M 2-methyl 2,4-pentanediol, 10 mM ß-mercaptoethanol, 1 tablet (per 50 ml of buffer) of protease inhibitor cocktail complete Mini, EDTA-free (11836170001, Roche). The resuspended lysate was filtered through 2 layers of miracloth into a new 50 ml falcon tube on ice. The filtrate about 25 ml was centrifuged at 1000 x g for 20 min at 4 °C with centrifuge brakes switched off. The supernatant was discarded and the pellet was gently washed and re-suspended in 15 ml of wash buffer M2 containing 10 mM sodium phosphate pH 7, 0.1 M NaCl, 1 M 2-methyl 2,4-pentanediol, 10 mM ß-mercaptoethanol, 1 tablet (per 50 ml of buffer) of protease inhibitor cocktail complete Mini, EDTA-free (11836170001, Roche), 10 mM magnesium chloride and 0.5% Triton X-100 (Sigma) and centrifuged at 1000 x g for 10 min at 4 °C with centrifuge brakes switched off. After centrifugation, the supernatant was discarded and the pellet was gently washed and partially resuspended in 7.5 ml wash buffer M3 containing 10 mM sodium phosphate pH 7, 0.1 M NaCl, 10 mM ß-mercaptoethanol, 1 tablet (per 50 ml of buffer) of The re-suspended samples were centrifuged at 1000 x g for 10 min at 4 °C with centrifuge brakes switched off. The supernatant was discarded and the clean nuclei pellet of creamy colour was gently resusupended in 1 ml of sonication buffer containing 0.5 M Hepes, 150 mM NaCl, 5 mM magnesium chloride and 10% TRITON X-100 and ½ a tablet buffer of protease inhibitor cocktail complete Mini, EDTA-

free (11836170001, Roche). In order to optimise the sonication in the water bath sonicator, the 1 ml of nuclei suspension were divided into two 1.5 ml Eppendorf tubes with corresponding a) and b) labels in order to be fused again at the column purification step. Sonication was performed in Bioruptur waterbath sonicator with cooling unit at 4 °C (2 x 5 min high power level with 30 sec on/30 sec off cycles) resulting in an average fragment size of 500 bp. After sonication, samples were centrifuged for 15 min full speed at 4 °C. The supernatant was transferred to a new 1.5 ml Eppendorf tube and the centrifugation step repeated. The supernatant was transferred to fresh tube and the pellet was discarded.

10.15.3. Chromatin immunoprecipitation, elution and cross-linking reversal

Before continuing with the immunoprecipitation, 1/10 of the supernatant (50 µl of a) and b) samples) was transferred to a tube as DNA input sample and kept on ice. To the remaining supernatant, 500 µl of immunoprecipitation buffer containing 0.5 M Hepes, 150 mM NaCl, 5 mM magnesium chloride and 10% TRITON X-100 (Sigma) and 1 mg/ml BSA (Sigma) and 25 µl of anti-GFP µMACS Microbeads (Milteyi Biotec) were added. The tubes were gently inverted and transferred to ice for 30 min incubation. Samples were gently inverted once after 20 min. After incubation the a) and b) samples of every biological replicate were loaded on a µ Column (Milteyi Biotec) that had been placed into the magnetic µMACS separator (Milteyi Biotec) and equilibrated with 200 µl immunoprecipitation buffer. Once the total samples volume of 1 ml had passed the column, the beads were washed with 2x 400 µl and 2x 200 µl of immunoprecipitation buffer and 2x 200 µl TE buffer (100 mM Tris pH 8, 10 mM EDTA pH 8). For elution, elution buffer containing 50 mM Tris pH8, 10 mM EDTA, 50 mM DTT (freshly added) and 1% SDS was preheated to 96 °C and a set of 1.5 ml low binding tubes were place under the µ columns for collection of the elute. In a first step, 20 µl of hot elution buffer were applied to the column and incubated for 5 min, followed by 2 x 50 µl of hot elution buffer for final elution. After elution of a total volume of 100 µl, 100 µl of TE-buffer and 9 µl of 25 mg/ml Proteinase K were added to the samples. Similarily, 100 µl of TE-buffer and 9 µl of 25 mg/ml Proteinase K were added to the input samples. Elution and input DNA samples were incubated at 37 °C overnight. The next day, 9 µl of 25 mg/ml Proteinase K were added to the samples and the samples were incubated at 65 °C in a heatblock for 8 hours.

10.15.4. DNA purification

Subsequently, 250 µl of Phenol:Chloroform:Isoamyl Alcohol 25:24:1, saturated with 10 mM Tris pH 8.0, 1 mM EDTA (P2069, Sigma) was added to the samples followed by a 10 min centrifugation step at full speed. The supernatant was transferred to a 1.5 ml Eppendorf tube and supplemented with 25 µl of 3 M sodium acetate, 1 µl of glycogen and 750 µl of EtOH. DNA was precipitated at -20 °C overnight. The pellet was precipitated by a centrifuge step at full speed for 30 min at 4 °C and the pellet was washed in 300 µl of 70% EtOH with a centrifugation step at full speed for 5 min at 4 °C. The pellet was air-dried for 20 min under the fumehood and resuspended in 100 µl PCR-grade water (Lightcyclerkit). Subsequently, the input DNA and immunoprecipitated DNA were extracted using PCR purification Kit (28104, Qiagen) following the manufacturer's instructions. Purified DNA was eluted in 30 µl Qiagen elution buffer and stored at -80 °C.

10.15.5. Quantification of enrichments

For quantification of the enrichment, 1 µl of the purified immune-precipiated DNA and of the purified input samples was used per 10 µl PCR-reaction to perform Q-PCR in technical triplicates using the LightCycler System (Roche) as described above. Enrichment of promoter regions was calculated from ΔCt values (Ct immunoprecipitated DNA – Ct input DNA) using $2^{-\Delta\Delta Ct}$ method (Livak and Schmittgen, 2001). Unpaired two-sample Student's t test was used to test for significant differences in enrichment between *pJAG:JAG-GFP jag-2* and wild-type L-*er* samples.

10.16. ChIP-oligonucleotides

For promoter analysis and oligos amplifying specific regions, the primer design tool "PRIMER3" http://frodo.wi.mit.edu/primer3/ was used. The efficiency of ChiP-oligos was tested using a dilution series of the same dilution factors as described above of mixed ChIP-Input DNA. Because, ChIP-oligos were predominantly designed to bind to A/T-rich promoter regions, ChIP-oligos were tested at different annealing temperatures starting from 61° C to 57° C in order to find the optimum annealing temperature for individual oligo pairs. The LC480 software was used to generate standard curves and to calculate

the slope (optimum -3.3), the oligo amplification efficiency (amplification factors between 1.85 and 2 (=100%) were considered as acceptable). In addition, it was checked that the melting curve gave one single clear peak and that the non-template controls did not give any signal. The following oligos were used to confirm DNA binding sites of JAG:

BEL-1877-F TCTGAGAAAAGCCTGAACTC

BEL-1877-R GTTGGTGTATAGATGGAGAGGT

BEL-288-F CTTCTCTCTCCCTCTTCACC

BEL-288-R AGCTCCTAAAACCCTACAAGA

BP-2609-F GGCAGTGCAATGAAGTGAAA

BP-2609-R CCCGAAACATAAAACCTACACG

BP-1064-F GCAAGACTTGGATGTTTTTGG

BP-1064-R TCGGATAGTGTGATCTCTCCAC

PTL-1056-F CACACATGCCTCTGGAGTTT

PTL-1056-R TCCATTAGAGGTTAACCGAGTCA

PTL-476-F CAAAGACGAGTGCCTCCATCTA3’

PTL-476-R TGTTTTGCAACATGTGTCTAGC3’

PTL+1322-F GCTCTGGTCGATTCAGTGTG

PTL+1322-R GGGAATAGGGACAAAAGGAGA

KRP2-1616-F TGATTGAGTATGCAGCTCGTG

KRP2-1616-R AATGCCGTCGTTCTGTATCG

KRP2-159-F CAAAACGAAGATCGTCACCA

KRP2-159-R TCACTCGTTATGTGTGCGTGT

KRP2+1342-F CCCACGAGGCAAAGATTTTA

KRP2+1342-R GTGGAGAAAAAGACTCCAGCTC

KRP4-1691-F GTCTGCAAGTCATGACAAATCC

KRP4-1691-R CCTGAGCTCTCTGCTATTTCTTCT

KRP4+295-F GGGTTTAGCGTTTAGGGTTTAGAG

KRP4+295-R GAATGCAGAGTCCCCCTGTA

Mu-like-F GATTTACAAGGAATCTGTTGGTGGT

Mu-like-R CATAACATAGGTTTAGAGCATCTGC

10.17. ChIP-Illumina Deep Sequencing: library preparation, deep sequencing, and data analysis

The six Illumina TruSeq ChIP-Seq libraries (three *pJAG: JAG-GFP* replicates and three wild-type controls) were produced with library insert sizes of 250-500 bp in collaboration with TGAC and subsequent quality checks and sequencing was performed by TGAC. Library insert sizes were verified using an Agilent Technologies 2100 Bioanalyzer and a High Sensitivity DNA chip. The concentration was measured using a High Sensitivity Qubit assay (Invitrogen) and normalised to 10 nM. Subsequent processing for Illumina HiSeq 2500 (Rapid-Run mode) clustering and sequencing using 50 bp single-end reads was performed as described by the manufacturer (Illumina).

For quality control: reads that failed the CASAVA filter were eliminated. Sequence reads in FASTQ format were mapped to the unmasked Arabidopsis genome (TAIR10; ftp://ftp.arabidopsis.org/) using the SOAPaligner (v2) program (Li et al., 2008). A maximum of two mismatches and no gaps were allowed. Reads mapping in multiple genomic location, to the chloroplast or mitochondrial genome were discarded. ChIP-Seq peaks were first detected using the online software tool PRI-CAT http://www.ab.wur.nl/pricat/ (Muiño et al., 2011) and subsequently analysed by Jose Muiño using CSAR (Muiño et al., 2011a) with default parameter values except for “backg”, which was set to 20. Sequences from each JAG-GFP library were analyzed independently in comparison with a single negative control with all three wild-type libraries combined. Mapped reads were extended directionally to 300 bp and the distribution of the number of extended mapped reads overlapping each nucleotide in the JAG-GFP library and in the negative control were normalized to have the same mean and variance. Enrichment relative to control was calculated as the ratio of normalized extended reads between JAG-GFP and control sample. Regions having less than 20 reads mapped in the control were set to 20 (parameter “backg”=20 in CSAR) to avoid false positives due the low coverage of the control in some regions. False discovery rate (FDR) thresholds were estimated by permutation of reads between sample and control using CSAR for each biological replicate independently. Candidate JAG target genes were defined as genes containing a significant (FDR<0.01) binding event in all three replicates, in the region between 3 kb upstream of the start codon and 1.5 kb downstream of the stop codon.

For *de novo* motif finding, DREME (Bailey, 2011) was used with default parameters on the set of sequences within 50 bp of a peak (101 bp region in total) for the top 1000 binding events located in the region 3 kb upstream and 1.5 kb downstream among the three replicates. Once the motifs were identified by DREME, and to validate their relationship with the ChIP-Seq scores, the proportion of binding sites associated with the motif for each ChIP-Seq score threshold value was plotted.

10.18. Gene ontology analysis

Gene ontology term enrichment analysis was performed with the module BINGO (Maere et al., 2005) from Cytoscape (Saito et al., 2012). Plots of gene ontology term enrichment versus ChIP-Seq score threshold were produced in R. The gene ontology database (*GO.db* v2.9.0) and the mapping of *Arabidopsis* genes to gene ontology terms (*org.At.tair.db v2.9.0*) were downloaded from Bioconductor (http://www.bioconductor.org/). The ChIP-Seq score attributed to each gene was the minimum value for the ChIP-Seq score of each of the three biological replicates. The proportion of genes associated with a particular gene ontology term was then plotted for each ChIP-Seq threshold.

10.19. Combined modified pseudo-Schiff-propidium iodide and EdU imaging

In preparation for combined modified pseudo-Schiff-propidium iodide (mPS-PI) staining modified after Truernit et al. (2008) and EdU (5-ethynyl-2-deoxyuridine) labelling modified after Salic and Mitchison et al. (2008), buds larger than 0.5 mm were removed from inflorescences and the inflorescence stem cut in 10 mm distance. For further dissection under the stereomicroscope with about 4-8X magnification, the floral apices were inserted into a solidified 1% agarose block placed in a box and flooded with aqua dest. Additional buds were removed following the phyllotactic spiral using a syringe needle until the inflorescence meristem surrounded by the 15-20 youngest buds was clearly visible. Then, the stem of the dissected apices was cut in a 45° angle at a distance of 6-8 mm from the base of the apices. Dissected apices were placed in sterile GM boxes

sealed with micropore surgical tape and grown for 45 h at 16° C under continuous light; for JAG-GR activation, the media also contained 10 µM dexamethasone (from 10 mM stock in ethanol), or 0.1% ethanol for mock-treatment. Apices were then transferred to boxes with the same medium supplemented with 10 µM EdU (Invitrogen), sealed with micropore surgical tape and incubated in the same conditions for another 3 h.

Subsequently, the apices were removed from the media, place into Eppendorf tubes and subjected to incubation in 15%, 30%, 50%, 70%, 85%, 95% and 100% ethanol for 15 min each at room temperature and protected from light. Subsequently, the floral apices were inserted into a solidified 1% agarose block placed in a box and flooded with 100% ethanol for further dissection, leaving only the inflorescence meristem and the youngest surrounding buds up to position 15-17. Then, the apices were removed from the agarose block in order to cut the stem as parallel as possible in order to make the apices sit facing straight upwards. Subsequently, the samples were placed into a 24-multi-well plate (up to 4-5 samples/well) filled with 100% ethanol and incubated at -20 °C overnight. Then, the samples were rehydrated through the same ethanol series, washed in water and incubated at 37 °C overnight in alpha-amylase solution containing 0.3 mg/mL alpha-amylase (A4551, Sigma) in 20 mM phosphate buffer pH 7.0, 2 mM NaCl, 0.25 mM $CaCl_2$.

All subsequent steps were performed at room temperature with gentle rocking on a shaker protected from light: the apices were rinsed in water three times and once in TBS pH 7.4 (1 l containing 8 g NaCl, 0.2 g KCl, 3 g Tris base and the pH adjusted with HCl) before being incubated in Alexa prestaining solution containing 10 µM Alexa488-azide (A10266, Invitrogen, prepared as a 10 mM stock solution with 0.5 mg dissolved in 58 µl of DMSO) in 100 mM Tris pH 8.5 for 1 hour followed by incubation in Alexa staining solution containing 10 µM Alexa488-azide, 100 mM Tris pH 8.5, 1 mM $CuSO_4$ and 100 mM ascorbic acid (freshly dissolved and last added) for 30 min. For both the prestaining and the staining solution vacuum-degassed water was used. Subsequently, samples were washed three times in water and incubated in 1% periodic acid (freshly dissolved in aqua dest) for 1 hour, followed by two washes in water. Then, the samples were incubated in Schiff-PI reagent for 2 h. For this, 625 µl HCl 12 N were added to 49 ml aqua dest, then 0.95 g sodium bisulfite were dissolved in the solution. An aliquot of this solution was used to prepare the PS-PI solution with a final propidium iodide concentration of 20 µg/ml (from a stock solution of 1mg/ml propidium iodide (81845, Sigma) dissolved in water, kept

frozen at -20 °C protected from light) after Truernit et al. (2008), followed by two washes in water. Subsequently, the samples were individually placed on single cavity depression slides (76 x 25 x 1.25 mm) (AGL4090, Agar Scientific) and immediately covered with a drop of chloral hydrate solution (40 g chloral hydrate dissolved in 10 ml aqua dest and 5 ml glycerol) for final clearing and left protected from light for about 20 min. Then, the excess chloral hydrate surrounding the samples was removed with a filter paper without touching the sample and replaced by a drop (about 100 – 150 µl) of Hoyer's Medium (40 g chloral hydrate dissolved in 10 ml aqua dest, 5 ml glycerol, 6 g gum Arabic (G9752, Sigma)) after Truernit et al. (2008) that had been kept protected from light and was centrifuged for 30 min prior to use. The samples were arranged in the center of the depression with the apices facing upwards as straight as possible before being covered with a 22 x 22 mm glass cover slip thickness No 0 (VWR International). Prepared slides were left to dry overnight protected from light and imaged within the following two days.

For imaging a Zeiss 510 Meta confocal microscope with a 25X water immersion objective was used with laser excitation at 488 nm and emission filters set to 572-625 nm for the PI signal (false color red in the images) and 505-600 nm for the EdU signal (false colour green in the images). Images were obtained by 512x512 pixel size using 4X mean averaging. For z-stacks, the image thickness was set to 0.5 µm and the pinhole to an optical thickness of airy 1. The detector gain was adjusted according to the signal intensity for both channels independently. Images were saved in .lsm file format and displayed in Fiji.

10.20. Quantitative 3D image analysis

Image processing was performed with Fiji, BioImageXD, custom Fiji macros and custom python scripts. Using Fiji and the macro "TIF_for_inr_import", confocal image stacks were opened, cropped, despeckled and saved as separate TIFF stacks for the PS-PI and EdU channels. The python script "TIF_import" was used to convert the TIFF stacks into compressed image files in inr.gz format and to subtract from the PS-PI image any background signal arising from EdU fluorescence. After converting the subtracted image back to a TIFF stack with the Fiji macro "TIF_S_fom_inr", the image was opened in BioImageXD (Kaankaanpaa et al., 2012), cells were segmented in 3D using a

morphological watershed algorithm, and the segmented image was converted to inr.gz format using the python script “inr”. The Fiji macro “select_landmarks” in combination with the Fiji plugins 3D Viewer (Schmid et al., 2010) and Point Picker (http://bigwww.epfl.ch/thevenaz/pointpicker/) was used to select landmarks on the summit of meristem and primordium and on primordium boundaries. Furthermore, custom scripts were developed to automatically determine the center of mass and volume of each individual cell (“cell_data_table”) and cell positions relative to the meristem summit and to primordium boundaries in order to locate cells in the meristem or primordium and to attribute cell layers (“select_meristem_primordia”), to detect artifacts of under and over-segmentation (“segmentation_quality”), and to select cells with EdU labeling from non-EdU labeled cells (“score_EdU”). Fiji macros were used to display the images and manually re-check the EdU scoring (“EdU_check”), segmentation quality and location of selected cells (“segmentation_selection”). At last, remaining errors were corrected manually in both the images and final cell data tables using the python script “delete_cells”. All macros and annotated python scripts along with instructions for installation and use are available from Robert Sablowski.

10.21. Live-Imaging of single flowers

Flowers at full anthesis (bud open, petals fully visible, elongated stamen level with stigma, described as stage 13 in Smyth et al. (1990) were used for live-imaging of single flowers. Inflorescence overview images and single flower images were taken in a Leica 205A stereomicroscope using 12X and 30X magnification, respectively, with reflective light mode (LED settings).

10.22. Sepal and Petal imaging for size measurements

Flowers at full anthesis (as described above) from the inflorescences that had developed between three and five siliques were detached and dehydrated in a 15%, 30%, 50% and 70% EtOH series and stored at 70% EtOH at 4 °C. For imaging, sepals and petals of single flowers were dissected in 70% EtOH and mounted on a slide. Images were

obtained using Leica DM6000 microscope equipped with an automatic stage for tiling mode with bright field settings using 10X magnification. Sepal and petal measurements were obtained using Fiji (http://fiji.sc).

10.23. Confocal live imaging

For live imaging of *pJAG::JAG:GFP jag-2*, *KRP2:KRP2-GFP* in *jag-1* and wild type *Col*, floral apices were dissected under water and imaged in boxes halfway filled with 1% agarose (as described above). Floral apices were recovered for 24 h on germination medium in boxes sealed with micropore surgical tape under normal growth conditions. Before imaging, a drop of 50 µg/ml N-(4-triethylammoniumpropyl)-r-(p-dietheylaminophenylhexatrienyl pyridium dibromide) (FM4-64) (Invitrogen) was applied to the apices still kept in the medium in the sealed box to retain the humidity and incubated for 10 min. Alternatively, the apices were removed from the medium and placed into 0.2 ml PCR-tubes containing 40 µl of 50 µg/ml FM4-64 solution and incubated for 10 min with the lid of the tube closed. Subsequently, the apices were placed in boxes with 1% agarose and covered with water. For confocal imaging a Zeiss 510 Meta confocal microscope equipped with a 20X water dipping lense was used with laser excitation at 488 nm. Samples were imaged with the confocal microscope Zeiss 510 Meta detecting FM4-64 emission signal at 571.8-625 nm and GFP emission signal at 505-600 nm. To screen for expression of GFP in *KRP2:KRP2-GFP* lines and to screen for CYPET expression in *KRP4:KRP4-CYPET* lines, in the root and shoot of young seedlings, young seedlings were placed on a slide submerged in water under a coverslip and imaged using same settings as described above for GFP and for CyPet (excitation at 435 nm/emission at 477 nm). 3D reconstructions and virtual sections of whole inflorescences and single floral buds based on the cell wall images were generated using 3D Viewer and Orthogonal Views plugins of Fiji (Schmid et al., 2000). Photoshop CS6 (Adobe Inc.) was used for final editing of images.

10.24. Scanning electron microscopy

For scanning electron microscopy, petals and sepals of flowers at full anthesis were mounted on the surface of an aluminium stub with optimal cutting temperature compound (Miles Scientific), plunged into liquid nitrogen slush at approximately -210 °C to cryo-preserve the tissue, and transferred to the cryo-stage of an Alto 2500 cryotransfer system (Gatan, Oxford) attached to a Zeiss Supra 55 VP field emission gun scanning electron microscope (Zeiss SMT, Germany). The surface frost was sublimed at -95 °C for 3 min before the samples were sputter coated with platinum for 2 min at 10 mA at below -110 °C. The samples were imaged on a cryostage at -130 °C and viewed at 1.2 to 5.0 kV. Overview images of petals and close-ups of the distal lobe region were taken at 40X and 1000X magnification, repectively. Sepal images were taken at 200X. All images were saved as TIF graphic files.

10.25. Statistical analysis

Statistical analysis of cell volume data was performed in R (http://www.r-project.org/). The RCommander package was used for box plots and unpaired Wilcoxon signed rank tests. The "boot'" package was used to calculate confidence intervals for the difference in volumes between EdU-positive and EdU-negative cells (nonparametric, ordinary bootstrap with 999 replicates, 95% confidence level).

For statistical analysis of petal and sepal measurements the RCommander package was used for box plots and to test for normal distribution using the "Shapiro-Wilk" test for normality. Subsequently, One-Way ANOVA with "pairwise comparisons of means" using "Tuckey Contrasts" was used.

For analysis of the global expression array and ChIP-seq data, the Fisher's exact test was used to test the significance of specific groups of genes within the total number of genes analysed.

References

1. Achard P*, et al.* (2006) Integration of plant responses to environmentally activated phytohormonal signals. *Science* 311(5757):91-94.
2. Achard P & Genschik P (2009) Releasing the brakes of plant growth: how GAs shutdown DELLA proteins. *Journal of Experimental Botany* 60(4):1085-1092.
3. Achard P, Herr A, Baulcombe DC, & Harberd NP (2004) Modulation of floral development by a gibberellin-regulated microRNA. *Development* 131(14):3357-3365.
4. Achard P*, et al.* (2009) Gibberellin Signaling Controls Cell Proliferation Rate in Arabidopsis. *Current Biology* 19(14):1188-1193.
5. Aida M & Tasaka M (2006) Morphogenesis and patterning at the organ boundaries in the higher plant shoot apex u. *Plant Molecular Biology* 60(6):915-928.
6. Allen RS*, et al.* (2007) Genetic analysis reveals functional redundancy and the major target genes of the Arabidopsis miR159 family. *Proceedings of the National Academy of Sciences of the United States of America* 104(41):16371-16376.
7. Alonso-Peral MM, Sun C, & Millar AA (2012) MicroRNA159 Can Act as a Switch or Tuning MicroRNA Independently of Its Abundance in Arabidopsis. *Plos One* 7(4).
8. Anastasia SD*, et al.* (2012) A link between mitotic entry and membrane growth suggests a novel model for cell size control. *Journal of Cell Biology* 197(1):89-104.
9. Anastasiou E*, et al.* (2007) Control of plant organ size by KLUH/CYP78A5-dependent intercellular signaling. *Developmental Cell* 13(6):843-856.
10. Andriankaja M*, et al.* (2012) Exit from Proliferation during Leaf Development in Arabidopsis thaliana: A Not-So-Gradual Process. *Developmental Cell* 22(1):64-78.
11. Asl LK*, et al.* (2011) Model-Based Analysis of Arabidopsis Leaf Epidermal Cells Reveals Distinct Division and Expansion Patterns for Pavement and Guard Cells. *Plant Physiology* 156(4):2172-2183.
12. Bacon MA, Wilkinson S, & Davies WJ (1998) pH-regulated leaf cell expansion in droughted plants is abscisic acid dependent. *Plant Physiology* 118(4):1507-1515.
13. Bai Y, Falk S, Schnittger A, Jakoby MJ, & Huelskamp M (2010) Tissue layer specific regulation of leaf length and width in Arabidopsis as revealed by the cell

autonomous action of ANGUSTIFOLIA. *Plant Journal* 61(2):191-199.

14. Bailey TL (2011) DREME: motif discovery in transcription factor ChIP-seq data. *Bioinformatics* 27(12):1653-1659.
15. Balasubramanian S & Schneitz K (2000) NOZZLE regulates proximal-distal pattern formation, cell proliferation and early sporogenesis during ovule development in Arabidopsis thaliana. *Development* 127(19):4227-4238.
16. Balasubramanian S & Schneitz K (2002) NOZZLE links proximal-distal and adaxial-abaxial pattern formation during ovule development in Arabidopsis thaliana. *Development* 129(18):4291-4300.
17. Barkoulas M, Galinha C, Grigg SP, & Tsiantis M (2007) From genes to shape: regulatory interactions in leaf development. *Current Opinion in Plant Biology* 10(6):660-666.
18. Baskin TI (2005) Anisotropic expansion of the plant cell wall. *Annual Review of Cell and Developmental Biology* 21:203-222.
19. Baumann K*, et al.* (2007) Control of cell and petal morphogenesis by R2R3 MYB transcription factors. *Development* 134(9):1691-1701.
20. Bellaoui M*, et al.* (2001) The Arabidopsis BELL1 and KNOX TALE homeodomain proteins interact through a domain conserved between plants and animals. *Plant Cell* 13(11):2455-2470.
21. Belles-Boix E*, et al.* (2006) KNAT6: an Arabidopsis homeobox gene involved in meristem activity and organ separation. *Plant Cell* 18(8):1900-1907.
22. Bemis SM & Torii KU (2007) Autonomy of cell proliferation and developmental programs during Arabidopsis aboveground organ morphogenesis. *Developmental Biology* 304(1):367-381.
23. Bencivenga S, Simonini S, Benkova E, & Colombo L (2012) The Transcription Factors BEL1 and SPL Are Required for Cytokinin and Auxin Signaling During Ovule Development in Arabidopsis. *Plant Cell* 24(7):2886-2897.
24. Benjamini Y & Hochberg Y (1995) CONTROLLING THE FALSE DISCOVERY RATE - A PRACTICAL AND POWERFUL APPROACH TO MULTIPLE TESTING. *Journal of the Royal Statistical Society Series B-Methodological* 57(1):289-300.
25. Benjamins R, Quint A, Weijers D, Hooykaas P, & Offringa R (2001) The PINOID protein kinase regulates organ development in Arabidopsis by enhancing polar

auxin transport. *Development* 128(20):4057-4067.

26. Benkova E*, et al.* (2003) Local, efflux-dependent auxin gradients as a common module for plant organ formation. *Cell* 115(5):591-602.
27. Bergonci T*, et al.* (2014) Arabidopsis thaliana RALF1 opposes brassinosteroid effects on root cell elongation and lateral root formation. *Journal of Experimental Botany*.
28. Besnard F, Vernoux T, & Hamant O (2011) Organogenesis from stem cells in planta: multiple feedback loops integrating molecular and mechanical signals. *Cellular and Molecular Life Sciences* 68(17):2885-2906.
29. Besson A, Dowdy SF, & Roberts JM (2008) CDK inhibitors: Cell cycle regulators and beyond. *Developmental Cell* 14(2):159-169.
30. Bischoff V*, et al.* (2010) TRICHOME BIREFRINGENCE and Its Homolog AT5G01360 Encode Plant-Specific DUF231 Proteins Required for Cellulose Biosynthesis in Arabidopsis. *Plant Physiology* 153(2):590-602.
31. Bischoff V, Selbig J, & Scheible W-R (2010a) Involvement of TBL/DUF231 proteins into cell wall biology. *Plant signaling & behavior* 5(8):1057-1059.
32. Blomme J, Inzé D, & Gonzalez N (2013) The cell-cycle interactome: a source of growth regulators? *Journal of Experimental Botany*.
33. Bolduc N, O'Connor D, Moon J, Lewis M, & Hake S (2012) How to pattern a leaf. *Cold Spring Harbor symposia on quantitative biology* 77:47-51.
34. Bolduc N & Hake S (2009) The Maize Transcription Factor KNOTTED1 Directly Regulates the Gibberellin Catabolism Gene ga2ox1. *Plant Cell* 21(6):1647-1658.
35. Bossinger G & Smyth DR (1996) Initiation patterns of flower and floral organ development in Arabidopsis thaliana. *Development* 122(4):1093-1102.
36. Bouche N (2010) New insights into miR398 functions in Arabidopsis. *Plant signaling & behavior* 5(6):684-686.
37. Breuer C*, et al.* (2009) The Trihelix Transcription Factor GTL1 Regulates Ploidy-Dependent Cell Growth in the Arabidopsis Trichome. *Plant Cell* 21(8):2307-2322.
38. Breuil-Broyer S*, et al.* (2004) High-resolution boundary analysis during Arabidopsis thaliana flower development. *Plant Journal* 38(1):182-192.
39. Breuninger H & Lenhard M (2010) CONTROL OF TISSUE AND ORGAN GROWTH IN PLANTS. *Plant Development* 91:185-220.

40. Brewer PB*, et al.* (2004) PETAL LOSS, a trihelix transcription factor gene, regulates perianth architecture in the Arabidopsis flower. *Development* 131(16):4035-4045.
41. Burian A*, et al.* (2013) A correlative microscopy approach relates microtubule behaviour, local organ geometry, and cell growth at the Arabidopsis shoot apical meristem. *Journal of Experimental Botany* 64(18):5753-5767.
42. Byrne ME*, et al.* (2000) Asymmetric leaves1 mediates leaf patterning and stem cell function in Arabidopsis. *Nature* 408(6815):967-971.
43. Byrne ME, Simorowski J, & Martienssen RA (2002) ASYMMETRIC LEAVES1 reveals knox gene redundancy in Arabidopsis. *Development* 129(8):1957-1965.
44. Carraro N, Peaucelle A, Laufs P, & Traas J (2006) Cell differentiation and organ initiation at the shoot apical meristem. *Plant Molecular Biology* 60(6):811-826.
45. Chae K*, et al.* (2012) Arabidopsis SMALL AUXIN UP RNA63 promotes hypocotyl and stamen filament elongation. *Plant Journal* 71(4):684-697.
46. Cheng H*, et al.* (2004) Gibberellin regulates Arabidopsis floral development via suppression of DELLA protein function. *Development* 131(5):1055-1064.
47. Cheng Y*, et al.* (2013) Downregulation of multiple CDK inhibitor ICK/KRP genes upregulates the E2F pathway and increases cell proliferation, and organ and seed sizes in Arabidopsis. *Plant Journal* 75(4):642-655.
48. Cheong YH*, et al.* (2007) Two calcineurin B-like calcium sensors, interacting with protein kinase CIPK23, regulate leaf transpiration and root potassium uptake in Arabidopsis. *Plant Journal* 52(2):223-239.
49. Chickarmane VS, Gordon SP, Tarr PT, Heisler MG, & Meyerowitz EM (2012) Cytokinin signaling as a positional cue for patterning the apical-basal axis of the growing Arabidopsis shoot meristem. *Proceedings of the National Academy of Sciences of the United States of America* 109(10):4002-4007.
50. Chiu WL*, et al.* (1996) Engineered GFP as a vital reporter in plants. *Current Biology* 6(3):325-330.
51. Cho D*, et al.* (2012) Vacuolar CAX1 and CAX3 Influence Auxin Transport in Guard Cells via Regulation of Apoplastic pH. *Plant Physiology* 160(3):1293-1302.
52. Cho HT & Cosgrove DJ (2000) Altered expression of expansin modulates leaf growth and pedicel abscission in Arabidopsis thaliana. *Proceedings of the National Academy of Sciences of the United States of America* 97(17):9783-9788.

53. Christensen SK, Dagenais N, Chory J, & Weigel D (2000) Regulation of auxin response by the protein kinase PINOID. *Cell* 100(4):469-478.
54. Chuck G, Lincoln C, & Hake S (1996) KNAT1 induces lobed leaves with ectopic meristems when overexpressed in Arabidopsis. *Plant Cell* 8(8):1277-1289.
55. Churchman ML*, et al.* (2006) SIAMESE, a Plant-Specific Cell Cycle Regulator, Controls Endoreplication Onset in Arabidopsis thaliana. *The Plant Cell Online* 18(11):3145-3157.
56. Clark SE, Williams RW, & Meyerowitz EM (1997) The CLAVATA1 gene encodes a putative receptor kinase that controls shoot and floral meristem size in Arabidopsis. *Cell* 89(4):575-585.
57. Clough SJ & Bent AF (1998) Floral dip: a simplified method for Agrobacterium-mediated transformation of Arabidopsis thaliana. *Plant Journal* 16(6):735-743.
58. Coen ES & Meyerowitz EM (1991) THE WAR OF THE WHORLS - GENETIC INTERACTIONS CONTROLLING FLOWER DEVELOPMENT. *Nature* 353(6339):31-37.
59. Cohen SM & Jurgens G (1989) PROXIMAL DISTAL PATTERN-FORMATION IN DROSOPHILA - CELL AUTONOMOUS REQUIREMENT FOR DISTAL-LESS GENE ACTIVITY IN LIMB DEVELOPMENT. *Embo Journal* 8(7):2045-2055.
60. Cole M, Nolte C, & Werr W (2006) Nuclear import of the transcription factor SHOOT MERISTEMLESS depends on heterodimerization with BLH proteins expressed in discrete sub-domains of the shoot apical meristem of Arabidopsis thaliana. *Nucleic Acids Research* 34(4):1281-1292.
61. Conlon I & Raff M (2003) Differences in the way a mammalian cell and yeast cells coordinate cell growth and cell-cycle progression. *Journal of biology* 2(1):7-7.
62. Cosgrove DJ (2005) Growth of the plant cell wall. *Nature Reviews Molecular Cell Biology* 6(11):850-861.
63. Dathan N*, et al.* (2002) The Arabidopsis SUPERMAN protein is able to specifically bind DNA through its single Cys(2)-His(2) zinc finger motif. *Nucleic Acids Research* 30(22):4945-4951.
64. Daviere J-M & Achard P (2013) Gibberellin signaling in plants. *Development* 140(6):1147-1151.
65. De Veylder L*, et al.* (2001) Functional analysis of cyclin-dependent kinase inhibitors of Arabidopsis. *Plant Cell* 13(7):1653-1667.

66. De Veylder L, Joubes J, & Inze D (2003) Plant cell cycle transitions. *Current Opinion in Plant Biology* 6(6):536-543.

67. De Veylder L, Beeckman T, & Inze D (2007) The ins and outs of the plant cell cycle. *Nature Reviews Molecular Cell Biology* 8(8):655-665.

68. De Veylder L, Larkin JC, & Schnittger A (2011) Molecular control and function of endoreplication in development and physiology. *Trends in Plant Science* 16(11):624-634.

69. Deeken R*, et al.* (2002) Loss of the AKT2/3 potassium channel affects sugar loading into the phloem of Arabidopsis. *Planta* 216(2):334-344.

70. Deeken R, Sanders C, Ache P, & Hedrich R (2000) Developmental and light-dependent regulation of a phloem-localised K+ channel of Arabidopsis thaliana. *Plant Journal* 23(2):285-290.

71. Denicourt C & Dowdy SF (2004) Cip/Kip proteins: more than just CDKs inhibitors. *Genes & Development* 18(8):851-855.

72. Dennison KL*, et al.* (2001) Functions of AKT1 and AKT2 potassium channels determined by studies of single and double mutants of arabidopsis. *Plant Physiology* 127(3):1012-1019.

73. Depuydt S & Hardtke CS (2011) Hormone Signalling Crosstalk in Plant Growth Regulation. *Current Biology* 21(9):R365-R373.

74. Dewitte W*, et al.* (2003) Altered cell cycle distribution, hyperplasia, and inhibited differentiation in arabidopsis caused by the D-type cyclin CYCD3. *Plant Cell* 15(1):79-92.

75. Dewitte W*, et al.* (2007) Arabidopsis CYCD3 D-type cyclins link cell proliferation and endocycles and are rate-limiting for cytokinin responses. *Proceedings of the National Academy of Sciences of the United States of America* 104(36):14537-14542.

76. DeYoung BJ*, et al.* (2006) The CLAVATA1-related BAM1, BAM2 and BAM3 receptor kinase-like proteins are required for meristem function in Arabidopsis. *Plant Journal* 45(1):1-16.

77. Dinneny JR, Weigel D, & Yanofsky MF (2006) NUBBIN and JAGGED define stamen and carpel shape in Arabidopsis. *Development* 133(9):1645-1655.

78. Dinneny JR, Yadegari R, Fischer RL, Yanofsky MF, & Weigel D (2004) The role of

JAGGED in shaping lateral organs. *Development* 131(5):1101-1110.

79. Disch S*, et al.* (2006) The E3 ubiquitin ligase BIG BROTHER controls Arabidopsis organ size in a dosage-dependent manner. *Current Biology* 16(3):272-279.
80. Dissmeyer N, Weimer AK, De Veylder L, Novak B, & Schnittger A (2010) The regulatory network of cell-cycle progression is fundamentally different in plants versus yeast or metazoans. *Plant signaling & behavior* 5(12):1613-1618.
81. Donnelly PM, Bonetta D, Tsukaya H, Dengler RE, & Dengler NG (1999) Cell cycling and cell enlargement in developing leaves of Arabidopsis. *Developmental Biology* 215(2):407-419.
82. Enugutti B, Kirchhelle C, & Schneitz K (2013) On the genetic control of planar growth during tissue morphogenesis in plants. *Protoplasma* 250(3):651-661.
83. Eriksson S, Stransfeld L, Adamski NM, Breuninger H, & Lenhard M (2010) KLUH/CYP78A5-Dependent Growth Signaling Coordinates Floral Organ Growth in Arabidopsis. *Current Biology* 20(6):527-532.
84. Escobara NM*, et al.* (2003) High-throughput viral expression of cDNA-Green fluorescent protein fusions reveals novel subcellular addresses and identifies unique proteins that interact with plasmodesmata. *Plant Cell* 15(7):1507-1523.
85. Fahlgren N*, et al.* (2006) Regulation of AUXIN RESPONSE FACTOR3 by TAS3 ta-siRNA affects developmental timing and patterning in Arabidopsis. *Current Biology* 16(9):939-944.
86. Ferjani A*, et al.* (2013) Enhanced Cell Expansion in a KRP2 Overexpressor is Mediated by Increased V-ATPase Activity. *Plant and Cell Physiology* 54(12):1989-1998.
87. Fleet CM, Ercetin ME, & Gillaspy GE (2009) Inositol phosphate signaling and gibberellic acid. *Plant signaling & behavior* 4(1):73-74.
88. Fleming AJ, McQueenMason S, Mandel T, & Kuhlemeier C (1997) Induction of leaf primordia by the cell wall protein expansion. *Science* 276(5317):1415-1418.
89. Francis D (1998) The cell cycle and plant growth. *Inherent Variation in Plant Growth: Physiological Mechanisms and Ecological Consequences*:5-20.
90. Friml J*, et al.* (2004) A PINOID-dependent binary switch in apical-basal PIN polar targeting directs auxin efflux. *Science* 306(5697):862-865.
91. Fuglsang AT*, et al.* (2007) Arabidopsis protein kinase PKS5 inhibits the plasma

membrane H+-ATPase by preventing interaction with 14-3-3 protein. *Plant Cell* 19(5):1617-1634.

92. Fukao Y & Ferjani A (2011) V-ATPase dysfunction under excess zinc inhibits Arabidopsis cell expansion. *Plant signaling & behavior* 6(9):1253-1255.
93. Furutani M*, et al.* (2004) PIN-FORMED1 and PINOID regulate boundary formation and cotyledon development in Arabidopsis embryogenesis. *Development* 131(20):5021-5030.
94. Gaamouche T*, et al.* (2010) Cyclin-dependent kinase activity maintains the shoot apical meristem cells in an undifferentiated state. *Plant Journal* 64(1):26-37.
95. Gallego-Bartolome J*, et al.* (2012) Molecular mechanism for the interaction between gibberellin and brassinosteroid signaling pathways in Arabidopsis. *Proceedings of the National Academy of Sciences of the United States of America* 109(33):13446-13451.
96. Gallois JL, Woodward C, Reddy GV, & Sablowski R (2002) Combined SHOOT MERISTEMLESS and WUSCHEL trigger ectopic organogenesis in Arabidopsis. *Development* 129(13):3207-3217.
97. Geisler M, Frangne N, Gomes E, Martinoia E, & Palmgren MG (2000) The ACA4 gene of arabidopsis encodes a vacuolar membrane calcium pump that improves salt tolerance in yeast. *Plant Physiology* 124(4):1814-1827.
98. Geldner N, Friml J, Stierhof YD, Jurgens G, & Palme K (2001) Auxin transport inhibitors block PIN1 cycling and vesicle traficking. *Nature* 413(6854):425-428.
99. Gharaibeh RZ, Fodor AA, & Gibas CJ (2008) Background correction using dinucleotide affinities improves the performance of GCRMA. *Bmc Bioinformatics* 9.
100. Gille S*, et al.* (2011) O-Acetylation of Arabidopsis Hemicellulose Xyloglucan Requires AXY4 or AXY4L, Proteins with a TBL and DUF231 Domain. *Plant Cell* 23(11):4041-4053.
101. Gille S & Pauly M (2012) O-acetylation of plant cell wall polysaccharides. *Frontiers in Plant Science* 3.
102. Gjetting KSK, Ytting CK, Schulz A, & Fuglsang AT (2012) Live imaging of intra- and extracellular pH in plants using pHusion, a novel genetically encoded biosensor. *Journal of Experimental Botany* 63(8):3207-3218.

103. Gomez-Mena C, de Folter S, Costa MMR, Angenent GC, & Sablowski R (2005) Transcriptional program controlled by the floral homeotic gene AGAMOUS during early organogenesis. *Development* 132(3):429-438.

104. Gonzalez N*, et al.* (2010) Increased Leaf Size: Different Means to an End. *Plant Physiology* 153(3):1261-1279.

105. Goranov AI*, et al.* (2009) The rate of cell growth is governed by cell cycle stage. *Genes & Development* 23(12):1408-1422.

106. Goubet F*, et al.* (2009) Cell wall glucomannan in Arabidopsis is synthesised by CSLA glycosyltransferases, and influences the progression of embryogenesis. *Plant Journal* 60(3):527-538.

107. Grandjean O*, et al.* (2004) In vivo analysis of cell division, cell growth, and differentiation at the shoot apical meristem in arabidopsis. *Plant Cell* 16(1):74-87.

108. Gregis V, Sessa A, Colombo L, & Kater MM (2008) AGAMOUS-LIKE24 and SHORT VEGETATIVE PHASE determine floral meristem identity in Arabidopsis. *Plant Journal* 56(6):891-902.

109. Gregis V, Sessa A, Dorca-Fornell C, & Kater MM (2009) The Arabidopsis floral meristem identity genes AP1, AGL24 and SVP directly repress class B and C floral homeotic genes. *Plant Journal* 60(4):626-637.

110. Grewal SS & Edgar BA (2003) Controlling cell division in yeast and animals: does size matter? *Journal of biology* 2(1):5-5.

111. Griffith ME, Conceicao AD, & Smyth DR (1999) PETAL LOSS gene regulates initiation and orientation of second whorl organs in the Arabidopsis flower. *Development* 126(24):5635-5644.

112. Gunesekera B, Torabinejad J, Robinson J, & Gillaspy GE (2007) Inositol polyphosphate 5-phosphatases 1 and 2 are required for regulating seedling growth. *Plant Physiology* 143(3):1408-1417.

113. Guo M, Thomas J, Collins G, & Timmermans MCP (2008) Direct repression of KNOX loci by the ASYMMETRIC LEAVES1 complex of Arabidopsis. *Plant Cell* 20(1):48-58.

114. Ha CM*, et al.* (2003) The BLADE-ON-PETIOLE 1 gene controls leaf pattern formation through the modulation of meristematic activity in Arabidopsis. *Development* 130(1):161-172.

115. Ha CM, Jun JH, Nam HG, & Fletcher JC (2007) BLADE-ON-PETIOLE1 and 2 control

Arabidopsis lateral organ fate through regulation of LOB domain and adaxial-abaxial polarity genes. *Plant Cell* 19(6):1809-1825.

116. Hackbusch J, Richter K, Muller J, Salamini F, & Uhrig JF (2005) A central role of Arabidopsis thaliana ovate family proteins in networking and subcellular localization of 3-aa loop extension homeodomain proteins. *Proceedings of the National Academy of Sciences of the United States of America* 102(13):4908-4912.
117. Halder G & Johnson RL (2011) Hippo signaling: growth control and beyond. *Development* 138(1):9-22.
118. Hamant O*, et al.* (2008) Developmental Patterning by Mechanical Signals in Arabidopsis. *Science* 322(5908):1650-1655.
119. Harashima H, Dissmeyer N, & Schnittger A (2013) Cell cycle control across the eukaryotic kingdom. *Trends in Cell Biology* 23(7):345-356.
120. Haruta M*, et al.* (2010) Molecular Characterization of Mutant Arabidopsis Plants with Reduced Plasma Membrane Proton Pump Activity. *Journal of Biological Chemistry* 285(23):17918-17929.
121. Haruta M, Monshausen G, Gilroy S, & Sussman MR (2008) A cytoplasmic Ca2+ functional assay for identifying and purifying endogenous cell signaling peptides in Arabidopsis seedlings: Identification of AtRALF1 peptide. *Biochemistry* 47(24):6311-6321.
122. Haruta M & Sussman MR (2012) The Effect of a Genetically Reduced Plasma Membrane Protonmotive Force on Vegetative Growth of Arabidopsis. *Plant Physiology* 158(3):1158-1171.
123. Hase Y*, et al.* (2005) Ectopic endoreduplication caused by sterol alteration results in serrated petals in Arabidopsis. *Journal of Experimental Botany* 56(414):1263-1268.
124. Hasson A*, et al.* (2011) Evolution and Diverse Roles of the CUP-SHAPED COTYLEDON Genes in Arabidopsis Leaf Development. *Plant Cell* 23(1):54-68.
125. Hay A*, et al.* (2002) The gibberellin pathway mediates KNOTTED1-type homeobox function in plants with different body plans. *Current Biology* 12(18):1557-1565.
126. Hay A, Barkoulas M, & Tsiantis M (2006) ASYMMETRIC LEAVES1 and auxin activities converge to repress BREVIPEDICELLUS expression and promote leaf development in Arabidopsis. *Development* 133(20):3955-3961.

127. Hay A & Tsiantis M (2010) KNOX genes: versatile regulators of plant development and diversity. *Development* 137(19):3153-3165.
128. Heisler MG*, et al.* (2005) Patterns of auxin transport and gene expression during primordium development revealed by live imaging of the Arabidopsis inflorescence meristem. *Current Biology* 15(21):1899-1911.
129. Henriques R, Bögre L, Horváth B, & Magyar Z (2014) Balancing act: matching growth with environment by the TOR signalling pathway. *Journal of Experimental Botany*.
130. Hibara K-i*, et al.* (2006) Arabidopsis CUP-SHAPED COTYLEDON3 regulates postembryonic shoot meristem and organ boundary formation. *Plant Cell* 18(11):2946-2957.
131. Himanen K*, et al.* (2002) Auxin-mediated cell cycle activation during early lateral root initiation. *Plant Cell* 14(10):2339-2351.
132. Holst K, Schmuelling T, & Werner T (2011) Enhanced cytokinin degradation in leaf primordia of transgenic Arabidopsis plants reduces leaf size and shoot organ primordia formation. *Journal of Plant Physiology* 168(12):1328-1334.
133. Hong-Hermesdorf A, Brux A, Gruber A, Gruber G, & Schumacher K (2006) A WNK kinase binds and phosphorylates V-ATPase subunit C. *Febs Letters* 580(3):932-939.
134. Horiguchi G, Kim GT, & Tsukaya H (2005) The transcription factor AtGRF5 and the transcription coactivator AN3 regulate cell proliferation in leaf primordia of Arabidopsis thaliana. *Plant Journal* 43(1):68-78.
135. Hu YX, Xie O, & Chua NH (2003) The Arabidopsis auxin-inducible gene ARGOS controls lateral organ size. *Plant Cell* 15(9):1951-1961.
136. Hunter C, Sun H, & Poethig RS (2003) The Arabidopsis heterochronic gene ZIPPY is an ARGONAUTE family member. *Current Biology* 13(19):1734-1739.
137. Hunter C*, et al.* (2006) Trans-acting siRNA-mediated repression of ETTIN and ARF4 regulates heteroblasty in Arabidopsis. *Development* 133(15):2973-2981.
138. Ikezaki M*, et al.* (2010) Genetic networks regulated by ASYMMETRIC LEAVES1 (AS1) and AS2 in leaf development in Arabidopsis thaliana: KNOX genes control five morphological events. *Plant Journal* 61(1):70-82.
139. Inze D & De Veylder L (2006) Cell cycle regulation in plant development. *Annual Review of Genetics* 40:77-105.

140. Ivakov A & Persson S (2013) Plant cell shape: modulators and measurements. *Frontiers in Plant Science* 4.

141. Jacobs J & Roe JL (2005) SKS6, a multicopper oxidase-like gene, participates in cotyledon vascular patterning during Arabidopsis thaliana development. *Planta* 222(4):652-666.

142. Jakoby MJ*, et al.* (2006) Analysis of the subcellular localization, function, and proteolytic control of the Arabidopsis cyclin-dependent kinase inhibitor ICK1/KRP1. *Plant Physiology* 141(4):1293-1305.

143. Jasinski S*, et al.* (2005) KNOX action in Arabidopsis is mediated by coordinate regulation of cytokinin and gibberellin activities. *Current Biology* 15(17):1560-1565.

144. Jegu T*, et al.* (2013) Multiple Functions of Kip-Related Protein5 Connect Endoreduplication and Cell Elongation. *Plant Physiology* 161(4):1694-1705.

145. John PCL & Qi R (2008) Cell division and endoreduplication: doubtful engines of vegetative growth. *Trends in Plant Science* 13(3):121-127.

146. Jorgensen P & Tyers M (2004) How cells coordinate growth and division. *Current Biology* 14(23):R1014-R1027.

147. Jun JH, Ha CM, & Fletcher JC (2010) BLADE-ON-PETIOLE1 Coordinates Organ Determinacy and Axial Polarity in Arabidopsis by Directly Activating ASYMMETRIC LEAVES2. *Plant Cell* 22(1):62-76.

148. Jurgens G (2005) Cytokinesis in higher plants. *Annual Review of Plant Biology* 56:281-299.

149. Kankaanpaa P*, et al.* (2012) BioImageXD: an open, general-purpose and high-throughput image-processing platform. *Nature Methods* 9(7):683-689.

150. Kanrar S, Onguka O, & Smith HMS (2006) Arabidopsis inflorescence architecture requires the activities of KNOX-BELL homeodomain heterodimers. *Planta* 224(5):1163-1173.

151. Kato N & Esaka M (1999) Changes in ascorbate oxidase gene expression and ascorbate levels in cell division and cell elongation in tobacco cells. *Physiologia Plantarum* 105(2):321-329.

152. Kaufmann K*, et al.* (2009) Target Genes of the MADS Transcription Factor SEPALLATA3: Integration of Developmental and Hormonal Pathways in the

Arabidopsis Flower. *Plos Biology* 7(4):854-875.

153. Kaufmann K*, et al.* (2010) Orchestration of Floral Initiation by APETALA1. *Science* 328(5974):85-89.

154. Kepinski S & Leyser O (2005) The Arabidopsis F-box protein TIR1 is an auxin receptor. *Nature* 435(7041):446-451.

155. Khan M*, et al.* (2012) Antagonistic Interaction of BLADE- ON-PETIOLE1 and 2 with BREVIPEDICELLUS and PENNYWISE Regulates Arabidopsis Inflorescence Architecture. *Plant Physiology* 158(2):946-960.

156. Kim GT*, et al.* (2002) The ANGUSTIFOLIA gene of Arabidopsis, a plant CtBP gene, regulates leaf-cell expansion, the arrangement of cortical microtubules in leaf cells and expression of a gene involved in cell-wall formation. *Embo Journal* 21(6):1267-1279.

157. Kim JH, Choi DS, & Kende H (2003) The AtGRF family of putative transcription factors is involved in leaf and cotyledon growth in Arabidopsis. *Plant Journal* 36(1):94-104.

158. Kim JH & Kende H (2004) A transcriptional coactivator, AtGIF1, is involved in regulating leaf growth and morphology in Arabidopsis. *Proceedings of the National Academy of Sciences of the United States of America* 101(36):13374-13379.

159. Kleine-Vehn J*, et al.* (2009) PIN Auxin Efflux Carrier Polarity Is Regulated by PINOID Kinase-Mediated Recruitment into GNOM-Independent Trafficking in Arabidopsis. *Plant Cell* 21(12):3839-3849.

160. Koyama T, Furutani M, Tasaka M, & Ohme-Takagi M (2007) TCP transcription factors control the morphology of shoot lateral organs via negative regulation of the expression of boundary-specific genes in Arabidopsis. *Plant Cell* 19(2):473-484.

161. Koyama T, Mitsuda N, Seki M, Shinozaki K, & Ohme-Takagi M (2010) TCP Transcription Factors Regulate the Activities of ASYMMETRIC LEAVES1 and miR164, as Well as the Auxin Response, during Differentiation of Leaves in Arabidopsis. *Plant Cell* 22(11):3574-3588.

162. Koyama T, Ohme-Takagi M, & Sato F (2011) Generation of serrated and wavy petals by inhibition of the activity of TCP transcription factors in Arabidopsis thaliana. *Plant signaling & behavior* 6(5):697-699.

163. Krizek BA (1999) Ectopic expression AINTEGUMENTA in Arabidopsis plants results

in increased growth of floral organs. *Developmental Genetics* 25(3):224-236.

164. Krizek BA & Fletcher JC (2005) Molecular mechanisms of flower development: An armchair guide. *Nature Reviews Genetics* 6(9):688-698.

165. Krizek BA, Lewis MW, & Fletcher JC (2006) RABBIT EARS is a second-whorl repressor of AGAMOUS that maintains spatial boundaries in Arabidopsis flowers. *Plant Journal* 45(3):369-383.

166. Krizek BA (2009) AINTEGUMENTA and AINTEGUMENTA-LIKE6 Act Redundantly to Regulate Arabidopsis Floral Growth and Patterning. *Plant Physiology* 150(4):1916-1929.

167. Krizek BA (2009a) Making bigger plants: key regulators of final organ size. *Current Opinion in Plant Biology* 12(1):17-22.

168. Kuchen EE*, et al.* (2012) Generation of Leaf Shape Through Early Patterns of Growth and Tissue Polarity. *Science* 335(6072):1092-1096.

169. Kumar R*, et al.* (2007) The Arabidopsis BEL1-LIKE HOMEODOMAIN proteins SAW1 and SAW2 act redundantly to regulate KNOX expression spatially in leaf margins. *Plant Cell* 19(9):2719-2735.

170. Kurakawa T*, et al.* (2007) Direct control of shoot meristem activity by a cytokinin-activating enzyme. *Nature* 445(7128):652-655.

171. Kurasawa K*, et al.* (2009) The AtXTH28 Gene, a Xyloglucan EndotransglucosylaseHydrolase, is Involved in Automatic Self-Pollination in Arabidopsis thaliana. *Plant and Cell Physiology* 50(2):413-422.

172. Kuroha T*, et al.* (2009) Functional Analyses of LONELY GUY Cytokinin-Activating Enzymes Reveal the Importance of the Direct Activation Pathway in Arabidopsis. *Plant Cell* 21(10):3152-3169.

173. Lampugnani ER, Kilinc A, & Smyth DR (2012) PETAL LOSS is a boundary gene that inhibits growth between developing sepals in Arabidopsis thaliana. *Plant Journal* 71(5):724-735.

174. Lampugnani ER, Kilinc A, & Smyth DR (2013) Auxin controls petal initiation in Arabidopsis. *Development* 140(1):185-194.

175. Laskowski M*, et al.* (2008) Root System Architecture from Coupling Cell Shape to Auxin Transport. *Plos Biology* 6(12):2721-2735.

176. Laufs P, Peaucelle A, Morin H, & Traas J (2004) MicroRNA regulation of the CUC

genes is required for boundary size control in Arabidopsis meristems. *Development* 131(17):4311-4322.

177. Lee Y & Kende H (2002) Expression of alpha-expansin and expansin-like genes in deepwater rice. *Plant Physiology* 130(3):1396-1405.
178. Leyser O (2010) The Power of Auxin in Plants. *Plant Physiology* 154(2):501-505.
179. Li CX, Potuschak T, Colon-Carmona A, Gutierrez RA, & Doerner P (2005) Arabidopsis TCP20 links regulation of growth and cell division control pathways. *Proceedings of the National Academy of Sciences of the United States of America* 102(36):12978-12983.
180. Li R, Li Y, Kristiansen K, & Wang J (2008) SOAP: short oligonucleotide alignment program. *Bioinformatics* 24(5):713-714.
181. Li X, Qin G, Chen Z, Gu H, & Qu L-J (2008) A gain-of-function mutation of transcriptional factor PTL results in curly leaves, dwarfism and male sterility by affecting auxin homeostasis. *Plant Molecular Biology* 66(3):315-327.
182. Li Y, Zheng L, Corke F, Smith C, & Bevan MW (2008) Control of final seed and organ size by the DA1 gene family in Arabidopsis thaliana. *Genes & Development* 22(10):1331-1336.
183. Liepman AH*, et al.* (2007) Functional genomic analysis supports conservation of function among cellulose synthase-like a gene family members and suggests diverse roles of mannans in plants. *Plant Physiology* 143(4):1881-1893.
184. Lincoln C, Long J, Yamaguchi J, Serikawa K, & Hake S (1994) A KNOTTED1-LIKE HOMEOBOX GENE IN ARABIDOPSIS IS EXPRESSED IN THE VEGETATIVE MERISTEM AND DRAMATICALLY ALTERS LEAF MORPHOLOGY WHEN OVEREXPRESSED IN TRANSGENIC PLANTS. *Plant Cell* 6(12):1859-1876.
185. Livak KJ & Schmittgen TD (2001) Analysis of relative gene expression data using real-time quantitative PCR and the 2(T)(-Delta Delta C) method. *Methods* 25(4):402-408.
186. Ljung K (2013) Auxin metabolism and homeostasis during plant development. *Development* 140(5):943-950.
187. Long JA, Moan EI, Medford JI, & Barton MK (1996) A member of the KNOTTED class of homeodomain proteins encoded by the STM gene of Arabidopsis. *Nature* 379(6560):66-69.

188. Maere S, Heymans K, & Kuiper M (2005) BiNGO: a Cytoscape plugin to assess overrepresentation of Gene Ontology categories in Biological Networks. *Bioinformatics* 21(16):3448-3449.

189. Mangeon A*, et al.* (2010) The tissue expression pattern of the AtGRP5 regulatory region is controlled by a combination of positive and negative elements. *Plant Cell Reports* 29(5):461-471.

190. Marshall WF*, et al.* (2012) What determines cell size? *Bmc Biology* 10.

191. Menges M, de Jager SM, Gruissem W, & Murray JAH (2005) Global analysis of the core cell cycle regulators of Arabidopsis identifies novel genes, reveals multiple and highly specific profiles of expression and provides a coherent model for plant cell cycle control. *Plant Journal* 41(4):546-566.

192. Michniewicz M*, et al.* (2007) Antagonistic regulation of PIN phosphorylation by PP2A and PINOID directs auxin flux. *Cell* 130(6):1044-1056.

193. Mitchum MG*, et al.* (2006) Distinct and overlapping roles of two gibberellin 3-oxidases in Arabidopsis development. *Plant Journal* 45(5):804-818.

194. Mizukami Y & Fischer RL (2000) Plant organ size control: AINTEGUMENTA regulates growth and cell numbers during organogenesis. *Proceedings of the National Academy of Sciences of the United States of America* 97(2):942-947.

195. Mockaitis K & Estelle M (2008) Auxin Receptors and Plant Development: A New Signaling Paradigm. *Annual Review of Cell and Developmental Biology* 24:55-80.

196. Moore I, Galweiler L, Grosskopf D, Schell J, & Palme K (1998) A transcription activation system for regulated gene expression in transgenic plants. *Proceedings of the National Academy of Sciences of the United States of America* 95(1):376-381.

197. Moseley JB, Mayeux A, Paoletti A, & Nurse P (2009) A spatial gradient coordinates cell size and mitotic entry in fission yeast. *Nature* 459(7248):857-U858.

198. Muino JM, Hoogstraat M, van Ham RCHJ, & van Dijk ADJ (2011) PRI-CAT: a web-tool for the analysis, storage and visualization of plant ChIP-seq experiments. *Nucleic Acids Research* 39:W524-W527.

199. Muino JM, Kaufmann K, van Ham RCHJ, Angenent GC, & Krajewski P (2011a) ChIP-seq Analysis in R (CSAR): An R package for the statistical detection of protein-bound genomic regions. *Plant Methods* 7.

200. Nath U, Crawford BCW, Carpenter R, & Coen E (2003) Genetic control of surface curvature. *Science* 299(5611):1404-1407.

201. Nawy T*, et al.* (2010) The GATA Factor HANABA TARANU Is Required to Position the Proembryo Boundary in the Early Arabidopsis Embryo. *Developmental Cell* 19(1):103-113.

202. Neff MM, Turk E, & Kalishman M (2002) Web-based primer design for single nucleotide polymorphism analysis. *Trends in Genetics* 18(12):613-615.

203. Nemhauser JL, Hong F, & Chory J (2006) Different plant hormones regulate similar processes through largely nonoverlapping transcriptional responses. *Cell* 126(3):467-475.

204. Neto-Silva RM, Wells BS, & Johnston LA (2009) Mechanisms of Growth and Homeostasis in the Drosophila Wing. *Annual Review of Cell and Developmental Biology* 25:197-220.

205. Nicol JW, Helt GA, Blanchard SG, Jr., Raja A, & Loraine AE (2009) The Integrated Genome Browser: free software for distribution and exploration of genome-scale datasets. *Bioinformatics* 25(20):2730-2731.

206. Norberg M, Holmlund M, & Nilsson O (2005) The BLADE ONPETIOLE genes act redundantly to control the growth and development of lateral organs. *Development* 132(9):2203-2213.

207. O'Maoileidigh DS, Graciet E, & Wellmer F (2014) Gene networks controlling Arabidopsis thaliana flower development. *New Phytologist* 201(1):16-30.

208. Ohno CK, Reddy GV, Heisler MGB, & Meyerowitz EM (2004) The Arabidopsis JAGGED gene encodes a zinc finger protein that promotes leaf tissue development. *Development* 131(5):1111-1122.

209. Olsen AN, Mundy J, & Skriver K (2002) Peptomics, identification of novel cationic Arabidopsis peptides with conserved sequence motifs. *In Silico Biology* 2(4):441-451.

210. Ori N, Eshed Y, Chuck G, Bowman JL, & Hake S (2000) Mechanisms that control knox gene expression in the Arabidopsis shoot. *Development* 127(24):5523-5532.

211. Ormenese S*, et al.* (2004) Analysis of the spatial expression pattern of seven kip related proteins (KRPs) in the shoot apex of Arabidopsis thaliana. *Annals of Botany* 93(5):575-580.

212. Palatnik JF*, et al.* (2003) Control of leaf morphogenesis by microRNAs. *Nature* 425(6955):257-263.

213. Pan D (2010) The Hippo Signaling Pathway in Development and Cancer. *Developmental Cell* 19(4):491-505.

214. Paredez AR, Somerville CR, & Ehrhardt DW (2006) Visualization of cellulose synthase demonstrates functional association with microtubules. *Science* 312(5779):1491-1495.

215. Parent B*, et al.* (2009) Drought and Abscisic Acid Effects on Aquaporin Content Translate into Changes in Hydraulic Conductivity and Leaf Growth Rate: A Trans-Scale Approach. *Plant Physiology* 149(4):2000-2012.

216. Park J, Khoa Thi N, Park E, Jeon J-S, & Choi G (2013) DELLA Proteins and Their Interacting RING Finger Proteins Repress Gibberellin Responses by Binding to the Promoters of a Subset of Gibberellin-Responsive Genes in Arabidopsis. *Plant Cell* 25(3):927-943.

217. Pastore JJ*, et al.* (2011) LATE MERISTEM IDENTITY2 acts together with LEAFY to activate APETALA1. *Development* 138(15):3189-3198.

218. Pearce G, Moura DS, Stratmann J, & Ryan CA (2001) RALF, a 5-kDa ubiquitous polypeptide in plants, arrests root growth and development (vol 98, pg 12843, 2001). *Proceedings of the National Academy of Sciences of the United States of America* 98(26):15394-15394.

219. Peaucelle A*, et al.* (2011) Pectin-Induced Changes in Cell Wall Mechanics Underlie Organ Initiation in Arabidopsis. *Current Biology* 21(20):1720-1726.

220. Peaucelle A*, et al.* (2008) Arabidopsis Phyllotaxis Is Controlled by the Methyl-Esterification Status of Cell-Wall Pectins. *Current Biology* 18(24):1943-1948.

221. Perrot-Rechenmann C (2010) Cellular Responses to Auxin: Division versus Expansion. *Cold Spring Harbor Perspectives in Biology* 2(5).

222. Persson S*, et al.* (2007) Genetic evidence for three unique components in primary cell-wall cellulose synthase complexes in Arabidopsis. *Proceedings of the National Academy of Sciences of the United States of America* 104(39):15566-15571.

223. Pignocchi C, Fletcher JM, Wilkinson JE, Barnes JD, & Foyer CH (2003) The function of ascorbate oxidase in tobacco. *Plant Physiology* 132(3):1631-1641.

224. Pignocchi C*, et al.* (2006) Ascorbate oxidase-dependent changes in the redox state

of the apoplast modulate gene transcript accumulation leading to modified hormone signaling and orchestration of defense processes in tobacco. *Plant Physiology* 141(2):423-435.

225. Powell AE & Lenhard M (2012) Control of Organ Size in Plants. *Current Biology* 22(9):R360-R367.

226. Qi R & John PCL (2007) Expression of genomic AtCYCD2;1 in arabidopsis induces cell division at smaller cell sizes: Implications for the control of plant growth. *Plant Physiology* 144(3):1587-1597.

227. Ragni L, Belles-Boix E, Guenl M, & Pautot V (2008) Interaction of KNAT6 and KNAT2 with BREVIPEDICELLUS and PENNYWISE in Arabidopsis inflorescences. *Plant Cell* 20(4):888-900.

228. Reddy GV, Heisler MG, Ehrhardt DW, & Meyerowitz EM (2004) Real-time lineage analysis reveals oriented cell divisions associated with morphogenesis at the shoot apex of Arabidopsis thaliana. *Development* 131(17):4225-4237.

229. Reinhardt D*, et al.* (2003) Regulation of phyllotaxis by polar auxin transport. *Nature* 426(6964):255-260.

230. Reinhart BJ*, et al.* (2013) Establishing a Framework for the Ad/Abaxial Regulatory Network of Arabidopsis: Ascertaining Targets of Class III HOMEODOMAIN LEUCINE ZIPPER and KANADI Regulation. *Plant Cell* 25(9):3228-3249.

231. Reiser L*, et al.* (1995) THE BELL1 GENE ENCODES A HOMEODOMAIN PROTEIN INVOLVED IN PATTERN-FORMATION IN THE ARABIDOPSIS OVULE PRIMORDIUM. *Cell* 83(5):735-742.

232. Ren H, Santner A, Carlos del Pozo J, Murray JAH, & Estelle M (2008) Degradation of the cyclin-dependent kinase inhibitor KRP1 is regulated by two different ubiquitin E3 ligases. *Plant Journal* 53(5):705-716.

233. Richmond TA & Somerville CR (2000) The cellulose synthase superfamily. *Plant Physiology* 124(2):495-498.

234. Rieu I*, et al.* (2008) Genetic Analysis Reveals That C-19-GA 2-Oxidation Is a Major Gibberellin Inactivation Pathway in Arabidopsis. *Plant Cell* 20(9):2420-2436.

235. Rieu I*, et al.* (2008a) The gibberellin biosynthetic genes AtGA20ox1 and AtGA20ox2 act, partially redundantly, to promote growth and development throughout the Arabidopsis life cycle. *Plant Journal* 53(3):488-504.

236. Rodriguez RE*, et al.* (2010) Control of cell proliferation in Arabidopsis thaliana by microRNA miR396. *Development* 137(1):103-112.

237. Rodriguez-Navarro A (2000) Potassium transport in fungi and plants. *Biochimica Et Biophysica Acta-Reviews on Biomembranes* 1469(1):1-30.

238. Roeder AHK*, et al.* (2010) Variability in the Control of Cell Division Underlies Sepal Epidermal Patterning in Arabidopsis thaliana. *Plos Biology* 8(5).

239. Rutjens B*, et al.* (2009) Shoot apical meristem function in Arabidopsis requires the combined activities of three BEL1-like homeodomain proteins. *Plant Journal* 58(4):641-654.

240. Ryu H*, et al.* (2007) Nucleocytoplasmic shuttling of BZR1 mediated by phosphorylation is essential in Arabidopsis brassinosteroid signaling. *Plant Cell* 19(9):2749-2762.

241. Sablowski RWM & Meyerowitz EM (1998) A homolog of NO APICAL MERISTEM is an immediate target of the floral homeotic genes APETALA3/PISTILLATA. *Cell* 92(1):93-103.

242. Sablowski R & Carnier Dornelas M (2013) Interplay between cell growth and cell cycle in plants. *Journal of Experimental Botany*.

243. Saddic LA*, et al.* (2006) The LEAFY target LMI1 is a meristem identity regulator and acts together with LEAFY to regulate expression of CAULIFLOWER. *Development* 133(9):1673-1682.

244. Sainsbury F, Thuenemann EC, & Lomonossoff GP (2009) pEAQ: versatile expression vectors for easy and quick transient expression of heterologous proteins in plants. *Plant Biotechnology Journal* 7(7):682-693.

245. Saito R*, et al.* (2012) A travel guide to Cytoscape plugins. *Nature Methods* 9(11):1069-1076.

246. Sakamoto T, Kamiya N, Ueguchi-Tanaka M, Iwahori S, & Matsuoka M (2001) KNOX homeodomain protein directly suppresses the expression of a gibberellin biosynthetic gene in the tobacco shoot apical meristem. *Genes & Development* 15(5):581-590.

247. Salic A & Mitchison TJ (2008) A chemical method for fast and sensitive detection of DNA synthesis in vivo. *Proceedings of the National Academy of Sciences of the United States of America* 105(7):2415-2420.

248. Sanz L*, et al.* (2011) The Arabidopsis D-Type Cyclin CYCD2;1 and the Inhibitor ICK2/KRP2 Modulate Auxin-Induced Lateral Root Formation. *Plant Cell* 23(2):641-660.

249. Sauret-Gueeto S, Schiessl K, Bangham A, Sablowski R, & Coen E (2013) JAGGED Controls Arabidopsis Petal Growth and Shape by Interacting with a Divergent Polarity Field. *Plos Biology* 11(4).

250. Sawa S*, et al.* (2002) The HAT2 gene, a member of the HD-Zip gene family, isolated as an auxin inducible gene by DNA microarray screening, affects auxin response in Arabidopsis. *Plant Journal* 32(6):1011-1022.

251. Scheer JM, Pearce G, & Ryan CA (2005) LeRALF, a plant peptide that regulates root growth and development, specifically binds to 25 and 120 kDa cell surface membrane proteins of Lycopersicon peruvianum. *Planta* 221(5):667-674.

252. Schiessl K, Kausika S, Southam P, Bush M, & Sablowski R (2012) JAGGED Controls Growth Anisotropy and Coordination between Cell Size and Cell Cycle during Plant Organogenesis. *Current Biology* 22(19):1739-1746.

253. Schmid B, Schindelin J, Cardona A, Longair M, & Heisenberg M (2010) A high-level 3D visualization API for Java and ImageJ. *Bmc Bioinformatics* 11.

254. Schmid JA & Neumeier H (2005) Evolutions in science triggered by green fluorescent protein (GFP). *Chembiochem* 6(7):1149-+.

255. Schmidt M*, et al.* (2002) Cell cycle inhibition by FoxO forkhead transcription factors involves downregulation of cyclin D. *Molecular and Cellular Biology* 22(22):7842-7852.

256. Schomburg FM, Bizzell CM, Lee DJ, Zeevaart JAD, & Amasino RM (2003) Overexpression of a novel class of gibberellin 2-oxidases decreases gibberellin levels and creates dwarf plants. *Plant Cell* 15(1):151-163.

257. Schoof H*, et al.* (2000) The stem cell population of Arabidopsis shoot meristems is maintained by a regulatory loop between the CLAVATA and WUSCHEL genes. *Cell* 100(6):635-644.

258. Schopfer P (2006) Biomechanics of plant growth. *American Journal of Botany* 93(10):1415-1425.

259. Schulze S, Schaefer BN, Parizotto EA, Voinnet O, & Theres K (2010) LOST MERISTEMS genes regulate cell differentiation of central zone descendants in

Arabidopsis shoot meristems. *Plant Journal* 64(4):668-678.

260. Schumacher K*, et al.* (1999) The Arabidopsis det3 mutant reveals a central role for the vacuolar H+-ATPase in plant growth and development. *Genes & Development* 13(24):3259-3270.

261. Sedbrook JC, Carroll KL, Hung KF, Masson PH, & Somerville CR (2002) The Arabidopsis SKU5 gene encodes an extracellular glycosyl phosphatidylinositol-anchored glycoprotein involved in directional root growth. *Plant Cell* 14(7):1635-1648.

262. Si-Ammour A*, et al.* (2011) miR393 and Secondary siRNAs Regulate Expression of the TIR1/AFB2 Auxin Receptor Clade and Auxin-Related Development of Arabidopsis Leaves. *Plant Physiology* 157(2):683-691.

263. Smirnoff N (2000) Ascorbic acid: metabolism and functions of a multi-facetted molecule. *Current Opinion in Plant Biology* 3(3):229-235.

264. Smith LG, Greene B, Veit B, & Hake S (1992) A DOMINANT MUTATION IN THE MAIZE HOMEOBOX GENE, KNOTTED-1, CAUSES ITS ECTOPIC EXPRESSION IN LEAF-CELLS WITH ALTERED FATES. *Development* 116(1):21-&.

265. Smith ZR & Long JA (2010) Control of Arabidopsis apical-basal embryo polarity by antagonistic transcription factors. *Nature* 464(7287):423-U121.

266. Smyth DR, Bowman JL, & Meyerowitz EM (1990) EARLY FLOWER DEVELOPMENT IN ARABIDOPSIS. *Plant Cell* 2(8):755-767.

267. Song SK & Clark SE (2005) POL and related phosphatases are dosage-sensitive regulators of meristem and organ development in Arabidopsis. *Developmental Biology* 285(1):272-284.

268. Spartz AK*, et al.* (2012) The SAUR19 subfamily of SMALL AUXIN UP RNA genes promote cell expansion. *Plant Journal* 70(6):978-990.

269. Srivastava R, Liu J-X, Guo H, Yin Y, & Howell SH (2009) Regulation and processing of a plant peptide hormone, AtRALF23, in Arabidopsis. *Plant Journal* 59(6):930-939.

270. Stevenson CEM*, et al.* (2013) Investigation of DNA sequence recognition by a streptomycete MarR family transcriptional regulator through surface plasmon resonance and X-ray crystallography. *Nucleic Acids Research* 41(14):7009-7022.

271. Sundaresan V*, et al.* (1995) PATTERNS OF GENE-ACTION IN PLANT DEVELOPMENT

REVEALED BY ENHANCER TRAP AND GENE TRAP TRANSPOSABLE ELEMENTS. *Genes & Development* 9(14):1797-1810.

272. Sunkar R, Kapoor A, & Zhu J-K (2006) Posttranscriptional induction of two Cu/Zn superoxide dismutase genes in Arabidopsis is mediated by downregulation of miR398 and important for oxidative stress tolerance. *Plant Cell* 18(8):2051-2065.
273. Sze H, Li XH, & Palmgren MG (1999) Energization of plant cell membranes by H+-pumping ATPases: Regulation and biosynthesis. *Plant Cell* 11(4):677-689.
274. Szyroki A*, et al.* (2001) KAT1 is not essential for stomatal opening. *Proceedings of the National Academy of Sciences of the United States of America* 98(5):2917-2921.
275. Tabata R*, et al.* (2010) Arabidopsis AUXIN RESPONSE FACTOR6 and 8 Regulate Jasmonic Acid Biosynthesis and Floral Organ Development via Repression of Class 1 KNOX Genes. *Plant and Cell Physiology* 51(1):164-175.
276. Takeda T*, et al.* (2002) Suppression and acceleration of cell elongation by integration of xyloglucans in pea stem segments. *Proceedings of the National Academy of Sciences of the United States of America* 99(13):9055-9060.
277. Tanaka K*, et al.* (2003) Physiological roles of brassinosteroids in early growth of Arabidopsis: Brassinosteroids have a synergistic relationship with gibberellin as well as auxin in light-grown hypocotyl elongation. *Journal of Plant Growth Regulation* 22(3):259-271.
278. Teixeira LT*, et al.* (2000) p27(Kip1)-deficient mice exhibit accelerated growth hormone-releasing hormone (GHRH)-induced somatotrope proliferation and adenoma formation. *Oncogene* 19(15):1875-1884.
279. Tokunaga H*, et al.* (2012) Arabidopsis lonely guy (LOG) multiple mutants reveal a central role of the LOG-dependent pathway in cytokinin activation. *Plant Journal* 69(2):355-365.
280. Torres Acosta JA*, et al.* (2004) Molecular characterization of Arabidopsis PHO80-like proteins, a novel class of CDKA;1-interacting cyclins. *Cellular and molecular life sciences : CMLS* 61(12):1485-1497.
281. Torres Acosta JA, Fowke LC, & Wang H (2011) Analyses of phylogeny, evolution, conserved sequences and genome-wide expression of the ICK/KRP family of plant CDK inhibitors. *Annals of botany* 107(7):1141-1157.

282. Truernit E*, et al.* (2008) High-resolution whole-mount imaging of three-dimensional tissue organization and gene expression enables the study of phloem development and structure in Arabidopsis. *Plant Cell* 20(6):1494-1503.

283. Tzur A, Kafri R, LeBleu VS, Lahav G, & Kirschner MW (2009) Cell Growth and Size Homeostasis in Proliferating Animal Cells. *Science* 325(5937):167-171.

284. Uchida N, Shimada M, & Tasaka M (2013) ERECTA-Family Receptor Kinases Regulate Stem Cell Homeostasis via Buffering its Cytokinin Responsiveness in the Shoot Apical Meristem. *Plant and Cell Physiology* 54(3):343-351.

285. Van Leene J*, et al.* (2010) Targeted interactomics reveals a complex core cell cycle machinery in Arabidopsis thaliana. *Molecular Systems Biology* 6.

286. van Steensel B, Delrow J, & Bussemaker HJ (2003) Genomewide analysis of Drosophila GAGA factor target genes reveals context-dependent DNA binding. *Proceedings of the National Academy of Sciences of the United States of America* 100(5):2580-2585.

287. Veit B (2009) Hormone mediated regulation of the shoot apical meristem. *Plant Molecular Biology* 69(4):397-408.

288. Venglat SP*, et al.* (2002) The homeobox gene BREVIPEDICELLUS is a key regulator of inflorescence architecture in Arabidopsis. *Proceedings of the National Academy of Sciences of the United States of America* 99(7):4730-4735.

289. Verkest A*, et al.* (2005) The cyclin-dependent kinase inhibitor KRP2 controls the onset of the endoreduplication cycle during Arabidopsis leaf development through inhibition of mitotic CDKA;1 kinase complexes. *Plant Cell* 17(6):1723-1736.

290. Vroemen CW, Mordhorst AP, Albrecht C, Kwaaitaal M, & de Vries SC (2003) The CUP-SHAPED COTYLEDON3 gene is required for boundary and shoot meristem formation in Arabidopsis. *Plant Cell* 15(7):1563-1577.

291. Wachsman G, Heidstra R, & Scheres B (2011) Distinct Cell-Autonomous Functions of RETINOBLASTOMA-RELATED in Arabidopsis Stem Cells Revealed by the Brother of Brainbow Clonal Analysis System. *Plant Cell* 23(7):2581-2591.

292. Wang H, Zhou YM, Gilmer S, Whitwill S, & Fowke LC (2000) Expression of the plant cyclin-dependent kinase inhibitor ICK1 affects cell division, plant growth and morphology. *Plant Journal* 24(5):613-623.

293. Wang S, Chang Y, Guo J, & Chen J-G (2007) Arabidopsis Ovate Family Protein 1 is a

transcriptional repressor that suppresses cell elongation. *Plant Journal* 50(5):858-872.

294. Wang S*, et al.* (2011) Arabidopsis Ovate Family Proteins, a Novel Transcriptional Repressor Family, Control Multiple Aspects of Plant Growth and Development. *Plos One* 6(8).

295. Wang Y*, et al.* (2003) The Arabidopsis homeobox gene, ATHB16, regulates leaf development and the sensitivity to photoperiod in Arabidopsis. *Developmental Biology* 264(1):228-239.

296. Wang Y, Chu Y-J, & Xue H-W (2012) Inositol polyphosphate 5-phosphatase-controlled Ins(1,4,5)P-3/Ca2+ is crucial for maintaining pollen dormancy and regulating early germination of pollen. *Development* 139(12):2221-2233.

297. Wartlick O & Gonzalez-Gaitan M (2011) The missing link: implementation of morphogenetic growth control on the cellular and molecular level. *Current Opinion in Genetics & Development* 21(6):690-695.

298. Weigel D, Alvarez J, Smyth DR, Yanofsky MF, & Meyerowitz EM (1992) LEAFY CONTROLS FLORAL MERISTEM IDENTITY IN ARABIDOPSIS. *Cell* 69(5):843-859.

299. Weinl C*, et al.* (2005) Novel functions of plant cyclin-dependent kinase inhibitors, ICK1/KRP1, can act non-cell-autonomously and inhibit entry into mitosis. *Plant Cell* 17(6):1704-1722.

300. Weinl S & Kudla J (2009) The CBL-CIPK Ca2+-decoding signaling network: function and perspectives. *New Phytologist* 184(3):517-528.

301. Wellmer F, Alves-Ferreira M, Dubois A, Riechmann JL, & Meyerowitz EM (2006) Genome-wide analysis of gene expression during early Arabidopsis flower development. *Plos Genetics* 2(7):1012-1024.

302. Werner T*, et al.* (2003) Cytokinin-deficient transgenic Arabidopsis plants show multiple developmental alterations indicating opposite functions of cytokinins in the regulation of shoot and root meristem activity. *Plant Cell* 15(11):2532-2550.

303. William DA*, et al.* (2004) Genomic identification of direct target genes of LEAFY. *Proceedings of the National Academy of Sciences of the United States of America* 101(6):1775-1780.

304. Winter CM*, et al.* (2011) LEAFY Target Genes Reveal Floral Regulatory Logic, cis Motifs, and a Link to Biotic Stimulus Response. *Developmental Cell* 20(4):430-443.

305. Wolf S & Greiner S (2012) Growth control by cell wall pectins. *Protoplasma* 249:169-175.

306. Wolf S, Hematy K, & Hoefte H (2012) Growth Control and Cell Wall Signaling in Plants. *Annual Review of Plant Biology, Vol 63* 63:381-407.

307. Wolf S, Rausch T, & Greiner S (2009) The N-terminal pro region mediates retention of unprocessed type-I PME in the Golgi apparatus. *Plant Journal* 58(3):361-375.

308. Wood E & Nurse P (2013) Pom1 and cell size homeostasis in fission yeast. *Cell Cycle* 12(19):3228-3236.

309. Wu C-Y, Rolfe PA, Gifford DK, & Fink GR (2010) Control of Transcription by Cell Size. *Plos Biology* 8(11).

310. Wu J & Cohen SM (1999) Proximodistal axis formation in the Drosophila leg: subdivision into proximal and distal domains by Homothorax and Distal-less. *Development* 126(1):109-117.

311. Wu J*, et al.* (2007) NaRALF, a peptide signal essential for the regulation of root hair tip apoplastic pH in Nicotiana attenuata, is required for root hair development and plant growth in native soils. *Plant Journal* 52(5):877-890.

312. Wuest SE*, et al.* (2012) Molecular basis for the specification of floral organs by APETALA3 and PISTILLATA. *Proceedings of the National Academy of Sciences of the United States of America* 109(33):13452-13457.

313. Xia T*, et al.* (2013) The Ubiquitin Receptor DA1 Interacts with the E3 Ubiquitin Ligase DA2 to Regulate Seed and Organ Size in Arabidopsis. *Plant Cell* 25(9):3347-3359.

314. Xu B*, et al.* (2008) Arabidopsis genes AS1, AS2, and JAG negatively regulate boundary-specifying genes to promote sepal and petal development (vol 146, pg 566, 2008). *Plant Physiology* 146(4):2054-2054.

315. Xu J*, et al.* (2006) A protein kinase, interacting with two calcineurin B-like proteins, regulates K+ transporter AKT1 in Arabidopsis. *Cell* 125(7):1347-1360.

316. Yamaguchi N*, et al.* (2013) A Molecular Framework for Auxin-Mediated Initiation of Flower Primordia. *Developmental Cell* 24(3):271-282.

317. Yamamoto A*, et al.* (2005) Suppressed expression of the apoplastic ascorbate oxidase gene increases salt tolerance in tobacco and Arabidopsis plants. *Journal of Experimental Botany* 56(417):1785-1796.

318. Yanai O*, et al.* (2005) Arabidopsis KNOXI proteins activate cytokinin biosynthesis. *Current Biology* 15(17):1566-1571.

319. Yu LP, Miller AK, & Clark SE (2003) POLTERGEIST encodes a protein phosphatase 2C that regulates CLAVATA pathways controlling stem cell identity at Arabidopsis shoot and flower meristems. *Current Biology* 13(3):179-188.

320. Zenoni S*, et al.* (2011) Overexpression of PhEXPA1 increases cell size, modifies cell wall polymer composition and affects the timing of axillary meristem development in Petunia hybrida. *New Phytologist* 191(3):662-677.

321. Zhang J*, et al.* (2009) AtSOFL1 and AtSOFL2 Act Redundantly as Positive Modulators of the Endogenous Content of Specific Cytokinins in Arabidopsis. *Plos One* 4(12).

322. Zhang X*, et al.* (2013) Transcription Repressor HANABA TARANU Controls Flower Development by Integrating the Actions of Multiple Hormones, Floral Organ Specification Genes, and GATA3 Family Genes in Arabidopsis. *Plant Cell* 25(1):83-101.

323. Zhao XA*, et al.* (2012) A General G1/S-Phase Cell-Cycle Control Module in the Flowering Plant Arabidopsis thaliana. *Plos Genetics* 8(8).

324. Zhao YX*, et al.* (2004) HANABA TARANU is a GATA transcription factor that regulates shoot apical meristem and flower development in Arabidopsis. *Plant Cell* 16(10):2586-2600.

325. Zhao Y (2010) Auxin Biosynthesis and Its Role in Plant Development. *Annual Review of Plant Biology, Vol 61* 61:49-64.

326. Zhou YM, Li GY, Brandizzi F, Fowke LC, & Wang H (2003) The plant cyclin-dependent kinase inhibitor ICK1 has distinct functional domains for in vivo kinase inhibition, protein instability and nuclear localization. *Plant Journal* 35(4):476-489.

327. Zhou YM*, et al.* (2002) Control of petal and pollen development by the plant cyclin-dependent kinase inhibitor ICK1 in transgenic Brassica plants. *Planta* 215(2):248-257.

328. Zhou Y, Fowke LC, & Wang H (2002a) Plant CDK inhibitors: studies of interactions with cell cycle regulators in the yeast two-hybrid system and functional comparisons in transgenic Arabidopsis plants. *Plant Cell Reports* 20(10):967-975.

Appendices